The Effect of X-ray Absorption in Thin Film Microanalysis

Khalid Mahmood Khan

Department of Physics And Astronomy, University of Glasgow, Glasgow G12 8QQ, Scotland.

A Thesis submitted for the degree
of the Doctor of Philosophy
in the University of Glasgow.

August 1990

ProQuest LLC.
789 East Eisenhower Parkway
P.O. Box 1346
Ann Arbor, MI 48106 – 1346

Declaration

This thesis has been written solely by me, and is an account of my research work undertaken in the department of Physics and Astronomy, The University of Glasgow, Glasgow. The work described is my own apart from where otherwise mentioned.

The specimens used for the analysis of biological work in chapter 5 were provided by Dr H Y Elder. The experimental spectra from these specimens were recorded by J D Pediani on a JEOL 100 C electron microscope in The Institute of Physiology, Glasgow University, Glasgow.

The specimens used for the work described in chapters 6 and 7 were provided by A J McGibbon and J L Martin respectively. The experimental spectra from these specimens were recorded by Dr W A P Nicholson on an extended VG HB5 electron microscope in the Department of Physics and Astronomy, Glasgow University, Glasgow.

All the computer programmes listed in appendix 2 were written in collaboration with Dr. W A P Nicholson, except for programme for calculating mass absorption coefficients which was written with Dr. A J Garratt-Reed (Massachusetts Institute of Technology, Boston USA).

The following papers have been published, or will be submitted for publication, presenting results mentioned in this thesis.

(a) Absorption Corrections for Thin Specimens.
K M Khan, W A P Nicholson, J N Chapman and A J Mc Gibbon.
In: EMAS Workshop Proceedings (Antwerp, 1989).

(b) Corrections for Self Absorption in EDX Microanalysis

of Semi-thin Specimens.

W A P Nicholson, K M Khan, J N Chapman and A J Mc Gibbon.

In: SCANNING 89/EM West Proceedings (Long Beach, 1989).

(c) Background Modelling by the MBH Method for the Microanalysis of Thin Biological Sections.

K M Khan, W A P Nicholson, J D Pediani and H Y Elder.

In: EMAG-MICRO 89 (Inst. Phys. Conf. Ser No 98 ; Chapter 16) Volume 2, P 691.

(d) Absorption Correction for Quantitative Microanalysis of Semi-thin Specimens (in preparation).

(e) Quantitative Methods for Microanalysis (in preparation).

No part of this thesis has been previously submitted in any application for a degree.

To

My parents, whose sacrifices made this Degree possible .

CONTENTS

ACKNOWLEDGEMENT

I would like to thank all who helped in the work presented in this thesis. In particular, I am especially grateful to my supervisor Dr W A P Nicholson for many hours of discussion, encouragement and sound advice during my research period. In fact, this research work would not have been possible without his continuous guidance and cooperation. He is also responsible for settling me down not only in this department but also in Glasgow and it is due to him that I always felt at home. I am also thankful to him for recording experimental spectra for me.

I am also grateful to Professors R P Ferrier and J N Chapman for their encouragement and for the provision of research facilities within the Solid State Physics Group in the Physics and Astronomy Department.

My thanks must also go to Dr H Y Elder who made available the biological samples and facilities of the Electron Microscopy Unit, The Institute of Physiology, Glasgow University. I am also thankful to him for reading chapter 5 and appendix 5 of this thesis. I am also indebted to Mr J D Pediani for recording biological spectra for me and providing some useful information about the preparation of biological samples. I am also thankful to Dr. A J McGibbon and Mr. J L Martin for providing me with the semiconductor specimens used in the work of absorption corrections.

I am thankful to my wife, Shabana Naz, who provided me great encouragement during the days of depression. I am also thankful to my sons, Sohail and Sajid, who provided good and

quiet atmosphere whenever I worked at home. I also wish to thank my parents and other members of the family and all my friends in Glasgow, especially Mr and Mrs Noor, for their continuous encouragement.

I am also indebted to Mrs M Waterson for her help with some of the diagrams presented in this thesis.

Finally, I would like to thank the Federal Ministry of Education, Government of Pakistan, for their financial help for this research work, without which this study would have been impossible. I am also thankful to Link Analytical for providing computer equipment.

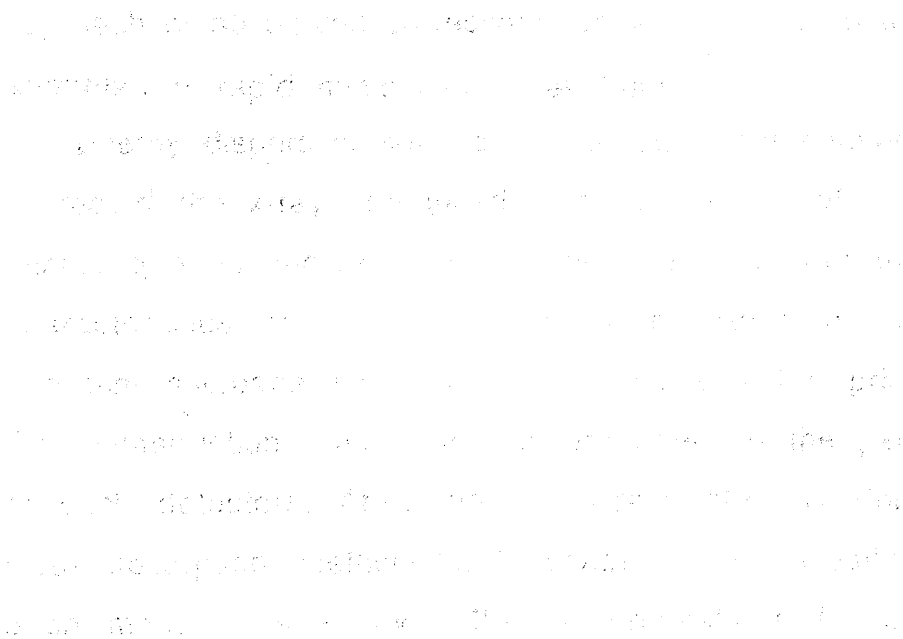

SUMMARY

Accurate knowledge of the production of characteristic and Bremsstrahlung x-rays when an monoenergetic beam of electrons is incident on a thin sample is of considerable importance in the technique of x-ray microanalysis. Chapter 2 describes the production of both the characteristic as well as Bremsstrahlung x-rays.

The main motivation of this work has been to investigate the possibility of developing a quantitative technique, based on the intensity of the characteristic x-rays, which can correct the x-ray lines for specimen self absorption effects. Chapter 3 first reviews the methods and problems of performing for the absorption of low energy lines and then describes an alternative approach of absorption corrections which is simple to use and is suitable for rapid minicomputer evaluation.

Energy dispersive solid state detectors are commonly used to record the x-rays produced when the beam of an electron microscope is incident on a specimen. Understanding the characteristics of such detectors is important in quantitative thin film microanalysis. Chapter 4 describes the principles of their construction and some factors affecting the performance of such detectors. Absorption of x-rays strongly depends on mass absorption coefficients. In chapter 4 an investigation has been made to see how different formulations for calculating mass absorption coefficients affect the predicted detector parameters for a number of detectors.

Extraction of the characteristic x-ray counts from a

measured spectrum of a thin specimen involves separation of these x-rays from the Bremsstrahlung signal. Extraction of the characteristic x-ray counts from a measured spectrum of a biological specimen is more complicated as peaks of interest are not well-separated and most of the peaks lie in the low energy region where the rate of background variation is more rapid. Chapter 5 first reviews some conventional methods of separating the characteristic x-rays from the measured spectrum and then describes an alternative approach which was developed to separate the characteristic signal from the Bremsstrahlung signal in organic samples. This background modelling method was used with a particular biological sample and results are compared with a conventional method of separating x-rays from the background signal.

Chapters 6 and 7 contain details of the experimental work carried out to investigate the technique of self absorption corrections discussed in chapter 3. Compound semiconductor multilayer systems were selected for this investigation as these are wedge shaped so that the thickness and hence the amount of self absorption varies significantly within the specimen and thus are ideal for such an investigation.

Finally chapter 8 reviews the preceding chapters, and suggests improvement and areas for further study.

TABLE OF FREQUENTLY USED SYMBOLS

Z = Atomic number.

Z' = Mean atomic number

C_i = Atomic fraction of element i

W = Atomic weight

W' = Mean atomic weight

w'_i = Weight fraction of element i

ρ = Density

μ/ρ = Mass absorption coefficient

ε_L = Detector efficiency at low photon energies

ε_H = Detector efficiency at high photon energies

ε = Detector efficiency (at low or high photon energies)

λ = Wave length of photons

P_K = Photon energy (in eV or keV)

T_0 = Incident electron energy (in eV or keV)

I_{0i} = Generated intensity of element i

N_i = Measured intensity of element i

t = Specimen thickness

L = X-ray absorption path length

ψ = A constant used to convert x-ray counts into absorption path length

M = Mass path length ($=\rho.L$)

G = A geometric factor which relates t and L

k_{AB} = k-factor for element A and B (used in the ratio method of quantitation).

K = $k_{AB}(C_B/C_A)$, a constant (used in absorption corrections).

S_K = Partition function

ω = Fluorescence yield

CHAPTER 1

Introduction

1.1 Energy Dispersive X-ray Microanalysis

Figure 1.1 shows a number of the most important interactions which occur when an electron beam is incident on a solid specimen. Electrons may be backscattered from the front face of the specimen with little or no energy loss or may interact with surface atoms of the specimen which may produce low energy secondary electrons. Some electrons may be absorbed by the specimen with a transfer of energy as heat, or visible light may be emitted as cathodo-luminescence. The electrons which are transmitted through the specimen may scatter through a range of angles or continue in the same direction as that of the incident electron beam. These scattered electrons may lose some energy (inelastically scattered electrons) or suffer no energy loss (elastically scattered electrons). The energy lost by inelastically scattered electrons is transmitted to the specimen and may produce Auger electrons or x-rays.

Each of the above mentioned events can provide information about the specimen, but in this thesis we will restrict ourselves to the generation of x-rays by high energy electrons when they interact with a specimen in an electron microscope. These generated x-rays carry information about the atoms

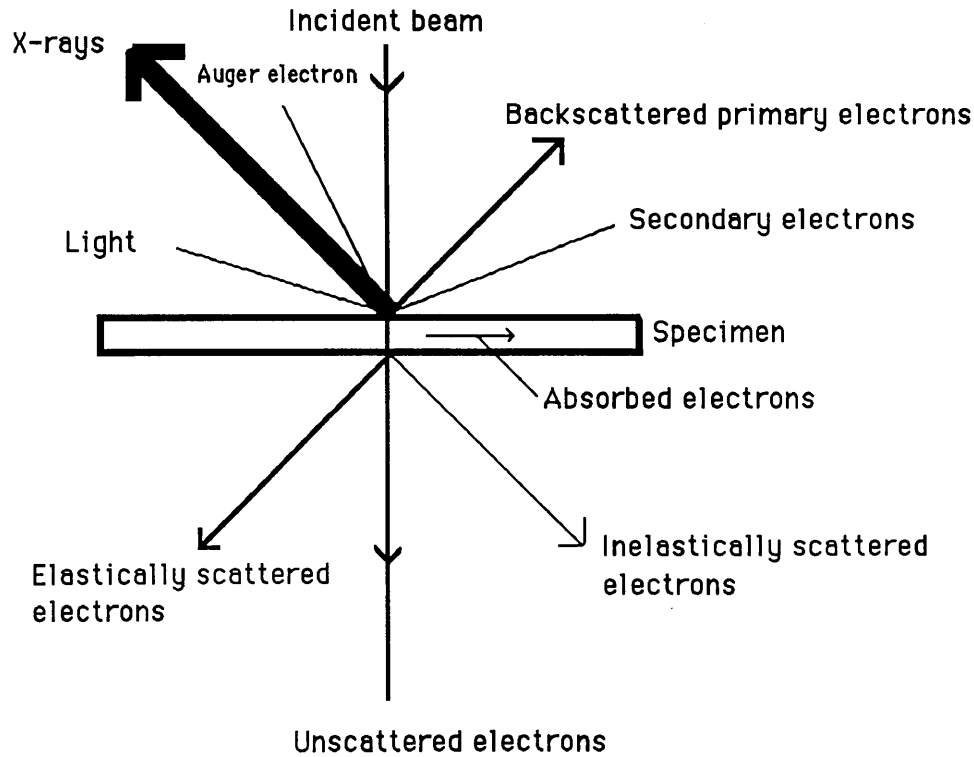

Figure 1.1

The various effects of electron-specimen interaction.

within the specimen in the region being irradiated; specifically they may be characteristic of the atoms in the specimen.

Therefore, the x-rays can be used to identify and quantify the elements present in the sample. A number of techniques have been used in the electron microscope for the extraction of quantitative information on the chemical composition of materials (See Venables 1981, Goodhew and Castle 1983 for reviews). One widely used technique is energy dispersive x-ray spectrometry (EDX), which became a standard analysis technique following the introduction of the energy dispersive solid state detectors in the early 1970's. During the last few years there has been an expanding amount of work utilizing the EDX technique with thin films in the electron microscopes. The major reasons for the interest in this technique are the small volume of material which can be analysed and the relative simplicity by which quantitative analyses can be obtained.

1.2 Absorption Correction in Thin Specimen Microanalysis

Among the problems remaining in EDX is that of the correction of x-rays for self absorption. X-ray self absorption is a phenomenon in which some low energy x-rays are absorbed within the specimen before reaching the detector and hence the x-ray signal measured is reduced in intensity.

Zaluzec (1979) has shown that the amount of x-ray self absorption can be calculated provided the density, geometry and the thickness of the sample are known. However, these parameters are often difficult to determine accurately in

practice. More difficulties are encountered in the specimens where the specimen thickness varies significantly within the sample. McGibbon (1989) used Zaluzec's approach of absorption corrections to correct the Al signal which was absorbed in an AlGaAs/GaAs multilayer system. The thickness of the specimen used was measured by convergent-beam diffraction patterns (Kelly et al, 1975). However, since such samples are wedge shaped, the requirement of uniform thickness severely restricts the area of the specimen for which the calculations would be valid.

Craven and Adam (1985) and Garratt-Reed et al (1987) have shown that with a knowledge of the Bremsstrahlung cross-sections and the detector efficiency, it is possible to derive the x-ray self absorption for a particular analysis. The method uses a comparison of the theoretical background with the experimental one in the energy range where the self absorption is significant (i.e, photon energy of 2 keV or less). This region must be free from characteristic lines and the background not be distorted by such effects as incomplete charge collection. It also requires that the atomic ratios of the main elements present in the sample be known approximately to calculate the theoretical background spectrum shape for the sample under investigation. The applicability of this approach has been further examined for biological samples in this thesis. These samples are ideal for the approach because peaks of interest are usually small so that incomplete charge collection is generally not a problem. Also biological spectra are usually free from peaks in the spectral region below 1 keV (Na K peak).

Adam (1986) has applied the method of specimen self

absorption corrections using the Bremsstrahlung to superalloys. Absorption corrections were performed for low energy peaks (Al K and Ni L) present in the sample. For these samples there were problems in the choice of low energy region used to match the theoretical and experimental backgrounds, because large peaks of Al K and Ni L and some small peaks of Co L and Cr L were all present in the low energy region. Incomplete charge collection distortion from high energy peaks (e.g Ni K_{α}) and high incomplete charge collection tailing from the close proximity of the Al K peak also caused problems by raising the experimental background above the Bremsstrahlung background. The fits obtained were poor in the low energy end and consequently large uncertainties were obtained in the absorption corrections of the low energy lines. Adam concluded that because of the above problems it is very difficult to perform the self absorption corrections for Al K and Ni L lines for this type of sample.

The main intention of this work was to develop a technique which can deal with the x-ray self absorption problem for a variety of samples. A technique has been investigated for x-ray self absorption corrections, which can correct the characteristic lines of a particular sample for this effect without knowing the density or geometry of the sample. The method depends only on the data contained in the x-ray spectra collected from analysis points at a range of specimen thicknesses and a knowledge of the general form of the absorption function. Compound semiconductor multilayer structures were selected for this work because of their current commercial importance and also these are ideal samples for investigating any technique for x-ray self absorption

corrections as the thickness varies significantly within the sample in the wedge shaped samples used.

1.3 Separation of Characteristic and Bremsstrahlung Signals in a Measured Spectrum

An inherent feature of all electron-excited x-ray spectra is the presence of a background upon which the characteristic peaks of interest are superimposed. To extract the x-ray intensity of the characteristic lines of interest, it is necessary to subtract this background, which may be due to both specimen generated Bremsstrahlung and extraneous sources, from a measured x-ray spectrum. Some conventional methods of background subtraction do not give sufficiently accurate results in biological analysis where the peaks of interest are not well-separated and most of the peaks lie in the region where the background is appreciably curved (see section 5.2). An alternative approach of background subtraction for such samples is investigated which involves a knowledge of Bremsstrahlung production. This method of theoretical background modelling is particularly suitable for biological samples as well as other samples with an organic matrix.

1.4 Structure of the Thesis

The ultrastructural information in the electron microscope image can be associated with the chemical analysis of very small regions of the specimen. For this the understanding of the generation of x-rays is important; this is described in detail in chapter 2. Chapter 3 contains a description of x-ray self

absorption, the difficulties involved in corrections and some existing techniques of the self absorption corrections of x-rays. An alternative technique is also developed for absorption corrections and this is the main interest of this thesis.

The purpose of the x-ray detector is to receive as many as possible of the x-rays that emerge from the volume of the specimen being irradiated. These x-rays are separated in energy so that the elements in the volume irradiated may be identified. The detector must be placed as close as possible to the specimen to ensure a high collecting power (high solid angle of detection). Because of its simple construction a solid state [Si(Li)] detector may be placed close to the source of the x-rays in the electron microscope without interfering with optics of the electron lenses.

However, a feature of the energy dispersive detector is that some low energy photons are absorbed by the protective windows of the detector before entering in the active region of the detector. Also some high energy photons pass right through the active region without being detected. This decrease in the number of photons detected at high and low photon energies produces a reduced detector efficiency in these spectral regions. The operation and some artifacts of such a detector as well as the measurement of low and high detector efficiencies are described in detail in chapter 4.

In chapter 5 of the thesis the theoretical background modelling for thin biological sections is examined in detail. Application of this method to the cells of the adrenal zona glomerulosa is described. The results are compared with a conventional procedure based on estimating background windows

on either side of the peaks (Nicholson and Dempster, 1980). It is also shown that the background modelling method allows calculations of the amount of x-ray self absorption for such organic specimens.

In chapter 6, the applicability of the approach of x-ray self absorption correction, discussed in chapter 3, is examined for two model samples. First a simple wedge shaped sample of stochiometric GaP, which was prepared by ion beam thinning, was chosen. After analysis of this simple sample, a more complex sample of crystalline InP with a few percent of Ga and As included was chosen to examine how small variations in specimen composition would affect the analytical technique.

In chapter 7, the absorption correction technique is applied to a AlGaAs/GaAs multilayer system. This system was grown in such a way that the atomic concentration of Al (x) in each layer is different. By treating the data from all the layers as if it were from one sample, the effect of large compositional variations on the analytical technique could be examined.

The final chapter discusses the conclusions of the results presented in the preceding chapters. Some future considerations are also discussed. In appendix 1 the analytical representation of MBH equation is given. The description and listings of all computer programmes used for this work are given in appendix 2. Appendix 3 discusses the geometry of absorption path length. The detail of the preparation of the biological sample used in chapter 5 is given in appendix 4. In appendix 5 the derivation of the Hall equation used for the quantitation of biological samples is presented.

CHAPTER 2

X-Ray Production

2.1 Introduction

Thin film x-ray microanalysis involves the separation of characteristic counts from the background in the spectrum. The characteristic signals are then used to deduce elemental concentrations. It is helpful to have an understanding of both the production of characteristic x-rays and the background x-rays; this is discussed in this chapter. Section 2.2 discusses the origin and nature of the characteristic x-ray spectrum. In the next four sub-sections the characteristic emission energies, intensity of characteristic lines, absorption edges, and the partition function are described. To predict the intensity of the characteristic x-rays generated when an electron beam is incident on a thin foil also requires a knowledge of the fluorescence yield (section 2.2.5) and the ionisation cross section (section 2.2.6).

In section 2.3 of this chapter the generation of the Bremsstrahlung spectrum is described. The use of a theoretical model to describe the Bremsstrahlung gives the facility of indicating any artifacts in the spectrum which cause the background shape to differ from the predicted form. Theoretical models of Bremsstrahlung production are discussed in the next two sub-sections. A discussion of x-ray absorption is given in

section 2.4. In the last section of this chapter x-ray fluorescence is briefly described.

2.2 The Characteristic Line Spectrum

The x-ray line spectrum consists of series of discrete energies characteristic of the emitting element. The x-ray line spectrum of an element arises when electrons are expelled from the inner orbits (K,L,M) of its atoms and electrons from orbits farther out fall into the vacancies. Each such transition constitutes an energy loss, which may appear as an x-ray photon. The study of x-ray spectra of the elements strongly suggests that the electrons in the atom are arranged in different groups or shells round the nucleus, all the electrons having the same total quantum number, n, forming one shell. Thus the innermost shell, known as the K-shell, consists of electrons whose total quantum number n = 1 ; the next shell, called the L-shell, contains electrons for which n = 2 and so on.

Figure 2.1 shows the electron transitions that give rise to the principal x-ray spectral lines, along with values of total quantum number " n ", an orbital quantum number " l ", which may take any integral value between zero and (n - 1) inclusively and the total angular quantum number " j ", which refers to the resultant angular momentum of the electron due to both orbital and spin motions, is the numerical value of the vector sum of l and spin quantum number " s " . The x-ray energy states are designated by the capital letters K, L, M, N , specifying the shell to which they refer. Each of these states is not only characterised by a total quantum number n, but also all the

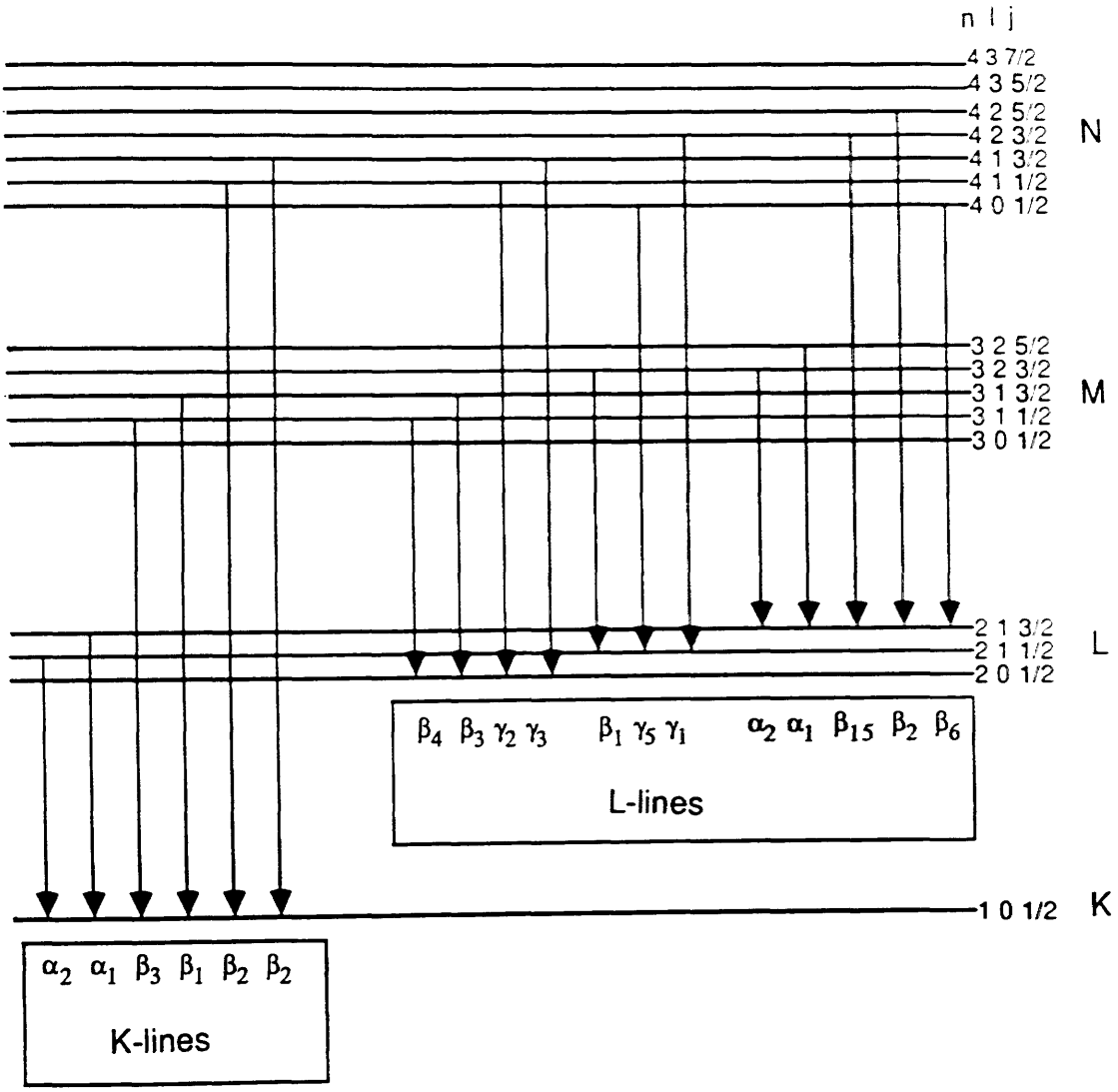

Figure 2.1

Some principal x-ray spectral lines with values of n, l and j quantum numbers.

states, except the K, are further split into subgroups; the L into two (n=2, l=0,1), M into three (n=3, l=0,1,2), N into four (n=4, l=0,1,2,3), etc. The first subgroup of the L state (n=2, l=0) gives rise to one term while the second subgroup (n=2, l=1) two terms corresponding to the two different values of j, viz; 3/2 and 1/2. Thus, the L state having three possible terms is a triplet. In a similar way the three subgroups of the M state give rise to quintet (5 possible terms) and 4 subgroups of N state give rise to septet (seven possible terms). However, the term multiplicity does not go on increasing. Pauli's principle putting a limit, the next O state is a quintet and P state a triplet. There are in all 24 different terms which are quite sufficient to represent completely the x-ray spectra of all the elements. They are denoted by the Roman numerals attached to the capital letters representing the states, e.g,

K, L_1 L_{11} L_{111}, M_1 M_{11} M_{111} M_{1v} M_v, etc.

They indicate all the possible combinations of l and j for a given value of n.

An electron transition cannot occur from any higher to any lower orbital. There are some rules, which must be satisfied. These rules are called selection rules and can be summarized as,

(1) The first selection rule is $\Delta n \geq 1$, i.e only those lines are observed for which the value of n changes by a number greater than or equal to one. For example, a L_{111} to L_1 transition would violate this rule. However, in electron-electron (radiationless) Coster-Kronig transitions a L_{111} to L_1 transition occurs.

(2) Most of the observed spectral lines are due to transitions between states, in which a single electron jumps from one orbit to another, and in such a case the selection rule is $\Delta l = \pm 1$ i.e

only those lines are observed for which the value of l changes by ±1. For example, a M_{1v} to L_1 transition would violate this rule.
(3) Spectral lines arise only when transition take place between states for which $\Delta j = \pm 1$ or zero. For example, a M_v to $L_{1\,1}$ transition would violate this rule.

The transition can only occur subject to the condition that these selection rules are obeyed (other "non-allowed" transitions do occur, but their probability is much lower), so that the number of possible transitions between two states is thereby considerably reduced and in consequence the number of fine structure components of the x-ray lines will be limited.

2.2.1 Characteristic Emission Energies

The photon energy of an x-ray spectral line is the difference in energy between the initial and final energy levels involved in the intra-atomic electron transition from which that line originates. The photon energy is the property used in energy dispersive x-ray spectrometry. The slight discrepancies in the tabulated energies in the literature may arise from small errors in rounding off the table values. Photon energy and wave length can be related as follows,

$$P_K = h \nu / \lambda e$$

Substituting the values for Planck's constant h, the velocity of light c, and the electronic charge e, the above equation may be written as,

$$\lambda = 123.96 / P_K \qquad (2.1)$$

Where P_K is in keV and λ is in nanometer (nm).

For a specified element, the photon energy of the lines increases from series M to L to K because the electron must "fall " farther to fill vacancies successively closer to the nucleus. The L_1, L_{11}, and L_{111} sub-series orbits lie closer in energy than do the various orbits from which electron transitions into them originate.

For a specified spectral line, the photon energy increases as the atomic number increases because positive nuclear charge, binding of orbital electrons, and inter-orbital energy differences all increase with increasing atomic number. Table 2.1 illustrates this with x-ray data selected for elements occurring in analyses described later in this thesis. All the values shown in this table are taken directly from the literature (Bearden, 1967).

2.2.2 Intensity of the Characteristic Line

The characteristic x-ray lines vary in intensity and it is those with the greatest intensity that are most easily detected and are thus most useful for characterising the atom. In practice the most intense lines are $K_{\alpha 1}$ lines, followed by $L_{\alpha 1}$ lines, followed by M_{α} lines. The relative intensities of three strong lines of the L-series and that of K_{α} and K_{β} are given as,

$L_{\alpha 1} : L_{\beta 1} : L_{\alpha 2} \approx 9 : 5 : 1$ and

$K_{\alpha} : K_{\beta} \approx 10 : 1$

The energy of the bombarding electrons affect the relative intensities of lines associated with different sub-shells. Hirst and Alexander (1935) have reported that the $L_{\alpha 2} : L_{\alpha 1}$ and $L_{\beta 2} : L_{\alpha 1}$ intensity ratios are independent of bombarding energy, but the

Atomic Number	Characteristic Emission Energy (keV)					Absorption Edge Energies (keV)			
	K-Lines		L-Lines			K-Lines	L-Lines		
	K_α	K_β	L_α	L_β	L_γ	K_{ab}	L_{1ab}	L_{11ab}	L_{111ab}
Be 4	.11	-	-	-	-	.12	-	-	-
C 6	.28	-	-	-	-	.29	-	-	-
O 8	.52	-	-	-	-	.53	-	-	-
Al 13	1.49	1.55	-	-	-	1.56	.09	.07	.072
Si 14	1.74	1.83	-	-	-	1.84	.12	.10	.098
P 15	2.02	2.13	-	-	-	2.14	.15	.13	.128
Ti 22	4.51	4.93	.45	.46	-	4.96	.53	.46	.45
Ga 31	9.25	10.26	1.10	1.12	-	10.37	1.30	1.13	1.12
As 33	10.54	11.73	1.28	1.32	-	11.86	1.53	1.36	1.32
In 49	24.21	27.27	3.29	3.49	3.92	27.93	4.24	3.94	3.73
Au 79	68.79	77.97	9.71	11.44	13.38	80.71	14.35	13.73	11.92

Table 2.1

A tabulation of atomic number, x-ray spectral line energy, and absorption edge energy for selected elements.

$L_{\beta 1}$: $L_{\alpha 1}$ ratio rises with bombarding energy due to variation of the relative probability of Coster-Kronig transitions. Victor (1961) and Goldberg (1961) have discussed such effects in greater detail.

Some intensity rules have been devised to supplement the selection rules and to predict the intensity of the lines that occur. These rules were originally postulated on an empirical basis in the study of optical and x-ray spectra. Later, a full theoretical derivation was given on a wave mechanical basis. These rules are as follows:

(a) Those transitions are strong, giving rise to intense lines, in which I and j change in the same sense : the transitions are the weaker the more the change in direction of I and j is different, i.e,

$\Delta I = -1$, $\Delta j = -1$: most intense line

$\Delta I = -1$, $\Delta j = 0$: less intense.

(b) A transition in the decreasing sense (I ---> I-1) is stronger than a transition in the increasing sense (I ---> I+1), i.e,

$\Delta I = +1$, $\Delta j = +1$: weaker

$\Delta I = +1$, $\Delta j = 0$: weakest (Also from (a)).

(c) The case of an oppositely directed transition does not occur, because it would lead to a final state, in which (j-I) would be two units greater than in the initial state, which is forbidden, i.e,

$\Delta I = -1$, $\Delta j = +1$: no line

$\Delta I = +1$, $\Delta j = -1$: no line.

2.2.3 Absorption Edge or Excitation Potential Energy

The excitation potential (absorption edge) energy is the minimum bombarding electron energy that can expel an electron from a specified orbital in an atom of a specified element. Thus it is the minimum energy which can excite a specified x-ray line series for that element. Each element has as many excitation potentials as it has subgroups : one K, three L, five M, etc.

For each element, the excitation potential increases for levels progressively closer to the nucleus, i.e

$V_K > V_{L_1} > V_{L_{11}} > V_{L_{111}} > V_{M_1} > \ldots\ldots\ldots\ldots$

This is because the closer an electron lies to the nucleus, the more firmly it is bound and thus the greater is the energy required to expel it. For each level, say V_K, the excitation potential increases with increasing atomic number, because with increasing atomic number the positive charge in the atomic nucleus increases and thus all electrons are more firmly bound. Table 2.1 illustrates this effect.

An electron that has enough energy to expel a K electron obviously can also expel L or M electrons. However, an electron having just enough energy to expel, say L_{11} electron, can also expel L_{111}, M and N electrons, but not L_1 and K electrons. The column 2 and 3 of table 2.1, provides the relationship of absorption edges and spectral lines. The spectral lines must have less energy than their absorption edges. The absorption edge energy is equivalent to the energy required to create an inner-orbital vacancy by lifting an electron from that level clear out of the atom to the free state. On the other hand the energy of a spectral line is equivalent to the energy emitted on

filling that vacancy; this is affected by an electron transition, not from outside the atom, but from an outer orbital. The farther out the orbital from which the electron falls, the more nearly equivalent is the transition to expulsion, and closer the line lies to the absorption edge. Typical absorption edges seen in mass absorption coefficients are illustrated in figures 2.4 (a) and (b).

2.2.4 The Partition Function

The partition function is the ratio of the sub-line to the total x-ray yield. This function is denoted by " S_K " and for a K-line, it can be written as,

$$S_K = K_\alpha / K_\alpha + K_\beta \qquad (2.2)$$

Scofield (1974) has calculated the values for the ratio of $K\alpha$ intensity to the total K-shell yield. These have been calculated using a relativistic Hartree-Fock solution for the atom in both initial and final states. The matrix element calculation includes exchange effects. Berenyi et al (1978) and Heinrich et al (1979) have experimentally verified these values with agreement within 0.5% for a range of elements. Keith et al (1978) have verified experimentally for nickel (Ni) with agreement within 0.7%.

Khan and Karimi (1980) have reviewed experimental data for the partition function and have presented a set of the most probable values for a range of elements with atomic number between 12 and 94. Crozier (1986) has reported that these values closely agree with the theoretical calculations presented by Scofield (1974). The values of the partition function given by

Scofield (1974) will be used as required in the present work.

2.2.5 X-ray Fluorescence Yield

When a vacancy in an inner shell is filled, the atom changes to a state of lower energy. This energy may be released in two ways; an x-ray photon may be emitted (radiative transition) or alternatively an Auger electron (Burhop 1952) may be released from the outer shell (radiationless transition). The probability of the photon being emitted is called the x-ray fluorescence yield, denoted by ω. We can also say that the x-ray fluorescence yield is the probability that the filling of a vacancy in a specified shell will result in emission of a characteristic x-ray photon. The fluorescence yield increases with atomic number and has larger values for K-line emission than L-line emission. The lower values of fluorescence yield is a significant factor which limits the detection of low atomic number elements.

Langenberg and Van Eck (1979) have reviewed the values for the fluorescence yield of the K-shell, with a quoted error of $< 2.5\%$ for the lowest atomic numbers. They obtained the mean values of the fluorescence yield for 62 elements, selected from several experimental values measured by various authors, and corrected these for systematic differences. The resulting accuracy of these values is about four times better than the accuracy of previously recommended empirical values (see, Bambynek et al 1972, Freund 1975). Gray (1981) has listed the values for fluorescence yield for elements Z=11 to Z=50, some of which has been taken directly from the table of Langenberg and Van Eck (1979), and some are obtained by interpolation from a diagram of the fluorescence yield as a function of atomic

number, with quoted error of ≤ 5.0%. The values of x-ray fluorescence yield given by Gray (1981) will be used as required in the present work.

2.2.6 Ionisation Cross Sections

Quantitation of EDX spectra requires the ability to predict the probability that a particular type of inelastic scattering involving the K or L shell of an atom will occur. Atomic theories are often used to describe the interaction, the probability of which is usually expressed as a cross-section. The ionisation cross-section is proportional to the probability per unit path length of an electron of a given energy causing ionisation of a particular shell of an atom in the specimen. Berenyi and Hock (1978) have shown that the characteristic radiation is emitted isotropically.

The most frequently used method for calculating ionisation cross section follows the Bethe model (Bethe 1930). The K-shell ionisation cross section σ_{iK} is given by,

$$\sigma_{iK} = \frac{2\,N'\,\pi\,e^4\,b_K\,\ln\left(c_K\,\frac{T_0}{I_K}\right)}{T_0\,I_K} \qquad (2.3)$$

where N' is the electron occupancy of the K-shell (=2), I_K is the K-shell ionisation energy, T_0 is the energy of incident electron, and b_K and c_K are two parameters which may be calculated empirically. The relativistic form of equation 2.3 has been given by Inokuti (1971).

Powell (1976) has listed the values of the parameters b_K and c_K derived both theoretically and from the best fits to experimental data. Powell was able to fit all the data to a common curve. However, the range of the values of the parameters b_K and c_K as recommended by him is limited to low atomic number elements. Schreiber and Wims (1981), Zaluzec (1984a), and Rez (1984) have investigated the variation of these parameters with atomic number Z. Gray et al (1983) deduced the values of these parameters by fitting to experimental data over a range of low and medium atomic number elements ($13 < Z < 47$), and with electron energies ranging from 40 keV to 100 keV. They predicted the values ($b_K = 0.69$ and $c_K = 0.89$) for these parameters over that range of conditions with a mean error of 7% and a maximum error of 14%. More recently Paterson et al (1989) have examined the data from three different electron microscopes over a wider range of electron energies and elements in an attempt to discover whether a universal pair of parameters could fitted satisfactorily to their experimental data. They used the Bethe formula as a fitting function and obtained relativistic as well non-relativistic sets of parameters. However, they have reported that from the goodness of fit there is no advantage of using the relativistic form of the equation. They obtained the non-relativistic values of these parameters as $b_K = 0.62$ and $c_K = 0.90$ with a mean error of 7% and a maximum error of 19%.

The ionisation cross section calculations of Rez (1984) has suggested that the Bethe model could also be applied to L-shell. Paterson et al (1989) have investigated the application of the Bethe model to the L-shell over a wider range of elements, and have determined the L-shell ionisation cross sections by using

the experimental measured K_α/L shell production ratios and comparing them with the predictions of the Bethe model. Their comparison of experimentally measured K_α/L shell production cross section ratios with the prediction of the Bethe model generally supported the theoretical calculations of Rez (1984), which suggest that the Bethe functional form should provide a good description of L-shell cross sections. The uncertainties in the published values of L-shell fluorescence yields precluded them from a more detailed investigation in this direction. However, their work indicated that the Bethe model may be used to calculate L-shell cross sections. The L-shell ionisation cross section, σ_{Lj}, can be given as,

$$\sigma_{Lj} = \frac{2\, N'_j\, \pi\, e^4\, b_L \ln\left(c_L \frac{T_0}{I_{Lj}}\right)}{T_0\, I_{Lj}} \qquad (2.4)$$

Where b_L and c_L are the L-shell parameters and N'_j is the electron occupancy of the L_j sub-shell (i.e $N'_1 = N'_2 = 2$ and $N'_3 = 4$). Paterson et al (1989) data did not allow b_L and c_L to be clearly determined. However, they suggest that b_L should be the same as b_K and the value of c_L may be taken 0.5 for a non-relativistic model. With these values of b_L and c_L their investigation gave the best agreement with experimental data. The Paterson et al (1989) non-relativistic values of Bethe parameters for both K and L-shells will be used as required in the present work.

2.3 The Bremsstrahlung X-ray Spectrum

The Bremsstrahlung spectrum is emitted as a result of the deflection of the incident electrons by the strong fields surrounding the nuclei of the atoms of the target element, in contrast to the characteristic x-ray spectrum which arises due to changes in the internal energy of the atoms of the target element ionised by the incident electron. If an electron passes close to the positive nucleus, its path about the nucleus will be a hyperbola. The acceleration of such an electron, according to the classical theory, will cause the emission of a pulse of radiation at some angle to the incident beam.

This interaction produces a negligible change in the energy of the nucleus, but the electron may lose anything from zero to its total energy. The radiation produced (x-ray) has the energy lost by the electron in the transition, which is why radiation energy is not characteristic of the atom. The spectrum intensity varies continuously with photon energy which is why the Bremsstrahlung spectrum is frequently referred to as the continuum. The spectrum of such radiation decreases in intensity with increasing photon energy.

As mentioned in chapter one, the Bremsstrahlung radiation forms the major part of the x-ray background, upon which the characteristic lines are superimposed.

2.3.1 Theoretical Models of Bremsstrahlung Production

The classical theory of Kramers (1923) for the intensity distribution of the Bremsstrahlung, which was derived as a

function of the emitted photon energy, does not fit well to the experimental data.

Various quantum mechanical treatments for Bremsstrahlung production have been developed in which relativistic and angular corrections have been incorporated. The basis for all such treatments is to consider a radiative transition of an electron between two states in the continuum with the emission of a Bremsstrahlung photon. By the use of time dependent perturbation theory, an expression for the differential cross section of Bremsstrahlung radiation can be derived (Bethe et al 1957). The exact solution of this expression is not possible due to lack of an accurate expression for the electronic wavefunction in a screened nuclear coulomb field. Tseng and Pratt (1971) have derived the best theoretical values. However, the time taken to compute cross sections by the Tseng and Pratt method is substantial and they have not provided data for all cross-sections relevant to all experimental conditions.

Chapman et al (1983) have investigated the accuracy of two models for Bremsstrahlung production, Sommerfeld (1931) and Bethe-Heitler (1934). They compared the predictions from these models with the results of exact numerical calculations of Pratt et al (1977) and with their experimental measurements, and came to the conclusion that modified Bethe-Heitler (MBH) theory (Koch and Motz 1959), most accurately represents the Bremsstrahlung production over the range of 3 keV to less than 20 keV photon energy. Gray et al (1983) found that MBH predicts the Bremsstrahlung intensity from thin samples with an average error of 10%. Adam (1986) compared the predictions of MBH with the exact numerical calculations of Kissel et al (1983) and found good agreement for photon energies down to zero. Garett-

Reed et al (1987) showed that MBH theory may be used for Bremsstrahlung production satisfactorily at low energies down to 500 eV. The work presented in this thesis will use the MBH theory as the basis of all Bremsstrahlung calculations.

2.3.2 The Modified Bethe-Heitler (MBH) Theory

The aim of this section is to present some ideas behind the development of this theory, and not its full derivation. One who is interested can find it in full in the literature (Koch and Motz,1959).

The classical expression for the Bremsstrahlung differential cross section may be evaluated without neglecting retardation and relativistic effects if the true wave functions are replaced by the appropriate Born approximation wave functions (Bethe 1930 and Heitler 1954). The resulting expression for the Bremsstrahlung differential cross section then can be integrated over all directions of the emerging electron. This result was first reported by Bethe and Heitler and hence called Bethe-Heitler (BH) theory.

The Born approximation becomes less reliable with the increase of atomic number, decrease of initial electron energy and when the photon energy approaches the high frequency limit. The breakdown of the theory is also due to the use of oversimplified wave functions. Elwert (1939) compared the non-relativistic Born approximation with the Sommerfeld (1931) calculations and derived a coulomb correction factor in the hope of overcoming the problem. The use of such a correction factor can not be justified in the high energy region of interest. Tseng and Pratt (1971) have given a discussion of the more

general coulomb correction factors.

In the relativistic Born approximation cross section, another correction factor must be considered to take account of the screening effect of the atomic electrons. A pure coulomb field was assumed in the derivation of the expression of the integrated Bremsstrahlung cross section (see Gluckstern and Hull, 1953 and Koch and Motz, 1959). For a general potential the integration over the emergent electron directions is not possible without recourse to numerical techniques. However, Gluckstern and Hull (1953) have shown that an approximate analytical expression for the cross section may be obtained if an approximate form of the potential is assumed. This potential can be given by,

$$V(r) = Z\, e^2 / r \exp(-r/a) \qquad (2.5)$$

where V(r) is the potential that determines the interaction for the Bremsstrahlung process, r is the radius vector and
$a = 108\, Z^{-1/3}\, (\hbar/mc)$.
Some justifications for the use of an simplified screened potential of the form of equation 2.5 are given by Tseng and Pratt (1971), who have shown numerically that the results are insensitive to the choice of screening model except at very low photon energies.

Therefore, an expression for the cross section, known as a modified Bethe-Heitler cross section, may be derived which takes account of both coulomb correction and screening. Such an expression is denoted by MBH and for the succeeding chapters of this thesis this notation will be used quite frequently. The

analytical representation of MBH theory has been given in appendix 1. The equation for MBH can be used to calculate the continuum x-ray production for pure elements and these can then be weighted numerically by the atomic fractions to calculate the continuum x-ray production for multi-element samples (see programme MBHBACK in appendix 2) .

2.4 Absorption Coefficients

When monochromatic photons are directed on a material, the incident photon intensity may be attenuated by absorption or scattering, as shown in figure 2.2. The top, middle and bottom rays in this figure show absorption, transmission and scattering respectively. The emergent beam consists of the transmitted rays and has an intensity which is given by Beer's law,

$$I_t = I_0 \exp(-\mu t) \qquad (2.6)$$

Where μ is known as linear absorption coefficient of the absorber of thickness t and has the unit reciprocal centimeter (cm^{-1}). The negative sign indicates that intensity always decreases on passing through matter.

When the photons pass through the absorber the linear absorption coefficients are the result of three phenomena, each having its own linear absorption coefficients and can be written as,

$$\mu = \tau' + \sigma' + \pi' \qquad (2.7)$$

where τ', σ' and π' represent losses by, respectively, true or

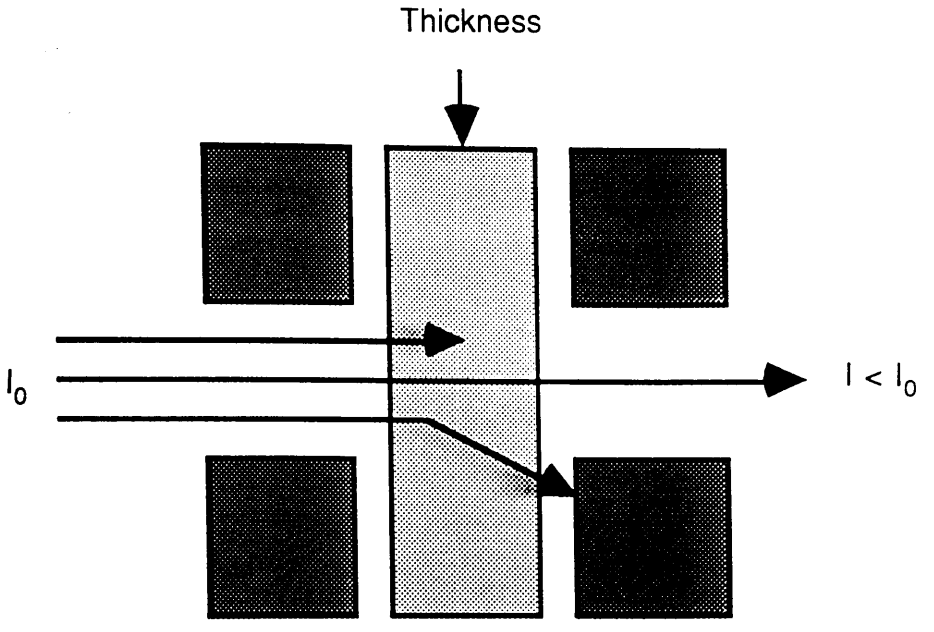

Figure 2.2

The interaction of x-rays with matter, showing absorption, transmission and scattering.

photoelectric absorption, scattering and pair production. In photoelectric absorption, x-rays are truly absorbed, expending all their energy in expelling and imparting kinetic energy to orbital electrons in absorber atoms. This is the process that may result in the emission of x-ray spectral lines. On the other hand in scattering, x-ray photons are not really absorbed, but only deflected from their paths in the absorber. In the case of Compton (inelastic) scattering, the incident x-ray interacts with the atomic electrons and loses a fraction of its energy, as a result of which it suffers a change in direction. In the case of Rayleigh (elastic) scattering the incident x-rays are scattered off very tightly bound electrons where no ionisation or energy loss takes place.

In pair production, x-ray photons interact with atomic nuclei, expending all their energy in creating electron-positron pairs. Since this phenomena occurs only at photon energies greater than or equal to 1.02 MeV, this can be neglected for this work.

In the spectral region of x-ray spectrometry (i.e 0-40 keV), photo electric absorption predominates over scattering except for the lightest elements at high photon energy. Figure 2.3 shows the relative sizes of τ' and σ' for Al. It can be seen from this figure that the dominant energy loss process is due to the photo electric effect. Therefore, for the work presented in this thesis $\mu \approx \tau'$.

The linear absorption coefficients are usually used in optics where the interaction cross section is affected by the density of the interacting medium. However, for x-ray spectrometry it is convenient to define the form in which absorption

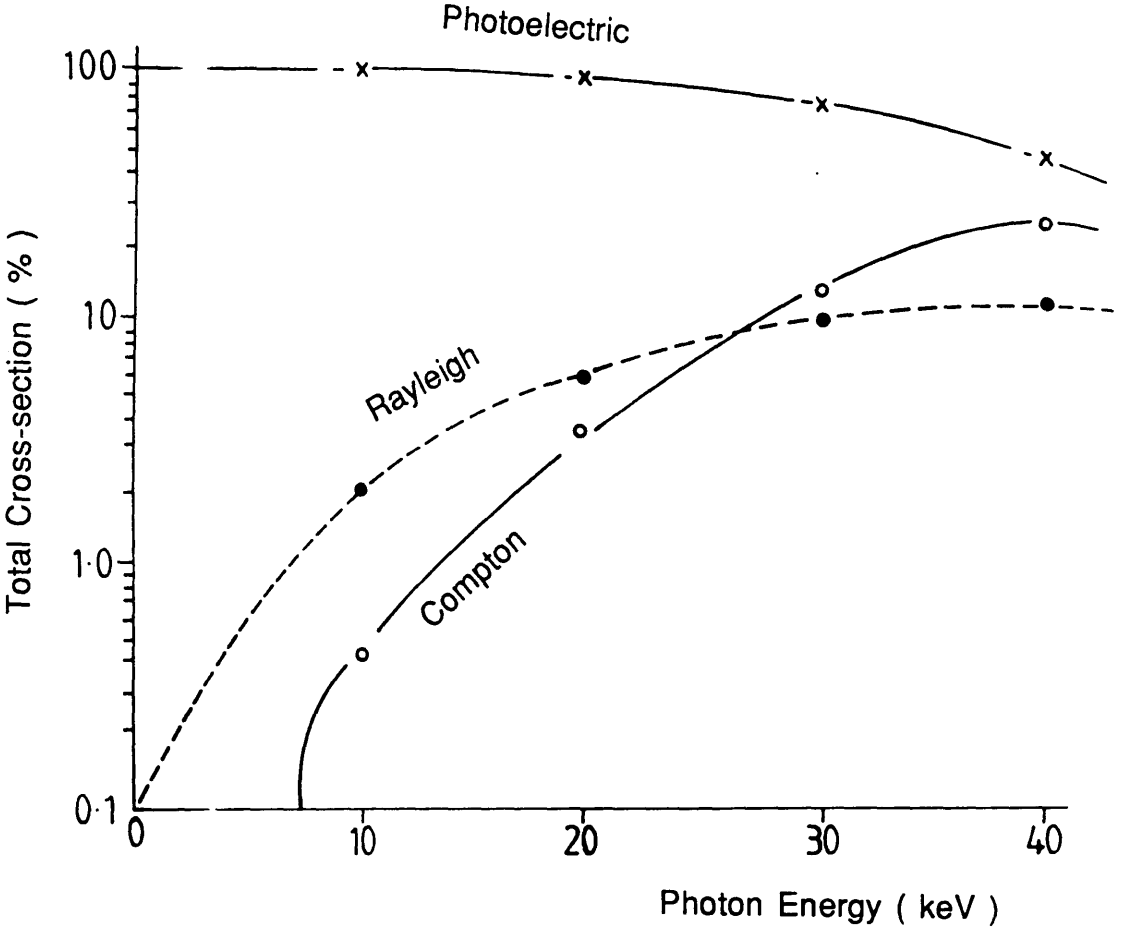

Figure 2.3

Relative order of magnitude of absorption and scattering processes for Al for x-ray in the energy range 0 to 40 keV.

coefficients are commonly quoted. This commonly used form is known as the mass absorption coefficient (μ/ρ) and has the unit centimeter square per gram (standard SI units are not used since even the most modern tabulations use $cm^2\ gm^{-1}$ for measurement of μ/ρ). The mass absorption coefficients are introduced because in x-ray spectrometry the interaction cross section is relatively unaffected by the density of the interacting medium and by the state of chemical combination. The mass absorption coefficient is an atomic property of elements. It is a measure of their x-ray opacity or stopping power, and is a function of photon energy and atomic weight. The value of mass absorption coefficients increases with decreasing photon energy (see figure 2.4) and increasing atomic weight. Linear absorption coefficients can be related to the mass absorption coefficients by the equation, $\mu = (\mu/\rho)\ \rho$, where ρ is the density of the absorber.

Mass absorption coefficient values for a compound, alloy, solution, or mixture may be calculated from the concentrations and coefficients of their constituents. The mass absorption coefficients for pure elements in the sample can be calculated and these then can be weighted numerically by the weight fractions to calculate mass absorption coefficients of a multi-element sample (see programme MABSCO in appendix 2). If the total mass absorption coefficient of a sample is denoted by $(\mu/\rho)_t$, then

$$(\mu / \rho)_t = \sum_{j=1}^{n} (\mu / \rho)_j \ w'_j \qquad (2.8)$$

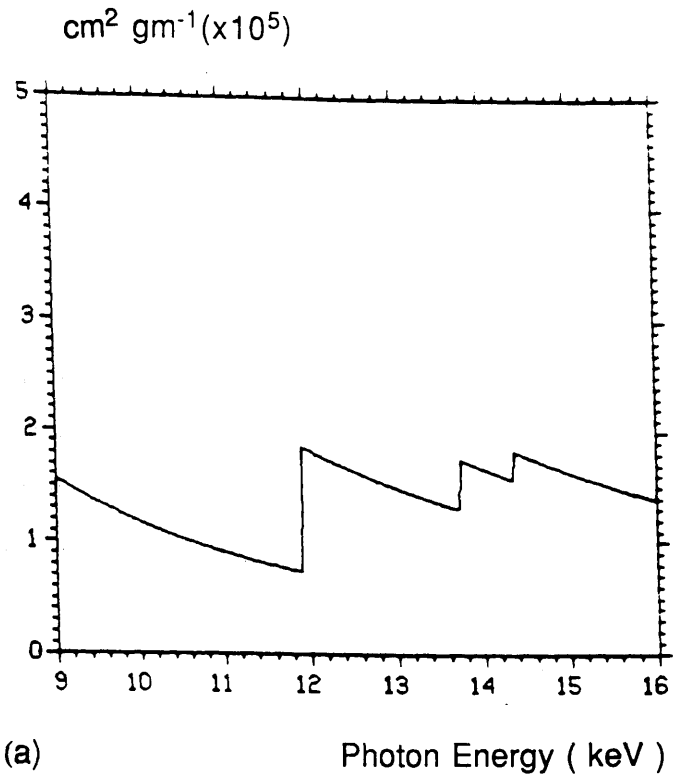

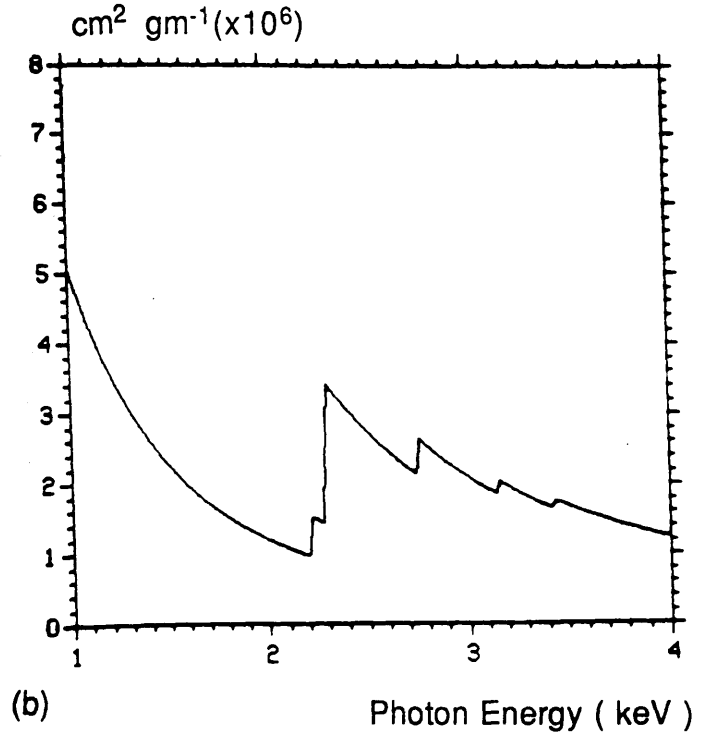

Figure 2.4

(a) L-subseries absorption edges for Gold.
(b) M-subseries absorption edges for Gold.

where n is number of elements in the sample, $(\mu/\rho)_j$ is mass absorption coefficient of element j for the measured photon energy and w'_j is equivalent weight fraction.

There are many formulations for mass absorption coefficients (Heinrich 1966, Bracewell and Veigele 1970, Henke et al 1974, Springer and Nolan 1976, Thinh and Leroux 1979, and Henrich 1987), two of which will be discussed here.

Springer and Nolan (1976) showed that the mass absorption coefficients exhibited a simple variation for each element as a function of wave length between any two successive absorption edges. This relationship is given by the equation,

$$\mu/\rho = c' \ \lambda^{n'} \tag{2.9}$$

where c′ and n′ are parameters that depend on the atomic number of the absorber, and λ is wave length.

Thinh and Leroux (1979) used the same type of relation as above but with somewhat different values of the parameters c′ and n′. More modern formulations use photon energy in place of photon wave length. Heinrich (1987) gave a new formulation with improved accuracy at low energies. This is,

$$\mu / \rho = c' \ (12397 / P_K)^{n'} \ \frac{Z^4}{W\left[1 - \exp\left\{\frac{(b' - P_K)}{a'}\right\}\right]} \tag{2.10}$$

Where c′, n′, a′, and b′ are parameters which vary with the atomic number of the absorber and the region between absorption edges. W is the atomic weight of an element and photon energy is in eV.

Heinrich (1987) presented a database which showed high consistency. Except for energies below 800 eV and regions close to or between absorption edges, an accuracy of 5% or better can be expected from this model. He claims that the uncertainties of the set are mainly caused by lack of measurements or discrepancies among them, as well as by differences in the theoretical approaches where experimental data were not found. A large uncertainty exists close to absorption edges, perhaps due to the assumption of sharp discontinuties at the edge position which is often significantly inaccurate. He suggests that the use of x-ray lines close to edge or between sublevels, particularly between M_{1V} to M_V should therefore be avoided and the use for energies below 200 eV should be discouraged.

Figure 2.5 shows mass absorption coefficients for Be, calculated from both the Heinrich (1987) and Springer et al (1976) models, between 200 eV to 2 keV photon energy range. Both have the same general shape but the values predicted by former model are larger than that of latter model.

If x-ray line intensities and equation 2.6 are to be used as a basis of thickness measurement, it is clear that the result will depend on the mass absorption coefficients chosen. For example for a given I_t/I_0 for transmission through Be, the Springer coefficients would predict a greater thickness than that of Heinrich. A comparison of these formulations will be discussed further in chapter 4.

2.5 X-ray Fluorescence

When the incident electron beam strikes a specimen it may

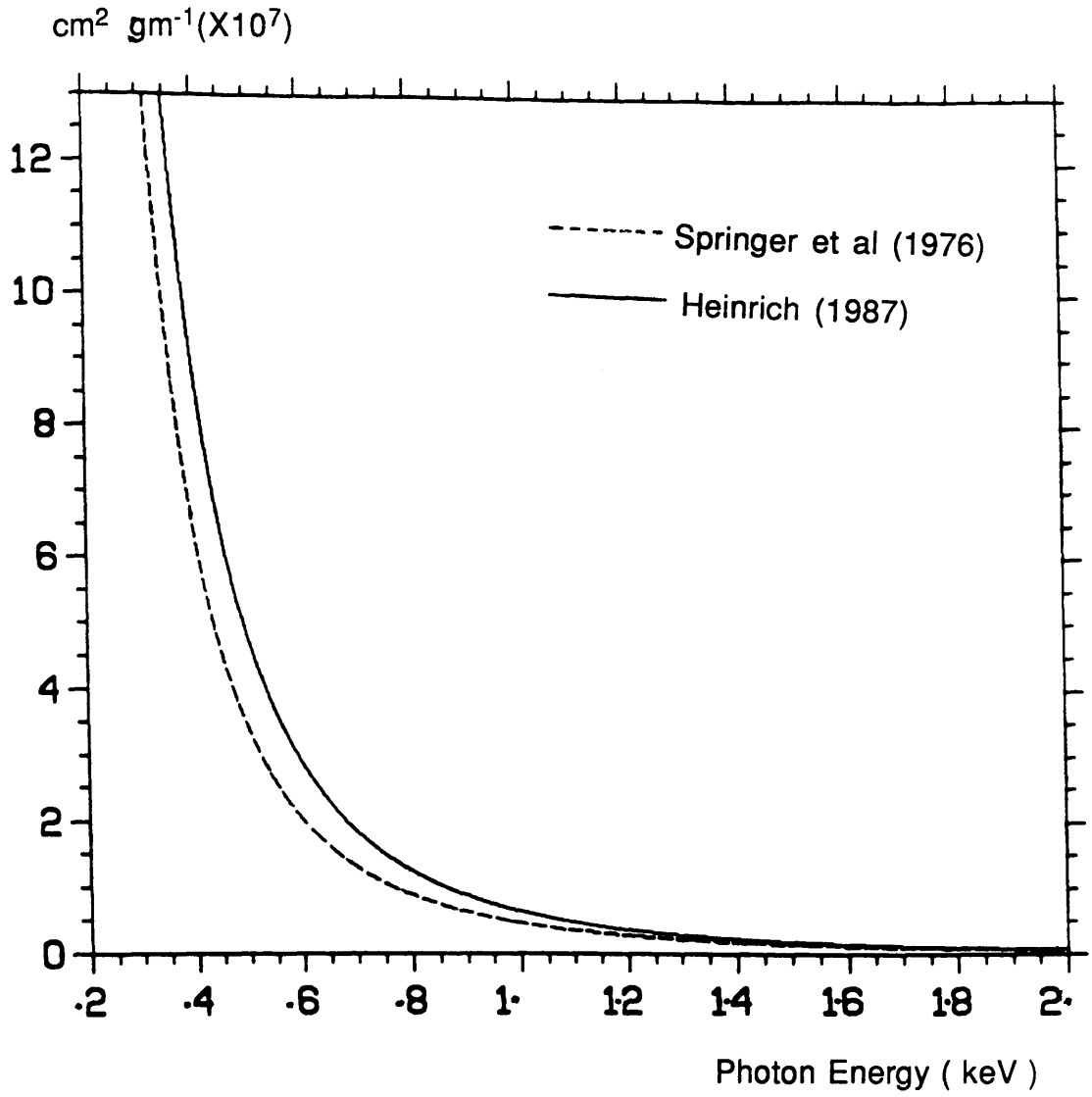

Figure 2.5

Comparison of mass absorption coefficients of Be for two models at low photon energies.

cause atoms to be ionised and some x-rays of high energy may be produced. These high energy x-rays may be absorbed by other atoms and thus cause a secondary ionisation, giving rise to further x-ray emissions. This effect is called x-ray fluorescence. The additional fluoresced x-rays can enhance the primary x-ray signal produced by the electron beam, which can cause some errors in quantitation. However, for thin films this effect is so small that it can be generally ignored.

CHAPTER 3

Quantitation of Spectra from Semi-thin Specimens

3.1 Introduction

Once the characteristic lines are separated from the background in a x-ray spectrum measured on a thin sample, the elemental composition may be obtained provided the assumption is made that the specimen self absorption and fluorescence effects may be neglected. This assumption is the basis of the thin film criterion. The concentration ratio of two elements is related to the corresponding characteristic count ratio by a constant factor. This is described in section 3.2 of this chapter in detail.

The first practical problem one is likely to encounter in thin film analysis is, at what point is the thin film approximation no longer valid? This is discussed in section 3.3. In section 3.4 the different ways of measuring specimen thickness found in the literature are reviewed. In section 3.5 specimen self absorption corrections in microanalysis are reviewed. The aim of this thesis is to investigate a new method of self absorption correction. The theory on which this method is based is described in detail in section 3.6.

3.2 Quantitation by the Ratio Technique

A number of techniques have been developed for quantitative thin film analysis. In this chapter we are only concerned with the ratio method (Cliff and Lorimer 1975).

In thin film x-ray microanalysis few electrons are backscattered and the length of the trajectory of the electron can also be assumed to be essentially the same as the thickness of the thin film t. We have seen in chapter two that the ionisation cross-section of an atom strongly depends on the incident electron energy. Zaluzec (1984b) has shown that when the electron path length lies in 500-600 nm range in a low to medium atomic number material, the change in K-shell ionisation cross-section relative to values at 100 keV electron energy is < 1%. Thus for the work presented here which is within these limits, we can safely ignore the effects of electron energy loss and can consider the ionisation cross-section to be a constant. Therefore, an expression for the intensity of photons generated in a thin specimen may be written as (Lorimer, 1983),

$$I_{oA} = N_0 D' \rho C_A \omega_A \sigma_{iA} S_A t / W_A \qquad (3.1)$$

where N_0 is a constant, W_A and C_A are the atomic weight and atomic concentration of element A respectively and D' is the electron dose.

From equation 3.1 it appears that the composition of the analysed region can be obtained simply by measuring the emitted intensity, I_{oA}, and by calculating the other terms. Unfortunately this can not be done easily since many of the

terms can not be evaluated accurately. In addition, the specimen thickness may vary from one point in the specimen to another. However, if the intensities of elements A and B are measured simultaneously and their ratio is taken, then the thickness t, constant N_0, electron dose term D′ and density cancel out and we are left with an equation of the form,

$$\frac{C_A}{C_B} = \frac{(\sigma_i \ \omega \ S/ \ W)_B}{(\sigma_i \ \omega \ S/ \ W)_A} \ \frac{I_{oA}}{I_{oB}} \qquad (3.2)$$

In equation 3.2 the terms within the parentheses are constant for a given operating voltage. Therefore, it is convenient to introduce,

$f(A) = (\sigma_i \ \omega \ S/W)_A$ and $f(B) = (\sigma_i \ \omega \ S/W)_B$

Where f(A) and f(B) are called the generation functions of element A and B respectively. Therefore equation 3.2 may be written as,

$$\frac{C_A}{C_B} = \frac{f(B) \ I_{oA}}{f(A) \ I_{oB}} \qquad (3.3)$$

The x-ray intensities which one measures, N_A, N_B, can differ from the generated intensities, because the intrinsic efficiency of the solid state Si(Li) detector varies with energy (see chapter 4). The measured intensity also differs because of the limited solid angle of the x-ray detector, typically 0.1 sr. The characteristic photons are generated isotropically. However,

since the solid angle is the same for elements A and B, the term for solid angle which occurs in the expression relating detected to generated intensities cancels in the ratio. Therefore, the measured x-ray intensity is proportional to the product of generated x-ray intensity and the detector efficiency. Therefore, equation 3.3 can thus be written as,

$$\frac{C_A}{C_B} = \frac{f(B)\ \varepsilon_B\ N_A}{f(A)\ \varepsilon_A\ N_B}$$

We can define a useful quantity k_{AB} defined by,

$$\frac{C_A}{C_B} = k_{AB}\ \frac{N_A}{N_B} \qquad (3.4)$$

So that,

$$k_{AB} = \frac{f(B)\ \varepsilon_B}{f(A)\ \varepsilon_A} \qquad (3.5)$$

k_{AB}, is the ratio of the product of the generation functions and the detector efficiencies of A and B is usually called the k-factor.

The use of measured intensity ratios for quantitation was first suggested by Cliff and Lorimer in 1975, who used standards to determine the k-factors (k_{AB}). Thus the technique is frequently known as the Cliff-Lorimer method. The above development assumes that the sample being analysed is thin, i.e; the generated x-ray intensity is equal to the x-ray intensity

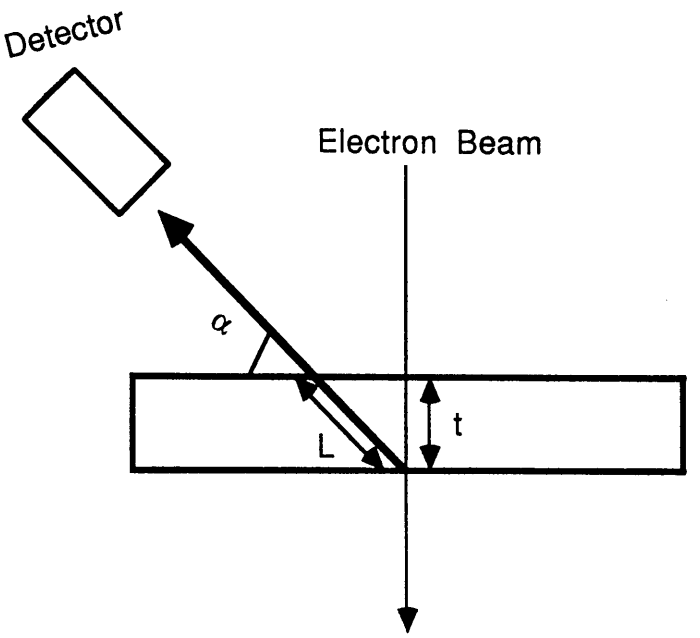

Figure 3.1

Relationship between specimen thickness and x-ray absorption path length. (L= t G, where G is a geometrical factor = cosec α)

leaving the sample, which means that x-ray absorption and fluorescence may be neglected. This assumption is known as the thin film criterion. The validity of these assumptions are examined below. An experimental technique to ensure the suitability of the standards used to determine the k-factors is also discussed (see section 3.5.1). An alternative approach to the measurement of standards
(Paterson et al 1989) is to use theoretical cross-sections to calculate k-factors, the approach which will be frequently used in this thesis.

3.3 Limitations of the Thin Film Criterion

Tixier and Philibert (1969) and Goldstein et al (1977) have defined the thin film criterion, which describes when absorption corrections may be neglected. Since absorption is a function of path length and mass absorption coefficients, these factors are used to define the thin film criterion.

Tixier and Philibert (1969) set forth the criterion that when the relation of the type, $(\mu/\rho)_A L < 0.1$ cm^3 g^{-1} is satisfied for all analysed x-ray lines, then absorption effects can be safely ignored. The $(\mu/\rho)_A$ in the above relation is the mass absorption coefficient of element A in the sample and L is the maximum absorption path length (see figure 3.1). Goldstein et al (1977) give an alternative criterion for any two elements A and B considered for quantitation, the relation $[(\mu/\rho)_B - (\mu/\rho)_A]L/2 < .1$ cm^3 g^{-1} must be satisfied, for absorption effects to be safely ignored. If we compare these criteria, it is seen that the second emphasizes that the difference in mass absorption coefficients is the more important parameter. It may be noted that for a

more conservative criterion, the limit of < 0.1 cm^3 g^{-1} in both relations may be decreased. For example, a limit of < .01 cm^3 g^{-1} ensures that no more than 0.5 to 1% of emitted x-rays are absorbed in the thin film. The criterion of Goldstein et al limits the differential absorption to < 5%. If the thin film criterion is not satisfied, the intensities will have to be corrected for absorption before equation 3.4 can be used accurately.

3.4 Measurement of Film Thickness

The major limitations to performing absorption corrections are the difficulty of determining accurately the thickness of specimens and the geometry of x-ray collection (absorption path length) at the analysis point. So far in our discussion the variations of the specimen thickness have been ignored. However, many thin foils are known not to be of uniform thickness; they may also be buckled. Large variations in path length are also frequently encountered in thinned wedge shaped specimens.

Several ways to measure the specimen thickness t have been reported in the literature. The contamination spot-separation method first used by Lorimer et al (1976) is useful if the contamination can be generated. During analysis, a contamination spot is produced on the top and bottom of the foil. The foil is then tilted through an appropriate angle and a micrograph is taken of the two contamination spots observed. The distance between the two spots is measured, and by simple geometry from a knowledge of the magnification, the thickness t can be calculated. In general, contamination is better avoided

since the carbon contamination causes extra electron scattering which may reduce the spatial resolution of the analysis. However, the method may only give an approximate measure of thickness. Love et al (1977) have pointed out that this method determines the total foil thickness including any surface film. Stenton et al (1981) reported errors with this method from 50 % to 200 %, with the contamination spot invariably overestimating the thickness, and thus causing an overcorrection for any absorption. Rae et al (1981) have reported the presence of relatively broad contamination deposits beneath the sharp cones and pointed out that the method overestimates the thickness.

Another frequently cited method which determines the foil thickness for crystalline materials is that of measuring the spacing of the fringes in convergent-beam diffraction patterns (Kelly et al.,1975). This method often requires a double-tilt holder to set up the correct diffraction conditions. The range of applicability of this method has been examined in detail by Allen (1981). He has reported that in practice, the required conditions are not always easy to obtain at precisely the region of interest. Moreover, it is not always possible to reproduce the exact diffraction conditions, particularly if Kikuchi lines are not visible because of specimen dimensions or local deformation. If the Kikuchi lines are not present, the specimen is probably thin enough to neglect the absorption effects.

Joy and Maher (1975) have suggested a method for measuring film thickness using a calibration curve developed from the relative transmission of the primary electron beam through the specimen. The reported accuracy of this method ±10% for thicknesses greater than 200 nm is reasonable.

However, in many practical cases, the thickness less than 200 nm can also give rise to significant amount of absorption.

Joy (1979) has presented a method to measure the specimen thickness which involves electron energy loss spectroscopy (EELS). According to this method the ratio of the probabilities of exciting the zero loss to that of the first plasmon is a function of the ratio of the specimen thickness and the plasmon mean free path. The probabilities ratio is just the measurement of the relative heights of the zero loss and first plasmon peaks in an EEL spectrum. Therefore, if the plasmon mean free path is known, the thickness can be calculated. Although the plasmon mean free path is usually between 50 and 150 nm at 100 kV (Joy, 1979), the data for the plasmon mean free path is not available for many materials. If specimen thickness is greater than the plasmon mean free path then the specimen is probably too thick for microanalysis using the inner shell losses using EELS.

3.5 Corrections for Self Absorption in Microanalysis

This section describes in detail the new method of self absorption correction. The method depends only on the data contained in the x-ray spectra collected from different analysis points and a knowledge of the general form of the absorption function. The method measures the absorption path length. However, this needs to be related to thickness for comparison with other methods. The factor which relates them is a geometrical constant which is often difficult to determine

accurately.

The maximum x-ray absorption path length (L) and the specimen thickness (t) may be related through a general equation,

$$L = t\,G \qquad (3.6)$$

where G (= cosec α, see figure 3.1) is the geometrical factor. The calculation of G for geometries, which are used commonly for x-ray microanalysis are discussed in appendix 3.

If the specimen is assumed to be homogeneous and of total thickness t, then the number of counts of element A measured at the surface of the sample, dN_A, from a thin layer of thickness dt is given by:

$$dN_A = I_{oA} \exp\{(-\mu/\rho)_A\, \rho\, Gz\}\, dz \qquad (3.7)$$

Where I_{oA} is the intensity of element A generated by the electron beam in a thin layer dz at depth z, $(\mu/\rho)_A$ is the mass absorption coefficient of element A in the sample. Integrating equation 3.7 in the limits zero to total thickness t, we get (Zaluzec, 1979),

$$N_A = I_{oA} \frac{\left[1 - \exp\left\{-(\mu/\rho)_A\, \rho\, L\right\}\right]}{(\mu/\rho)_A\, \rho\, L} \qquad (3.8)$$

If the assumption is made that the absorption of one of the lines in the sample e.g N_X, is negligible then N_X is proportional to the specimen thickness (equation 3.1) and through G to L,

$$t = \phi\, N_X \quad ; \quad L = G\, \phi\, N_X \qquad (3.9)$$

where ¢ is a constant having dimensions of length. Therefore equation 3.8 can be written as,

$$N_A = I_{oA} \frac{\left[1 - \exp\{-(\mu / \rho)_A \rho G¢ N_X\}\right]}{(\mu / \rho)_A \rho G¢ N_X} \qquad (3.10)$$

The relationship between N_A and N_X given in equation 3.10 may be used to evaluate the absorption of N_A under certain conditions discussed later. However, it is convenient at this point to examine the recent work of Horita et al (1986, 1987). A discussion of their method is included here because of the close similarity of their analytical development to the one presented in this thesis (section 3.6).

3.5.1 Horita's Method for Measuring k-factors

Horita et al (1986) have discussed an extrapolation method for the determination of Cliff-Lorimer k-factors (k_{AB}). They used the exponential form of the absorption function to calculate limits below which absorption in the standards used for k_{AB} determination could be neglected. In a later paper (1987) they pointed out that if a suitable characteristic line were available, i.e. one for which absorption could be assumed negligible, then its intensity would be proportional to thickness, thus avoiding many thickness measurements. However, they recommended some thickness measurements be made to ensure this assumption was valid.

Using equation 3.10 for two elements A and B and taking ratios, Horita et al developed an equation under the assumption

that all x-rays are generated at the mid point of the foil thickness. Their equation with the notation used in this chapter can be written as,

$$\log (N_B/N_A) = \log (I_{oB}/I_{oA}) + (\Delta_{AB}\ \mathcal{C})\ N_X \qquad (3.11)$$

Where,

$\Delta_{AB} = 0.217\ [\ (-\mu/\rho)_A - (-\mu/\rho)_B]\ \rho\ G$

The characteristic x-ray intensities are measured and the logarithmic intensity ratio, $\log (N_B/N_A)$, is plotted as a function of N_X. The extrapolation to $N_X = 0$ gives the absorption free intensity ratio, (I_{oB}/I_{oA}), which is used for the compositional analysis.

With similar assumptions they also developed an equation for k_{AB} factor which can be shown as,

$$\log (k_{AB}) = \log (k_{AB})_0 + (\Delta_{AB}\ \mathcal{C})\ N_X \qquad (3.12)$$

where, $(k_{AB})_0$ is the absorption free k-factor. The logarithm of k_{AB} is plotted as a function of N_X. The extrapolation to $N_X = 0$ gives the absorption free k-factor $(k_{AB})_0$.

Although their method indicates that such graphical plotting could be used to give absorption path length at thicker points, they restricted their interest to obtaining absorption free k-factors and intensity ratios to deduce the sample composition. However, it must be noted that their method is not suitable for single point analysis. To make the extrapolation feasible, several data points are necessary for the method. The further requirements they stipulate for the method are that the beam current and x-ray acquisition time should be kept constant

in the series of x-ray intensity measurement and the sample must contain at least one element whose characteristic x-rays show negligible absorption.

3.6 Determination of Absorption Path Length

In this section a method is presented which allows the path length along which absorption takes place in the specimen to be determined for each analysis point. This may then be used to correct x-ray intensities generated at that point for self absorption. If assumptions are made about geometry, the specimen thickness may also be calculated.

For samples in which self absorption is not negligible, we can apply equation 3.10 to the measured counts ratio in equation 3.4 which becomes,

$$\frac{N_B}{N_A} = k_{AB} \frac{C_B}{C_A} \frac{(\mu / \rho)_A}{(\mu / \rho)_B} \frac{\left[1 - \exp\{-(\mu / \rho)_B \rho G\text{¢} N_X\}\right]}{\left[1 - \exp\{-(\mu / \rho)_A \rho G\text{¢} N_X\}\right]} \quad (3.13)$$

There are difficulties involved with determining the geometric factor G and the density (ρ) of thin specimens. Thus it is often convenient to introduce another quantity, mass path length (M), defined by,

$$M = \rho L = \rho G \text{¢} N_X \quad (3.14)$$

Defining the constant, $\Psi = \rho G \text{¢}$ (having dimensions of gm cm^{-2}), equation 3.14 becomes

$$M = \Psi N_X \qquad (3.15)$$

Making this substitution into equation 3.13, and with the assumption that absorption of one line, say A, is negligible, it becomes,

$$\frac{N_B}{N_A} = k_{AB} \frac{C_B}{C_A} \frac{\left[1 - \exp\left\{ -(\mu / \rho)_B \Psi N_A \right\}\right]}{(\mu / \rho)_B \Psi N_A} \qquad (3.16)$$

In principle, equation 3.16 is true for any analysis point and may be evaluated provided the specimen thickness t and the constant of proportionality relating it to the counts may be determined.

If several spectra are recorded from regions of the specimen of various thicknesses including very thin regions, a plot may be made of the counts of one line against the other. Here it must be noted that the data must be normalized to electron dose. Usually the intensity of the lower energy line (line having self absorption) is plotted on the Y-axis (see figure 6.4). If the K lines from two elements A and B are used, then to progress further, the assumption must be made that their composition ratios is known to be constant. As in Horita's method, data must be taken from a number of points from within the sample. Some points should be from " thicker " regions so that they exhibit significant (around > 5%) absorption of the lower energy x-ray line. A line plotted through the data points should be straight for the thin regions but will deviate from the extrapolation of the straight line as absorption becomes significant. This procedure has the advantage that k_{AB} is then truly a constant. However, variations in specimen composition

may still effect the values of mass absorption coefficients. These approaches are investigated experimentally in chapters 6 and 7 to evaluate over what range of compositions the procedure might be useful.

If n is the number of data points recorded from the various thicknesses of a specimen, then equation 3.16 may be written as,

$$\frac{N_{iB}}{N_{iA}} = K_i \frac{\left[1-\exp\left\{-(\mu/\rho)_{iB}\ \Psi\ N_{iA}\right\}\right]}{(\mu/\rho)_{iB}\ \Psi\ N_{iA}} \qquad (3.17)$$

where i = 1,2,3, ...n and $K_i = k_{AB}\ C_B/C_A$. If the composition does not vary too much, equation 3.7 may be fitted by treating K_i and $(\mu/\rho)_{iB}$ as constants. Equation 3.17 may then be fitted through the data points to give the best value of the parameter Ψ, which relates the counts of N_A to specimen thickness. The slope of the graph near the origin will give the value of $k_{AB}(C_B/C_A)$. It can be seen that the above equation depends on the mass absorption coefficient of element B in the sample at each analysis point, which is the function of the specimen composition at that particular point. Obviously, the specimen composition is initially an unknown quantity, but the assumption is made that variations in composition do not affect the $(\mu/\rho)_{iB}$ significantly. In this case equation 3.17 may be further simplified to,

$$\frac{N_{iB}}{N_{iA}} = K \frac{\left[1-\exp\left\{-\eta\ N_{iA}\right\}\right]}{\eta\ N_{iA}} \qquad (3.18)$$

with $\eta = (\mu/\rho)_B\ \Psi$ (3.19)

and where η is a dimensionless constant. If absorption corrections are required for only one line, the constants K and η can be evaluated by a best fit of equation 3.18 through the data points.

Where composition variations are small but non-negligible, the assumption that K and $(\mu/\rho)_{iB}$ are constants may no longer be strictly valid. However, an iterative approach can be used to determine the best values of parameters K and Ψ in equation 3.17, by successive approximation to the values of $(\mu/\rho)_{iB}$ at each data point i.

As a first approximation, the composition of the specimen is determined using the Cliff-Lorimer method ignoring absorption effects and this is used to calculate initial mass absorption coefficients. These are then used in equation 3.17 to determine initial values of the mass path lengths from which initial absorption corrections can be made. A second approximation can then be made to the specimen composition to produce better values of mass absorption coefficients and hence the better value of mass path length. This procedure is repeated until a suitable convergences of the composition and mass path length are obtained. Once the mass path length at an analysis point is known, this may then be used to perform absorption corrections for the lines from other elements present in the sample.

If the composition variations are small enough to be neglected and the absorption corrections for more than one line are required, then the equation 3.18 may be used for each line required for analysis without the necessity of determining mass

absorption coefficients. If the characteristic counts for each line required for analysis are inserted into the programme MINIMISE (see appendix 2), a value for η for each line is obtained, from which the correction factors can be calculated.

CHAPTER 4

X-ray Detection and Modelling of X-ray Detector Efficiency

4.1 Introduction

This chapter starts with a section in which the operation of an energy dispersive detector is described. The deviations from the ideal detection process result in the loss of some information from the experimental spectrum of interest. In the subsequent sections some effects which give rise to such deviations are discussed. Sections 4.3, 4.4, 4.5 and 4.6 discuss peak broadening, peak distortion, Si escape peak and contamination respectively.

A most important parameter is the efficiency as a function of photon energy, since for an x-ray detector this determines both the shape of the measured Bremsstrahlung background and the sensitivity factors for standardless techniques such as the analysis of thin samples by the Cliff-Lorimer (1975) approach. The method by which detector efficiency can be measured is discussed in section 4.7.

A number of detectors (see table 4.1) were examined for different formulations of mass absorption coefficients to see how these affect predicted detector parameters for a particular detector (section 4.8). For this examination spectra

which were already available and had been recorded on a variety of x-ray detectors interfaced to different electron microscopes were used. A summary of the detectors and microscopes is given in table 4.1. The main aim here, was to attempt to decide which set of mass absorption coefficient was most suitable for future work. This is discussed in section 4.9.

4.2 Energy Dispersive X-ray Detector

Figure 4.1 shows a cross-sectional view of x-rays entering the detector. An energy dispersive x-ray detector consists of a Si crystal with Li ions diffused into it, and may have a surface area 30 mm^2 and a nominal thickness 3 mm. Two electrodes of gold are evaporated onto the crystal across which a bias of several hundreds volt can be applied. The Li diffusion usually takes place at a temperature of 100 C° and with an applied voltage of 500 volts (Link detector information manual). The detector crystal is kept under high vacuum and at liquid nitrogen temperature to minimize the electronic noise. This temperature also prevents the further diffusion of Li ions within the crystal under the action of applied field. At such a low temperature one can expect a Si(Li) semiconductor to behave like an insulator, since a shared valence electron is bound to its locality and there are no sources from which it can obtain the extra energy necessary to free itself from its bonds.

In conventional detectors the x-rays enter the detector through a Be window that maintains the detector vacuum against external atmospheric pressure and prevents light from reaching the detector. A major limitation of such a detector is that the Be window is the primary absorber of low energy x-

No.	Detector Type	Interfaced Electron Microscope
A	Link Be Window "Long Nose" detector	HB5 (Glasgow University)
B	Link Windowless (LZ 5) detector	HB5 (Glasgow University)
C	Kevex "Horizontal take-off" detector	JEOL 2000 FX (IBM Center)
D	Kevex Be Window detector	JEOL 100 C (Glasgow University)

Table 4.1

List of detectors used for the work of this thesis. All detectors used were of 30 mm^2 area. The crystal thickness of detector B was 5 mm, while the crystal of all other detectors shown was 3 mm thick.

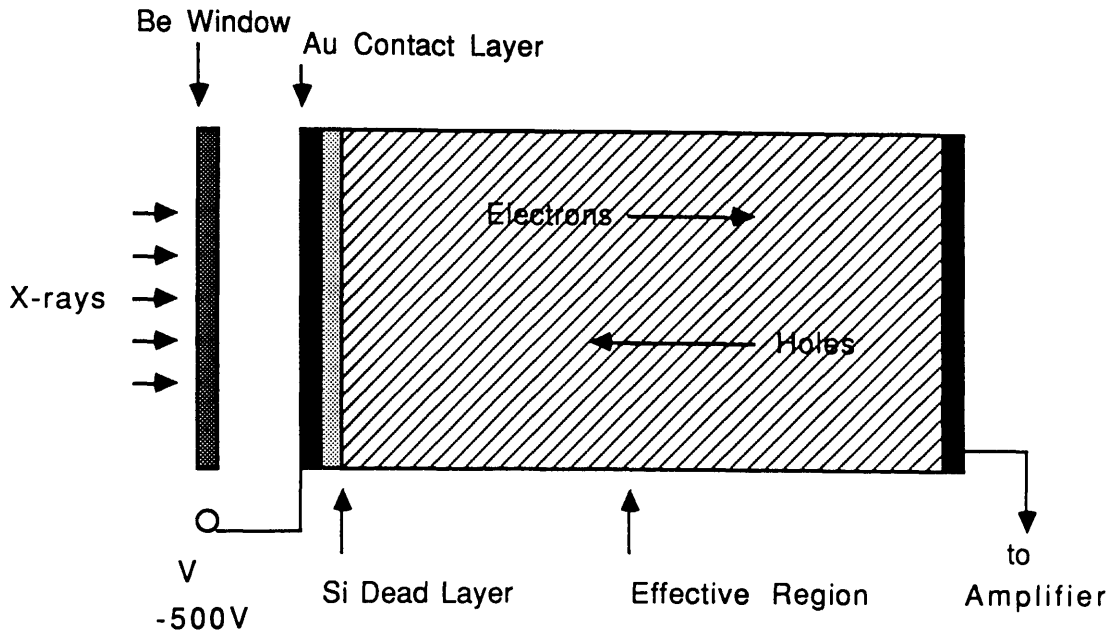

Figure 4.1

The schematic diagram of a typical Si(Li) windowed detector.

rays in the system. This fact accounts in part for the drop-off in intensity of the spectral background below 2 keV and the inability to detect characteristic peaks of energy below ≈ 1keV (e.g. Na K_α). However, new types of detector have been introduced. The Ultrathin Window (UTW) detector uses a gold coated formvar film, a few tens of nanometers thick, which protects the detector but absorbs fewer low energy x-rays than the conventional Be window and thus permits detection of x-rays from Boron (Z≈5) and higher atomic number materials. The drawback of these detectors is that the window may not be able to maintain the internal detector vacuum against atmospheric pressure. Therefore, there has to be an airlock system to protect the window when the microscope is vented to air. This air lock mechanism prevents the placement of the detector close to the specimen. Hence the collection efficiency is decreased.

A second new type of detector which has no window may also be used. As there is no protective window, it is preferable to use such detectors in an ultraclean environment; otherwise, contamination may form on the cold detector and degrade the performance. In many modern electron microscopes, the vacuum approaches suitable levels of cleanliness, and windowless detectors have been used successfully.

The x-rays which enter the detector are absorbed in the active region predominantly by the photoelectric effect. The absorption of photons ionizes the Si atom, which results in the formation of electron hole pairs. The number of these electron hole pairs, n, can be given as,

$$n = P_K/d \qquad (4.1)$$

where P_K is the x-ray energy and d is the mean energy required to create a pair and is of the order of 3.8 eV. These electron holes are collected by the applied bias to form a pulse. The total charge integrated at the electrodes is amplified by a field effect transistor (FET), which is built into the rear of the crystal. The output voltage pulse is then further amplified and passed to a multichannel analyser.

4.3 Peak Broadening

The ability to separate two adjacent peaks in the energy spectrum is determined by the energy resolution of the detector. It is generally measured as the full width of the peak at half the maximum intensity (FWHM), usually quoted at the Mn K_α energy position in the spectrum. This parameter is important when considering peak interferences, especially in quantitative analyses, where the removal of the interference is necessary for accurate determination of the composition.

The natural x-ray line width (typically a few eV) is degraded by the detection process in the Si (Li) detector typically to a value of 154 eV for Mn K_α energy. The degradation in width of the peak occurs due to two reasons namely,

1 There is a statistical distribution in the final number of electron-hole pairs created by capturing photons of a single energy.

2 An uncertainty is introduced by the thermal noise of the amplification process.

The distribution of number of charge carrier for a single photon energy is reasonably well described by a Gaussian distribution, shown schematically in figure 4.2. The FWHM (resolution) of the distribution can be calculated from the two sources of noise by quadrature addition according to the equation,

$$FWHM = \sqrt{(Noise)^2 + (D)^2}$$

where

$$D = 2.35 \sqrt{F d P_K}$$

F is the Fano factor, having a value somewhere in the region of 0.1 to 0.15. Thus,

$$FWHM = \sqrt{(Noise)^2 + \kappa P_K} \qquad (4.2)$$

where $\kappa = (2.35)^2 F d$ is a constant.

Since the noise term is a constant for a given detector, operated under a fixed set of conditions, equation 4.2 can be written in a form which is useful for comparing the width of a peak at an energy of interest to the width of a peak located at any other energy in a spectrum.

$$FWHM = \sqrt{\kappa \{ P_K - (P_K)_{ref} \} + (FWHM)_{ref}} \qquad (4.3)$$

All units are in eV. The immediate consequence of the peak broadening is a reduction in the height of the peak. The counts, Y_i,

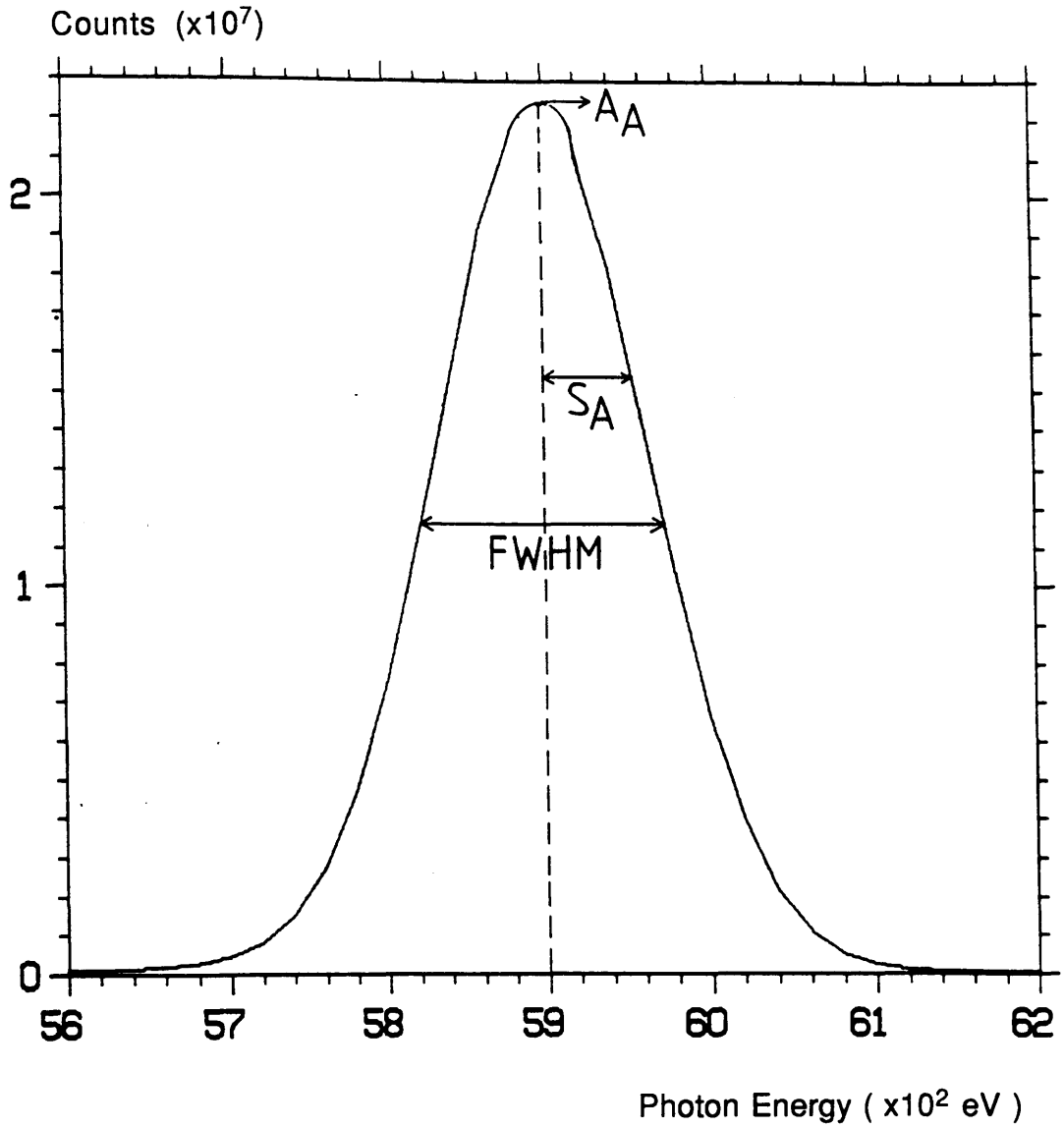

Figure 4.2

Theoretical Gaussian distribution which approximately describes an EDX peak.

of any given channel comprising a given Gaussian distribution can be calculated (Fiori and Newbury, 1978) from,

$$Y_i = A_A \exp\left[-0.5 \frac{\left\{(P_K)_A - (P_K)_i\right\}^2}{(Sig_A)^2}\right] \quad (4.4)$$

Where $(P_K)_i$ is the energy of the ith channel, $(P_K)_A$ is the centroid energy both in eV units of energy. A_A is the counts in the central channel (see figure 4.2). The parameter Sig_A specifies the standard deviation of the peak in the same units as energy and can be calculated from a simple relation,

$$Sig_A = FWHM/2.35 \quad (4.5)$$

Thus the net counts of an EDX peak can be calculated by integrating the theoretical Gaussian distribution (equation 4.4) over the whole peak width.

If a number of spectra for different elements for a particular detector are recorded, then fitting the experimental counts of each channel to equation 4.4 the best value of Sig_A for each line can be obtained and then using equation 4.5, the FWHM of each line can be calculated. Once the values of FWHM are known for different peaks of a particular detector, then a plot of FWHM vs P_K (see equation 4.2) can give the best value of constant κ (see figure 4.3). In the literature the value of κ is frequently cited as a constant 2.5. However, the data of detector A is best described by 2.67, which corresponds to a value of F 0.128. The resolution of a particular detector may vary with

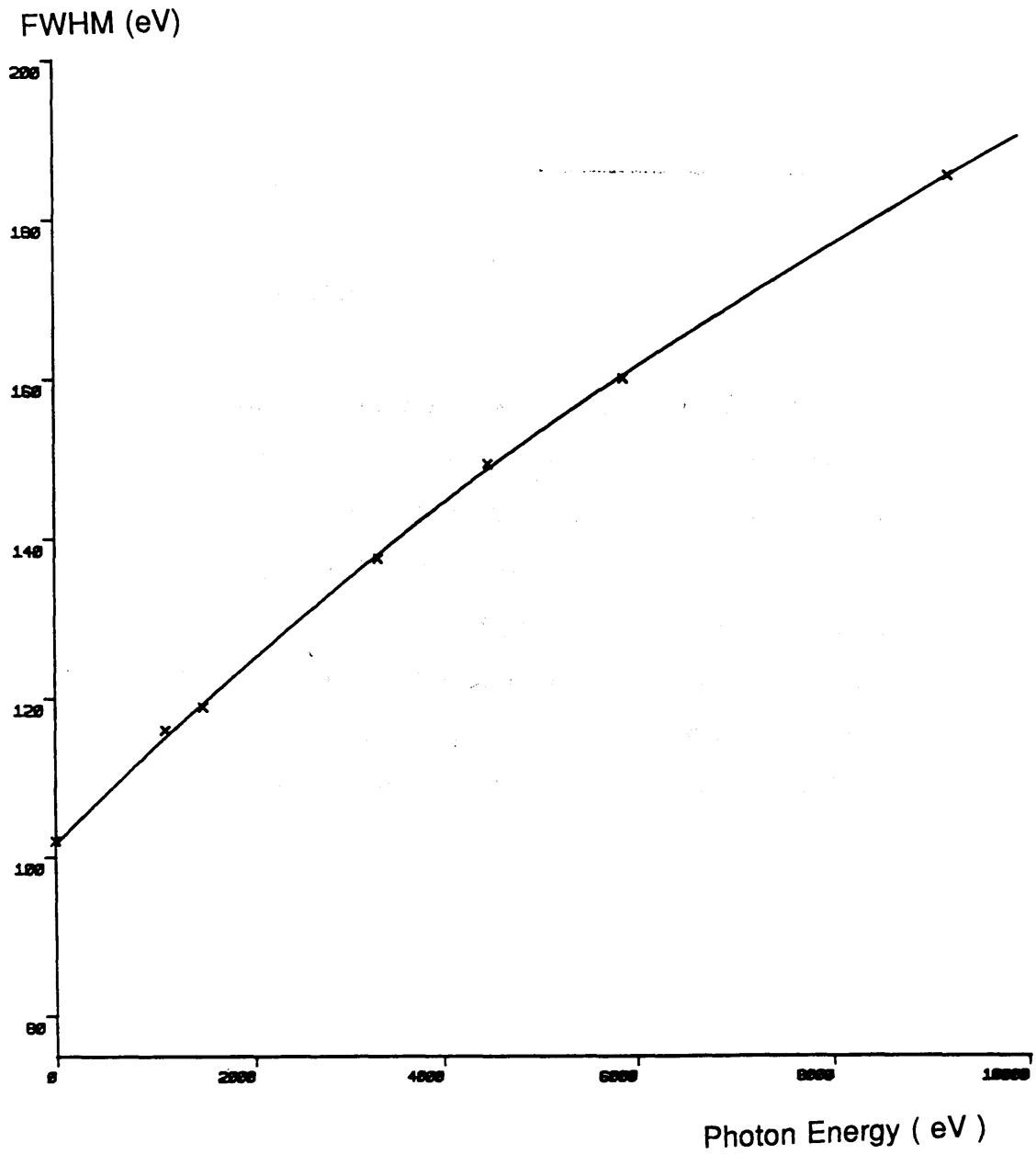

Figure 4.3

FWHM of a Be window detector (A), versus photon energy.

time depending on its history (Pears private communication). When the above data was collected from this detector (A) the electronic noise was found to be 102 eV, with the resolution (FWHM) of Mn K_α as 161 eV.

4.4 Peak Distortion

By distortion of the peak we mean the deviation from a Gaussian shape on the low energy side of the peak. The distortion mainly occurs due to incomplete charge collection (ICC). This is a phenomenon in which the collection of electron - hole pairs created in certain regions of the detector near the faces and sides is incomplete due to trapping and recombination of the electron-hole pairs (see Fiori and Newbury, 1978 and Craven et al, 1985). According to equation 4.1, this will lead to a reduction in the number of charges resulting from the incident photon and thus a fraction of their counts appears at lower energies in the spectrum. Here it should be noted that the ICC leads to a transfer of counts from the peak of interest to the entire energy region down to zero (see figure 4.4). The data for figure 4.4 was provided by K Pears.

4.5 Auger Electron and Si Escape Peaks

The generation of a photo-electron in the effective crystal region leaves the Si atom in an energetic state. If the photoelectron is emitted from the K-shell, the atom can subsequently undergo an electron transition to fill this K-shell vacancy, with subsequent emission of a Si K x-ray or an Auger

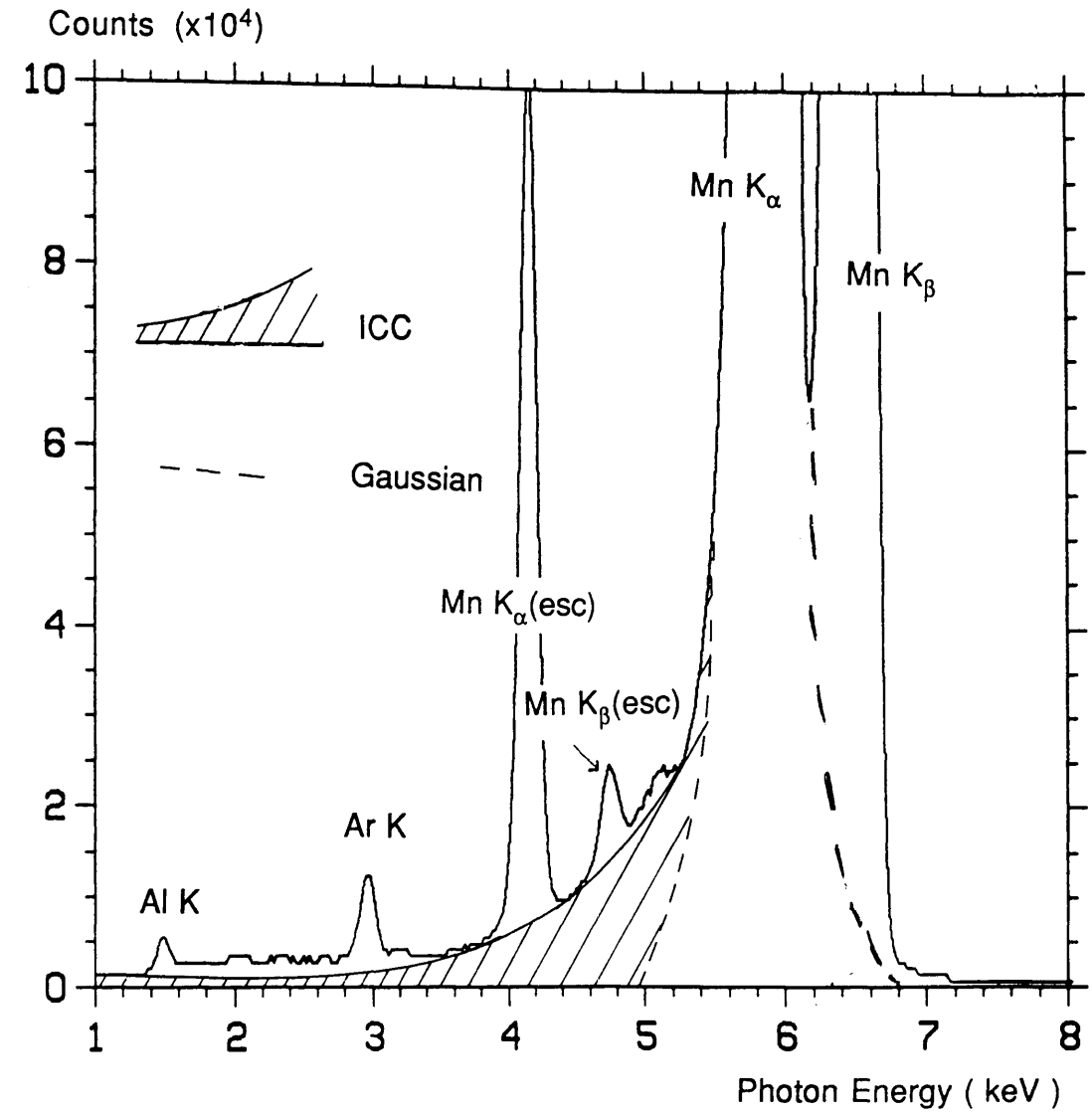

Figure 4.4

A typical EDX spectrum from Fe^{55} showing the main Mn K characteristic and escape peaks (data recorded on detector A). The ICC effect on the spectrum is also marked.

electron. It is highly probable that an Auger electron will be reabsorbed in the detector and contribute its energy to the formation of electron-hole pairs, as a result of which the total energy of the incident photon is deposited in the detector. The Si K x-ray, on the other hand, has greater probability of escaping the detector, which results in the formation of an escape peak at an energy equal to the energy of parent line minus the energy of the Si photon. For example a photon of energy P_K produces an escape peak at an energy equal to P_K-$(P_K)_{Si}$, where $(P_K)_{Si}$ is the energy of the escaping Si K_α photon. Here it should be noted that an escape peak can not occur for radiation with energy below the absorption energy of the Si K-shell (see figure 4.4).

The surface layer of the Si crystal is less efficient in collecting charge and is frequently referred to as the Si dead layer. The absorption of x-rays by the Si dead layer may cause fluorescence of a Si K photon, as a result of which a small peak appears in the spectrum, which is so called Si internal fluorescence peak. However, the probability of seeing the Si internal fluorescence peak is very small, because the Si dead layer is very thin (usually < 0.1 μm).

4.6 Contamination

Effects on x-ray intensities caused by contamination arise from the environment of the sample and the detector. The rate at which contamination builds up on a specimen is a complicated function of many parameters like, current density, specimen character, beam energy, residual gases in the vacuum system, and extraneous substances which exist on the surface of the specimen. Generally, the rate of contaminating is proportional

to the beam current density (see Fiori and Newbury, 1978). The specimen contamination has nothing to do with the x-ray detection process. However, its effect leads to spectral distortion which has to be considered when interpreting spectra. The contaminating layer absorbs low energy x-rays emerging from the specimen and hence measured x-ray intensities are affected. It is frequently difficult to separate this effect from changes in detector efficiency.

To minimise the contamination copper blades cooled to -196 C° with liquid nitrogen are employed around the specimen. It is also necessary to maintain a high vacuum in the specimen region, because a poor vacuum can cause rapid specimen contamination.

4.7 Modelling X-ray Detector Efficiency

As shown in figure 4.1, the electrical contact is made to a thin layer of Au (of a nominal thickness of 0.01 μm) which is evaporated on to the crystal surface. A so called Si dead layer (having a nominal thickness of 0.05 μm), may exist between the Au layer and the active crystal region. The photons entering the detector must pass through the Be window and these two layers. However, as mentioned in section 4.2 some low energy (< 3 keV) photons are absorbed within the Be window and may be also in the two surface layers of the detector. This absorption of low energy photons results in the reduction of detector efficiency at low energy region (Figure 4.5).

Although the absence of a Be window allows a windowless detector to detect low energy x-rays with a far greater

efficiency than the conventional one, some absorption still occurs in the Au contact and Si dead layers and the detection efficiency falls significantly below unity at the low energy end. The efficiency can be calculated if the layer thicknesses are known. Thomas (1984) has described the efficiency in terms of absorption in 20 nm of Au and a 0.15 μm of Si dead layer. However, Paterson (1988) suggested that since in the low energy region the mass absorption coefficients of Si and Au have similar shapes, the experimental background shape could be modelled in terms of absorption in either a Au or Si dead layer. However, the effective thickness of Au (t_{Au}) is the parameter frequently chosen to describe the efficiency of a particular windowless detector. It is important to be able to model the efficiency of windowless detectors as this is particularly sensitive to thin layers of ice which may form on the crystal.

Some high energy (> 16 keV) photons may pass right through the detector and are not detected, which results in the loss of detector efficiency at the high energy end (Figure 4.5). At the high energy end the efficiency is determined by the thickness of the crystal, so it is useful to know the effective Si crystal thickness.

We have already seen in chapter 2 that the Bremsstrahlung or background spectrum generated in a thin specimen by an electron beam can be accurately calculated with the MBH formula. In an experimental x-ray spectrum the shape of the recorded background depends on several factors. In the mid energy range (4 keV to 16 keV) the background shape depends only on the functional form of the Bremsstrahlung emitted from the specimen, as the efficiency of the Si(Li) detector is

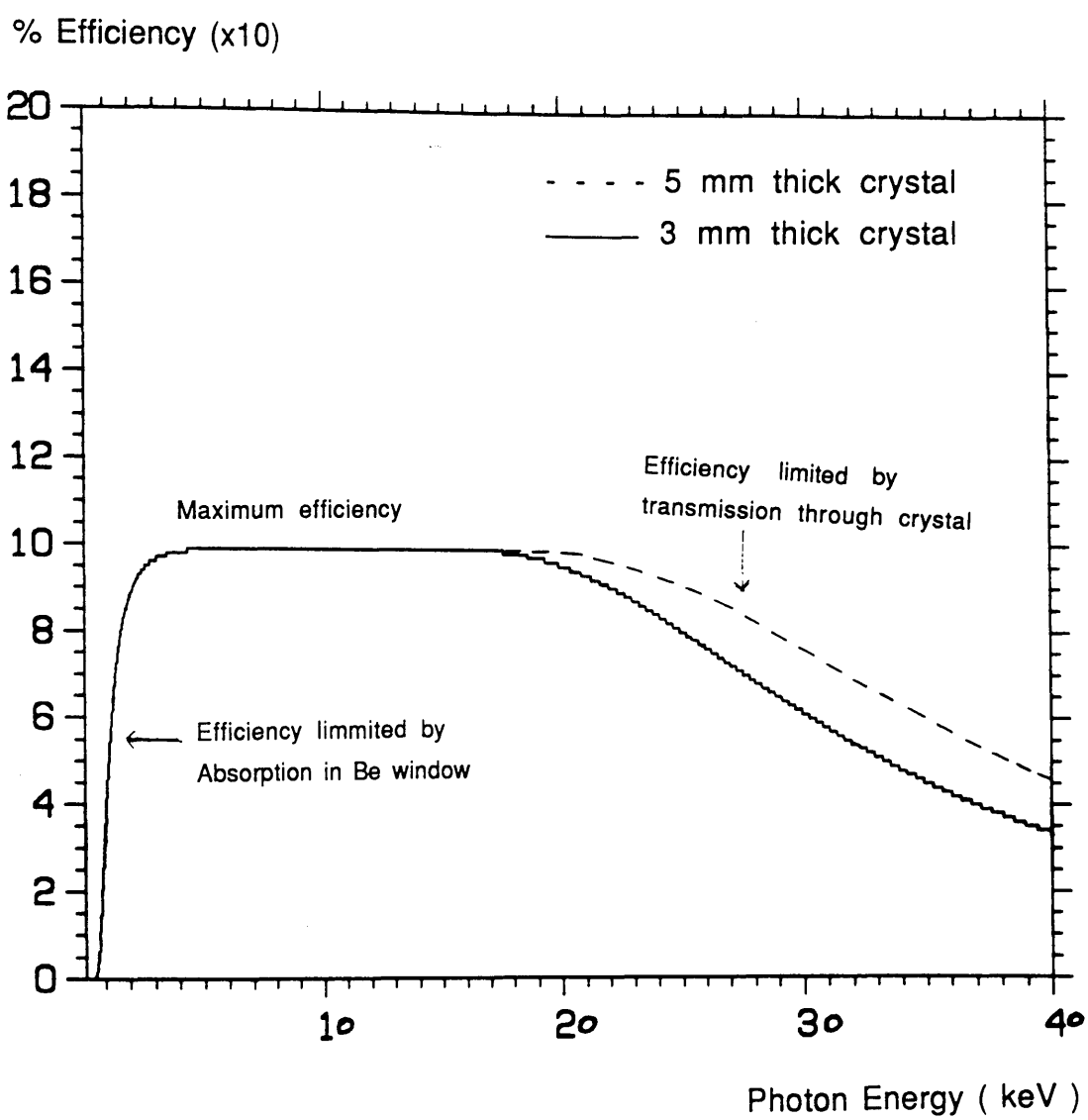

Figure 4.5

Percentage detection efficiency of EDX detectors over the x-ray energy range of interest.

essentially unity in this region and specimen self absorption is negligible. So the background shape should be that predicted by the MBH formula. The shape outside of this energy range is strongly influenced by the detector efficiency.

The difference between the predicted Bremsstrahlung shape and that observed experimentally may in principle be used to determine the x-ray detector efficiency at high and low energies (Nicholson et al, 1984). This is the approach which will be used here.

4.7.1 Detector Efficiency at Low Photon Energies

The low energy spectrum shape, Low (P_K), may be written as,

$$\text{Low } (P_K) = \text{MBH } (P_K)\ \ \varepsilon_L(P_K) \qquad (4.6)$$

Where MBH (P_K) represents the shape of the Bremsstrahlung predicted by the MBH equation. $\varepsilon_L(P_K)$ is the low energy efficiency of the x-ray detector, which may be written as,

$$\varepsilon_L(P_K) = \exp\left[\sum_i \left\{ -(\mu/\rho)_i\ \rho_i\ t_i \right\}\right] \qquad (4.7)$$

In this equation the exponent represents absorption of the incident x-rays in the various " layers " present before they actually enter the active Si(Li) region. $(\mu/\rho)_i$ is the mass absorption coefficients for x-rays of photon energy P_K in the layer of element i; ρ_i; and t_i; are respectively the density and thickness of that layer.

Implicit in the equation 4.7 is the assumption that the efficiency function can be modelled as a simple absorption process in a homogeneous material of uniform thickness. This is most certainly an approximation, since in all likelihood some deviations may exist. The Be window, which is usually made by a mechanical rolling process, can have irregular surfaces, and may be oxidized to greater or lesser extents depending on its handling (see Statham, 1981). The gold layer if thin enough may not be of uniform thickness, and Si dead layer is influenced by the bias employed.

Although absorption occurs in many non-uniform layers, we do not have enough information in a spectrum to separate out the absorption effects of each layer. Hence it is convenient, for a Be window detector, to assume for the purpose of the efficiency calculation that the thicknesses of Au and Si dead layers are zero, and that all the absorption takes place in the Be window which has thickness t_{Be}, so that t_{Be} may be considered as a convenient way of describing the efficiency of a particular Be window detector.

4.7.2 Detector Efficiency at High Photon Energies

The high energy spectrum shape, High (P_K), may be written as,

$$\text{High } (P_K) = \text{MBH } (P_K) \cdot \varepsilon_H(P_K) \qquad (4.8)$$

where $\varepsilon_H(P_K)$ is the high energy efficiency of the x-ray detector, which may be written as,

$$\varepsilon_H(P_K) = 1 - \exp\{-(\mu/\rho)_{Si} \quad \rho_{Si} \quad t_{Si}\} \qquad (4.9)$$

Here t_{Si} is the thickness of the effective region of the detector. The exponential term represents the absorption of the incident photons within the active region.

4.8 Experimental Determination of X-ray Detector Efficiency

Spectra were recorded from a variety of materials using several different x-ray detectors. A MBH theoretical background was calculated for each specimen using programme MBHBACK (see appendix 2), and fitted to the experimental spectrum of each thin specimen over peak free regions away from the extremes of energy range so that the efficiency of the detector could be assumed to be unity. Then the theoretical spectrum was corrected for absorption in a range of t_{Be}. Each time this corrected background spectrum was compared to the experimental spectrum over the region where the efficiency would be less than unity. This comparison was performed using a chi-squared test. The value of t_{Be}, which gave the minimum value of chi-square was taken as an effective value (see programme CORRECTION in appendix 2 and figure 4.6). The mass absorption coefficients required for this correction procedure were calculated using programme MABSCO (see appendix 2). A similar approach may be used to deduce the best value of t_{Si} and hence the high energy efficiency of a particular detector.

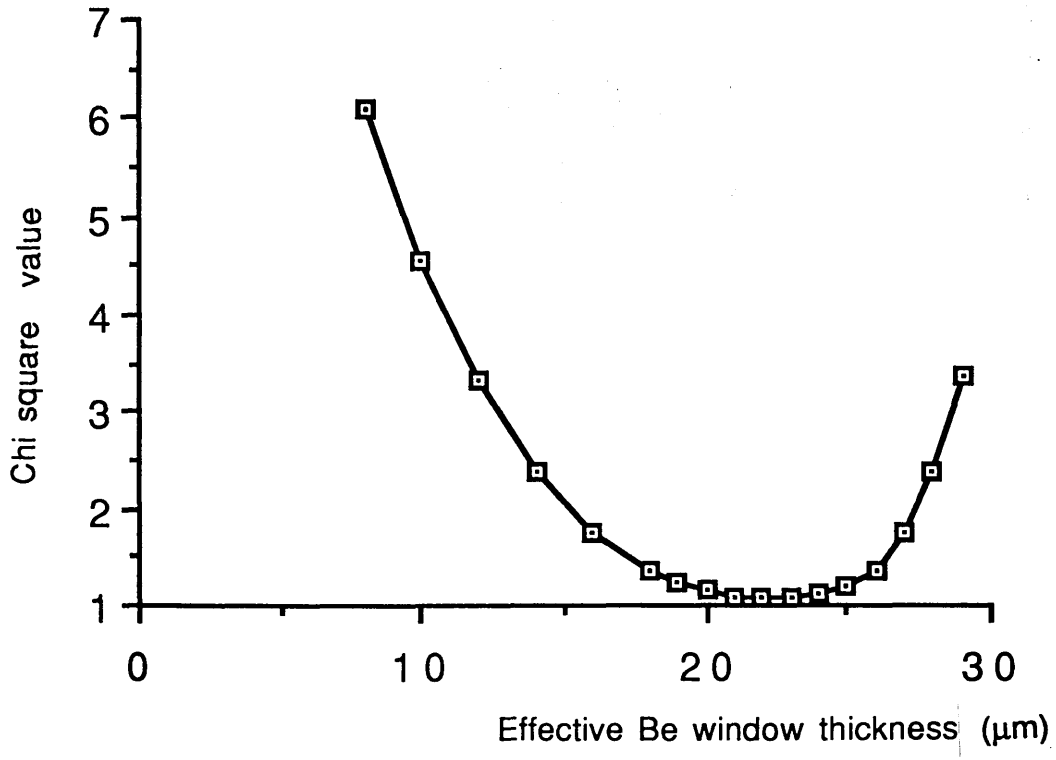

Figure 4.6

A plot of chi squared value versus effective Be window thickness.

4.8.1 Low Energy Efficiency of Conventional Be Window Detectors

A Link Analytical detector (A) fitted on an extended VG HB5 electron microscope was investigated to examine its low energy efficiency. Experimental spectra recorded on this detector from thin regions of a GaP specimen were available for this investigation. The preparation of the sample and the full experimental details used for the collection of the spectra are described in chapter 6. The spectra recorded from this sample were primarily intended to be used for determination of specimen self absorption (see chapter 6). Some suitable spectra were selected from the data set for which specimen self absorption could be neglected. This is important for measuring low energy detector efficiency as it is not possible to separate photon absorption in the specimen from that in the detector window. However, because of the short recording times used for the experiment for self absorption corrections, the spectra are rather noisy for efficiency determination.

The approach as described above, was used to deduce the best value of t_{Be} for this detector. The theoretical (MBH) and experimental background of GaP were scaled over a region of 10.6 to 15 keV photon energy and compared for a chi-square test in the regions 0.7 to 0.84 keV and 1.46 to 1.7 KeV. The best value of t_{Be} obtained for this detector was 9±1 μm when Heinrich's (1987) formulation of mass absorption coefficient was used. Springer et al (1976) formulation of mass absorption coefficient gave the value of t_{Be} as 12±1 μm. Figure 4.7 shows an experimental spectrum from a thin region of GaP recorded on

this detector (A) with the theoretical background spectrum corrected for absorption in 9.0 μm Be window (Heinrich's coefficients) superimposed.

A Kevex detector (D) fitted on a JEOL 100 C electron microscope was also investigated to examine its low energy efficiency. Experimental spectra from thin formvar foils (50 nm thick) were used for this investigation. The full experimental details used for the collection of spectra from this detector are described in chapter 5. Both the experimental and the theoretical spectra were scaled in the energy region of 5 to 15 keV and the chi-square test was performed in the energy region of 0.98 to 1.28 keV. The best values of t_{Be} obtained were 8±1 μm and 11±1 μm for the Heinrich and Springer et al formulations of mass absorption coefficients respectively. Figure 4.8 shows an experimental spectrum from thin formvar recorded on this detector with the theoretical background spectrum corrected for absorption in 8.0 μm Be superimposed.

It can be seen from figures 4.9 (a) and (b) that the low energy efficiency has essentially the same shape for the two formulations of mass absorption coefficients, but a different value for t_{Be} is obtained for a particular detector for each formulation.

4.8.2 Detector Contamination and Low Energy Efficiency

It has been noted that there is insufficient information in the low energy Bremsstrahlung shape to separate the effects of photon absorption in the specimen from that in the detector window. If the window or crystal become contaminated this may

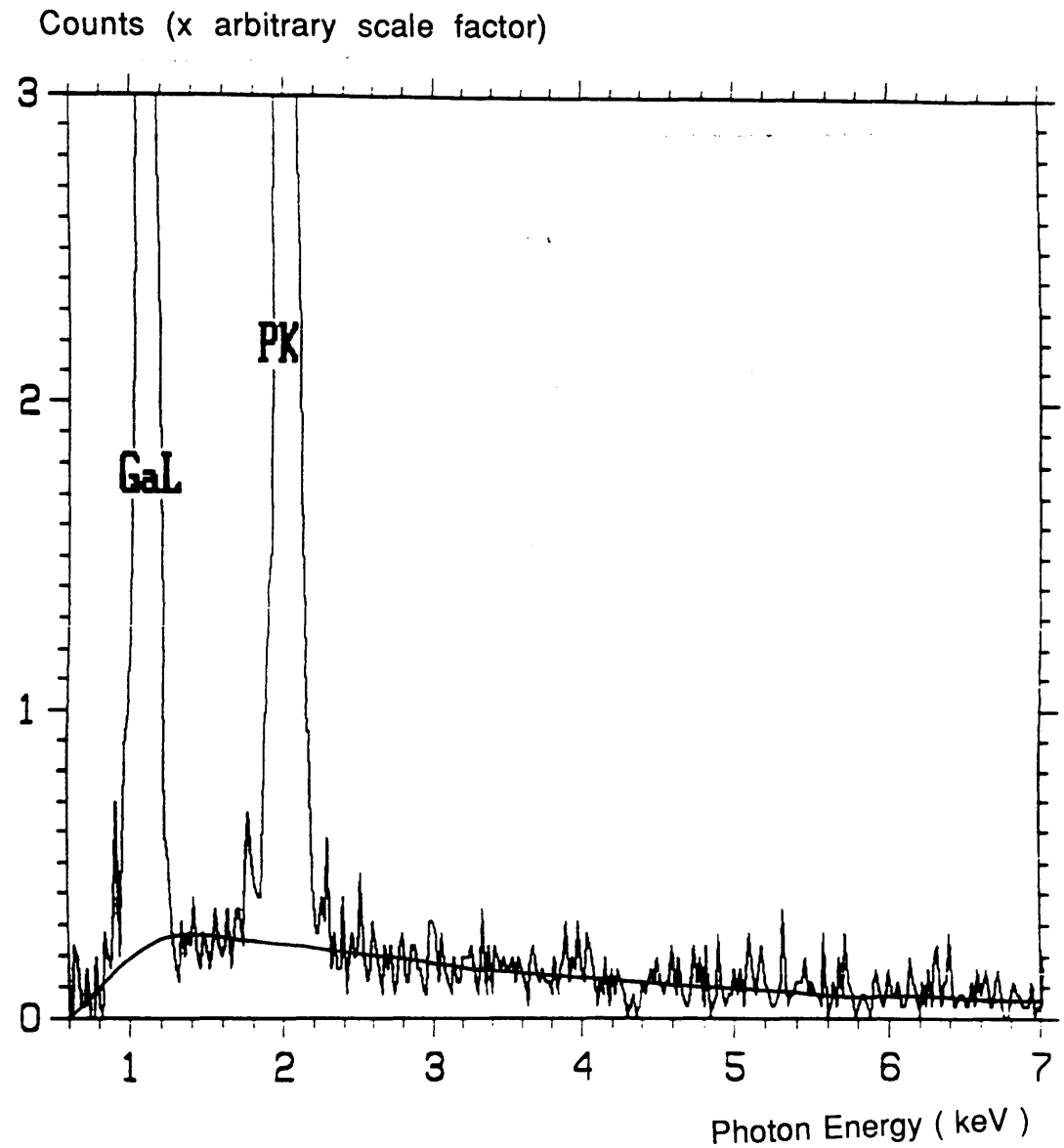

Figure 4.7

Experimental spectrum of GaP specimen with MBH shape corrected for loss in detector efficiency by absorption through 9 μm of Be using Heinrich's mass absorption coefficients superimposed. (Data recorded on detector A.)

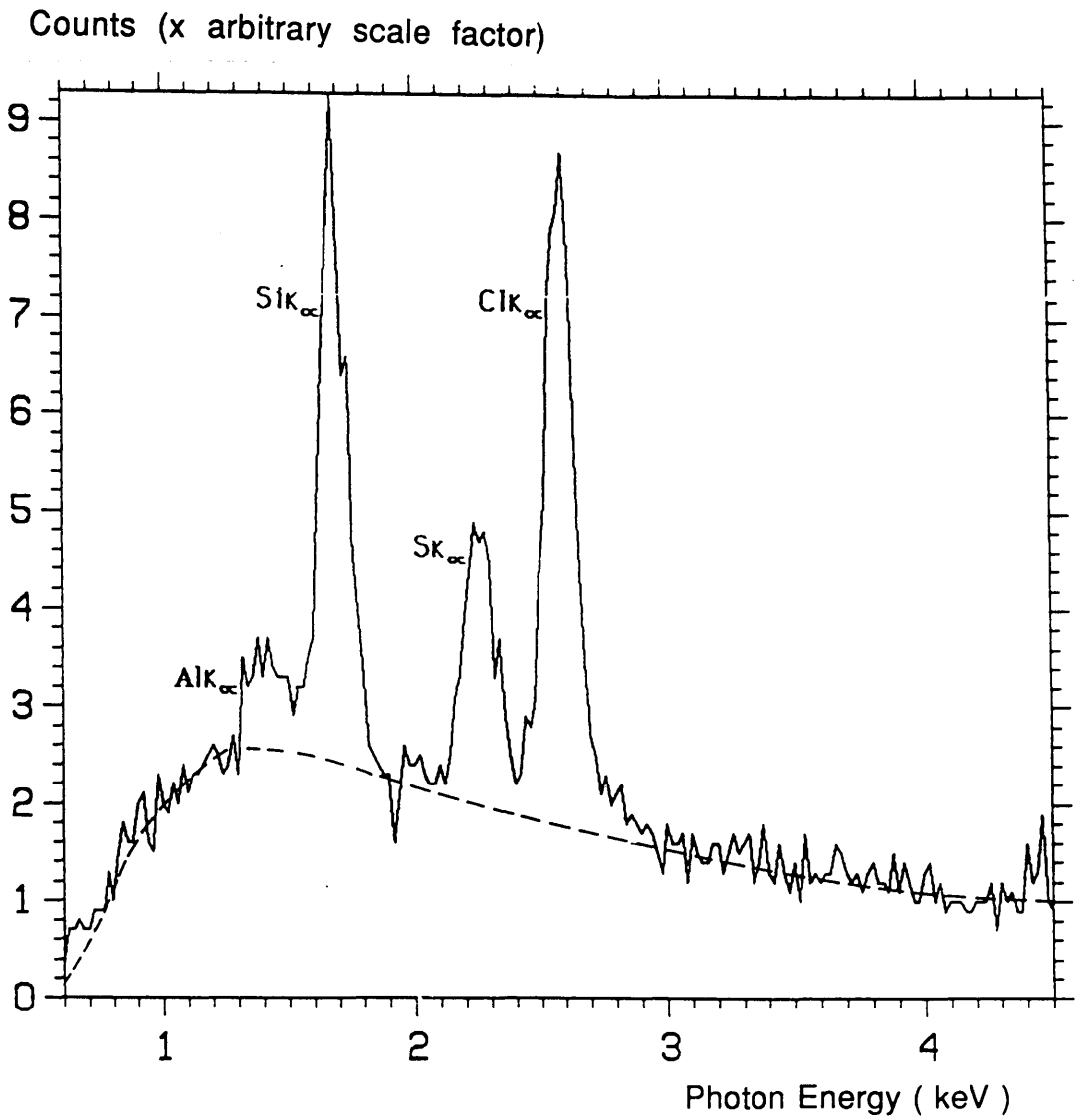

Figure 4.8

An experimental spectrum from 50 nm Araldite with MBH shape corrected for loss in detector efficiency by absorption through 8 μm of Be using Heinrich's mass absorption coefficients superimposed. (Data recorded on detector D.)

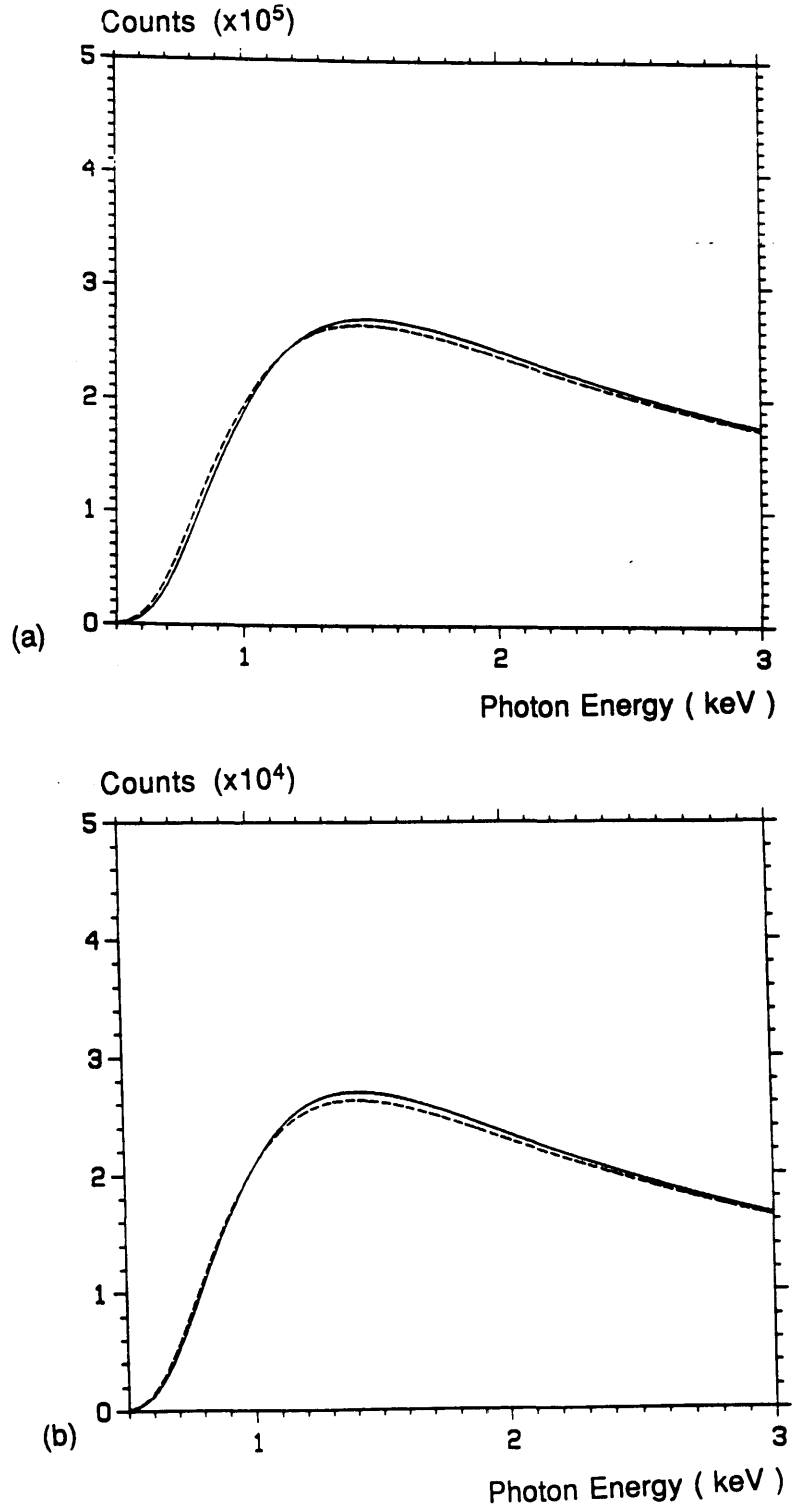

Figure 4.9

(a) GaP MBH shape corrected for absorption for 9 μm (Heinrich) and 12 μm (Springer et al) Be superimposed. (b) Formvar MBH shape corrected for absorption for 8 μm (Heinrich) and 11 μm (Springer et al) Be superimposed.

also reduce the low energy efficiency in a similar manner.

A Kevex Be window detector (C) fitted on JEOL 2000 FX electron microscope has been examined in detail by Paterson (1988) using the Springer et al (1976) formulation of mass absorption coefficients which gave a value of t_{Be} as 32 μm. This value is much greater than the nominal thickness (9 μm). This result is highly typical of all spectra recorded on this detector. Here, the same detector is examined by using Heinrich's (1987) formulation of mass absorption coefficients. Spectra from thin foils of Co, Cr and Cu recorded on this detector were used to deduce the low energy efficiency. These spectra were collected by Dr W A P Nicholson at IBM Almaden Research Center.

Single element specimens were used to ensure that the Bremsstrahlung was due as far as possible to the element under investigation in each case. In order to minimise non-sample contributions, these thin foils were supported on single hole mounts of Cu or Ti. In order to assess approximately the extent of the bulk contribution, bulk spectra were recorded from the material of the grid on which the specimen was mounted. However, the bulk contribution was at most 2 percent for any of these spectra (Paterson, 1988), so no bulk subtraction was done.

Figure 4.10 shows an experimental spectrum of a thin Co foil recorded on this detector. A theoretical background spectrum of Co was scaled to the experimental spectrum over the region 10.3 to 15 keV as in this region the efficiency of the detector is unity. The theoretical spectrum was then corrected for a range of values of t_{Be} and each time compared in the low energy region between 1 to 1.48 keV. A plot of chi-square values is shown in figure 4.6. It can be seen from this plot that

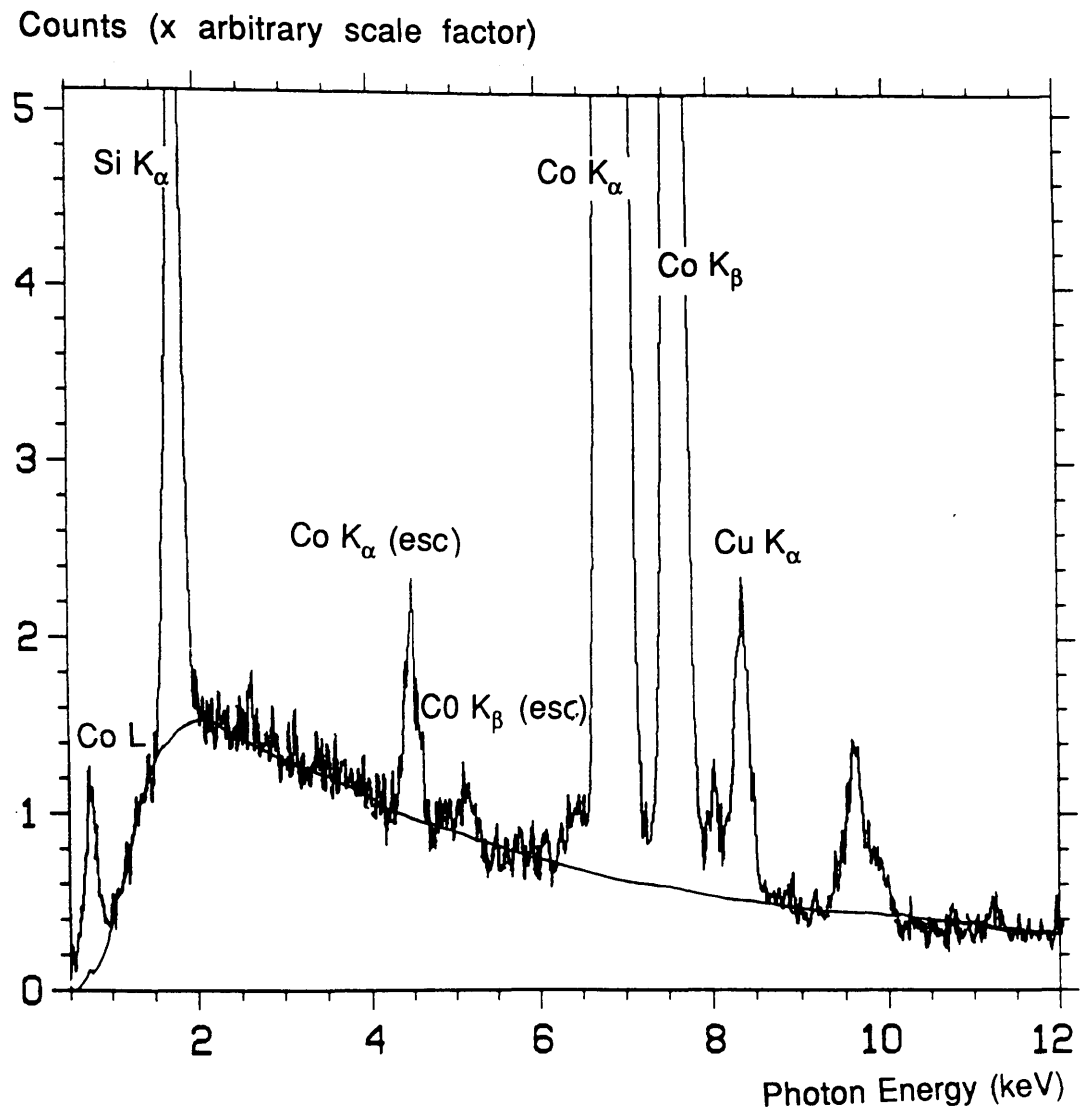

Figure 4.10

An experimental spectrum of Co with MBH shape corrected for absorption in 9 μm Be and 8.5 μm ice superimposed. (Data recorded from detector C.)

although at 22 μm the value of chi-square is minimum (1.08), the variation of chi-square is small in the thickness range 20 to 24 μm. Thus, the best value of t_{Be} is 22±2 μm for this detector, which is still greater than the nominal value for the window thickness.

It is unlikely that the window is really 22 μm thick, and such a difference could not be accounted for by realistic values of Au contact and Si dead layers. Therefore, there must have been some other source of absorption. Accumulation of a layer of ice on the window or the crystal could give rise to such an effect (Paterson, 1988). It is not possible to tell from fitting to the spectrum as described in what proportion the absorption is due to ice and the usual detector window. However, by assuming t_{Be} to be 9 μm, the effect of varying the value of effective thickness of ice (t_{ice}) could be investigated. As before a chi-square test in the region 1-1.48 keV was performed and thus a value of t_{ice} which best described the experimental background was obtained. The optimum value of t_{ice} was obtained as 8.5±1 μm. A spectrum from thin Co recorded on this detector with an MBH theoretical background spectrum corrected for absorption in 9 μm of Be and 8.5 μm of ice superimposed is shown in figure 4.10.

4.8.3 High Energy Efficiency

Two Link Analytical detectors having nominal thicknesses 3 mm (detector A) and 5 mm (detector B) respectively were examined to deduce their high energy efficiencies. Both these detectors were fitted at different times to the extended VG HB5

electron microscope in Glasgow University. Experimental spectra from an InP specimen were used to investigate the 3 mm detector and that from Carbon (C) for the 5 mm detector. The preparation of the InP sample and the full experimental details used for the collection of the spectra are described in chapter 6. The same experimental conditions were used for the collection of C spectra. However, for this sample carbon ribbon was evaporated onto a rock salt (NaCl) crystal. The film was "floated" off rock salt into distilled water. It was left for approximately one hour to dissolve away any crystals and was then picked off with a grid and finally dried.

The experimental and theoretical background spectra of InP were scaled in the energy region 12.5 to 16 keV. A chi-square test was performed in the energy region from 29 to 40 keV. The best value of t_{Si} for this detector was 3.1±0.1 mm for Heinrich's formulation of mass absorption coefficients and 2.8±0.1 mm for the Springer et al formulation of mass absorption coefficient. Figure 4.11 shows an experimental spectrum of InP with theoretical background and theoretical background corrected for loss in the high detector efficiency by transmission through 3.1 mm of Si superimposed.

Both the experimental and the theoretical background spectra of C were scaled in the energy region of 8.5 to 18 keV, while the chi-square region was chosen to be the same as that of for the InP spectra. The best value of t_{Si} was (4.7±0.2) mm for the Heinrich formulation and that of (4.3±0.2) mm for the Springer et al formulation of mass absorption coefficients. Figure 4.12 shows an experimental spectrum of C with theoretical background and theoretical background corrected for loss in the high detector efficiency by transmission through 4.7

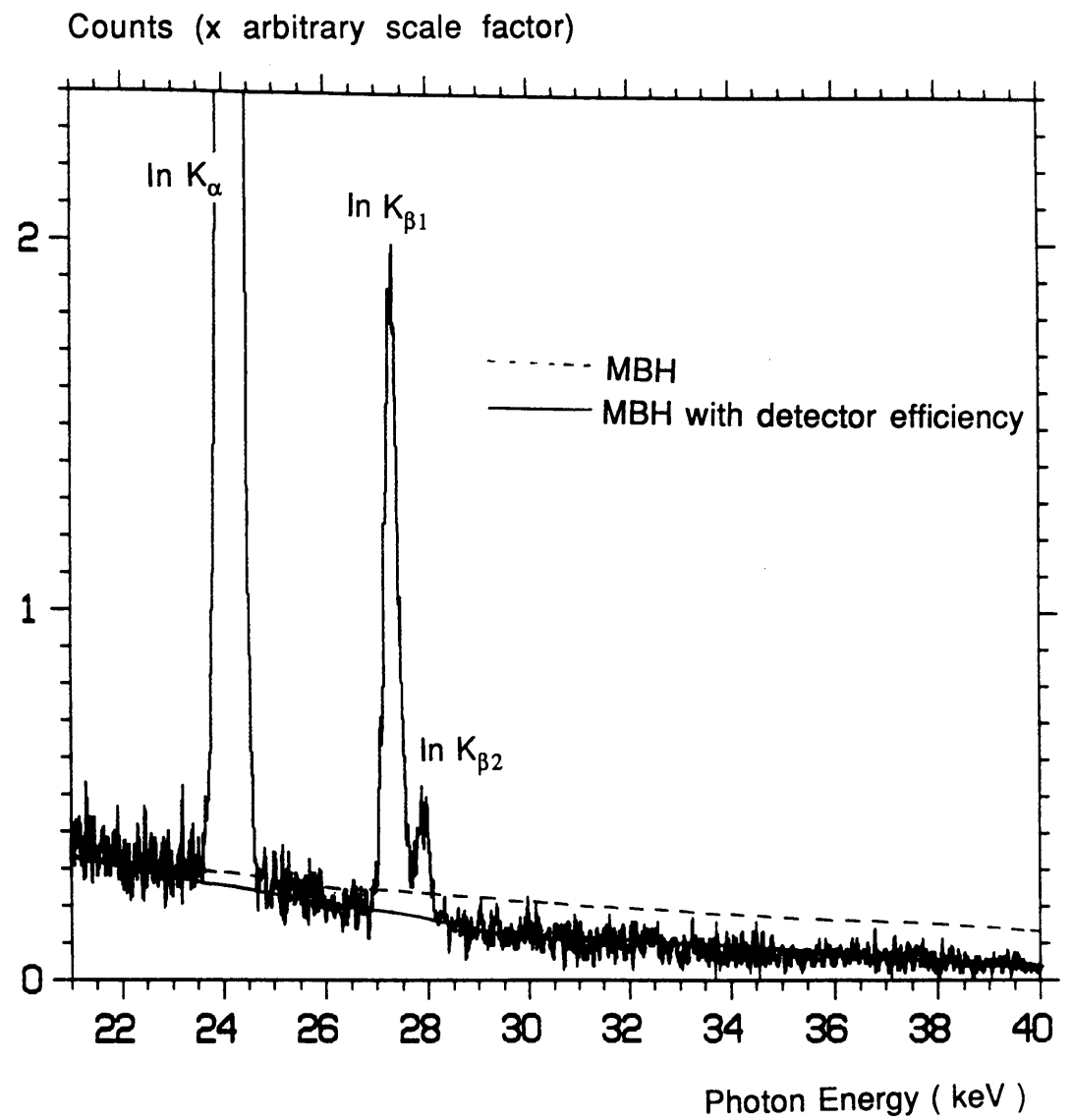

Figure 4.11

An experimental spectrum of InP with MBH and MBH corrected for loss in detector efficiency by transmission through 3.1 mm of Si using Heinrich's mass absorption coefficients superimposed. (Data recorded from detector A.)

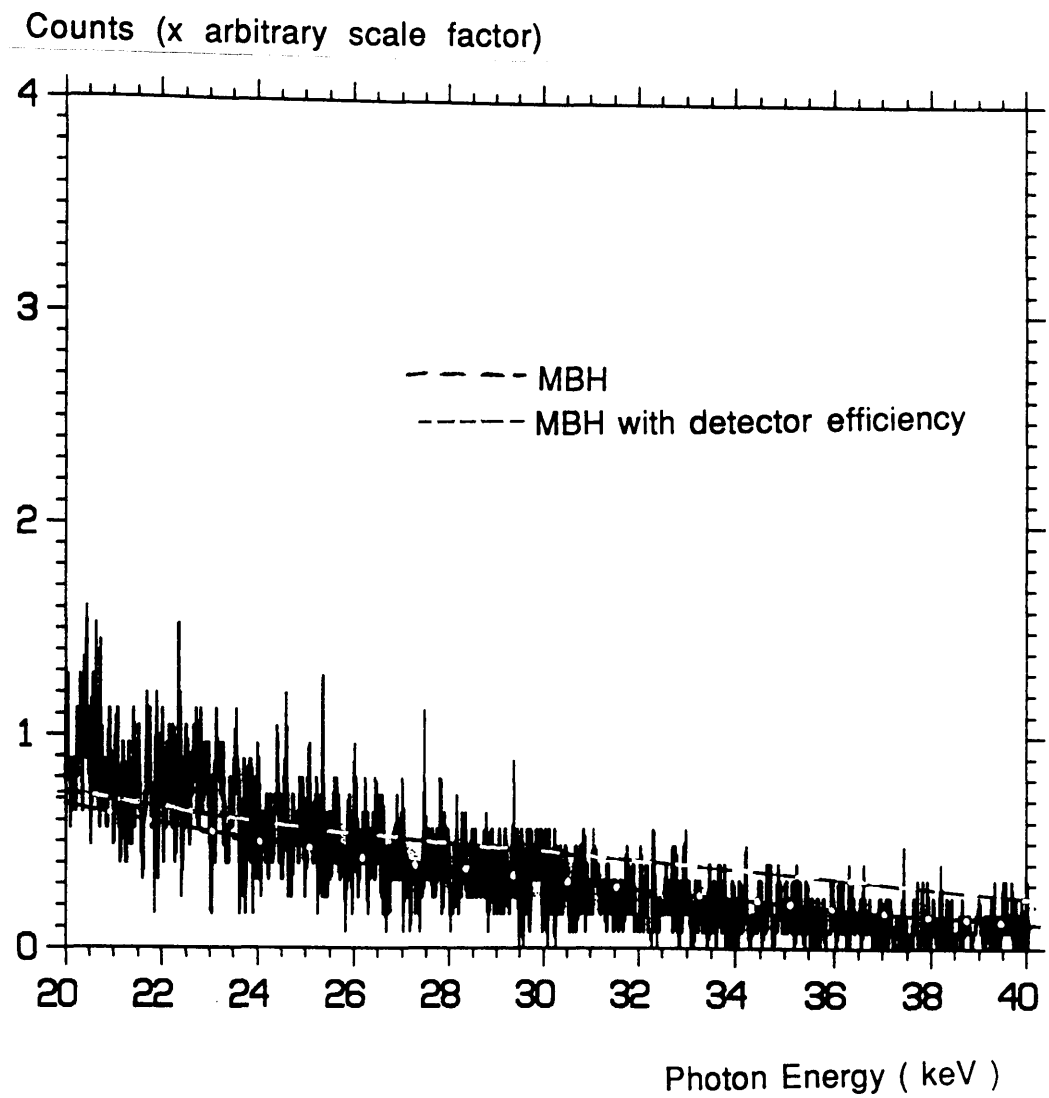

Figure 4.12

An experimental spectrum of C with MBH and MBH corrected for loss in detector efficiency by transmission through 4.7 mm of Si using Heinrich's mass absorption coefficients superimposed. (Data recorded from detector B.)

mm of Si superimposed.

It can be seen that the 5 mm thick crystal offers higher detector efficiency especially for photons of energy greater than 20 keV. For example, at the In K_α energy, the efficiency of a 3 mm thick crystal is 84%, whereas a 5 mm thick crystal has an efficiency of 95% for the same line.

4.9 Discussion

The low and high energy efficiencies of different EDX detectors attached to different electron microscopes have been investigated. A significant discrepancy exists between the various published tabulations of mass absorption coefficients which may be used to calculate the detector efficiencies. The overall shapes of the efficiencies are moderately independent of the choice of mass absorption coefficient formulations, but the values of t_{Be} and t_{Si} obtained are dependent upon the choice of coefficients used.

Because of the uncertainties in manufacturing, the differences in t_{Be} predicted by the two different models can not definitively select which is better, although t_{Be} predicted by the Heinrich formulation is closer to the manufacturer quoted value.

Discussion with Link Analytical failed to produce any physical explanation of how a crystal of a given thickness could perform as though it were effectively "thinner" provided that the high energy descriminators on the pulse processor were set to maximum. The values of t_{Si} predicted by Heinrich's formulation of mass absorption coefficients are in good agreement with the crystal thicknesses which were measured

by the manufacturers. It seems likely that these values are more realistic and will be used for the rest of this thesis.

CHAPTER 5

Theoretical Background Modelling and Absorption Corrections Using the Bremsstrahlung

5.1 Introduction

In this chapter the way in which the recorded spectrum from a thin biological section can be analysed to provide elemental concentration is discussed. The intensities of the characteristic lines are used to quantify elemental concentrations if these can be accurately separated from the background beneath. There are several conventional ways to separate the background beneath the characteristic peaks (see section 5.2). Here, the x-ray production theory and a knowledge of the detector efficiency response will be used to model the background as an alternative way of extracting peaks from the background.

As the theoretical Bremsstrahlung shape is a weak function of the mean atomic number of the specimen, a single background shape should fit spectra from all biological specimens since their mean atomic number lies in the range 6 to 15. In this chapter this possibility is examined and results are compared with conventional technique for measuring the background using windows (Nicholson and Dempster, 1980). A typical biological problem has been used to provide spectra for this investigation.

Also, in this chapter the absorption of the Bremsstrahlung will be used to determine mass path lengths so that characteristic line intensities can be also corrected for self absorption effects.

One approach, which is used for quantitation is the ratio method, as discussed in chapter 3. This method, which compensates for the variation of x-ray intensity with specimen thickness, is suitable for specimens in which all elements emit a detectable characteristic line. However, for biological specimens, this method only allows quantitation of elemental ratios rather than absolute concentrations. Another analytical approach which can be used for the microanalysis of thin biological specimens, provided suitable standard data is available, is called the continuum normalization(CN)method (Hall, 1971).

This chapter begins with a brief review of the procedures commonly used to separate the sample Bremsstrahlung beneath the characteristic peaks of interest to extract the characteristic data. To achieve accurate quantitation of the elemental composition from an x-ray spectrum, the first requirement is that the recorded spectrum is truly representative of the thin sample under analysis. In a spectrum measured from a thin biological section, two types of Bremsstrahlung are included. One is thin sample Bremsstrahlung and the other is non-sample Bremsstrahlung. Section 5.3 reviews the non-sample Bremsstrahlung and the method to subtract it from the measured Bremsstrahlung to give true thin sample Bremsstrahlung. The window method of specimen background subtraction is described in section 5.4 and section

5.5 discusses the background modelling method in detail. Section 5.6 discusses the approach of absorption corrections using the Bremsstrahlung. A brief discussion on how the information available in an EDX spectrum can be used to determine an elemental concentration by the use of CN method is given in section 5.7. A detailed discussion of the CN method can be found in appendix 5.

The next sections give a detailed description of how the samples are analysed to get the comparison of the results when both window method and MBH background modelling are used. The chapter closes with the conclusion of the analysed work.

5.2 Background Subtraction Procedures

Several different methods have been developed for separating the characteristic signal from the non-characteristic (background contribution) in an EDX spectrum. One of these methods, known as frequency filtering (Statham, 1976), takes advantage of the fact that the background is a slowly varying function of energy to differentiate it from the faster varying characteristic peaks. The separation is achieved by taking the Fourier transform of the spectrum and removing the low frequency components. Then the inverse transform is taken, the residual is the characteristic signal.

Another method, known as iterative stripping procedure (Statham,1976), removes the characteristic peak in stages until no discernible peak can be detected above the background.

Ekelund et al (1979) have reported a fast and simple procedure for the evaluation of net intensities from EDX

spectra, known as selective partitioning method. This method is based on some assumptions, namely, the detector resolution is known, the position in the spectrum for the peaks of interest are known, the peaks are of Gaussian shape, the background varies linearly below each peak, and the peak overlaps can be corrected by using the partit ion functions of parent peaks.

Another method, a simple interpolation and extrapolation method (Nicholson and Dempster, 1980), is based on background windows. The background under the peak of interest is estimated by setting background windows on either side of the peak(see figure 5.1).

It may be seen that all these methods require no *a priori* knowledge of the form of the background and perform well provided the background varies only slowly in the vicinity of the peak of interest. The background varies slowly with energy in the region above 3 keV photon energy. However, it has been seen in chapter 4 (Fig 4.5) that in the low energy part of the spectrum, the detection efficiency is rapidly decreasing and hence the rate of background variation is not slow in this region. An alternative procedure has been employed here which involves modelling the background using the currently available knowledge of x-ray physics and energy dispersive detectors. Results obtained by using this procedure will be compared with the window method.

5.3 Non-sample Bremsstrahlung Correction

Non-sample Bremsstrahlung may come from " stray " or scattered electrons which strike the solid material surrounding

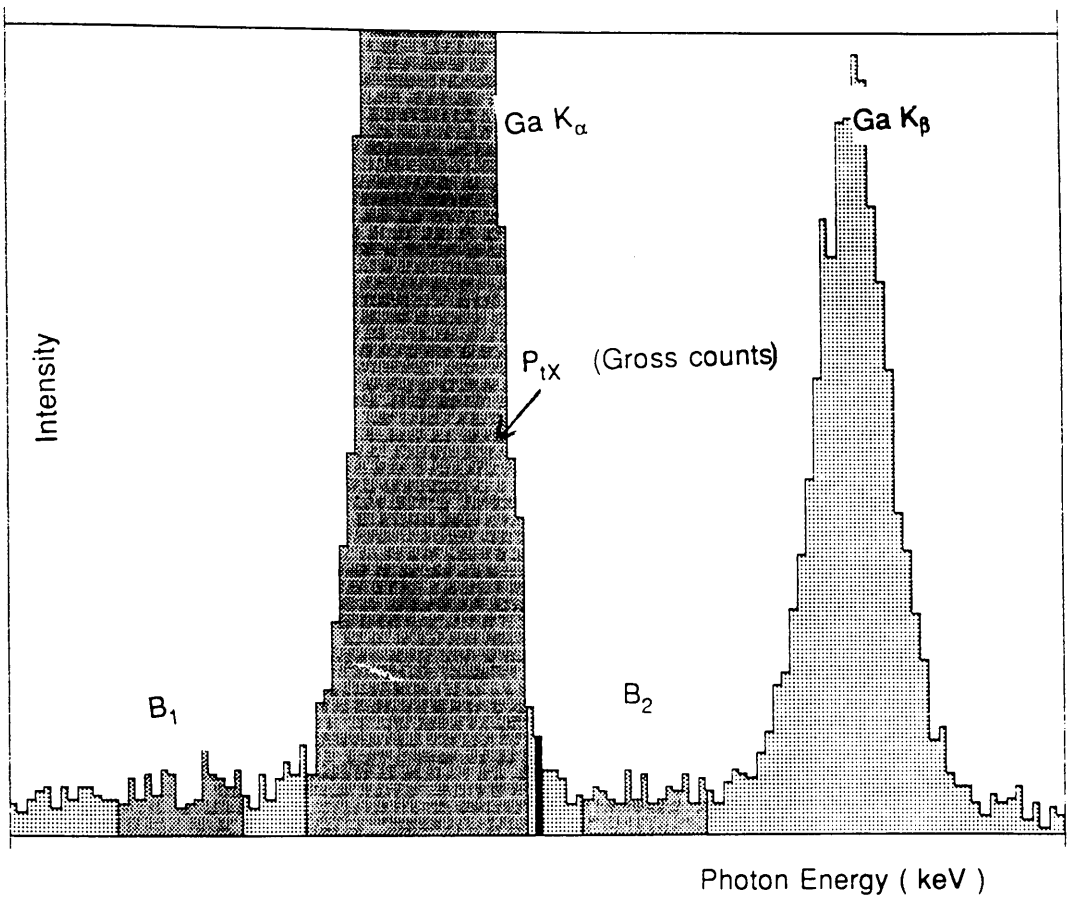

Figure 5.1

Peak of interest on a background along with background windows B_1 and B_2 on either side of the peak.

the specimen as well as from the foil which supports the sample. Evidently this extra background will reduce the peak to background ratio and reduce the detectability of the elements being analysed. Also the shape of "bulk" Bremsstrahlung is different from thin specimen Bremsstrahlung, so a correction may need to be made for the bulk to enable a good fit with a theoretical thin background to be made. If part of the Bremsstrahlung is used for measurement of specimen mass thickness as in the CN method, then erroneous results may be obtained. However, one of the experimental difficulties in application of the CN method is the separation of the thin sample Bremsstrahlung from this non-sample Bremsstrahlung. Methods of minimizing the instrumental contribution to the measured x-ray spectrum have been discussed extensively in the literature (see Goldstein and Wiliams, 1977; Hall and Gupta, 1979; Bentley et al, 1979, and Nicholson et al, 1982). A common method is by coating all the surrounding of the specimen, e.g. the specimen stage, the anticontaminator, etc, with a heavy layer of light elements (such as C or Be), and by it these spurious contribution can be reduced.

Here, in order to reduce and identify the sources of extraneous background, Nicholson et al (1982) have redesigned all instrumental parts of the electron microscope in use (a JEOL JEM 100 C) that either generate x-rays or scatter electrons towards the detector. New parts have been made from a low atomic number material typically Ti, which ensures that all solid materials which contribute x-rays to the spectrum produce a detectable characteristic line. By using the intensity of these lines, the instrumental contribution to the individual recorded spectrum can be estimated and then subtracted (see

Nicholson et al, 1982 and Nicholson et al, 1983).

The procedure of correcting the recorded spectrum for instrumental Bremsstrahlung is to record a spectrum from the pure solid material under the same instrumental conditions, i.e., accelerating voltage and the specimen detector geometry, as used for the specimen. This solid spectrum may then be scaled so that its characteristic peak (Ti K_α) has the same height as that in the measured thin spectrum to be corrected, and then subtracted. Thus a pure thin specimen spectrum is left (see figure 5.2).

Here, it must be noted that in this correction procedure the assumption is made that the solid Bremsstrahlung shape is the same in the two (pure and measured) cases. The pure solid spectrum is recorded with mono-energetic electrons and also the angle between the beam and the solid surface, and the take-off angle both are well defined. On the other hand, the stray solid contribution to the specimen spectrum is generated by electrons often multiply scattered through a range of angles and range of energies. So the intensity and shape of the Bremsstrahlung when normalized to the characteristic line will only be to a first approximation the same as the pure solid spectrum. However, a simple method for demonstrating the success (or otherwise) of the solid correction procedure is to determine how well the resulting corrected spectrum represents a thin specimen; that is, by examining how well the experimental spectrum fits to that predicted by MBH when an appropriate scaling factor is applied. Details of this will be given in the later sections of the chapter.

Normally thin samples are supported on some form of foil

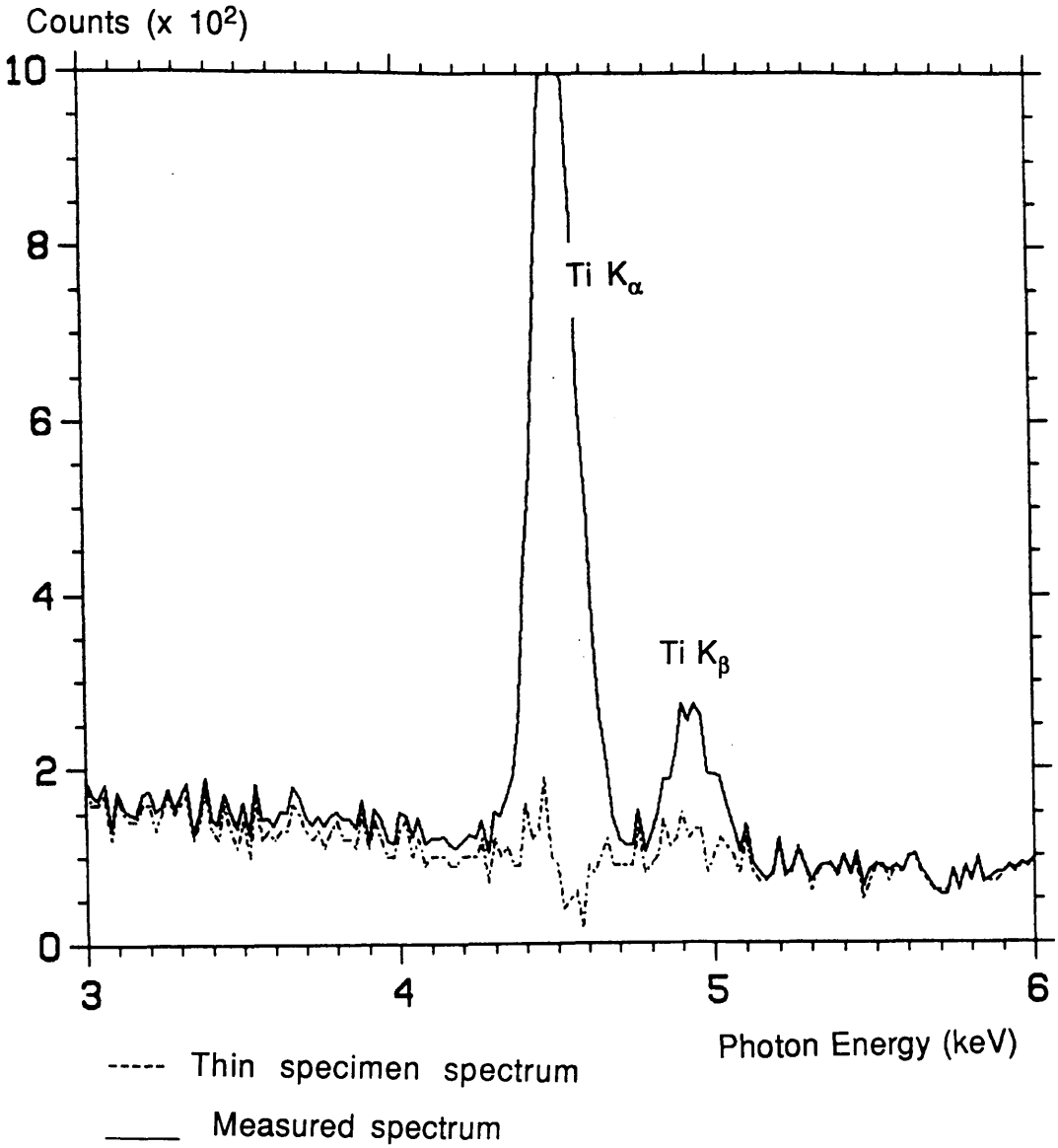

Figure 5.2

A pure thin specimen Bremsstrahlung after subtracting non-sample Bremsstrahlung from a measured spectrum.

(such as nylon, formvar, pioloform, etc), which being mainly hydrocarbon will also contribute Bremsstrahlung but no or very few characteristic x-rays to the measured spectrum. The Bremsstrahlung from the support foil can be estimated by putting the beam directly on the bare support foil (nylon in this work). When the beam is directed onto the nylon foil, the Bremsstrahlung is generated within the foil, and also within the bulk surrounding the foil by electrons scattered from the foil, which can be corrected in the same way as that corrected from the specimen.

There is some error in measuring the foil contribution, since these measurements must be made on regions of the foil surrounding the specimen. For a typical thin specimen of 100 nm of soft (or embedded) tissue supported on a 30 nm organic film, the Bremsstrahlung intensity from the support film is about one third that due to specimen, since their densities and mean atomic numbers are similar. However, support foils are generally very uniform, so that several measurements may be taken from the different areas of the foil to keep the error in this correction procedure close to that due to counting statistics, and then can be averaged. This correction procedure requires that the live time and the beam current of this average spectrum be normalised to match the measured spectrum live time and beam current.

In general, the thin specimen Bremsstrahlung can be given as,

$$W_{specimen} = W_{measured} - W_{solid(s)} - W_{support\ foil}$$

The separation of the non-sample Bremsstrahlung from the thin sample Bremsstrahlung in a measured spectrum, may be done on channel by channel basis (Nicholson et al, 1983), but for use with the continuum normalization method a simple numerical factor may be used to perform the correction(Barbi, 1979; and Hall and Gupta, 1979).

5.4 Window Method of Background Subtraction

The most critical part of this procedure involves the difficulty of setting windows which truly measure the background. When peaks are well separated, this presents little problem and the background can be measured directly on either side of each peak. However, when peaks are not well separated (as is often the case in biological sections), the problems are severe and difficulties are also encountered when the peaks have large tails on the low energy side (Figure 5.3).

The net characteristic counts for any element are obtained by using the equation,

$$P_{nx} = P_{tx} - n\,B \qquad (5.1)$$

where P_{nx} and P_{tx} are respectively net and total counts of the peak of element x. n is the number of channels in the peak width and B is the average background count per channel. The average background per channel can be worked out by setting background windows B_1 and B_2 on either side of the peak (see figure 5.1).

$$B \cdot = \cdot \frac{1}{2} \cdot \left(\frac{B_1}{n_1} + \frac{B_2}{n_2} \right)$$

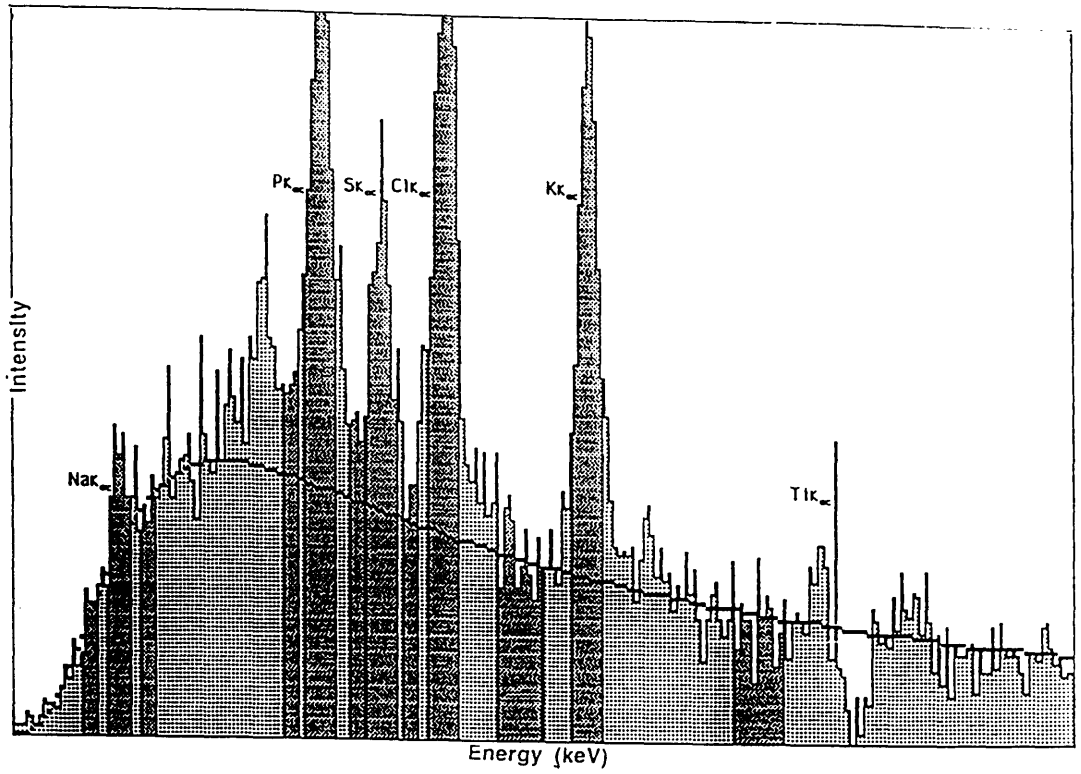

Figure 5.3

Spectrum with elements of interest, background windows and MBH background shape superimposed.

Where B_1 and B_2 are total counts in these windows, and n_1 and n_2 are the number of channels in windows B_1 and B_2 respectively. It assumes that the background between window B_1 and B_2 is approximately linear and some place is available on either side of the peak to set a suitable background window (i.e peaks do not overlap).

5.5 Background Subtraction by Theoretical Modelling

The overall accuracy of the analysis could be improved by improving the background subtraction procedure. Strictly speaking, in order to remove a background correctly, the true shape of the background is necessary. Since we know the precise shape of the Bremsstrahlung background (MBH), it should be possible to perform a direct fit to the peak free regions in the spectrum and, in principle, it can then be subtracted to get the characteristic peaks data.

Although the intensity of the Bremsstrahlung generated in thin specimen increases approximately as Z^2, the shape is a weak function of mean atomic number of the specimen (see figure 5.4). In this figure the thin Bremsstrahlung shape (with detector efficiency correction) of soft tissue ($Z \approx 6$) is scaled, in the energy region 7 - 14 keV, to that from hard tissue ($Z \approx 15$). It can be seen that there is some difference in the two values in the low energy end; however this becomes negligible when scaled to the experimental data.

Therefore, for a range of atomic number (Z) in the biological

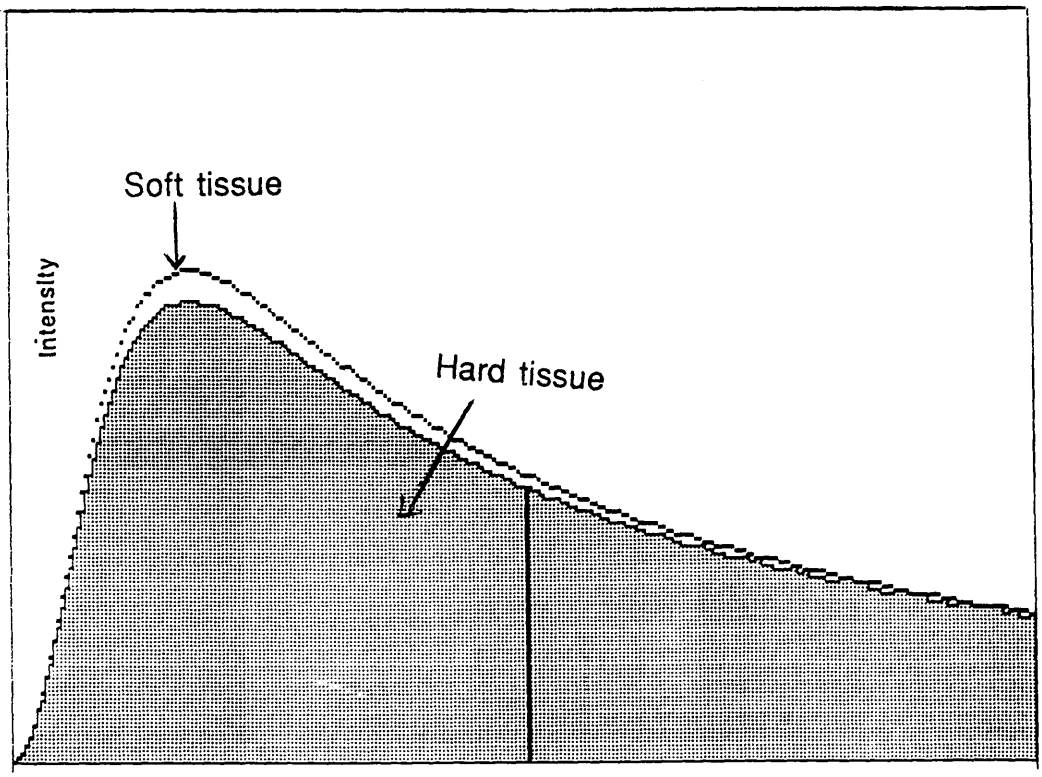

Figure 5.4

Comparison of thin specimen background spectrum of soft tissue (Z≈6) with that of hard tissue (Z≈15).

samples (Z ≈ 6 to 15), a single theoretical background shape should fit the experimental background well, from all thin specimen spectra, for a given electron energy and x-ray detector geometry (80 keV and 90° to the beam respectively in this chapter). It has been shown in chapter 4, that MBH predicts a continuous rise in intensity with decrease in photon energy, but in practice absorption in x-ray detector window modifies the shape below 3 keV (see figure 4.5). Thus the difference between the experimental background and that predicted theoretically should be due to the decrease in detector efficiency at low photon energies. This can be measured, and multiplied by the MBH shape to give a " universal " background shape, which can be scaled to the experimental data and subtracted. The scaling window must be chosen in a spectral region which must be free of peaks and where the detector efficiency is unity. Normally, it is the same as the continuum normalisation window.

5.6 Absorption Corrections Using the Bremsstrahlung

As mentioned in chapter 1, Craven and Adam (1985) and Garratt-Reed et al (1987) have shown that with a knowledge of the Bremsstrahlung cross-sections and the detector response, it is possible to derive the x-ray self absorption in a particular sample. The Bremsstrahlung background (MBH theory) contains, in principle, complete information about the absorption path length. For very thin regions where specimen self absorption is negligible, a theoretical thin specimen background (MBH corrected for low detector efficiency) fits the experimental

data (see chapter 4). For the spectra from the thicker regions, the differences between experiment and a theoretical thin specimen background are mostly due to specimen self absorption. The thin specimen background can be compared with the experimental background to get the value of mass path length as required for absorption corrections and thus modifying a theoretical thin specimen background for self absorption it is possible to get such a background shape which fits the experimental data well. This is the approach which will be used here.

Thus, if the universal thin specimen background does not fit the experimental background well in the very low energy end (i.e 1keV and below), then the differences are due to absorption of x-rays in the specimen itself (see figure 5.5). For quantitation using the CN method, some assumption has to made for the composition of the matrix. For soft tissue, embedded, or frozen hydrated specimens it is this matrix which is primarily responsible for the specimen self absorption. Concentrations of heavier elements from Na to Ca (Z=11 to Z=20) are usually sufficiently small that absorption in them is negligible. Therefore, adding a term to describe absorption in matrix to equation 4.6, the background shape in low energy end may be written as,

$$Low(P_K) = MBH(P_K)\ \varepsilon_L(P_K) \left[\frac{1 - \exp\left\{ -(\mu / \rho)_M\ \rho_M\ L \right\}}{(\mu / \rho)_M\ \rho_M\ L} \right] \qquad (5.2)$$

Where $(\mu/\rho)_M$ is the mean mass absorption coefficient of the matrix elements, and ρ_M is the density of the matrix.

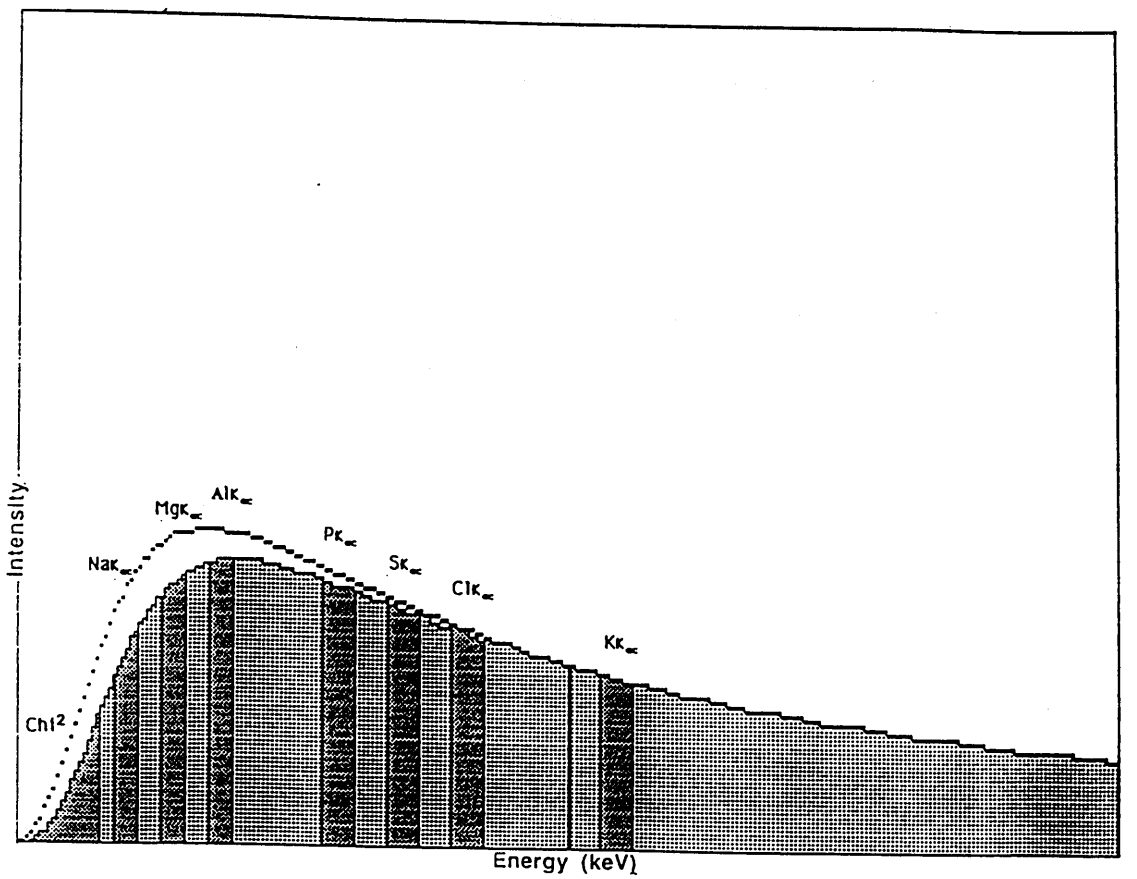

Figure 5.5

MBH background from thickest test section (≈ 200 nm) with position of elements of interest and the computed self absorption.

The modelled (universal background) shape can be matched to the measured (experimental) shape in the spectrum, by adjusting the product $\rho_M L$ (mass path length) for the best fit. If the Bremsstrahlung is modelled correctly in the region of a characteristic peak, it follows that the peak absorption will also be modelled correctly, since the absorption mechanisms are identical. Thus, this value of mass path length can then be used to correct the characteristic lines for absorption on the specimen (30 % for Na, 25 % for Mg in Figure 5.5). In order to compute a best fit of universal thin background to the experimental data, a chi-square test may be performed using a window below the Na peak (600 eV to 900 eV) as shown in figure 5.5.

5.7 Continuum Normalization Method of Quantitation

Continuum normalization method is based on the equation derived by Hall (1971), which has been widely accepted for the quantitation of thin biological samples. However it requires care in processing the data. The largest difficulty with this method occurs in obtaining accurate measurement of the Bremsstrahlung which originates from the sample only. However the advantages of the method are that concentrations obtained are independent of variation in section thickness and density, which are difficult to determine accurately, and it yields absolute values of dry weight concentrations, even though some elements (such as C, O, N, H, etc) may produce no detectable characteristic lines (when Be windowed detector is used).

A specimen is " thin " when its thickness is much less than the range of the incident electrons. It clearly depends upon the energy of the beam, density of the sample, and the section thickness. For unfixed and unstained soft biological samples this would be at least 0.5 μm in SEM and > 1.0μm in TEM instruments at higher accelerating voltages, provided no high atomic number atoms (such as Os, Pb, U, etc) of extrinsic origin or heavy deposits of intrinsic mineral [e.g hydroxyapatite, $Ca_5(PO_4)_3OH$] are present in the sample.

The derivation of quantitative data is based on the fact that the characteristic x-ray intensity is proportional to the number of atoms of the element in the volume of the sample excited by the electron beam, and the Bremsstrahlung intensity is a measure of mass thickness, provided the sections are thin. Hence the intensity of a part of the Bremsstrahlung free from characteristic lines, is used to normalize the characteristic lines of that spectrum against specimen mass thickness variations. This part of the Bremsstrahlung is often referred to as the " white window ", and must be set carefully in the region of the spectrum. Nicholson et al (1982) have pointed out that the assumption that the Bremsstrahlung production is proportional to Z^2 (as used by Hall) is an approximation and have evaluated its validity. They recommend criteria for selection of the white window to best satisfy this approximation. The analytical details of CN method are discussed in appendix 5.

5.8 Collection of Experimental Spectra

Cells of the bovine adrenal zona glomerulosa, known to exhibit an increased potassium efflux in response to

angiotensin, were used to produce test data. A batch of cells was divided into samples A (control) and B (stimulated). The full detail of the preparation of specimens and the standards is given in appendix 4. The ultrathin sections were examined in a J.E.O.L. J.E.M. 100C Transmission Electron Microscope (TEM) operating at 80 kV and equipped with a Kevex energy dispersive detector (EDS), having a detector area of 30 mm^2, the window thickness of 8 μm, and resolution rated at 142 eV and inclined at an angle of 90° with respect to the incident electron beam ($\theta_{\bullet}$). The specimen was tilted 30° with respect to the horizontal. The zero strobe peak and Ti K_α line were used to calibrate the analyser for gain and zero shifts. The spectra were collected over the range of 0 keV to 20 keV for 200 seconds live time at a resolution of 20 eV/channel.

The biological data were recorded by positioning a stationary electron beam inside the cytoplasm of the adrenal cell. Similarly for the aminoplastic standards, four different concentrations of each salt were examined using a stationary electron beam positioned over the section and at least 30 spectra were collected for each concentration. The spectra from the ultrathin sections of nylon were also examined using a stationary electron beam positioned by the side of the section.

5.9 Analysis of Thin Biological Spectra

Ten spectra were collected from each sample A & B using a Link Analytical model 290 analyser. The file format of these (290 format) spectra were converted into the format used by the Link Analytical AN10 analyser using a programme "CONVERT"

written by Paterson (1988).

Hall has not given any guidance for the optimum energy for the white window. However, he has suggested that the upper limit of the window must be below the average kinetic energy of the emergent electrons, so that throughout their trajectories the electrons remain capable of generating photons over the entire window. Shuman et al (1976) and Roomans et al (1980), suggest that this window should be near the maximum in the intensity of the thin specimen Bremsstrahlung, and minimum of any bulk signals. Shuman et al (1976) have suggested that the best region is 1.34-1.64 keV. However, for biological specimens, windows at low energies must be limited in width due to the presence of elemental peaks from the specimen and also it is undesirable that the window is set so low in energy that significant specimen self absorption occurs. Nicholson et al (1983) have reported that in determining the optimum window, the greatest importance must be given to the statistical accuracy of the white measurement. They suggest that a window several keV wide can be set in the photon energy range above 9 keV, with a higher statistical accuracy, even allowing for the increase in solid contributions to the Bremsstrahlung counts. This coincides with the window for which the Z^2 approximation holds good. Therefore, following them, a 5.0 keV wide window, which is centered at 12.0 keV is used for the work presented here.

The analysis of recorded biological spectra involves three stages. In first stage the recorded spectra are corrected for non-sample Bremsstrahlung. In the second stage net characteristic counts (background subtracted) are obtained from

the characteristic peaks of interest and in the third stage these net characteristic counts are converted into percentage absolute mass fractions by using the CN method.

The net characteristic counts of the peaks were obtained using window and background modelling methods as described in sections 5.4 and 5.5. Here, it may be noted that the window method uses a simple numerical factor for the correction of non-sample Bremsstrahlung contribution while the modelling method corrects the spectrum for this contribution on a channel by channel basis.

The extraction of net characteristic counts based on the window method were obtained by a fortran programme which is written for a Data General NOVA computer. The programme was written by Nicholson in 1977 and is still in use in the Physiology Institute of Glasgow University. In this method difficulties were involved in setting the windows on either side of the peaks. This can be seen from figure 5.3.

For the modelling method each recorded biological spectrum was corrected overall for the non-sample Bremsstrahlung contribution, so that pure "thin biological" spectra were obtained. The universal background spectrum was generated and then corrected for x-ray self absorption effect for each experimental spectrum by using computer programme AUTO. The details of the programme is given in appendix 2. Figures 5.6 and 5.7 show experimental spectra from samples A and B with universal background and the universal background corrected for self absorption superimposed.

Once the characteristic peak data are known, it is straight forward to use CN method for quantitation. Using the Hall

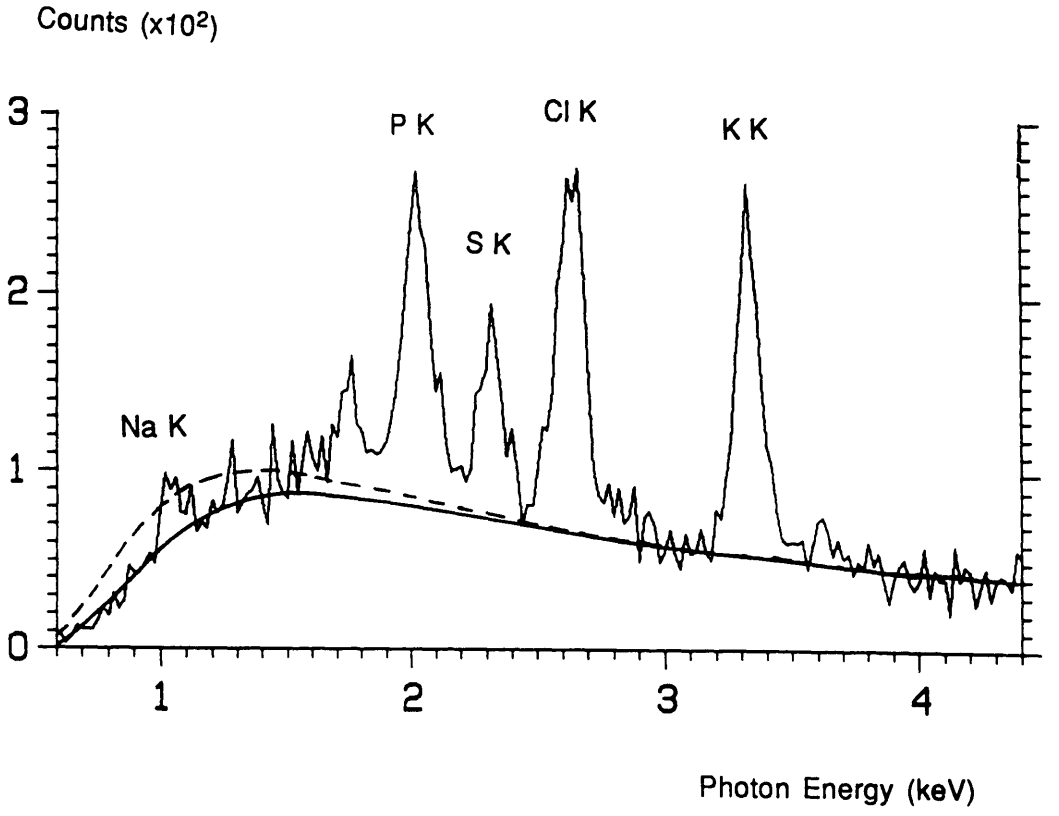

Figure 5.6

An experimental spectrum of sample A (control) with universal thin specimen background (broken line) and universal thin specimen background corrected for self absorption superimposed. (Data recorded on detector D.)

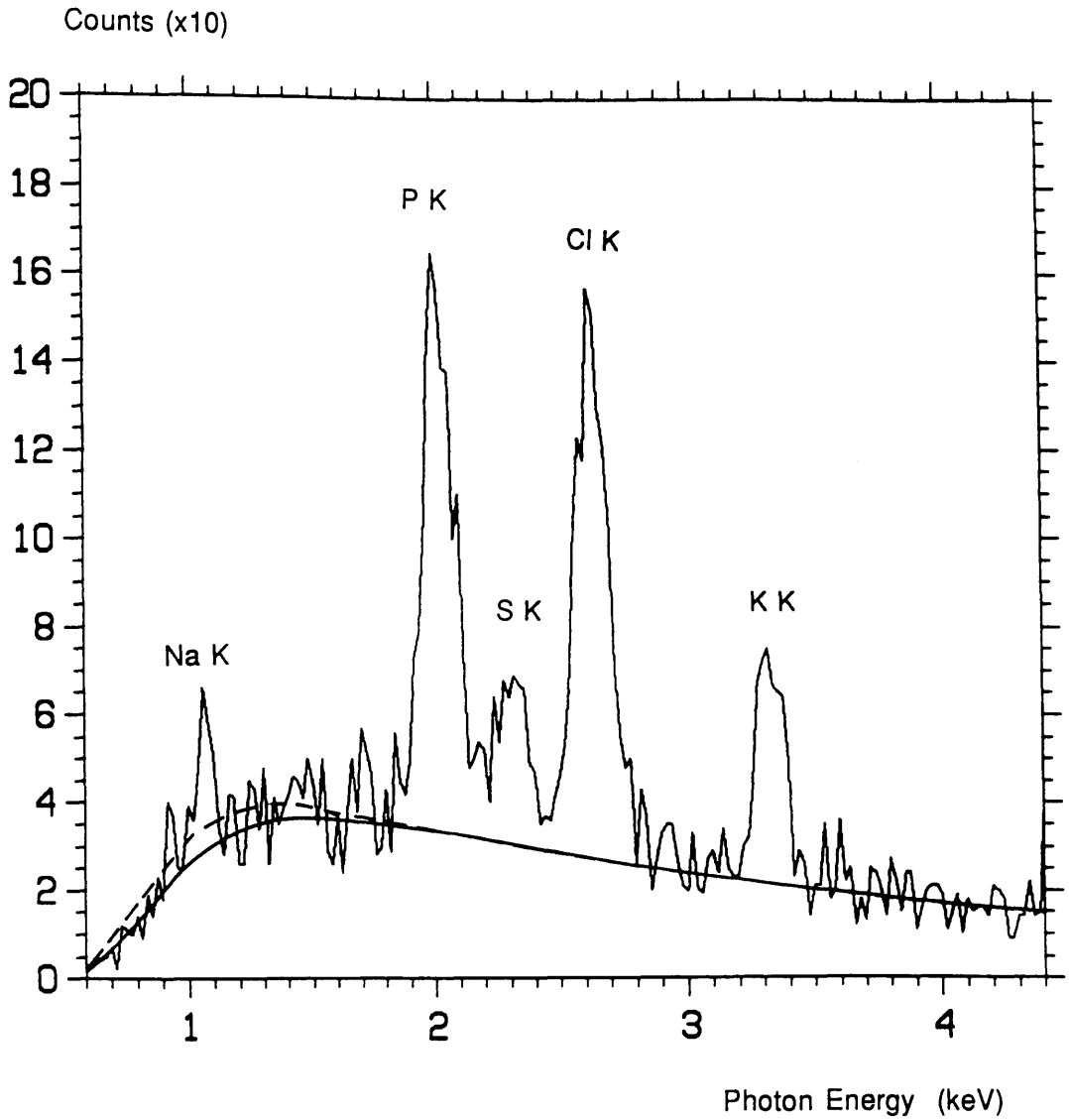

Figure 5.7

An experimental spectrum of sample B (stimulated) with universal thin specimen background (broken line) and universal thin specimen background corrected for self absorption superimposed. (Data recorded on detector D.)

equation as developed in appendix 5, the percentage mass fractions of each spectrum were obtained corresponding to the characteristic data obtained by window and modelling methods. These calculations were performed using programme HALL (see appendix 2). Then the values were combined to get a mean of Na, P, S, Cl, and K concentrations in a particular sample. These results are shown in table 5.1.

5.10 Error Analysis

The error in the counts of characteristic peaks may be obtained by reference to standard statistical arguments regarding counting experiments that follow Poisson statistics. The measured (gross) counts for a characteristic peak, say x, can be given:

$$P_{tx} = P_{nx} + B_t \tag{5.3}$$

where B_t is the total number of background counts under the characteristic peak. It can be shown (Zaluzec,1981) that corresponding error in the net counts for this situation is given by,

$$\frac{\Delta P_{nx}}{P_{nx}} = \sqrt{\frac{(P_{tx} + B_t)}{(P_{tx} - B_t)^2}} \tag{5.4}$$

In general, the statistical error in determining P_{tx} is negligibly small for EDX (Zaluzec, 1981).

In the window method of background subtraction, the

Method	Concentration ($mm\ kg^{-1}$)				
(a)	Na	P	S	Cl	K
Windows	125 ± 33	162 ± 16	100 ± 15	178 ± 15	99 ± 9
Modelling	106 ± 22	186 ± 8	118 ± 9	174 ± 7	95 ± 5
(b)					
Windows	153 ± 57	182 ± 29	91 ± 27	247 ± 27	75 ± 13
Modelling	157 ± 44	221 ± 14	111 ± 13	246 ± 12	71 ± 7

Table 5.1

Comparison between elemental concentrations computed in test adrenal cells by the MBH and windows methods of background subtraction for (a) control and (b) stimulated samples. Values are combined means ± statistical counting error.

background windows are a few channels wide. So the statistical error in B_t will be quite significant. Thus for that method, equation 5.4 is used to work out the statistical errors in the intensities of peaks of interest.

For modelling method, the background is predicted theoretically, so we can set a very wide window to minimise the statistical counting error. The same sort of size of error will be applicable for the background under the characteristic peaks. It was found that in this method this error was negligibly small. Therefore for such case equation 5.4 can be written as,

$$\frac{\Delta P_{nx}}{P_{nx}} = \sqrt{\frac{(P_{tx})}{(P_{nx})^2}} \qquad (5.5)$$

The other source of error in the modelling method is due to the error in determining the absorption path length when universal background shape is corrected for specimen self absorption. This type of error only effects the Na peak results.

The total error in the Na peak can be calculated by adding the errors in quadrature. For an example, a typical experimental spectrum background may be modelled by correcting the universal thin background for absorption in 600-800 nm of the specimen. When the scaled modelled background spectrum is subtracted from the measured one, say the net Na K counts is ≈ 400 on a background of 500 counts. Now the statistical error, accordind to equation 5.5, will be 7.5% (400 ± 30). The upper and lower limit(± 100 nm) of mass path length affects the Na K counts by 10 i.e. 2.5 %. Adding both

errors in quadrature, the total error in the net counts of the Na K line is ≈ 8%.

5.11 Results and Discussion

It can be seen from table 5.1 that at energies where the background is fairly flat and broad background windows can be placed, free of interference from other peaks, such as the K region, there is close agreement between the windows and modelling methods. However, the differences between the methods are significant for P and S peaks where, it is impossible to site background windows completely free from peak overlaps and the window method significantly underestimate the P. Moreover, the significant biological change in P concentration between the two samples which is shown by the modelling method is not apparent using the window method because of the poorer background counting statistics of this method. However, both methods reveal a significant intracellular fall of K ($P<0.02$) and rise in Na ($P<0.05$) and Cl ($P<0.01$) in the stimulated cells when the ten original spectral values in each group are compared by unpaired t-test.

From figure 5.5, it can be seen that specimen self absorption will significantly affect Na, Mg, and Al peaks, but for other characteristic peaks, this effect is so small that it can be neglected. A corollary of this statement is that if Na, Mg, and Al lines are not present in the sample, despite the fact that specimen self absorption is present in the sample, the universal thin background shape can be scaled to the experimental data and subtracted without modification.

CHAPTER 6

Specimen Self Absorption Corrections Using Characteristic Lines

6.1 Introduction

In this chapter the equations developed in chapter 3 to measure mass path length at each analysis point will be applied to different samples. The mass path lengths are then used to perform absorption corrections for the lower energy lines. Specimen thicknesses are also calculated. An ion beam thinned binary specimen of crystalline GaP was chosen as the model sample to test initially the viability of the approach. This is a simple and an ideal sample as it is of known composition and is wedge shaped so that spectra can be recorded from regions where the path length varies significantly from point to point. A more complex multilayer system is investigated to test the approach further. This system comprises alternating layers of InGaAs and InP, the former being approximately lattice matched to the latter. A description of such multilayer samples and their growth is discussed in detail in sections 6.2 and 6.3 respectively. The extent of beam broadening during the microanalysis of thicker specimens is an important effect, which is discussed in section 6.5.

The approach of measuring mass path length involves three

steps. Firstly, spectra are collected from a number of varying thicknesses of a particular sample, as discussed in section 6.4. Secondly, the characteristic data for the lines of interest are extracted from a measured spectrum, which is discussed in section 6.6 for GaP (and section 6.8.2 for InP). Finally, the characteristic counts of a particular line are used to determine the mass path length. This is discussed in sections 6.7 and 6.8 for GaP and InGaAs/InP respectively. In section 6.9 the results obtained from this approach are compared with the approach of absorption correction using the Bremsstrahlung. In section 6.10 the results obtained from this work are discussed briefly.

6.2 Multilayer Samples

For the past twenty years it has been possible to make semiconductor devices from compound semiconductors such as GaAs and InP, which are both capable of light emission and have higher carrier speeds than Si devices. Such III-V devices (so called because the materials comprise equal number of atoms from group III and V from the periodic table) have been fabricated on III-V material substrates.

Esaki and Tsu (1970) first introduced the growth of multilayer structures by the selective, alternate deposition of two compounds. A multilayer structure comprises layers of materials of differing compositions grown on a substrate. Some ternary (like $In_xGa_{1-x}As$ or $Al_xGa_{1-x}As$) and quaternary semiconductors (like $In_{1-x}Ga_xAs_yP_{1-y}$) in multilayers are common in use in a variety of optoelectronic applications. A major advantage of a ternary or quaternary semiconductor in

multilayers is that its electronic properties, such as the band gap, can be varied by changing the value of x or y. As a result, the growth of compound semiconductor multilayers has given rise to the development of multiple quantum wells.

One of the major applications for multiple quantum well structures has been in the development of semiconductor lasers for the telecommunications industry. Multiple quantum well lasers incorporating a $In_xGa_{1-x}As/InP$ superlattice have been of considerable interest because, depending on the value of well thickness and x, their emission wavelengths may be tuned to the wavelength range 1.1 to 1.6 μm (Mallard et al, 1987). One of the requirements for a good multiple quantum well laser is that layer thickness and interfacial abruptness can be accurately controlled.

The other most commonly used system for multilayer growth is the $Al_xGa_{1-x}As/GaAs$ system. This system has some advantages over the $In_xGa_{1-x}As/InP$ system. An advantage to using this particular configuration is that, irrespective of the value of x selected, the lattice parameter of $Al_xGa_{1-x}As$ is very similar to that of GaAs. Such close lattice matching enables the growth of high quality multilayers with very few misfit dislocations at interfaces. The majority of devices fabricated from this multilayer system have been used for fast logic and microwave applications. The band gap in the $Al_xGa_{1-x}As/GaAs$ system dictate that optoelectronic devices fabricated from the system operate at wavelengths of typically <850 nm.

In addition to systems as described above ($Al_xGa_{1-x}As/GaAs$, $In_{1-x}Ga_xAs_yP_{1-y}/InP$ and $In_xGa_{1-x}As/InP$), a wide range of materials can be used in the formation of compound

semiconductor multilayers (see Osbourne, 1983; Bean et al, 1984; Rosbec and Harper, 1987; Cullis et al,1987). However, in this thesis only $In_xGa_{1-x}As/InP$ and $Al_xGa_{1-x}As/GaAs$ multilayer samples have been analysed. They are particularly suitable for investigating the success of performing absorption corrections using the counts of the characteristic lines.

6.3 Growth of Multilayer Samples

Group III-V materials are usually obtained via epitaxial growth techniques such as molecular beam epitaxy (MBE) and metal-organic chemical vapor deposition (MOCVD). Epitaxial growth is widely used in both the III-V industry and research because it produces stacking of thin films of different materials. Layer growth is obtained by introducing atoms onto a atomically flat heated substrate.

The system investigated here (InGaAs/InP) has been grown by MOCVD. The system was grown on InP substrates from the reaction of the metal-organic gases trimethyl-indium and trimethyl-gallium with the hydrides arsine (AsH_3) and phosphine (PH_3) at atmospheric pressure in an MOCVD reaction chamber using hydrogen as the carrier gas. The hydrogen gas not only transferred the reactants to and from the chamber, but use of this gas also avoids the deposition of carbon in the chamber in the course of a reaction. Bass et al (1986 and 1987) have described the MOCVD reactor design and gas flow system in detail.

The AlGaAs/GaAs system investigated (see next chapter) was grown by MBE, which involves the generation of molecular beams from solid thermal sources. The generated thermal beams

interact on a heated crystalline substrate in a deposition chamber to produce a single crystal layer. The interaction of molecular beams with a crystalline substrate in the deposition chamber must occur under high vacuum (total pressure < 10^{-10} torr). In order to get deposition of epilayers, the substrate is heated to a suitable temperature (≈ 600 C°) and is rotated at a constant rate. The substrate rotation rate and the temperature are the two main factors which effect the quality of the material grown by this technique (see Alavi et al, 1983; Hull et al, 1986). Davies and Andrenes (1985) and Joyce (1985) have given a detailed review of this technique.

6.4 Instrumentation

The semiconductor specimens were prepared for electron microscopy following a method described by Chew and Cullis (1987). This technique involved reactive ion milling with iodine as the final stage of preparation. The thinned specimen has surface approximately parallel to the [110] pole so that the layers, grown on the [001] face of the substrate, run approximately vertically through the sample. The precise attainment of the condition in electron microscope was achieved through the use of Kikuchi patterns. The specimens were tilted through ≈ 22° from the [110] pole along the [004] Kikuchi band. In this orientation the layers remain parallel to the beam whilst the tilts of specimens away from the pole is desirable to minimise the electron channeling effects (Glas, 1986).

The specimen drift in the electron microscope was reduced

to a minimum by loading the specimen, supported in a double-tilt Be cartridge, into the microscope several hours before data acquisition was begun.

Both samples investigated in this chapter were examined in the Glasgow University extended VG HB5 STEM operating at 100 kV. It was equipped with a Link Systems conventional Be windowed x-ray detector (see table 4.1, detector A). The detector was located at an angle of ≈100° with respect to the incident beam direction (θ_0). GaP spectra were collected over the energy range of 0 to 20 keV and those of the InGaAs/InP multilayer system 0 to 40 keV at a resolution of 20 eV per channel. The spectra were recorded from the center of the layer.

The acquisition and processing of spectra were accomplished using a Link Analytical AN10000 System. The regions were selected so that spectra from both thin and thick areas were recorded. Using the experimental conditions defined, an acquisition time between 30 and 60 seconds was found to yield signals from thicker regions of the samples of sufficient statistical significance. For example, ≈9000 counts in the P K peak from the GaP specimen and ≈4000 counts in the P K peak from the InP specimen were recorded when the beam was centered at the thickest point of the particular specimen. However, for the spectra recorded from the thin areas, an acquisition time of 100 seconds was found to be required for sufficient statistical significance.

6.5 Beam Broadening in the Specimen

All of the electrons incident on a thin foil potentially

contribute to x-ray production and those scattered through the greatest angles define the effective width of the x-ray source size and hence the spatial resolution for analysis. The spatial resolution in a thin foil is a function of the mean atomic number Z', specimen thickness t and the incident electron energy T_0.

Goldstein et al (1977) have proposed a simple model for beam broadening in which it was assumed that each incident electron suffered a single, elastic, large-angle Rutherford scattering event at the center of the foil (see figure 6.1) and derived an analytical expression,

$$b = (6.25)10^5 \frac{Z'}{T_0}\left(\frac{\rho}{W'}\right)^{0.5} t^{1.5} \qquad (6.1)$$

where T_0 is in eV, W' is the mean atomic weight, ρ is in gm cm^{-3} and t is in cm, giving the value of the broadening parameter b in cm.

This analytical expression defines the x-ray source size as that in which 90 % of the transmitted electrons are contained. The parameter b is a measure of the beam spreading at the bottom surface of the foil for a scattering event which occurs at the center of the foil. This scattering model is discussed in detail by Goodhew and Chescoe (1980). Although the model of Goldstein et al is based on a single scattering treatment, the values of the beam broadening which it predicts agree remarkably well with the Monto-carlo calculations of Kyser and Geiss (1977) and with experimental measurements by Hutchins et al (1979) and Champness et al (1980).

Cliff and Lorimer (1981) have derived a simple model based

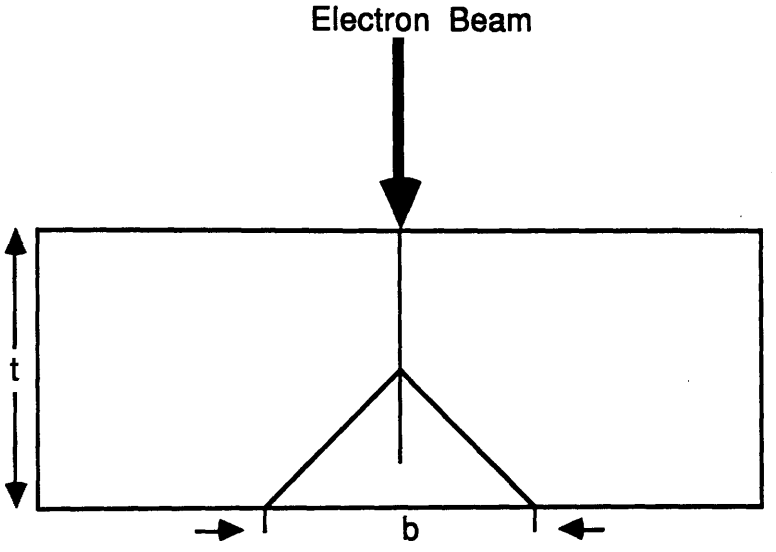

Figure 6.1
Single scattering model.

on the concepts of plural scattering and have shown that the expression for this model, with some assumptions, may be reduced to an expression identical to that of Goldstein et al. They have also shown that even for specimens for which the single scattering assumption is invalid, the expression of Goldstein et al can still be used to estimate the extent of the beam broadening in a thin foil. They claim that in such a case the results of the single scattering model of Goldstein et al are in good agreement with their experimental results upto a thickness of ≈400 nm but then diverge to give an overestimate of broadening.

6.6 Extraction of Characteristic Counts from Spectra of GaP

For this particular sample the characteristic x-ray counts from Ga K_α, Ga L and P K peaks are required for the investigation of absorption corrections. The background in the energy region of the Ga K_α peak is small and its energy variation slow; therefore, the characteristic x-ray counts of Ga K_α can be determined by a simple linear interpolation of the background on either side of the peak (see chapter 5). Figure 6.2 shows part of a spectrum from a thin region of GaP with a theoretical background (modelled as discussed in section 6.9). It can be seen that the variation of background intensity near the P K peak is slow. For the Ga L line the background variation is more rapid. However, the peak to background ratio is large and therefore use of linear interpolation is still reasonable.

All the recorded x-ray spectra analysed in this chapter were normalised to the same electron dose. Counting times were

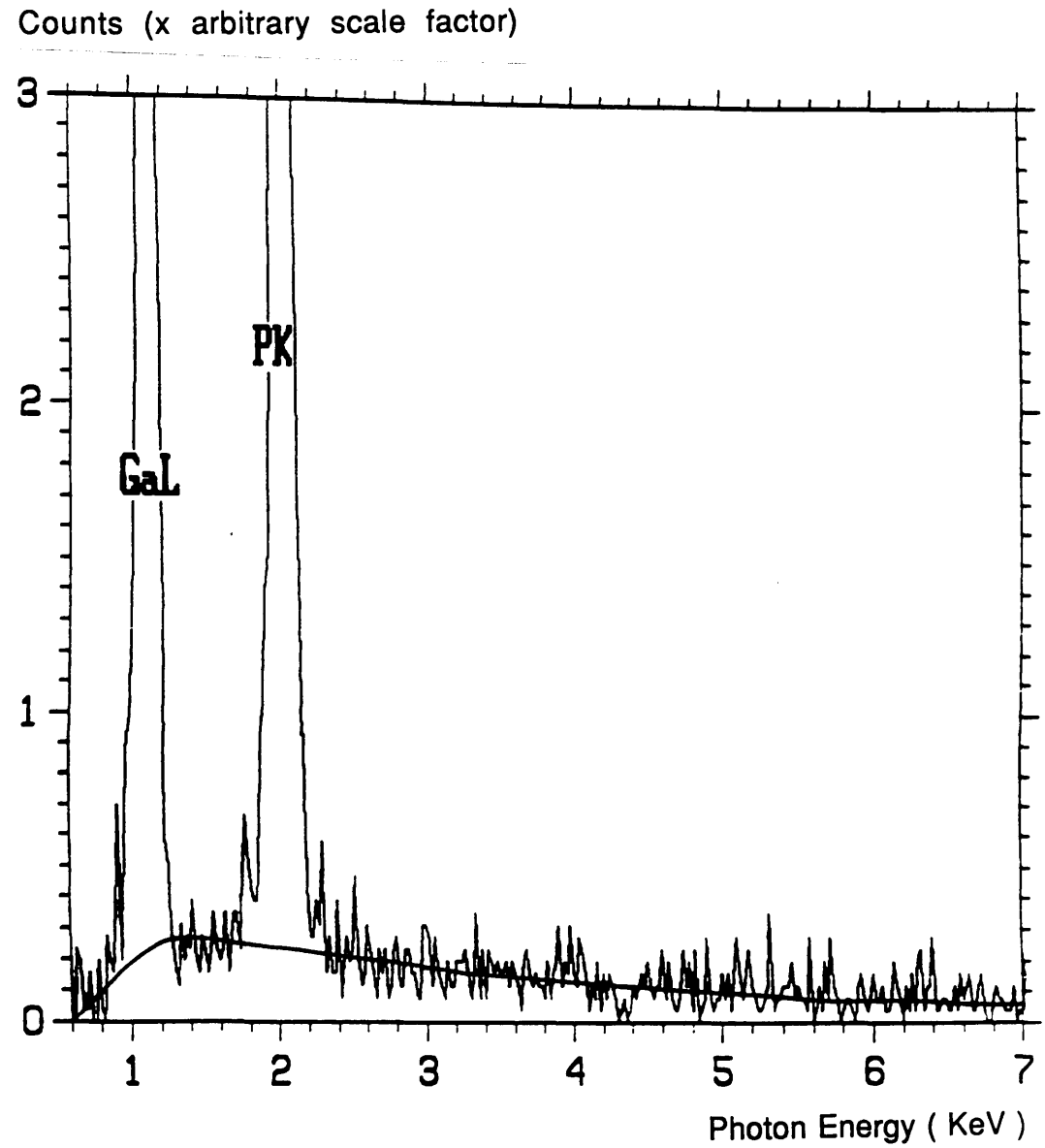

Figure 6.2

Experimental spectrum from GaP for a thin region (≈10 nm) with theoretical thin specimen background superimposed.

normalised to 100s. The current used for normalisation typically 100 nA, was that measured on the virtual objective aperture blade, situated before the first condenser lens in a plane approximately conjugate to that occupied by the real objective aperture. This current is proportional to the beam current (typically 0.4 nA) which was occasionally measured on the objective aperture blade for calibration of the virtual objective aperture current. Use of a virtual objective aperture had also advantages in eliminating undesirable artifacts from the x-ray spectra. For such large peaks on a small background, the error in the counts of characteristic peaks may be obtained by using equation 5.4.

6.7 Absorption Corrections for GaP

In this sample P K and Ga L signals are heavily absorbed in the thicker regions. However, it is assumed initially that absorption of the Ga K_α signal is negligible in this sample. Hence the Ga K_α intensity may be taken to be proportional to specimen thickness and used with the Ga L or P K intensity in equation 3.18 to deduce the mass path length.

6.7.1 Fitting of P K and Ga K_α Counts

Substituting N_{GaK} for N_A and N_{PK} for N_B, equation 3.18 can be written as,

$$N_{iPK} = K\ N_{iGaK}\ \frac{[\ 1-\exp(-\eta\ N_{iGaK})\ ]}{\eta\ N_{iGaK}} \qquad (6.2)$$

The index i in above equation (and in all such equations shown in this chapter) runs over the number of data points used for the fitting. When the data from 16 points were fitted to this equation, the values of the fitting parameters obtained were K=0.9 and $\eta = 7.0 \times 10^{-4}$ with relative errors of ≈2% and ≈6% respectively. For this particular sample the atomic concentrations of Ga and P are known. Therefore, mass fractions can be obtained by using the general equation,

$$w'_j = \frac{C_j \, W_j}{\sum_r (C_r \, W_r)} \qquad (6.3)$$

Where C_j is the atomic fraction or atomic concentration and W_j the atomic weight of the element j in the sample and sum r runs over all elements of the sample.

Once mass fractions are known, equation 2.8 can be used to calculate the mass absorption coefficient of P K (or Ga L) in the GaP sample. With mass ratios Ga : P = 0.69 : 0.31, the value of the mass absorption coefficient for the P K line was calculated using equation 2.8. This value of mass absorption coefficient (1893 $cm^2\ gm^{-1}$) when used in equation 3.19 gave the best value of the parameter Ψ. This value of Ψ [$(3.7 \pm 0.2) \times 10^{-7}$ gm cm^{-2}] was then used to convert N_{GaK} into mass path length at each analysis point using equation 3.15.

Figure 6.3 shows equation 6.2 which, with the best values of K and Ψ, passes through the origin within experimental error. The error bars shown represent the statistical counting errors of the P K line at the individual analysis points. (The statistical

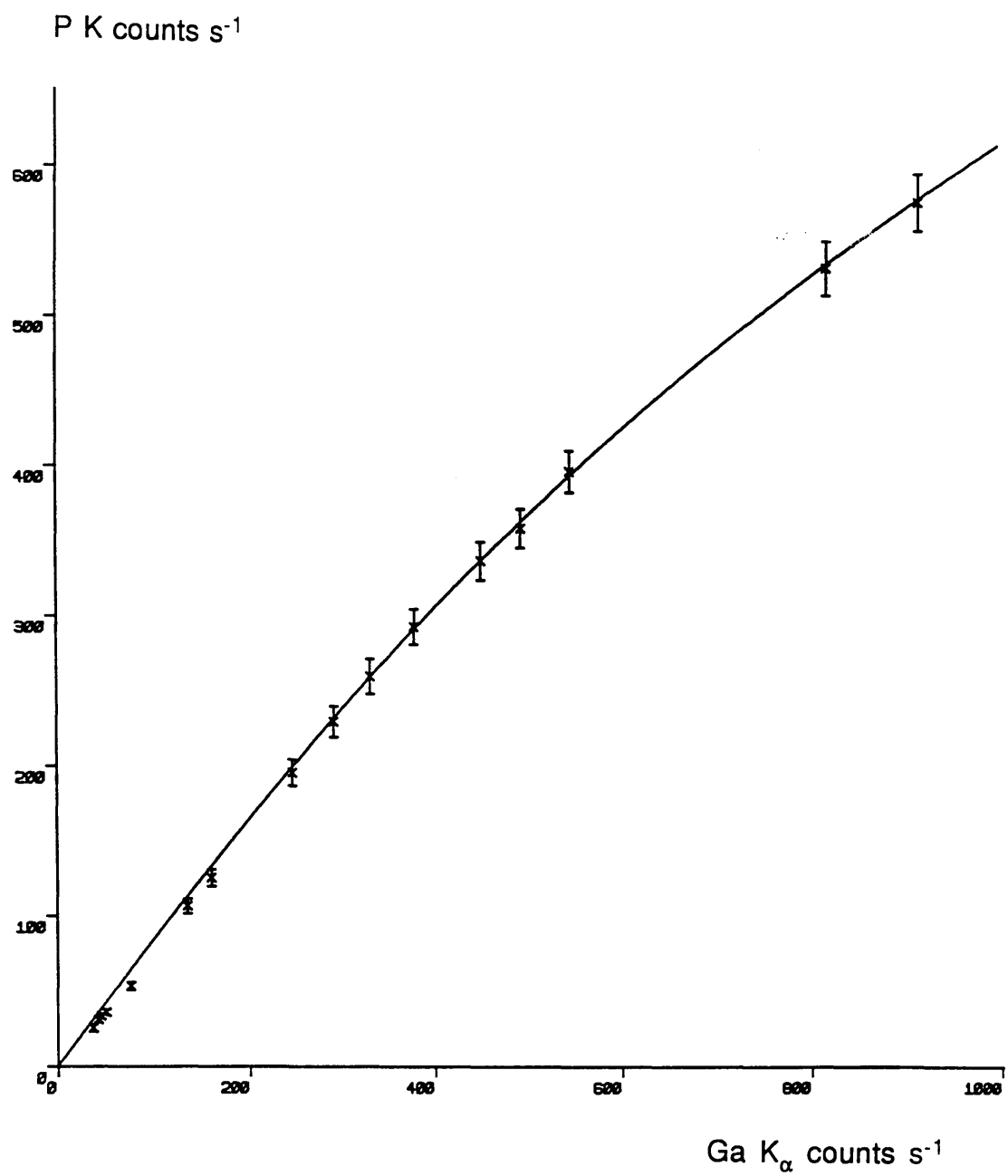

Figure 6.3

Experimental P K and Ga K_α counts s^{-1} with the best fit of equation 6.2 superimposed.

errors in the Ga K_α line, although not shown, were similar to those in the P K line.)

The density of this sample is known (ρ_{GaP}=4.13 gm cm^{-3}), therefore, the values of mass path length can be converted to an x-ray absorption path length by using equation 3.14. An approximate value of the geometric factor (G) can be calculated for this sample using equation A3.2 (see appendix 3) and thus use of equation 3.6 can give an approximate estimate of thickness at each analysis point. The value of the geometric factor calculated for this sample was 2.8, assuming the specimen to be parallel sided. In reality the samples investigated were approximately wedge shaped due to the ion beam thinning process. For such samples the wedge shaped geometry (see appendix 3) is required for the calculation of G. Due to the variability of the wedge shaped geometry and unavailability of wedge angle, thickness calculations were based on the rather simplistic parallel geometry so that the value of G may have large uncertainties.

Table 6.1 shows the best values of mass path length, x-ray absorption path length and approximate estimates of thickness along with the percentage absorption of the P K line at each analysis point. The relative error quoted for the mass path length and absorption path length is the fitting error. The error quoted for the absorption of individual lines was estimated numerically from the error in the individual fitting parameter (Ψ). Table 6.2 shows the values of mass absorption coefficient of the P K line and fitting parameters used in this analysis. The absorption of the Ga K_α signal at the thickest point (820 nm absorption path length) is 0.8%, which justifies the initial assumption that absorption of Ga K_α signal is negligible.

6.7.2 Fitting of Ga L and Ga K_α Counts

Substituting N_{GaK} for N_A and N_{GaL} for N_B , equation 3.18 can be written as,

$$N_{iGaL} = K' \, N_{iGaK} \, \frac{[\, 1 - \exp(-\eta' \, N_{iGaK}) \,]}{\eta' \, N_{iGaK}} \qquad (6.4)$$

In a similar way to that described in the previous section the data from 16 points were fitted to the above equation to get the best values of the fitting parameters. The values obtained were as $K' = 0.52 \pm 0.01$ and $\eta' = (5.3 \pm 0.4) \times 10^{-4}$ corresponding to relative errors of ≈2% and ≈9% respectively. The value of the mass absorption coefficient for Ga L in GaP was calculated to be 1400 $cm^2 \, gm^{-1}$. This value of mass absorption coefficient was used in equation 3.19 to get the value of the parameter Ψ' [$(3.8 \pm 0.3) \times 10^{-7}$ gm cm^{-2}]. Figure 6.4 shows equation 6.4 with the best values of K' and η' which again, within experimental error, passes through the origin. The error bars shown represent the statistical counting errors of the Ga L line at the individual analysis points. The values of the percentage absorption of Ga L signal are shown in table 6.1.

It can be seen from table 6.2 that the values of Ψ and Ψ' obtained from two fittings are in good agreement and can be used to calculate the thickness assuming a value for G. The value of the constant K ($=k_{GaP} \, . C_P/C_{Ga}$) obtained from P K and Ga K_α fitting is the same as Horita's $(k_{GaP})_0$ and could be used as an experimental k-factor for GaP for other samples where absorption is negligible. The value of K' obtained from Ga L and

Point	Mass P.Length ($gm\ cm^{-2}$) (10^{-4})	Absorption P.Length (nm)	Thickness (nm)	% Absorption of Lines PK	GaL
01	.13	32	11	1.2±0.1	0.9±.06
02	.15	36	13	1.4±0.1	1.0±.08
03	.16	40	14	1.5±0.1	1.1±.08
04	.18	45	16	1.7±0.1	1.2±0.1
05	.28	70	25	2.6±0.2	2.0±0.1
06	.50	120	45	4.6±0.3	3.4±0.2
07	.60	145	50	5.5±0.3	4.0±0.3
08	.90	220	80	8.0±0.5	6.0±0.4
09	1.1	270	95	10.0±0.7	7.0±0.5
10	1.2	290	100	11.0±0.7	8.0±0.5
11	1.4	340	120	12.0±1.0	9.0±0.7
12	1.7	410	150	14.0±1.0	11.0±0.8
13	1.8	440	160	15.0±1.0	12.0±0.8
14	2.	485	175	17.0±1.2	13.0±0.9
15	3.	730	260	24.0±1.5	18.0±1.1
16	3.4	820	300	26.0±1.6	20.0±1.2

Table 6.1

Results of the absorption corrections of GaP sample. The typical error is 6 % in both the mass and absorption path lengths.

Fitting	μ/ρ $cm^2\ gm^{-1}$	K	ψ $gm\ cm^{-2}$ $(x\ 10^{-7})$
P K : Ga K_α	1893	0.90±0.02	3.72±0.22
Ga L : Ga K_α	1400	0.52±0.01	3.80±0.30

Table 6.2

Fitting parameteres used in GaP analysis.

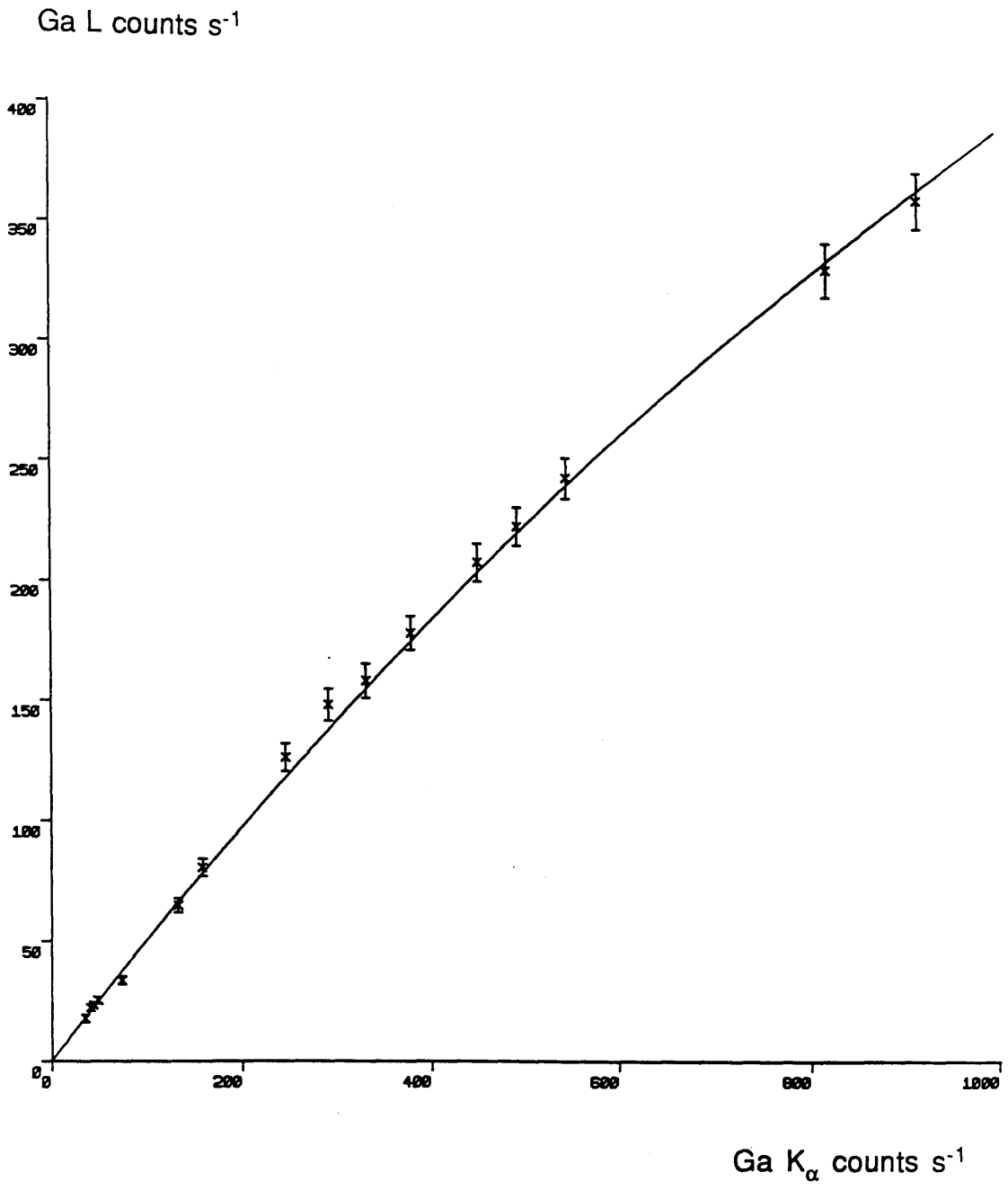

Figure 6.4

Experimental Ga L and Ga K_α counts s^{-1} with the best fit of equation 6.4 superimposed.

Ga K_α fitting can be used to determine the ionisation cross section ratio of the total Ga L to the Ga K_α by the insertion of suitable atomic constants (see equation 3.5). This gives a value of 14.1 which is in good agreement with Paterson et al (1989). From these results the technique looks promising and an investigation of a more complex sample in which some elemental concentrations are unknown is described in the next section.

6.8 Absorption Corrections for an InGaAs/InP Sample

6.8.1 Introduction

Spectra were collected from varying thicknesses and several layers of an InGaAs/InP multilayer sample. To minimise interference in the spectra due to x-rays being generated in neighbouring layers, the sample was carefully orientated so that the layers were parallel to the incident electron beam, but away from any strong diffraction condition since this is known to affect the relative intensities of the generated characteristic lines (Glas, 1986). No analysis was made of spectra from the InGaAs layers as absorption of lines In K_α, Ga K_α, and As K_α is not likely to be significant in any sample thin enough to be suitable for transmission electron microscopy.

However, the data recorded from InP layer proved suitable for this investigation. Figure 6.5 shows a typical EDX spectrum collected from an InP layer in an InGaAs/InP multilayer system. The presence of both Ga and As in the layer is indicated by their characteristic lines being visible in the spectra. Chew et al

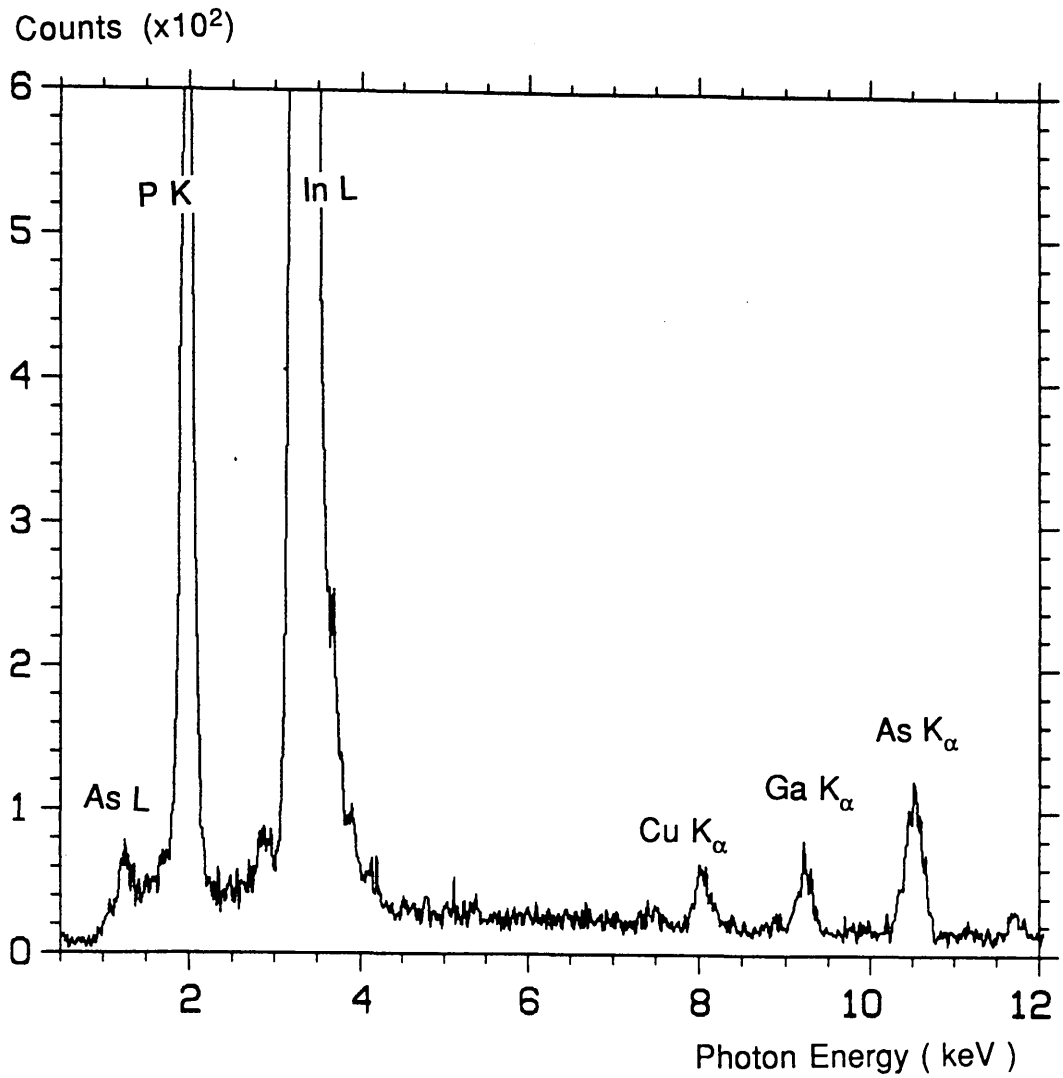

Figure 6.5

A typical EDX spectrum recorded from InP layer of InGaAs/InP multilayer sample.

(1987) and Barnett et al (1988) have reported that an appreciable As content was present in the InP layer for this particular sample. Chapman et al (1987) and McGibbon et al (1989) have reported the presence of Ga content as well as As in such samples.

Although the concentrations of Ga and As are small, they show significant variations which affect both the atomic concentrations (see table 6.4) and the mean mass absorption coefficients of the sample (particularly for P K_α, variation of which is within ≈ 8 %). Thus this system is a suitable specimen of greater complexity for absorption corrections. McGibbon (1989) provides analytical data from the same sample, but from regions in which specimen self absorption can be neglected.

6.8.2 Extraction of X-ray Counts from $In_{1-x}Ga_xAs_yP_{1-y}$ Spectra

The technique of linear interpolation is also applicable for the extraction of P K, In L, Ga K_α, As K_α, and In K_α line signals from this series of spectra. However, there is difficulty with the extraction of As K_α line, which overlap with Ga K_β . The difficulty with the As K line can be resolved by calculating the number of Ga K_β counts using a knowledge of the partitioning of the characteristic photons between the K_α and K_β lines for Ga and then subtracting these counts from the total counts of the combined peak of As K_α and Ga K_β . The partition function has a value of 0.873 for Ga.

The In L_α line overlaps with the other L sublines. A theoretical Gaussian distribution which describes an In L_α peak

can be calculated by using equation 4.4 as the peak amplitude (A_A) and the centroid energy $\{P_K\}_A$ are known, and the FWHM of the In L_α peak for this particular detector can be calculated using equation 4.5. However, the error in this technique may be large as it depends directly on the counts in the single centroid channel (A_A). The method used here is to first subtract the background by linear interpolation from just below the In L_α line to just above the In L_γ and, secondly, to record the number of counts in the lower energy half of the peak. By doubling this value, an estimate of the detected In L_α line is obtained. Figure 6.6 shows such an estimated In L_α line.

It is known that in this sample P K and In L_α signals are heavily absorbed in the thicker regions. However, it may be assumed that absorption of the In K_α signal is negligible in this sample and equation 3.18 can be used to deduce the mass path length. The possibilities of using either the combined peak of In L_α and In L_β or In L_α alone as the absorbed line are also examined.

6.8.3 Fitting of P K and In K_α Counts

It can be seen from figure 6.5 that the concentrations of Ga and As are much smaller than those of In and P. For a first approximation equation 3.18 can be used to correct the P K signal without the necessity of knowing any mass absorption coefficients. This can give a first set of approximate values for atomic fractions for each analysis point and then an iterative process can be used to get better values of atomic fractions in the sample. Substituting In K_α counts for N_A and P K counts for N_B, equation 3.18 can be rewritten as,

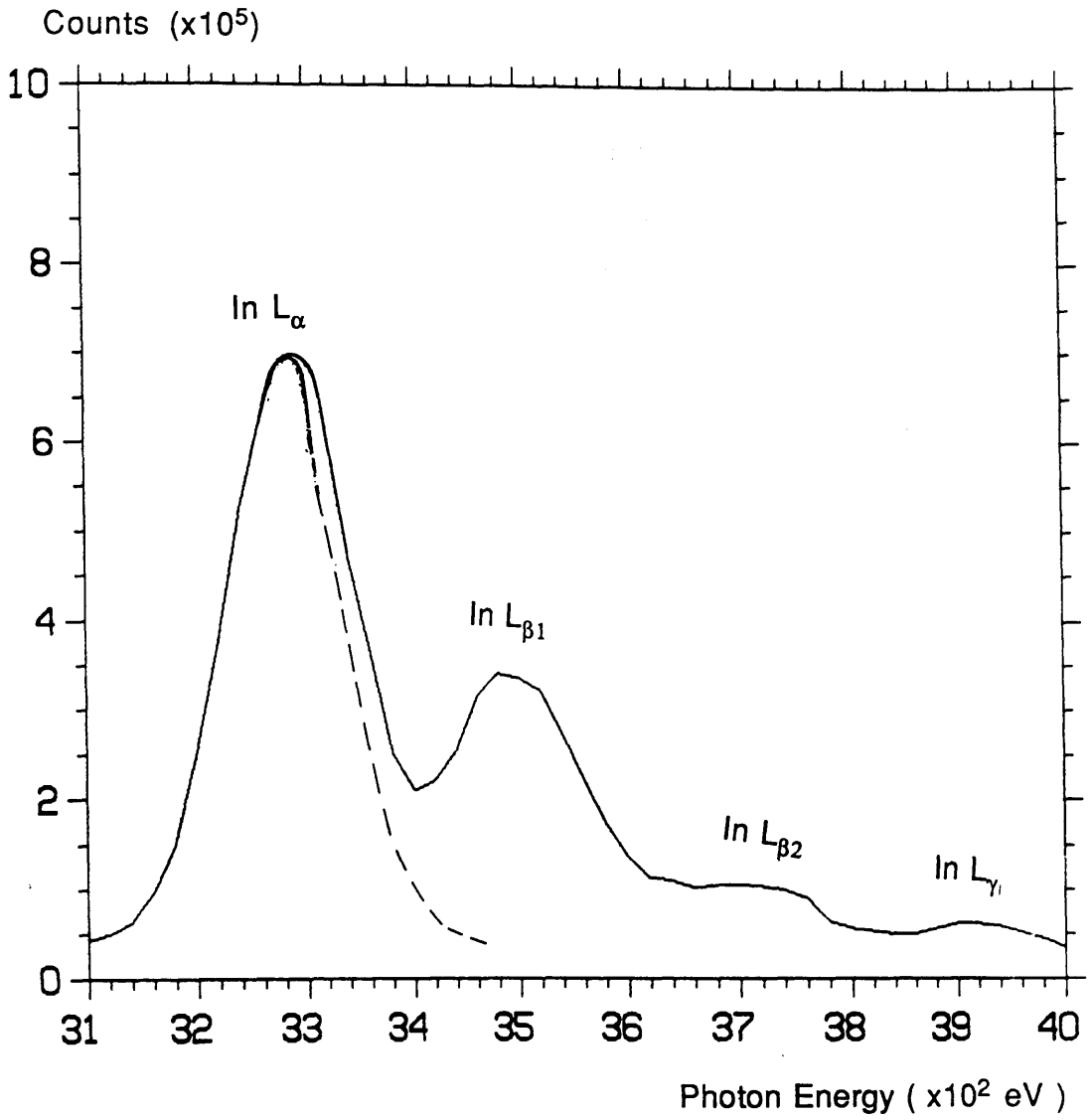

Figure 6.6

Experimental In L lines with the separated In L_α line superimposed.

$$N_{iPK} = K\ N_{iInK}\ \frac{[\ 1-\exp(-\eta\ N_{iInK})\ ]}{\eta\ N_{iInK}} \qquad (6.5)$$

Data were fitted to this equation and the values of the fitting parameters were obtained . The P K signal was corrected at each point and hence the first approximate atomic concentrations were calculated for the sample at each analysis point. For this particular compound sample equation 3.4 can be re-written as,

$$C_{In} = C_{Ga}\ R_1 \qquad (6.6)$$

$$C_{As} = C_{Ga}/R_2 \qquad (6.7)$$

$$C_P = C_{As}/R_3 = (C_{Ga}/R_2)/R_3 \qquad (6.8)$$

Where,

$R_1 = k_{InGa}\ (N_{In}/N_{Ga})$, $R_2 = k_{GaAs}\ (N_{Ga}/N_{As})$ and $R_3 = k_{AsP}\ (N_{As}/N_P)$.

The k-factor for GaAs (k_{GaAs}) was determined experimentally to be 0.90 from x-ray analysis of a pure GaAs specimen using standard experimental conditions but with longer acquisition times to reduce the statistical uncertainties. k-factor values may be interrelated by a chain rule defined by,

$$k_{ji} = k_{jl}\ k_{li} \qquad (6.9)$$

Using experimental values of k_{GaAs} (0.90) and k_{GaP} (0.90) in equation 6.9 the value of k_{AsP} was calculated to be 1.0 which agrees with the theoretical value within ≈ 2.0%. Similarly, the chain rule was used for deriving value for k_{InGa} as 4.62. Here, it

Because C_{Ga} is a small, calculations based on the equation of quantitation used could lead to large errors. This could be avoided by starting from the composition of one of the major elements such as In.

may be noted that the theoretical values for k-factors can be calculated by using the programme KVALUE (see appendix 2). This programme is based on the recent work of Paterson et al (1989).

In this sample, the sum of atomic fractions of elements of group III and those in group V must be equal to one as the material is known to be structurally perfect (group III atoms on one sub-lattice and group V atoms on the other). Therefore, using the normalization relationship (Σ C =2), $C_{In} + C_{Ga} + C_{As} + C_P = 2$, we can write as,

$$C_{Ga} = \frac{2}{\left(1 + R_1 + \frac{1}{R_2} + \frac{1}{R_2 . R_3}\right)}$$

Once C_{Ga} is known then equation 6.6, 6.7 and 6.8 can be used to work out the atomic ratios for the other three elements in the sample. The programme RATIO (see appendix 2) was used to first correct the P K signal for self absorption and then calculate initial values of the atomic concentrations of the four elements in the sample. These were used to calculate a set of mass absorption absorption coefficients for P K at each point and then equation 3.17 could be used. An iterative process was continued until convergence occurred (after the third iteration). The convergence criterion used was that the concentrations of In and P showed no change in the third significant digit between iterations. After the first iteration it became clear that the first three data points had substantially different compositions from the rest of the set. It was believed that the In

Although it is known that in the InGaAs/InP multilayer system the lattice constant changes with composition, the error in neglecting this (for the density calculation) is small compared to other errors in the calculation for which density is required.

concentration in these regions of the specimen were reduced by radiation damage (Bullock et al, 1987) and these points were excluded from the fitting procedure. Thus the final values of the fitting parameters K and Ψ were obtained. Figure 6.7 shows equation 3.17 fitted for this particular sample with the best values of K and Ψ. The best values of fitting parameters are shown in table 6.3, with a relative error of ≈3% in K and ≈8% in Ψ. Table 6.4 shows the best estimates of the atomic fractions of each element at each analysis point. The error quoted for atomic fractions of individual elements was estimated numerically from the errors in the individual fitting parameters.

The lattice constant for InP (a = 0.587 nm) can be used to estimate the sample density at each analysis point. The total mass of the sample in one unit cell can be calculated and then dividing it by the volume of the cell, the density of the sample is obtained. The best estimate of sample density at each analysis point is also shown in table 6.4. The error in the densities is primarily due to the error in the concentrations from which they are calculated. Thus the proportionate errors in the densities are similar to those for the concentrations shown in table 6.4. Using these densities, estimates of the absorption path length at each analysis point were obtained using equation 3.14. The geometric factor was estimated in a similar way as that in the GaP case. An approximate estimate of the value of G for this sample was 3.4. This value of G was used to convert absorption path length to approximate thickness of the analysis point. Table 6.5 shows the best estimates of mass path length and approximate estimates of absorption path length and thickness at each analysis point (excluding the first three

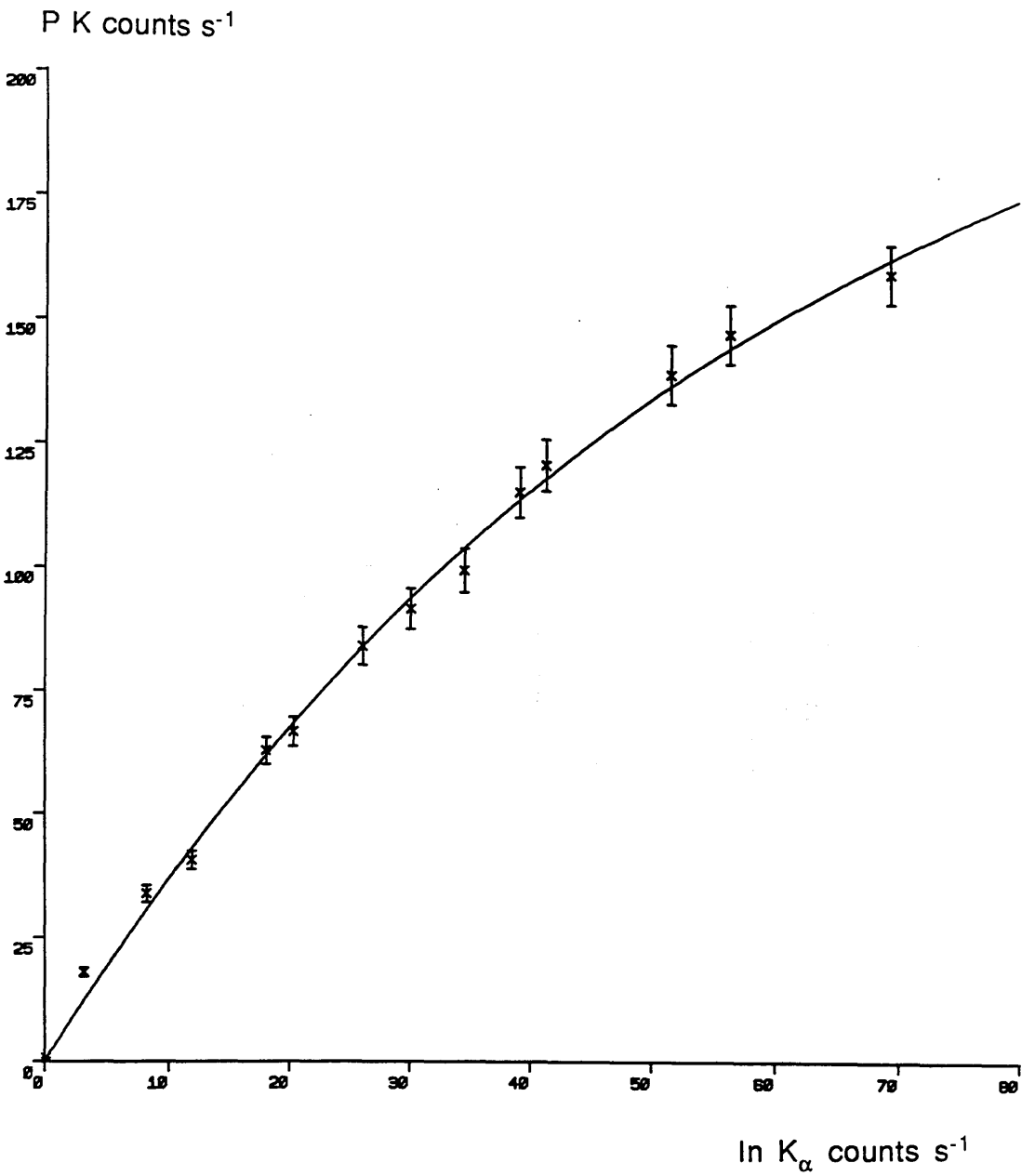

Figure 6.7

Experimental P K and In K_α counts s^{-1} with the best fit of theoretical equation superimposed.

Fitting	μ/ρ	K	ψ gm cm^{-2} ($\times 10^{-5}$)
P K : In K_α	P K	4.0±0.1	1.17 ±0.10
In L_α+In L_β : In K_α	In L_α	6.8±0.2	1.05 ±0.22
In L_α+In L_β : In K_α	weighted	6.8±0.2	1.10 ±0.18
In L_α : In K_α	In L_α	5.2±0.1	1.14 ±0.14

Table 6.3

Fitting parameter s used in InP analysis.

Point	% In	%Ga	% As	% P	ρ gm cm^{-3}
01	79 ±2	1.40±0.03	8.0±0.5	112±5	4.5
02	74 ±2	0.40±0.01	4.0±0.3	121±5	4.4
03	94 ±2	0.20±0.01	2.6±0.2	103±5	5.0±0.3
04	93.0±1.5	5.00±0.13	15.0±0.9	88±4	5.1
05	96.0±1.5	2.00±0.05	8.0±0.5	93±4	5.
06	93.0±1.4	5.00±0.13	12.0±0.8	90±4	4.9
07	99.0±1.3	0.80±0.02	5.0±0.3	96±4	5.4±0.2
08	100.0±0.9	1.00±0.03	3.4±0.3	96±3	5.5
09	100.0±0.9	1.00±0.03	4.6±0.3	95±3	5.4
10	97.0±1.0	2.00±0.05	5.6±0.3	94±3	5.2
11	99.0±1.0	0.80±0.02	7.0±0.4	94±2	5.3±0.2
12	98.0±1.0	2.60±0.07	5.6±0.3	94±2	5.2
13	98.0±0.8	2.40±0.06	6.6±0.3	94±2	5.2
14	98.0±0.7	2.60±0.07	8.0±0.5	93±2	5.1

Table 6.4

Atomic concentrations of In, Ga, As and P in InGaAsP sample. Some typical standard errors in the density are also shown.

points). The same table also shows the percentage absorption of the P K signal at a particular point. The absorption of the In K_α line at the thickest point is 0.4%, which again justifies our initial assumption.

6.8.4 Fitting of In L and In K_α Counts

Because of the success of calculating mass path lengths using the K and L lines from the same element for GaP, and the uncertainties encountered using the P K from InP due to the variability of the P concentration, the possibility of using the In L lines was investigated. Writing $N_{InK} = N_A$ and $N_{InL} = N_B$, equation 3.17 becomes,

$$N_{iInL} = K' \; N_{iInK} \; \frac{\left[\, 1 - \exp\{-(\mu / \rho)_{iInL} \; \Psi' \; N_{iInK}\} \,\right]}{(\mu / \rho)_{iInL} \; \Psi' \; N_{iInK}} \qquad (6.10)$$

Using the In L lines is more complex here, because there are a number of overlapping lines in the In L spectrum covering a range of photon energies (see figure 6.6) for which the sample mass absorption coefficient varies considerably (for example, for a typical point 13, the mass absorption coefficient of the In L_α line is 570 and that of the L_β line 480 $cm^2\ gm^{-1}$). The selection of both the characteristic counts and the mass absorption coefficient for substituting in equation 6.10 must be done with care. A number of approaches were examined. The most straight forward method was to take the total count for the In L_α and In L_β peaks and use the mass absorption coefficient for In L_α. This simple technique is the same as that used with

Point	Mass P.Length (gm cm^{-2}) (10^{-4})	Absorption P.Length (nm)	Thickness (nm)	% Absorption of Lines P K	In L
04	1.4	320	90	10.0±0.8	4.0±0.3
05	2.2	440	130	14.0±1.1	6.0±0.5
06	2.4	490	150	15.0±1.2	6.5±0.5
07	3.	550	160	18.0±1.5	8.0±0.6
08	3.5	640	190	20.0±1.7	9.0±0.7
09	4.	740	220	23.0±1.8	11.0±1.0
10	4.6	900	265	26.0±2.0	12.0±1.0
11	4.8	900	270	27.0±2.2	12.0±1.0
12	6.	1140	330	32.0±2.6	15.0±1.2
13	6.6	1270	370	35.0±2.8	17.0±1.4
14	7.8	1530	450	40.0±3.	20.0±1.6

Table 6.5

Results of the absorption corrections of InP sample. The typical error is 8 % in both the mass and absorption path lengths. The error in the thickness is approximately 40%.

the Ga L lines. When data for the combined peak of In L_α and In L_β were fitted to equation 6.10, the values of the fitting parameters obtained were $K' = 6.8 \pm 0.2$ and $\Psi' = (1.05 \pm 0.22) \times 10^{-5}$ corresponding to relative errors of ≈3% and ≈21% respectively.

A possibly more accurate way of calculating the required mass absorption coefficient for the combined peak is to weight the In L_α and In L_β mass absorption coefficients by their partition coefficients taken from tables. Using these mass absorption coefficients in equation 6.10, the values of the fitting parameters obtained were $K' = 6.8 \pm 0.2$ and $\Psi' = (1.10 \pm 0.18) \times 10^{-5}$. Thus, this choice of mass absorption coefficients reduced the error of fitting parameter Ψ' from 21% to ≈16%.

A further improvement can be obtained by calculating the number of counts in the In L_α alone as described in 6.8.2. Using the data from the In L_α line with its mass absorption coefficients in equation 6.10, values of fitting parameters obtained were $K' = 5.2 \pm 0.1$ and $\Psi' = (1.14 \pm 0.14) 10^{-5}$, corresponding to relative errors of ≈2.5% and 12% respectively. Thus with these data the error in the fitting parameters has been reduced further. The resulting parameters for the different approaches to fitting the InP data are summarised in table 6.3. It can be seen from this table that the value of the fitting parameter Ψ' obtained from the In L_α to In K_α fitting is in good agreement with that of Ψ obtained from the P K to In K_α fitting.

It should be noted that equation 6.5 is valid only if the fitting parameter $K (= k_{InP}.C_P/C_{In})$ is a constant as is assumed in the fitting procedure. From the data in table 6.4 it is clear that C_P/C_{In} varies from ≈ .94 upto ≈ 1.42. However, with the exception of first three points the ratio of the P and In

concentrations is constant within the experimental error (C_P/C_{In} ratio varies from ≈.95 upto ≈.97).

From table 6.5, it can be seen that nominal thicknesses upto 450 nm are obtained from the InP specimen. However, the value of thickness was estimated on the basis of the value of the geometric factor, G (=3.4) which has a large uncertainty (as discussed in section 6.7.1).

The effect of beam broadening on some thicker points of the sample was examined. An approximate estimate of b can be obtained by using mean values of Z′=33 and W′=97 in equation 6.1. Table 6.6 shows the values of the broadening parameter b corresponding to the nominal thickness at the point. It can be seen from this table that if the value of the broadening parameter is compared with the width of InP layer (which is 100 nm), only experimental data of points 12, 13 and 14 may be affected by beam broadening. At the thickness <350 nm the broadening is unlikely to affect this sample. The broadening at points 12, 13 and 14 means that electrons may be scattered into the neighbouring layer of InGaAs where the atomic concentration of In is ≈25%. This would produce a loss of In and P signals and increase in Ga and As signals at these points (12,13 and 14). The concentrations at these points shown in table 6.4 are not modified in this way suggesting their measurement is not affected by beam broadening. This indicates that their actual thickness may be of the order of 350 nm or less than it and that the geometric factor is consequently greater than 3.4 .

Point	t (nm)	b(nm)
11	270	66
12	340	91
13	370	107
14	450	140

Table 6.6

Values of beam broadening parameter at some thicker points for mean Z=33 and mean A=97.

6.9 Comparison of the Results with the Approach of Self Absorption Corrections Using the Bremsstrahlung

The theoretical thin specimen background corrected for self absorption using the values of mass path length obtained by the characteristic line ratio method should fit the experimental background. This will evidently be the case from thin regions, but should also be true from thicker regions of the specimen.

An experimental spectrum from a thin area of GaP with an MBH background corrected for detector efficiency (the ideal thin background) superimposed is shown in figure 6.2. Figures 6.8, 6.9 and 6.10 show experimental spectra from thicker regions of GaP with a "thin" background and "thin" background corrected for specimen self absorption (using values of absorption path length previously determined) superimposed. The MBH background spectrum was calculated using the programme MBHBACK. The mass absorption coefficients of Be and GaP were calculated by using the programme MABSCO. Then using the programme CORRECTION the MBH spectrum of GaP was corrected for detector efficiency to calculate the thin background spectrum. Next the thin background spectrum was corrected for specimen self absorption effects by using the same programme. The full listings of these programmes is given in appendix 2.

In a similar way, the thin specimen background spectra of InGaAsP were calculated and corrected for self absorption. Figures 6.11, 6.12 and 6.13 show experimental spectra from thicker regions of the InGaAsP sample with the thin background and the thin background corrected for absorption superimposed. The theoretical backgrounds shown in figures 6.11 to 6.13 were

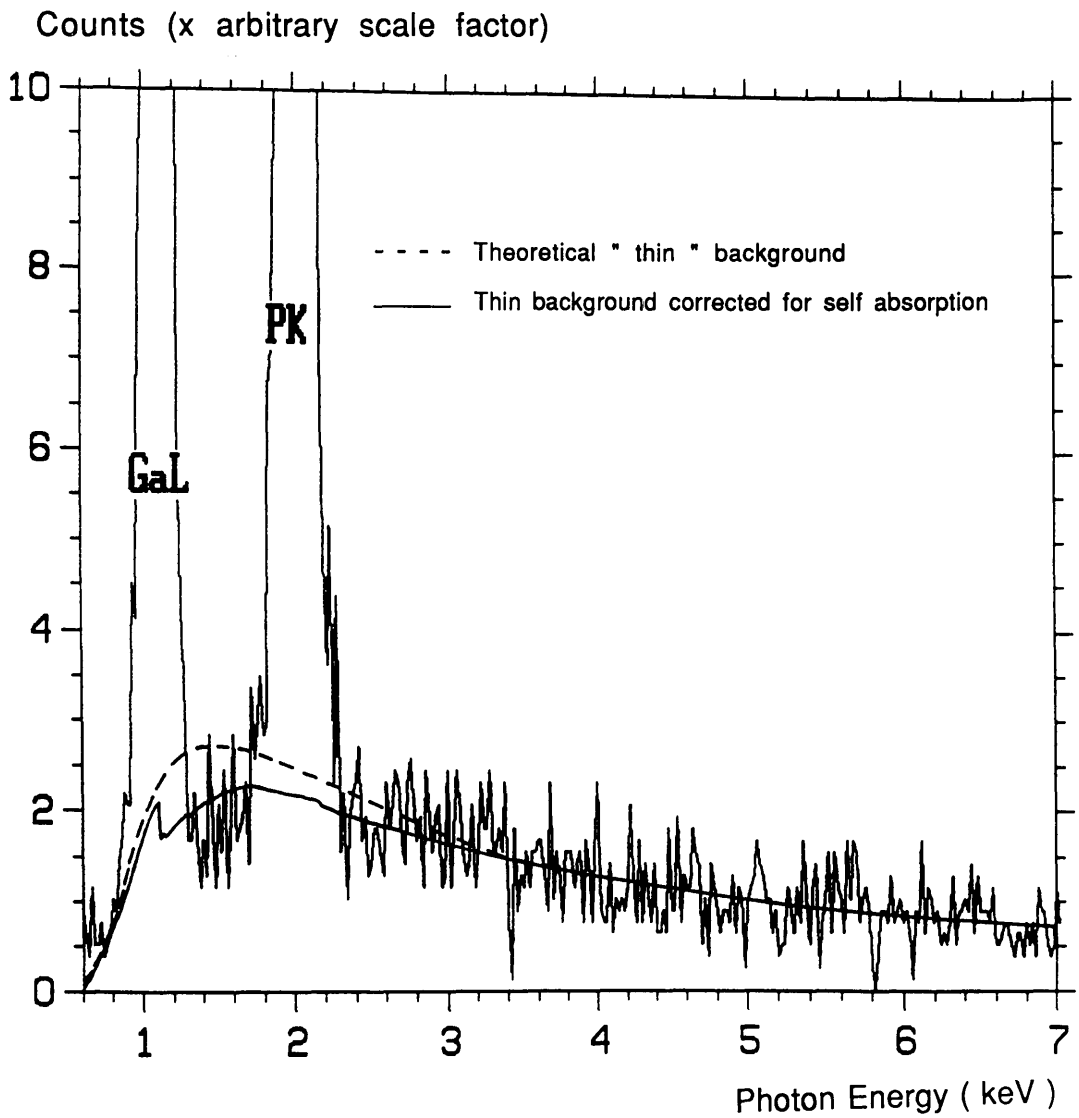

Figure 6.8

Experimental spectrum from GaP point 9, with theoretical thin background and thin background corrected for self absorption in 270 nm absorption path length superimposed.

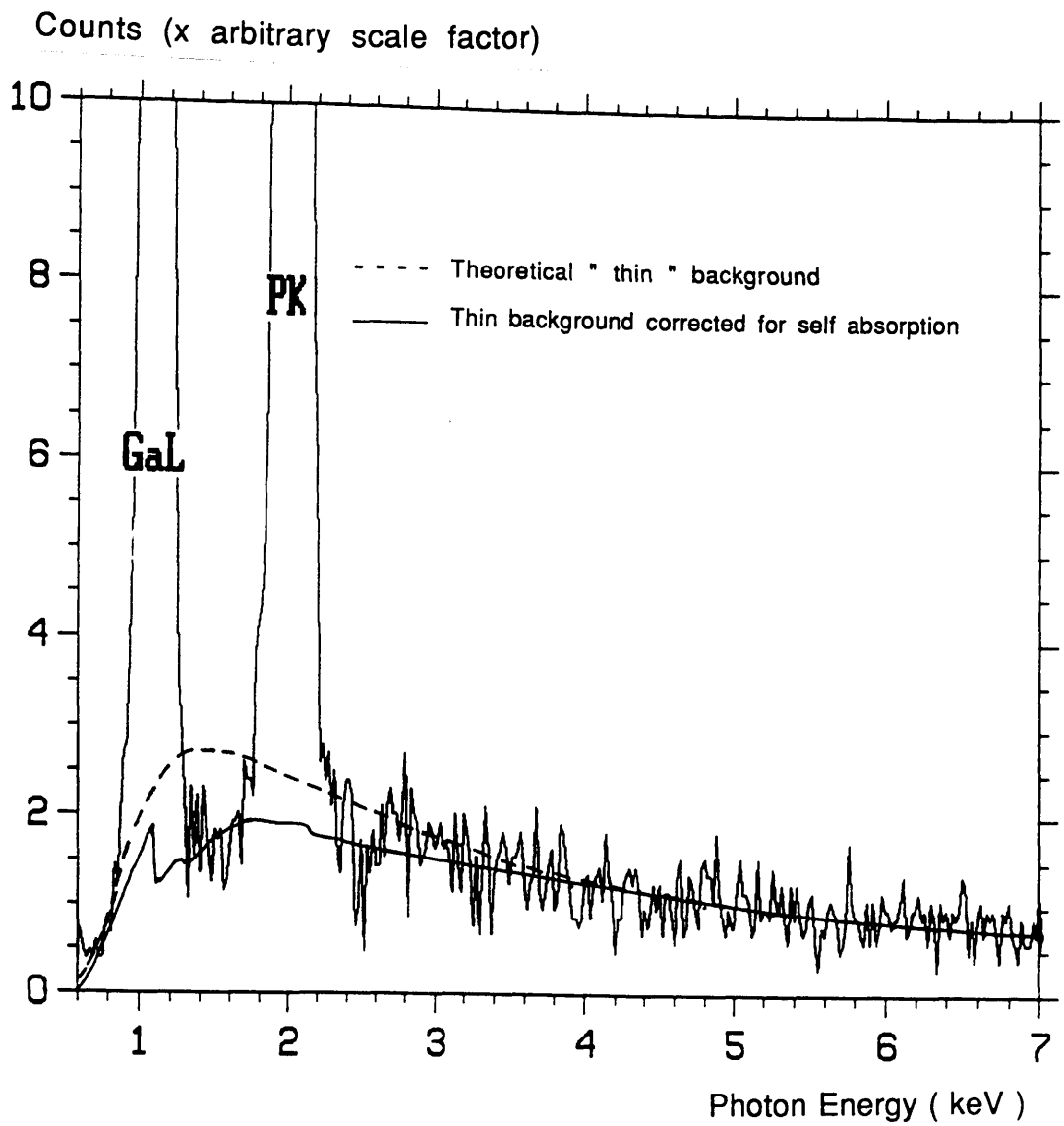

Figure 6.9

Experimental spectrum from GaP point 13, with theoretical thin background and thin background corrected for self absorption in 440 nm absorption path length superimposed.

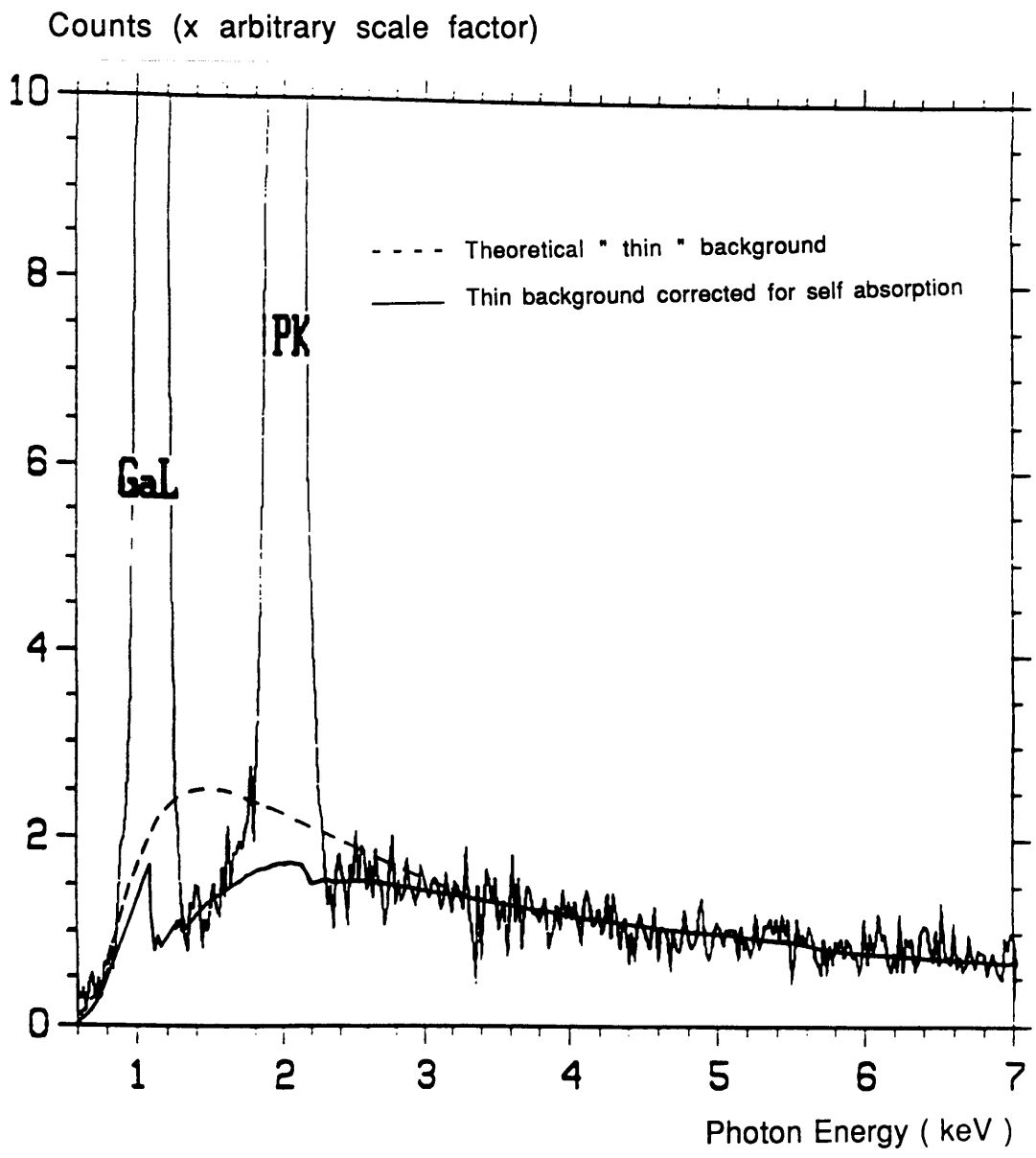

Figure 6.10

Experimental spectrum from GaP point 16, with theoretical thin background and thin background corrected for self absorption in 820 nm absorption path length superimposed.

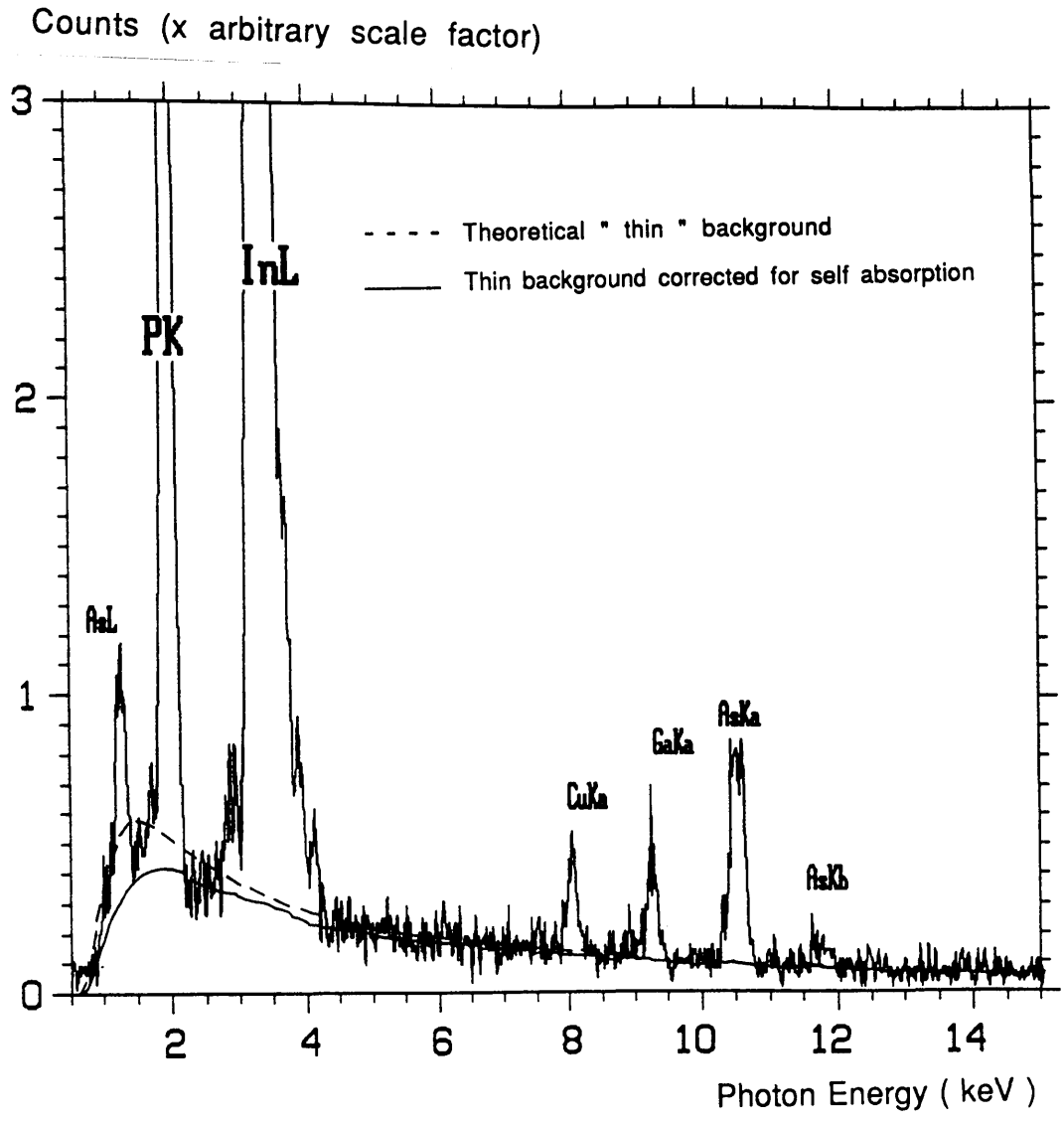

Figure 6.11

Experimental spectrum from InP point 7, with theoretical thin background and thin background corrected for self absorption in 550 nm absorption path length superimposed.

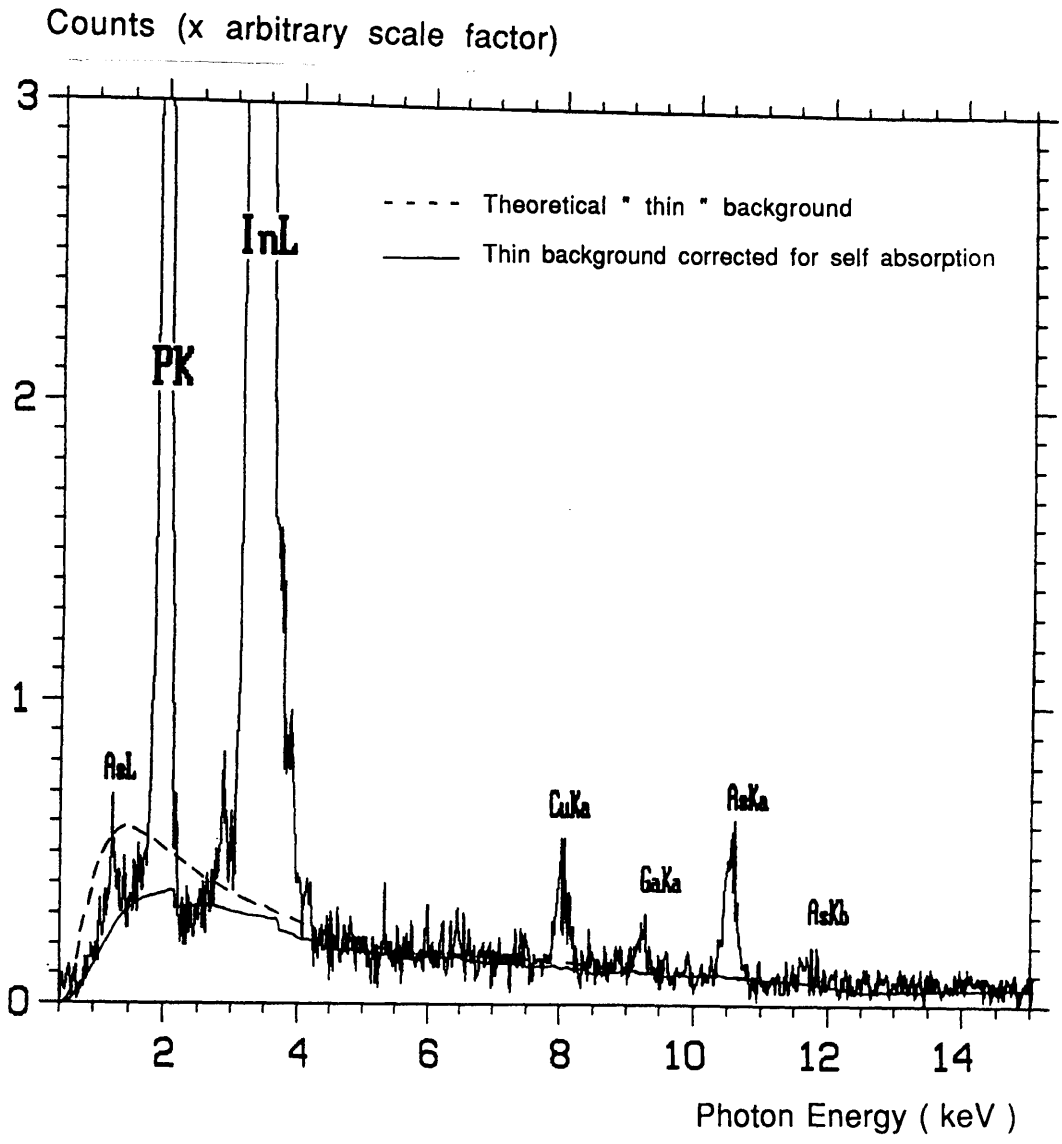

Figure 6.12

Experimental spectrum from InP point 12, with theoretical thin background and thin background corrected for self absorption in 1140 nm absorption path length superimposed.

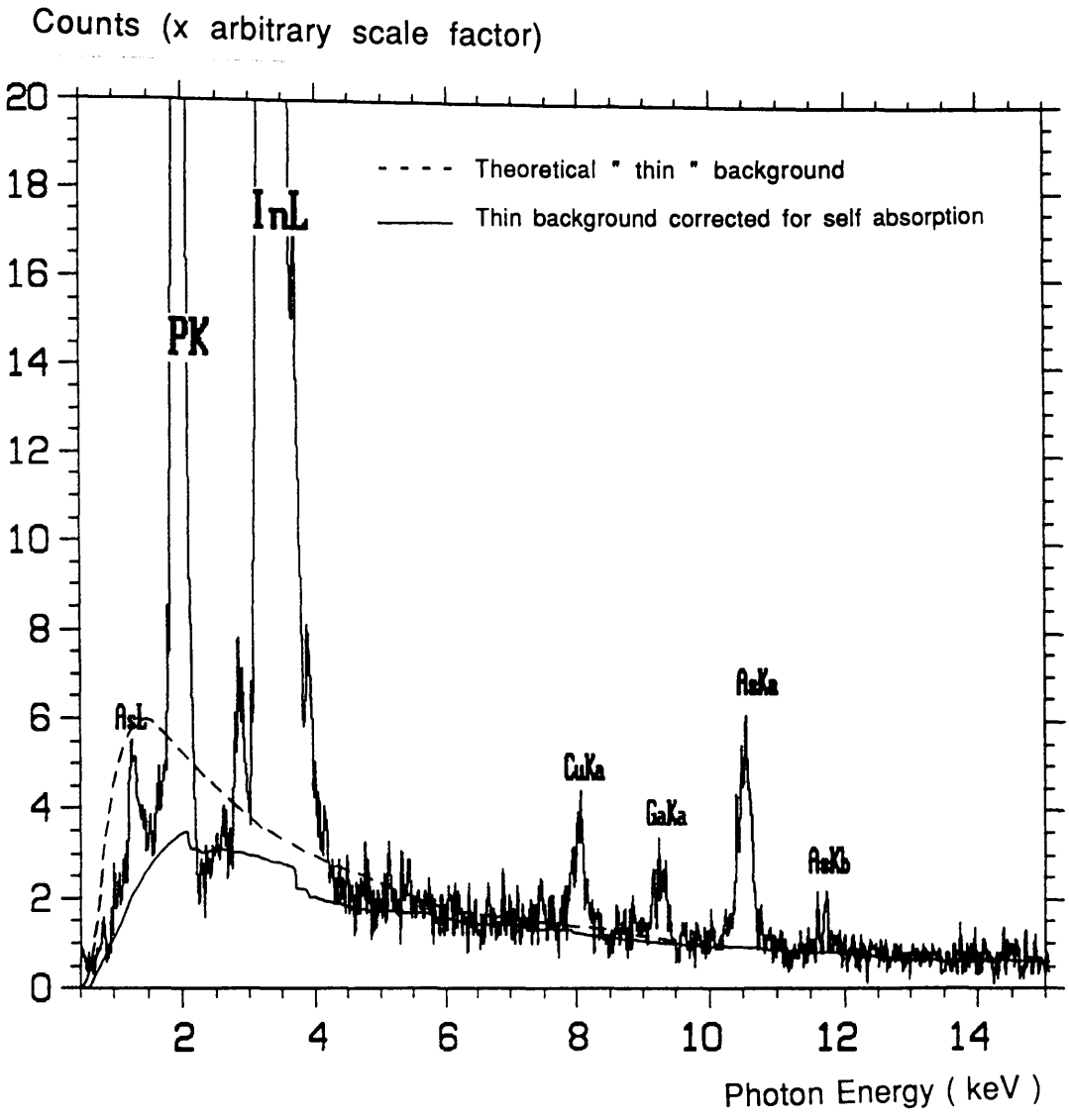

Figure 6.13

Experimental spectrum from InP point 14, with theoretical thin background and thin background corrected for self absorption in 1530 nm absorption path length superimposed.

calculated using mass path lengths which had been previously determined from the characteristic line method. It is thus to be expected that they fit the experimental data well. However, it is interesting to investigate how accurately the Bremsstrahlung background might be used to make an independent measure of mass path length.

The method of absorption corrections using Bremsstrahlung (described in chapter 5) was applied to the GaP sample to fit the theoretical background shape to the experimental one. A range of thicknesses around that predicted from characteristic line method were taken and the chi-square test was performed using the regions .78-.88 keV and 1.38-1.7 keV. The range of values of chi-square obtained, indicated that the absorption path length had a value of 430±50 nm for this typical analysis point (figure 6.9). Thus the Bremsstrahlung method of absorption corrections has ≈11% relative error in absorption path length for this typical spectrum, whereas for the same spectrum the characteristic line method has ≈ 6% relative error in absorption path length. The error in the measurement of the absorption path length (≈11%) is similar to that obtained for the biological samples i.e. ≈12%.

A further disadvantage in the Bremsstrahlung method is that it requires a fitting window in the low energy end free from artifacts for the comparison of theoretical and experimental backgrounds. This may not be practical if any large peak in the low energy end is affected by ICC. In figure 6.13 where the large P K peak from InP is affected by ICC, it would not be practical to use the Bremsstrahlung method for absorption corrections.

6.10 Results and Discussion

In this work it has been shown that it is possible to correct signals in a particular sample for x-ray self absorption using the data from the characteristic lines of the sample. A wide range of options are available for choosing the data for this correction procedure. It can be seen from figures 6.3, 6.4, 6.7 that the fit of N_B vs N_A is good apart from in the thinner regions. Small layers of contamination or the radiation damage which is more apparent in the thinner areas of the samples (Bullock et al, 1987) are thought to be the cause of differences between the fit and the experimental points from the thinner regions. It can also be seen from table 6.4 that in the thicker regions of the InP well, the requirement that the sum of the atomic ratios of group III and those of group V be one is satisfied within experimental error.

The multilayer material grown in this study was found to contain up to fourteen percent As and five percent Ga in the InP well (see point 4). It is improbable that some interference from the InGaAs layer comes in the InP layer when electron beam is incident on the area of InP because if this were so then one would expect that the As and Ga detected when the beam was in InP well would show with a rise with thickness of the specimen, which has not been seen in these experiments. This shows that the carry over of As and Ga into the InP well may be due to other reasons. It is possible that As and Ga get trapped in dead spaces in the reactor and is then incorporated into the InP even though AsH_3 supply has been closed. In addition to the effect of dead

spaces there may be a background incorporation of As, the most likely source of which is PH_3. Even a small concentration of AsH_3 in PH_3 could become significant due to the incorporation rate of AsH_3, which is $\approx$ 50 times greater than that of PH_3. A further possibility is the slow desorption of precursors from the pipework and the reactor walls, which could be the cause of the Ga content (McGibbon et al, 1989).

In the case of the In L line when the combined peak of In L_α and In L_β was taken as the line with significant absorption, the magnitude of the error in Ψ' was large when mass absorption coefficients of the In L_α line were used for the fitting technique. The magnitude of this error may be reduced by using the mass absorption coefficients of In L_α and In L_β weighted according to the intensity ratio. However, it is evident that these methods are over simplistic to give the best results. The magnitude of this error is further reduced when data from the single In L_α line with its mass absorption coefficients are used. This shows that mass absorption coefficients play an important role in this fitting process and have to be carefully selected.

In the case of the GaP investigation since the energy separation of the L_α and L_β line for this sample is very small, the mass absorption coefficients of the whole L line are very similar to that of L_α line. However, in the InP case the energy separation of In L_α and In L_β is large enough to produce a significant difference in the mass absorption coefficients and hence a large error is obtained. This indicates that for the higher atomic number elements ($Z > 50$), where the energy separation in the L sublines is larger, the size of the error in Ψ' may be correspondingly larger when the combined L peak is used with mass absorption coefficients of the L_α line. Therefore, for

the elements of atomic number Z < 40 it may be concluded that the counts from the combined L line along with mass absorption coefficients of the L_α line may be used without producing any significant increase in error in Ψ'. The fitting of two K lines is much more straight forward. However, difficulties may be encountered if the ratio of the concentration of two elements chosen for the fitting is not constant. This is investigated further in chapter 7.

The values of mass path length obtained by the characteristic line method of self absorption are compared with the method of MBH fitting and it can be seen that results are self consistent, although the MBH method measures mass path length less accurately. The analysis of the InGaAs/InP multilayer system as shown in this work also gives a good opportunity to understand the problems in their growth and hence to improve growth techniques further.

CHAPTER 7

Specimen Self Absorption Corrections for the AlGaAs/GaAs Multilayer System

7.1 Introduction

In chapter 6, the technique of absorption corrections using the characteristic lines has been examined for two different samples having relatively small variations in composition. In this chapter the same technique is applied on an AlGaAs/GaAs multilayer system to perform the absorption corrections of Al K signal which is heavily absorbed in thicker regions of the sample. This sample was grown in such a way that it comprised of 20 nm wide layers of GaAs separating AlGaAs layers of similar width. The Al concentration was nominally constant in the individual layers which had grown compositions of 10%, 20%, 30%, 40% and 50%. The main aim of the work presented here was to extend the absorption correction method to samples where composition is not constant.

Section 7.2 describes the experimental details used for the collection of the spectra and section 7.3 describes the extraction of the characteristic counts from the measured spectrum as required in the technique. In section 7.4 different methods of performing absorption corrections for the sample are discussed in detail. The possibility of correcting the data from a single point for absorption using its characteristic

counts without the use of a multi point fitting approach is also examined in section 7.5. In section 7.6 the results are discussed briefly.

7.2 Instrumentation

The sample investigated in this chapter was also examined in the Glasgow extended VG HB5 STEM discussed in section 6.4. This sample was grown by MBE (see chapter 6) in a Varian Modular Gen 11 system at a temperature of 625 C° so that the sticking coefficients of both Ga and Al were unity. As a consequence the ratios of Al to Ga in the layers were equal to the Al to Ga flux ratios which were accurately calibrated prior to the growth of the structure. Cross-sections suitable for microscope examination were prepared by mechanical thinning followed by ion-milling in Ar. The spectra were collected over the energy range 0 to 20 keV at a resolution of 20 eV per channel. An acquisition time of 90 s was found to yield signals of adequate statistical accuracy. For example, ≈ 6000 counts were recorded in the Ga K_α x-ray peak when the beam was centered at the point where the specimen had a calculated thickness of 60 nm. All other experimental conditions were the same as discussed in section 6.4.

7.3 Extraction of X-ray Counts From the Measured Spectrum

For this particular sample the characteristic counts of x-ray lines of Al K, Ga K_α, As K_α and Ga L are required so that the

first approximations to the compositions and mass absorption coefficients can be calculated. These can be then used for fitting with different data sets to enable the mass path length at each analysis point to be determined. The characteristic counts of Ga K_α and As K_α have high peak to backgrounds and can be obtained by simple straight line background fitting with a correction for the Ga K_β / As K_α overlap as discussed in section 6.6. However, there is a problem involved with the estimations of the Ga L and Al K lines which overlap with the As L line as shown in figure 7.1. This figure compares a spectrum acquired from an area of AlGaAs with that acquired from GaAs.

Figure 7.1 suggests that Al K line counts could be obtained by the subtraction of a pure thin GaAs spectrum from a spectrum measured from AlGaAs layer. Before any such subtraction, the thin GaAs spectrum would have to be scaled to the AlGaAs spectrum and each method has an associated problem. One approach would be to scale the thin GaAs spectrum to the As K_α peak. However, differential absorption between the As K_α and As L lines at different points would lead to a mismatch in the As L peaks between the two spectra. Another approach would be to scale the spectrum to the As L line, but for the AlGaAs spectrum the choice of scaling window is complicated due to the overlap with Ga L and Al K lines.

In this series of spectra, linear interpolation of the background on either side of the Al K peak may yield large uncertainties. The low energy background window would have to be chosen below the Ga L peak where the background variation is rapid and some problem is also involved in the choice of the high energy background window due to the presence of a small Ar

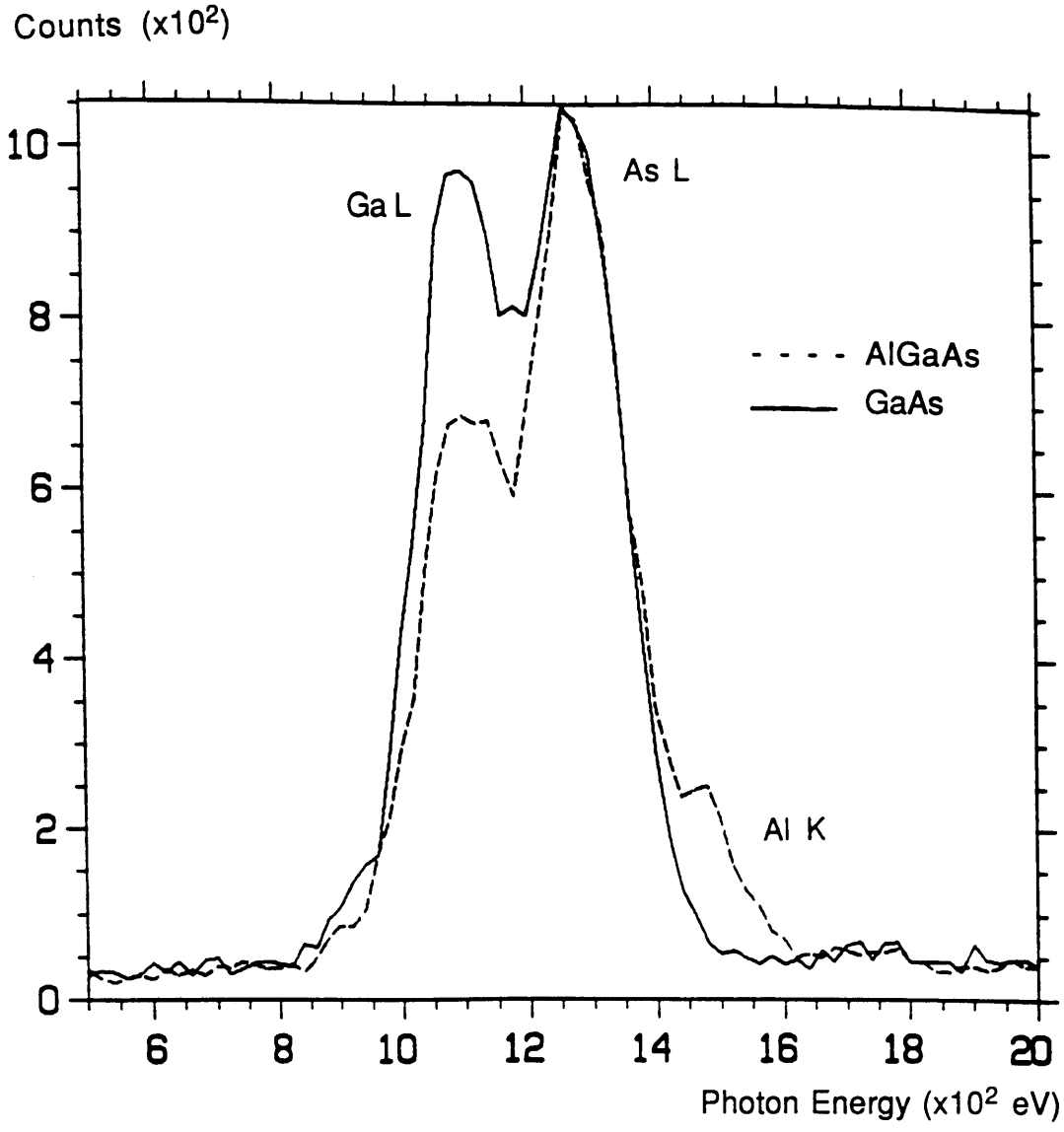

Figure 7.1

Experimental specta acquired from the regions of GaAs and AlGaAs, showing the overlap that occurs between the Ga L, As L and Al K peaks.

signal. Moreover, the peak to background ratio of Al K is small so that this approach of background estimation is likely to lead to large errors.

To overcome such problems, background modelling (see sections 5.4 and 5.5) was performed to estimate the background under the Al K and Ga L peaks. Fortunately for this particular sample a suitable window (.74 to .84 keV) was available below the Ga L line for background modelling. The computer programme AUTO was modified for this purpose. The modelled background spectrum was then subtracted from the measured one. The number of counts in the upper energy half of the Al K peak were recorded and then by doubling this value, a value for the Al K signal was obtained. A similar approach was used to estimate the counts of the Ga L line. It should be noted that the modelling approach of background subtraction reduces the statistical errors of the Ga L and Al K lines (see section 5.10). The characteristic x-ray counts of all lines were then normalized to the same electron dose (100 s acquisition time and 100 nA VOA current).

7.4 Absorption Corrections for the AlGaAs Layer

The most convenient way to express elemental composition in an $Al_xGa_{1-x}As/GaAs$ system is in terms of the atomic fraction ratios f_{Al} and f_{Ga}, where f_{Al} and f_{Ga} are the ratios of the number of atoms of Al, C_{Al}, and Ga, C_{Ga}, to the number of As atoms, C_{As}, respectively;

$$f_{Al} = \frac{C_{Al}}{C_{As}} = k_{AlAs} \frac{N_{Al}}{N_{As}} \quad (7.1)$$

$$f_{Ga} = \frac{C_{Ga}}{C_{As}} = k_{GaAs} \frac{N_{Ga}}{N_{As}} \quad (7.2)$$

where N_{Al}, N_{Ga} and N_{As} are the characteristic counts of Al, Ga and As respectively. In this specimen as C_{As} =1, f_{Al} and f_{Ga} are the same as x and 1-x respectively.

The k-factor for GaAs (k_{GaAs}) was determined in chapter 6 to be 0.9. However, the k-factor for AlAs (k_{AlAs}) was calculated theoretically as 1.1 using the programme KVALUE. Using equation 7.2, the value of f_{Ga} can be calculated and then the estimate of f_{Al} can be made on the assumption that $f_{Al}+f_{Ga}=1$. Table 7.1 shows such results. It should be noted that the concentration of As is 1 in this sample. In table 7.1, the layers 1, 2, 3, 4 and 5 nominally contain 10% Al and 90% Ga, 20% Al and 80% Ga, 30% Al and 70% Ga, 40% Al and 60% Ga, and 50% Al and 50% Ga respectively. The concentrations shown in table 7.1 can be used to calculate the mass absorption coefficient of Ga L line at each analysis point.

7.4.1 Fitting Data Where the Composition Varies

Examination of equation 3.17 shows that changes in specimen composition will affect the fitted parameters in two ways. The value of K ($=k_{AB}\ C_B/C_A$) will be directly modified by changes in C_A and C_B. Further, the mass absorption coefficients

Point	% Al	%Ga	C_{Al}/C_{Ga}
Layer 1 - 10% Al nominal			
01	12	88	0.14
02	10	90	0.11
03	08	92	0.09
04	03	97	0.03
Layer 2 - 20% Al nominal			
01	24	76	0.32
02	21	79	0.27
03	18	82	0.22
Layer 3 - 30% Al nominal			
01	28	72	0.39
02	33	67	0.49
03	31	69	0.45
04	28	72	0.39
05	24	76	0.32
Layer 4 - 40% Al nominal			
01	38	62	0.61
02	40	60	0.67
03	39	61	0.64

Point	% Al	%Ga	C_{Al}/C_{Ga}
04	37	63	0.59
05	36	64	0.56
06	31	69	0.45
Layer 5 - 50% Al nominal			
01	46	54	0.85
02	49	51	0.96
03	46	54	0.85
04	52	48	1.08
05	52	48	1.08
06	48	52	0.92
07	43	57	0.75

Table 7.1

Uncorrected atomic concentrations of Al and Ga in the AlGaAs sample. The % Ga is calculated from equation 7.2, the % Al is calculated by difference.

in the exponent and the denominator will also be modified by changes in composition. Only the latter of these effects could play a role for the case of fitting using L vs K line for a single element. Figures 7.2 and 7.3 show plots of the mass absorption coefficients of the Ga L line and the Al K line vs Al atomic concentration x, of an ideal $Al_xGa_{1-x}As$ sample. It can be seen that the variation for the Ga L line is much less than for the Al line. The next two sections examine the possibility of determining mass path lengths using the Ga L and Al K lines as the measure of absorption in the presence of variable Al concentration.

7.4.2 Fitting of Ga L and Ga K_α Counts

In this section an investigation will be made to treat the data of all five layers as one set and to fit it with a single theoretical line. For the case of the Ga L to Ga K ratio, equation 3.18 may be re-written as

$$N_{iGaL} = K' \; N_{iGaK} \; \frac{\left[1 - \exp\{ -\eta' \, N_{iGaK} \} \right]}{\eta' \, N_{iGaK}} \qquad (7.3)$$

where the index i runs over the data points.

When the data from the 25 points were fitted to equation 7.3, the best values of parameters K′ and η′ were obtained as 0.51 ± 0.01 and $(1.85 \pm 0.14) \times 10^{-5}$ respectively, corresponding to relative errors of ≈ 2% and ≈ 8% in K′ and η′. Figure 7.4 shows Ga L plotted against Ga K_α for points from all 5 layers. Since the mass absorption coefficients of Ga L do not vary strongly

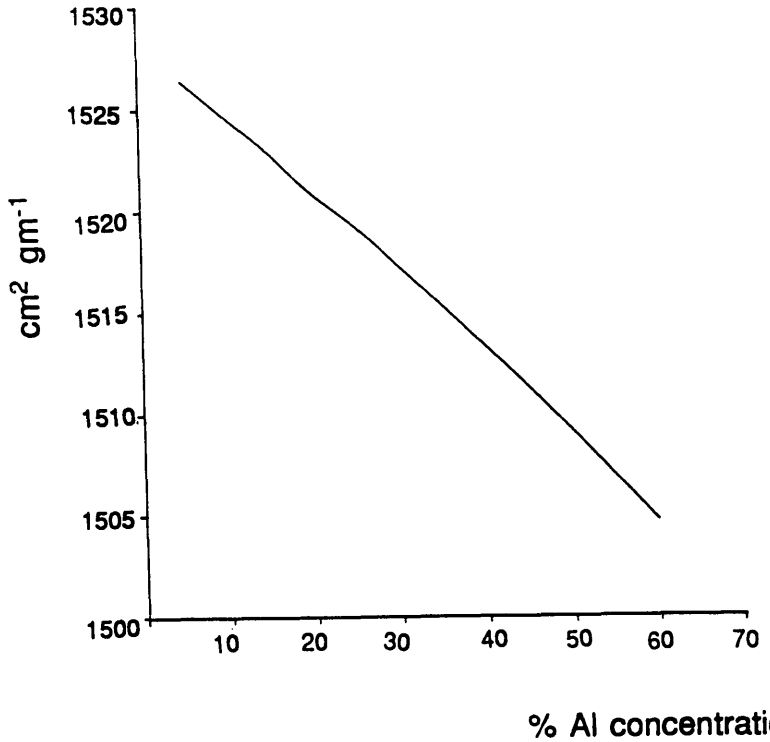

Figure 7.2

The variation of mass absorption coefficients of Ga L in $Al_xGa_{1-x}As$ as a function of Al concentration.

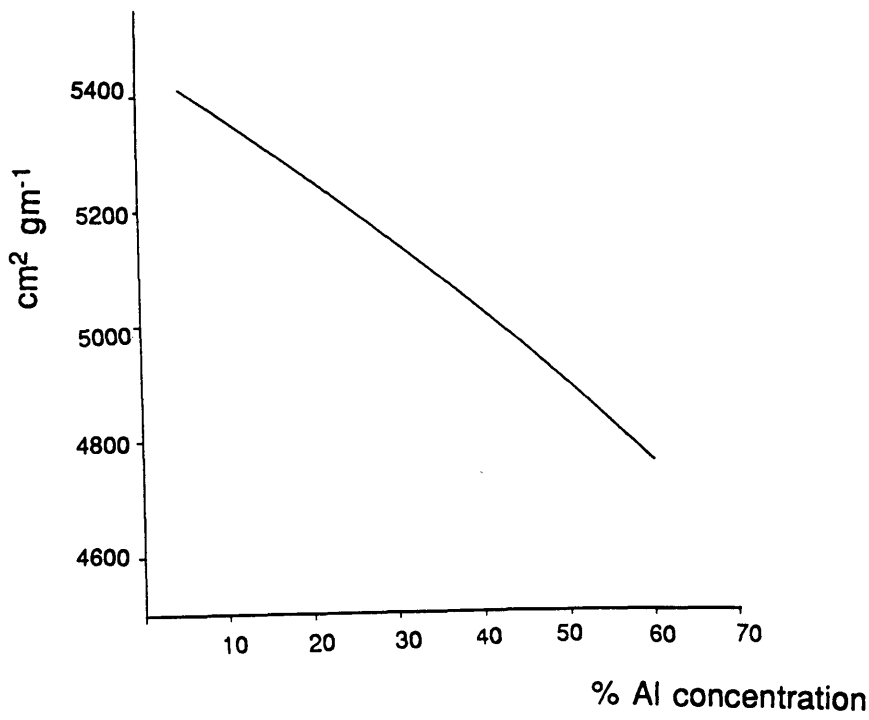

Figure 7.3

The variation of mass absorption coefficients of Al K in $Al_xGa_{1-x}As$ as a function of Al concentration.

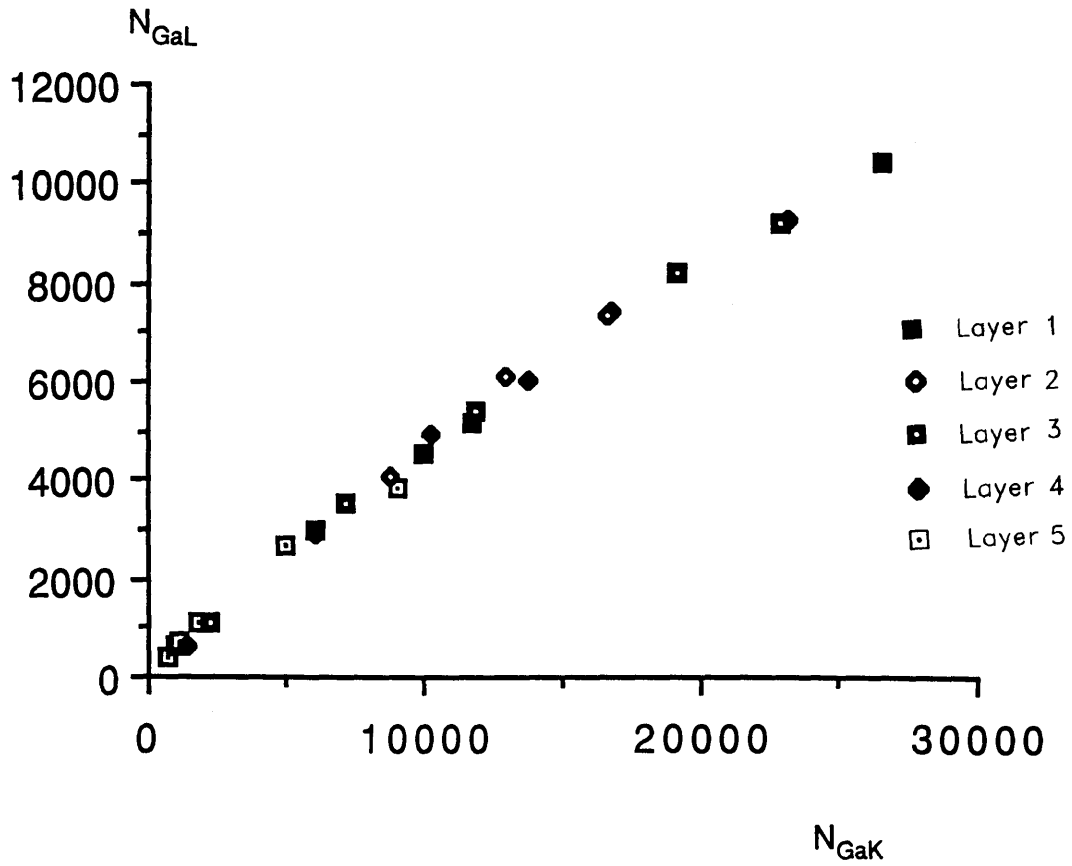

Figure 7.4

N_{GaL} vs N_{GaK} for 5 layers of differing composition in $Al_xGa_{1-x}As$.

with the variation of Al in the sample, the mass absorption coefficient of Ga L calculated from the uncorrected concentrations of the sample (table 7.1) can be used to get the best value of Ψ directly (i.e no iteration is required to get the mass absorption coefficients of the Ga L line). This value of Ψ [$(1.22 \pm 0.10)\times10^{-8}$] can then be used to convert Ga K_α counts into mass path lengths.

The value of mass path length obtained from fitting equation 7.3 can be used to correct the measured Al K line for absorption and hence the values of f_{Al} and f_{Ga} can be calculated for the data set using equations 7.1 and 7.2 respectively. The programme RATIO (with some modification) was used for this purpose. Table 7.2 shows the atomic concentrations of Al and Ga obtained by the use of absorption corrected data, and equations 7.1 and 7.2. Comparison of the Ga concentrations between tables 7.1 and 7.2 shows most data points are unchanged by the correction procedure. Only a few points are slightly lower in table 7.2. These are at the thickest regions where there is some absorption of As K_α in Ga and the correction decreases the Ga K/As K ratio (equation 7.2).

It can be seen from table 7.2 that the condition that $f_{Al+Ga} = 1$ is satisfied (within experimental error) by most of the points in layers 3, 4 and 5. However, for some points in these layers and particularly for the points in layers 1 and 2 where the Al concentration is small, this condition is not as well satisfied. This is probably due to the larger statistical error in these small Al peaks, typically 280 counts and 1600 counts in the 10% and 20% layers respectively. However, as a result of the good agreement between experiment and theory, a greater confidence can be placed in the value of K_{GaAs} used and hence in the

Point	% Al	%Ga	ρ (gm cm^{-3})
Layer 1 (10% Al nominal)			
01	10.0±1.3	88	5.16
02	8.0±1.2	90	5.18±0.65
03	6.0±1.0	92.0±0.3	5.22
04	2.0±0.5	95	5.27
Layer 2 (20% Al nominal)			
01	23.0±1.8	76	4.97
02	19.0±2.0	79.0±0.4	5.02±0.40
03	16.0±1.4	81	5.06
Layer 3 (30% Al nominal)			
01	27.0±1.0	72	4.9
02	32.0±1.5	67	4.83
03	31.0±1.3	69±0.4	4.87±0.18
04	27.0±1.8	72	4.9
05	23.0±1.5	75	4.96
Layer 4 (40% Al nominal)			
01	37.0±0.8	62	4.76
02	38.0±1.4	60±0.5	4.73
03	39.0±1.0	61	4.74
04	37.0±0.9	63	4.77±0.08
05	35.0±1.0	64	4.8
06	30.0±1.5	68	4.85

Point	% Al	%Ga	ρ (gm cm^{-3})
Layer 5 (50% Al nominal)			
01	44.0±1.0	54	4.62
02	47.0±0.9	51	4.6
03	46.0±0.7	54	4.63±0.05
04	52.0±0.5	48±0.5	4.54
05	51.0±0.9	48	4.54
06	48.0±0.6	52	4.6
07	42.0±0.8	56	4.67

Table 7.2

Atomic concentrations of Al and Ga in the AlGaAs sample calculated from equations 7.1 and 7.2 after correcting the characteristic lines for self absorption. Some typical standard errors in the density and Ga composition are also shown.

concentration calculations obtained by the use of absorption corrected data and equation 7.2.

The lattice constant for GaAs (a=.565 nm) can be used to estimate the sample density at each point in the same way as used for InP (chapter 6). An estimate of density at each point is shown in table 7.2. Using these values of density the best estimates of absorption path length were made. The geometric factor G was estimated to be 2.3 using the same technique as in chapter 6 for GaP and InP. Again, it is likely that this value of G will have a large error, probably 40%. Table 7.3 shows the best estimate of the mass and absorption path length and the approximate value of the thickness at each analysis point. The percentage absorption of Ga L line is also shown in the same table. The absorption of Ga K_α line at the thickest point (point 4 of layer 5) is $\approx$ 0.8% which justifies our initial assumption that absorption of Ga K_α line is negligible.

A comparison of the value of parameter K′ obtained from this fitting with that obtained in chapter 6 (GaP case) shows that the values agree within experimental error, which is an expected result as the ratio of Ga L to Ga K_α should be constant when absorption of the Ga L line is negligible.

For the purpose of this investigation the Al K, Ga L and Ga K_α counts have been treated as though they come from a single layer. Table 7.4 shows the results of the calculation for $Al_{0.1}Ga_{0.9}As$ (the layer with the highest mean atomic number) using equation 6.1 to predict the likely effect of beam spreading. It can be seen that this is likely to play a role in points where the specimen thickness is greater than 100 nm. The effect will be to scatter electrons from the AlGaAs layer

Point	Mass P.Length ($gm\ cm^{-2}$) (10^{-4})	Absorption P.Length (nm)	Thickness (nm)	% Absorption of Lines Al K	GaL
Layer 1 (10% Al nominal)					
01	0.7	130	60	16.0±2.0	5.0±0.5
02	1.2	230	100	26.0±3.0	9.0±1.0
03	1.4	270	120	30.0±3.0	10.0±1.0
04	3.2	610	270	50.0±5.0	21.0±2.0
Layer 2 (20% Al nominal)					
01	1.0	200	90	22.0±2.0	7.0±0.7
02	1.6	320	140	32.0±3.0	11.0±1.0
03	2.0	400	170	38..0±3.0	14.0±1.0
Layer 3 (30% Al nominal)					
01	.26	50	25	6.0±0.6	2.0±0.2
02	.9	190	80	20.0±2.0	6.5±0.5
03	1.4	290	130	28.0±2.0	10.0±0.8
04	2.3	470	200	42.0±3.0	16.0±1.0
05	2.7	540	230	46.0±3.0	18.0±1.0

Point	Mass P.Length (gm cm^{-2}) (10^{-4})	Absorption P.Length (nm)	Thickness (nm)	% Absorption of Lines Al K	GaL
Layer 4 (40% Al nominal)					
01	.2	40	20	4.0±0.3	1.5±0.1
02	.7	150	70	16.0±1.3	5.0±0.4
03	1.2	250	110	25.0±2.0	9.0±0.7
04	1.6	340	150	30.0±3.0	11.0±1.0
05	2.0	420	180	40.0±3.0	14.0±1.0
06	2.8	580	250	47.0±3.0	19.0±1.0
Layer 5 (50% Al nominal)					
01	.08	20	10	2.0±0.2	0.60±0.05
02	.11	25	10	2.7±0.2	0.80±0.06
03	.14	30	15	3.4±0.3	1.00±0.08
04	.20	45	20	5.0±0.3	1.5 ±0.1
05	.60	130	60	13.0±1.0	4.5 ±0.3
06	1.0	220	100	20.0±2	7.0 ±0.7
07	1.8	390	170	35.0±3.0	12.0 ±1.0

Table 7.3

Results of the absorption corrections of AlGaAs sample obtained from the fitting of equations. The typical error is 7% in both the mass and absorption path lengths.

into the neighbouring GaAs layers thus reducing the Al signal. The analysis point numbers in table 7.2 which have been underlined are those for which the nominal thickness is greater than 100 nm. Most points of greater thickness show a substantial reduction of Al concentration below the nominal layer composition, which is consistent with the effects of beam broadening.

7.4.3 Fitting of Al K and Ga K_α Counts

It can be seen from table 7.2 that the ratio of the Al concentration to the Ga concentration (C_{Al}/C_{Ga}) varies within each layer, but varies much more between the layers. The data from 5 layers may be treated individually and fitting parameters K_j and Ψ_j (see table 7.5) obtained for each layer j, using the technique described in chapter 6. Figure 7.5 show the data points with identification for the individual layers. If it were assumed that these points were all from a single specimen of unknown and variable composition it is clear that the scatter is so large no useful single fitting could be obtained.

Evidently, the parameter K of equation 3.17 is not truly a constant for the data from particular layer and varies considerably between layers. However, the k-factor of Ga and Al (k_{GaAl}) is a constant for the two elements for the whole data set. Re-writing equation 3.17 for this particular case,

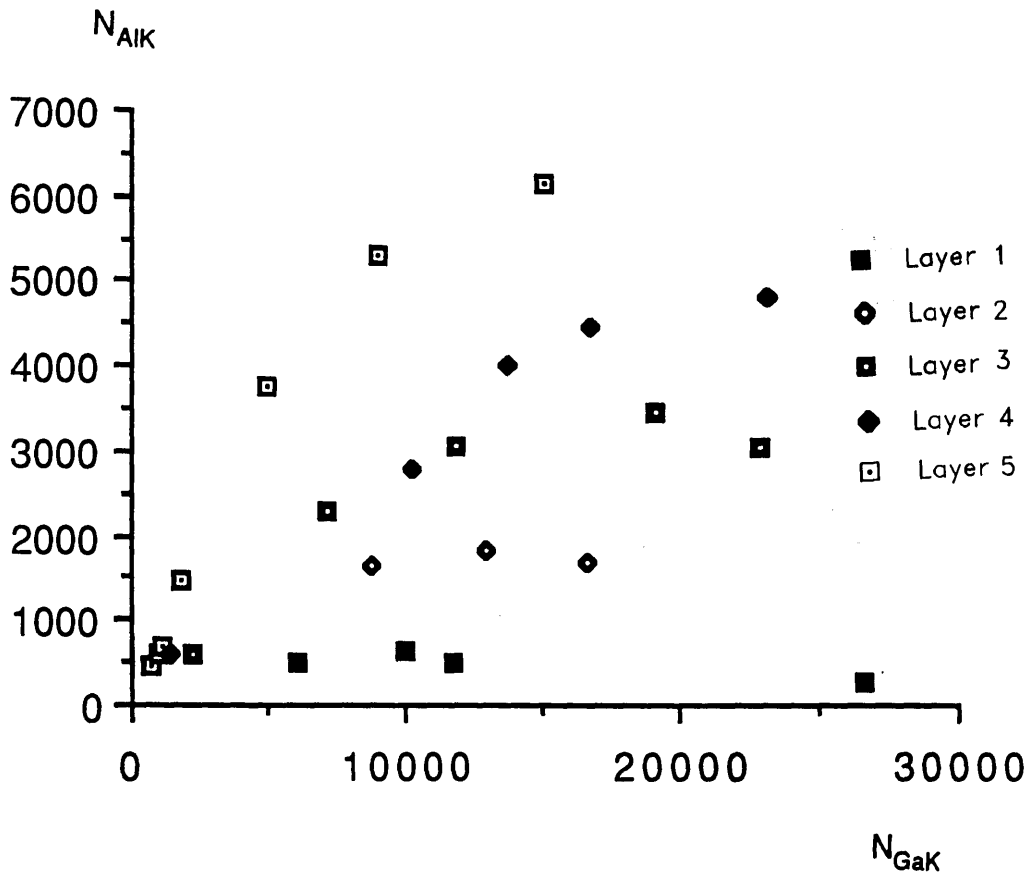

Figure 7.5

Measured Al K counts vs N_{GaK} (after normalisation) for the 5 layers in the $Al_xGa_{1-x}As$ sample.

t (nm)	b(nm)
50	6
100	16
150	30
200	45
250	65
300	85

Table 7.4

Values of beam broadening parameter at some thicker points for mean atomic number 31 and mean atomic weight 72.

Fitting	K	ψ gm cm^{-2} ($\times 10^{-8}$)
Layer 1 (10% Al)	Programme MINIMISE breaks down	
Layer 2 (20% Al)	0.52 ±0.25	5.6 ±3.0
Layer 3 (30% Al)	0.50 ±0.11	2.7 ±0.9
Layer 4 (40% Al)	0.72 ±0.09	2.8 ±0.6
Layer 5 (50% Al)	1.0 ±0.1	2.7 ±0.5

Table 7.5

Parameters obtained from the fitting of Al K and Ga K_α data for each layer using equation 7.3.

$$N_{iAlK} = k_{GaAl}\,(C_{Al}/\,C_{Ga})N_{iGaK}\frac{\left[\,1-\exp\{-(\mu/\rho)_{iAlK}\;\;\Psi_0\;\;N_{iGaK}\}\,\right]}{(\mu/\rho)_{iAlK}\;\;\Psi_0\;\;N_{iGaK}} \quad (7.4)$$

This suggests that if N_{iAlK} is plotted against $(C_{Al}/C_{Ga})N_{iGaK}$, where C_{Al}/C_{Ga} is the uncorrected ratio, a fit might be obtained to determine the two parameters k_{GaAl} and Ψ_0. In this particular case the mass absorption coefficient of the Al K line for each point is already known from the Ga L vs Ga K_α fitting. These values along with uncorrected data for the Al K and Ga K_α counts can be used with equation 7.4 to get 5 independent values of k_{GaAl}, as well as Ψ_0, for each layer. These values are shown in table 7.6 with their absolute errors. It can be seen from this table that the errors in the parameters are much larger for layers 1 and 2. This is mostly because for these two layers the Al concentration is small so that statistical accuracy for the Al K counts is poor. Also there are fewer data points for these layers. Figure 7.6 shows Al K counts of each layer plotted against $(C_{Al}/C_{Ga})N_{GaK}$ where C_{Al} has been calculated from $(1-C_{Ga})$.

It has been noted that the best values of $(\mu/\rho)_{AlK}$ obtained from the Ga L vs Ga K_α fitting were used in the calculations. However, even if these values were not known in advance, this technique is still feasible. First approximations of $(\mu/\rho)_{AlK}$ could be obtained from the uncorrected data. This could give a first approximation of the mass path lengths and hence the data can be corrected to get a second approximation of C_{Al}/C_{Ga} and $(\mu/\rho)_{AlK}$. This could be continued iteratively until a suitable convergence is obtained.

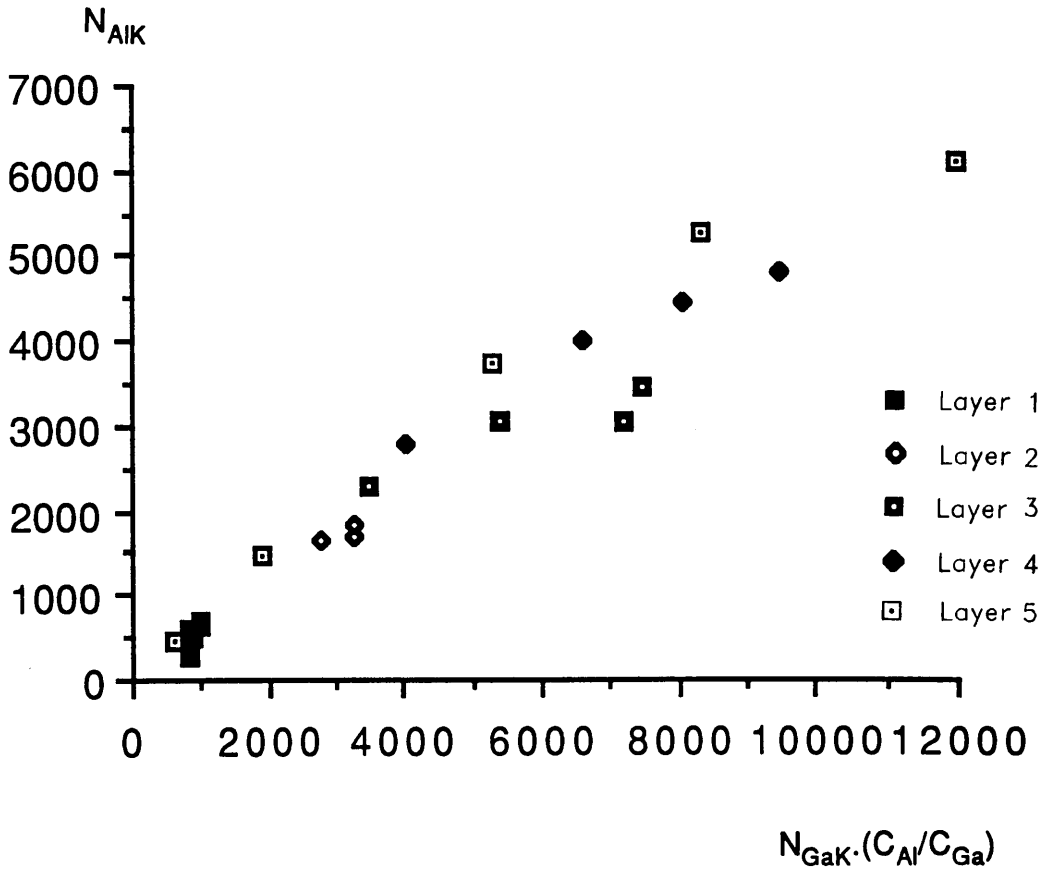

Figure 7.6

Measured Al K counts vs $N_{GaK}.(C_{Al}/C_{Ga})$ for the 5 layers in the $Al_xGa_{1-x}As$ sample.

Fitting	k_{GaAl}	ψ_0 gm cm^{-2} ($\times 10^{-8}$)
Layer 1 (10% Al)	0.76 ±0.08	1.36 ±0.40
Layer 2 (20% Al)	0.80 ±0.05	1.36 ±0.22
Layer 3 (30% Al)	0.82 ±0.02	1.26 ±0.10
Layer 4 (40% Al)	0.81 ±0.02	1.20 ±0.08
Layer 5 (50% Al)	0.79 ±0.01	1.15 ±0.10

Table 7.6

Parameters obtained from the fitting of Al K and Ga K_α data for each layer using equation 7.4.

Ga L : Ga K_α	$K' = 0.51\pm0.01$	$\psi' = (1.22\pm0.10)\times10^{-8}$
Al K : Ga K_α	$k'_{GaAl} = 0.80\pm0.03$	$\psi'_0 = (1.30\pm0.30)\times10^{-8}$

Table 7.7

Summary of fitting parameter s when data from 5 layers were taken as one set.

The scatter of the data in figure 7.6 is much greater than in figure 7.4 (the Ga L vs Ga K_α data). However, it was felt to be worthwhile to treat the data for figure 7.6 as a single set. This produced fitting parameters of k'_{GaAl} of 0.80 ±0.03 and Ψ'_0 of (1.3 ±0.3)x10^{-8} (see table 7.7). A comparison of the values of parameter Ψ obtained from the Ga L vs Ga K_α fitting [(1.22 ±0.10)x10^{-8}] with those obtained from the Al K vs Ga K_α fittings (see table 7.6) shows that these agree within experimental error.

The experimental value of k_{GaAl} along with experimental value of k_{GaAs} can be used to get the value of k_{AlAs} which is used in equation 7.1. Using equation 6.9, the value of k_{AlAs} obtained was 1.14 which agrees with the theoretical value (1.1) within ≈ 4%.

A check for consistency was made between the results obtained by this approach of absorption corrections with those obtained from the Bremsstrahlung method of absorption corrections as discussed in chapter 6. Figure 7.7 shows an experimental spectrum from a typical thicker region of the AlGaAs specimen with the thin background and the thin background corrected for absorption superimposed.

7.5 Calculation of Mass Path Length for a Single Point.

As has been discussed in chapter 6, the value of the parameter K′, which may be obtained from the fitting of L to K data of a single element may also be calculated using the

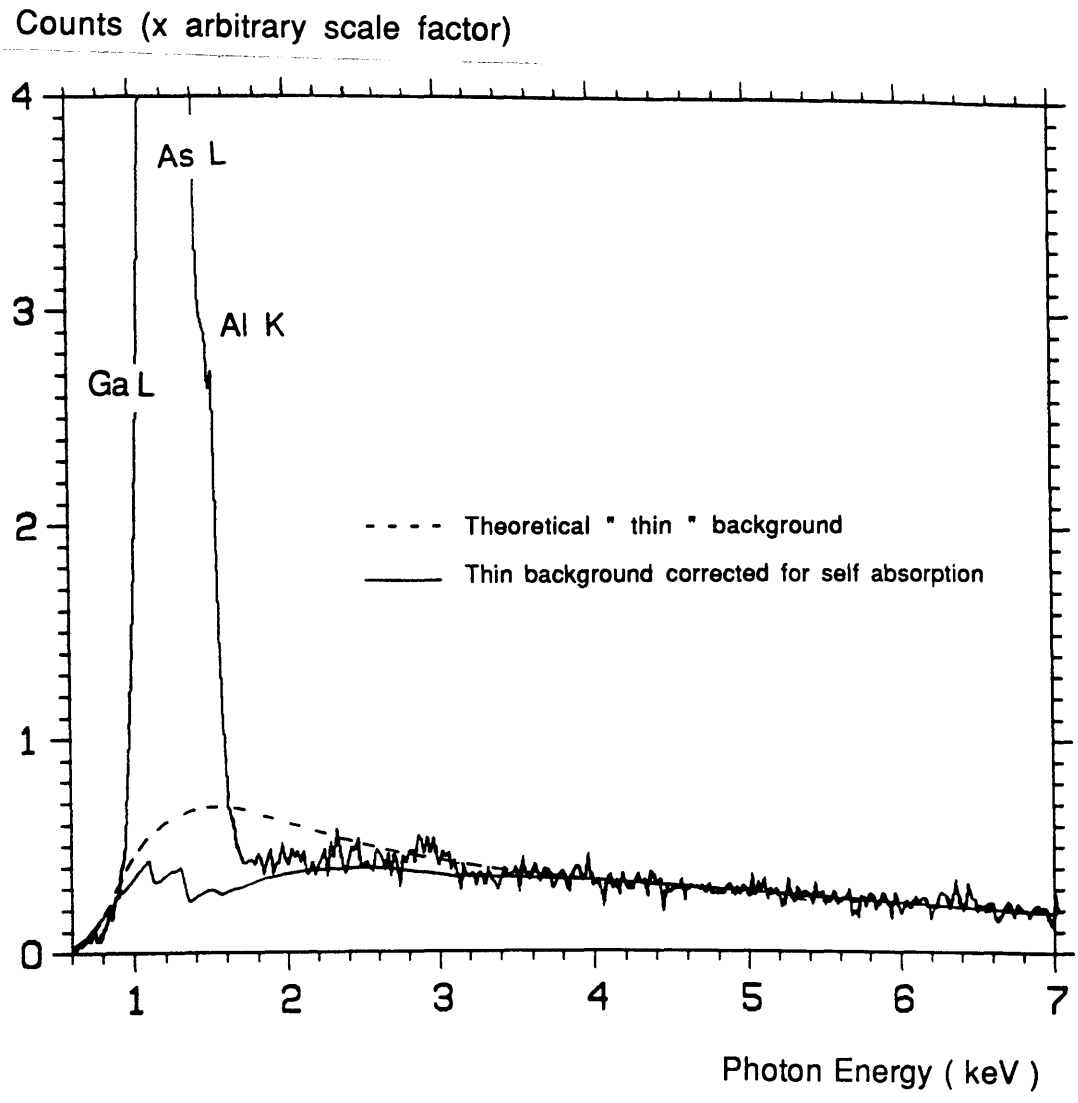

Figure 7.7

Experimental spectrum from AlGaAs point 6 of layer 4, with theoretical thin background and thin background corrected for self absorption in 580 nm absorption path length superimposed.

theoretical values of the ionisation cross sections of L and K_α lines. Similarly, the k-factor of elements A and B obtained by fitting can also be calculated theoretically. This suggests that an approximate value of mass path length of a single point could be calculated without a need for the fitting process. This possibility is investigated here in detail.

7.5.1 Using L and K lines of an Element

Re-writing equation 7.3 for a single point we get,

$$F = \frac{\left[1 - \exp\left\{ -(\mu / \rho)_L \, M \right\} \right]}{(\mu / \rho)_L \, M} \qquad (7.5)$$

where

$$F = N_L / K' N_K$$

and N_L and N_K are the measured counts of the L and K lines of an element and $(\mu/\rho)_L$ is the mass absorption coefficient of the L line. By expanding the exponential as a power series upto the cubic term and using the theoretical value of K′, equation 7.5 can be solved to give a simple relationship which relates the mass path length to the count ratio and the mass absorption coefficient of L line which can be given as,

$$M = \frac{3 \pm \sqrt{9 - 24(1 - F)}}{2(\mu / \rho)_L} \qquad (7.6)$$

Equation 7.6 gives results which agree with those calculated previously from the multipoint fit (see table 7.2), only if the

absorption of the L line is <30%. Once the mass path length of a single point is known; this can be used to correct the other lines of the sample for the absorption effect at that point.

7.5.2 Using K-lines of two elements

Re-writing equation 7.3 for a single point using the two K lines of two elements A and B,

$$F' = \frac{\left[1 - \exp\{-(\mu / \rho)_B \, M\} \right]}{(\mu / \rho)_B \, M} \qquad (7.7)$$

where,

$$F' = \frac{N_B}{N_A} \frac{C_A}{C_B} \frac{1}{k_{AB}} \qquad (7.8)$$

As before the exponential may be approximated to give an equation of the form 7.6. A first order approximation of C_B/C_A can be obtained from the composition of the sample calculated from the use of uncorrected data of that particular point. This ratio along with the theoretical value of k_{AB} can be used in equation 7.8 to get a first order approximation of F′ which can be used to calculate an approximate value of M. An iterative approach can be used to get the best value of M and $(\mu/\rho)_B$ and the corrected composition.

It may be noted that calculation of the factor F from L to K calculation is simple as it is less dependent on the specimen composition, whereas the factor F′ strongly depends on the specimen composition. This indicates that the use of the data of

two K lines may involve many calculations before getting best value of correction factor.

Table 7.8 compares some values of mass path length obtained from the fitting method with those obtained from the use of equations 7.5 and 7.7.

7.6 Results and Discussion

In this work it has been shown that it is possible to correct the Al signal in an AlGaAs/GaAs multilayer system (where composition is not a constant) for self absorption using the data from the characteristic lines of the sample. It can be seen from table 7.1 that the ratio of Al to Ga concentration varies significantly within a layer. This variation of concentration does not affect the absorption correction fitting approach if the Ga L and Ga K_α data are used. However, this variation affects the fitting approach if Al K and Ga K_α data are used with the condition that parameter K of equation 3.17 is a constant. However, it has been seen that the same data can be used with a modified approach since k_{AB} of equation 3.17 is a constant. Hence, both the Ga L vs Ga K_α and the Al K vs Ga K_α fittings discussed in this chapter provide alternative techniques when the composition of the sample is not constant. However, the L to K fitting is simpler to use as it is less dependent on the specimen composition.

A possibility of correcting data from a single point for absorption without the use of a fitting approach is also examined. This uses the count from two lines of a particular point and some constants which can be either taken from tables or can be calculated from first principles.

Point	Mass Path Length (gm cm^{-2})x10^{-4}		
	Fitting	Equation 7.5	Equation 7.7
2 of layer 1	1.2	1.27	1.26
1 of layer 2	1.0	0.98	1.03
3 of layer 3	1.4	1.4	1.44
3 of layer 4	1.2	1.26	1.24
6 of layer 5	1.0	0.98	0.97

Table 7.8

Comparison of values of mass path length obtained from fitting method to that of equations 7.5 and 7.7.

The values of mass path length obtained by the characteristic line method of self absorption are compared with the method of MBH fitting and it can be seen from figure 7.6 that results are self consistent.

CHAPTER 8

Conclusions

The data and discussions in this thesis has been mainly centered about x-ray absorption corrections. The general aim was to improve the accuracy of the standardless technique of thin film microanalysis. Absorption of low energy x-rays was divided into two parts. One absorption within the specimen (self absorption) and other absorption within the protective windows of the detector (low energy detector efficiency). Low energy detector efficiency as well as high energy detector efficiency (transmission of high energy photons through the crystal) appears to be the controlling factor in relating the accuracy of experimental and theoretical k-factors from system to system.

The detector efficiency depends on mass absorption coefficients and thickness of the absorbing materials. Several formulations are found in the literature. In chapter 4 two of them are investigated for a variety of detectors to see how these affect the detector efficiency of a particular detector. From this work following points have been concluded:

(1) The overall shapes of the detector efficiencies can be well characterised, essentially independently of the choice of mass absorption coefficient formulations.

(2) The values of the thicknesses of the absorbing materials are dependent upon the choice of the coefficient formulations. Every formulation of mass absorption coefficients will give different

value of the thickness of absorber. However, the Heinrich formulation gives values which are closer to the manufacturer quoted values. It is important to note that whenever value of the thickness of the absorber material is quoted, the formulation of mass absorption coefficient used should also be given.

(3) Enough information is not available in a spectrum to separate out the absorption effects of each individual protective layer present before the active region of the detector. For a Be window detector it is convenient to assume the absorption in the Be window only and for a windowless detector absorption in the Au layer can be assumed for the purpose of efficiency calculations.

In general, the specimen self absorption corrections using the Bremsstrahlung are difficult as problems may be encountered in comparing the theoretical MBH cross-sections with experimental backgrounds below 3 keV for a variety of reasons. Many of the phenomena which distort the shape of the experimental spectra below 3 keV can be broadly classified as detector effects. However, in this thesis this technique has been investigated for biological samples (or those with an organic matrix) as in such samples the detector effects are less of a problem. It has been seen that in such samples the Na K, Mg K and Al K characteristic lines are those mostly affected by specimen self absorption. For example, for a typical point of thickness $\approx$ 200 nm 30% signal of the Na K line was found to be absorbed.

The method of specimen self absorption corrections using the characteristic lines have been developed. For this method many of the characteristic line intensities in a measured

The specimen composition variation was almost certainly due to effects of electron scattering from AlGaAs into the neighbouring GaAs layers. However, for the purpose of this work the analysis treated this as being a composition variation within the layer.

spectrum are used. Two approaches have been used. One using the K_α and L characteristic lines of a single element and the other using the K characteristic lines of two elements present in the sample whose concentration ratios are assumed to be constant. The first approach is relatively simple as it is less dependent on specimen composition and variation in the composition. The second approach depends much on specimen composition and is more affected by composition variation.

It has been shown in chapter 7 that a modified technique can be used if specimen composition variation is a problem. However, this technique has some limitations. If the variation of the mass absorption coefficients of the K line of element B changes slowly with composition variation (as in Ga L and Ga K in an AlGaAs layer), then the data may be considered as a single set. However, if this is not the case (as has been seen in Al K and Ga K case in AlGaAs layer), then it is important to put a limit on the specimen composition variation. It can be seen in chapter 7 that the specimen composition varied within $\approx$ 15% in each AlGaAs layer and the modified technique worked well. However problems were encountered in fitting data from all five layers (where composition varies from $\approx$ 5% to $\approx$ 50%) due to the significant change in the mass absorption coefficients of Al K .

Although, the work presented in chapters 6 and 7 have provided good results for absorption corrections, the technique could still be investigated further. The accuracy and applicability could be investigated with a variety of samples so that this could possibly lead to a more general approach for absorption corrections. A common problem in thin film microanalysis is the overlap of low energy L lines. A detailed

investigation could be made by plotting the combined peak of two different L lines (as in AlGaAs where Ga L overlaps As L) against the line of element whose line is little absorbed. This might be possible if the mass absorption coefficient of the combined peak could be calculated by normalising the mass absorption coefficient of individual L lines. In multilayer samples investigated in chapter 7, some variations in measured composition were evidently due to beam broadening in the sample. It is possible that this experiment could be extended to give more information about the effects of beam broadening. A comparison of measured composition with actual composition would indicate the electron intensity scattered into neighbouring layers.

In this work, technique has been developed using K and L lines only. However, an investigation could be made using M lines (if they were present in the sample) with that of L or K lines. Also, in this technique a restriction is that one line in the sample must be present for which the absorption is negligible. An investigation could be made to determine if fittings were possible using any two lines present in the sample even if the higher energy one showed some effects of absorption.

The accuracy of the calculation of thickness from x-ray absorption path length depends on the geometry of the experiment. Work could be carried out measuring the relative positions (in X and Y) on the sample at which the analyses were made. The characteristic line method can provide the thickness of the sample, so it could be possible to calculate the wedge profile for a number of points. A better knowledge of the wedge angle would reduce the error in the geometric factor and hence

the conversion from absorption path length to thickness.

Background modelling for biological samples has been carried out for a specific sample. From this work, it has been seen that this method provides relatively more accurate concentration results especially for P K and S K signal than those of obtained from a conventional method (window method). More investigation is required before it can become a more common technique of background subtraction in such samples. A comparison of the results obtained by this method with other methods of background subtraction such as filter least square (FLS) fitting method will be useful to check the accuracy of the method.

APPENDIX 1

Analytical Representation of MBH Equation

In this appendix the analytical representation of MBH equation is presented. The subroutine MBHEQ is written to evaluate this equation. First a list of symbols, constants and energy-momentum relationships used are given.

E_0, E	Initial and final total energy of the electron in a collision, in m_0c^2 units.
p_0, p	Initial and final momentum of the electron in a collision, in m_0c^2 units.
T'_0, T′	Initial and final kinetic energy of the electron in a collision, in m_0c^2 units.
k_0, K_0	Energy and momentum of the emitted photon in m_0c^2 and m_0c units.
θ_0	Angle between p_0 and K_0 (MBH angle)
m_0	Rest mass of an electron (9.11×10^{-31} kg)
m_0c^2	Electron rest mass energy (511 keV)
r_0	Classical radius of an electron (= $e2/m_0c^2$ = 2.82×10^{-15} m)

$$E^2_0 = p^2_0 + 1 \qquad E^2 = p^2 + 1$$

$$E_0 = T'_0 + 1 \qquad E = T' + 1$$

$$p_0 = [T'_0(T'_0 + 2)]^{1/2} \qquad p = [T'(T' + 2)]^{1/2}$$

The reduced cross section (Chapman et al, 1983) can be given as,

$$\sigma'' = (2.31)10^{-2}\ \frac{\beta_0\left[1-\exp(-2\pi\ Z/\ 137\ \beta_0)\right]}{\beta\left[1-\exp(-2\pi\ Z/\ 137\ \beta\ )\right]}\cdot\frac{pT'}{p_0}$$

$$\left\{\frac{8\sin^2\theta_0\left(2E_0^{\ 2}+1\right)}{p_0^{\ 2}\Delta_0^{\ 4}}-\frac{2\left(5E_0^{\ 2}+2E.E_0+3\right)}{p_0^{\ 2}\Delta_0^{\ 2}}-\frac{2\left(p_0^{\ 2}-k_0^{\ 2}\right)}{Q^2\Delta_0 2}\right.$$

$$+\frac{4E}{p_0^{\ 2}\Delta_0}+\frac{L_0}{pp_0}$$

$$\left.x\left\{\left[\frac{4E_0\sin^2\theta_0\left(3k_0-p_0^{\ 2}E\right)}{p_0^{\ 2}\Delta_0^{\ 4}}+\frac{4E_0^{\ 2}\left(E_0^{\ 2}+E^2\right)}{p_0^{\ 2}\Delta_0^{\ 2}}\right.\right.\right.$$

$$\left.\left.\left.x\left[+\frac{2-2\left(7E_0^{\ 2}-3EE_0+E^2\right)}{p_0^{\ 2}\Delta_0^{\ 2}}+\frac{2k_0\left(E_0^{\ 2}+EE_0-1\right)}{p_0^{\ 2}\Delta_0}\right]-\frac{4\varepsilon_0}{p\Delta_0}+Q_0\right\}\right\}$$

where

$$L_0 = \ln\left[\frac{\left(EE_0-1+pp_0\right)^2}{k_0^{\ 2}+p_0^{\ 2}\ \exists^{-2}\ \Delta_0^{\ -2}}\right]$$

$$\Delta_0 = E_0-p_0\cos\theta_0 \quad ; \quad \varepsilon_0=\ln\left(\frac{E+p}{E-p}\right)$$

$$Q^2 = p_0^{\ 2}+k_0^{\ 2}-2p_0k_0\cos\theta_0 \quad ; \quad \exists=\frac{108}{Z^{1/3}}$$

$$Q_0 = \frac{\varepsilon'}{pQ}\left[\frac{4}{\Delta_0^{\ 2}}-\frac{6k_0}{\Delta_0}-\frac{2k_0\left(p_0^{\ 2}-k_0^{\ 2}\right)}{Q^2\Delta_0}\right]$$

and

$$\varepsilon' = \frac{1}{2}\ln\left[\frac{(Q+p)^4}{4\left(k_0^{\ 2}\Delta_0^{\ 2}+p_0^{\ 2}\ \exists^{-2}\right)}\right]$$

APPENDIX 2

Analysis Programmes

A2.1 Introduction

In this section the programmes are presented which were written for the analysis of spectral data in this thesis. Sections A2.2 to A2.9 describe the purpose of each programme. In section A2.10 the main programmes are listed. In section A2.11 the subroutines used by the main programmes are listed alphabetically.

A2.1 ANALYSIS

This programme presents a menu which allows the user to select which processing step is required. Information is passed from subroutine to subroutine for processing (mostly in labeled common). This can be summarised as follows:

(1) An experimental spectrum is read from the disk in INSPEC array in real (floating point) format via subroutine RDSPAN, which automatically reads spectra in either 16 bit integer or 32 bit double precision integer format.

(2) The MBH theoretical background spectrum is read in OUTSPEC array in real format again via subroutine RDSPAN.

(3) A secondary short menu is used in subroutine EFFIC which allows the user to correct the theoretical background spectrum for low and high detector efficiencies and the specimen self

absorption effect. Files of mass absorption coefficient are directly read from the disk via subroutine RDSPAN. These would have been created previously using the programme MABSCO (section A1.6).

(4) The regions of the spectrum required for analysis are selected via subroutine SETWIND, which allows the user to set upto 30 windows. The selected window channel numbers are written in common to pass this information to other subroutines.

(5) The corrected MBH spectrum may be scaled to the real experimental spectrum according to the ratio of counts in a chosen window or windows of the spectrum via subroutine SCALE.

(6) The scaled MBH spectrum may be then compared with the experimental spectrum over a selectable range or ranges of interest. A reduced chi-square value of the fit over the range(s) may be calculated via a subroutine CHISQUARED.

(7) The corrected MBH spectrum is then written to the disk in AN10 format using subroutine WRSPAN. This subroutine uses another subroutine ERRMESS which outputs to the console error messages corresponding to the error numbers in the Link Fortran Manual.

(8) The subroutine HEADER and PRESET are also used in this programme. The subroutine PRESET sets the spectrum parameters e.g number of channels, energy per channel,etc. The subroutine HEADER sets up a spectrum header block default values to allow writing files to disk in the Link AN10 format that the data can be read into the x-ray analyser as a spectrum for visualization.

(9) An option is introduced in the programme to allow the user to change the preset values of the parameters used in the programme.

A2.3 AUTO

This programme is based on MBH theoretical modelling and is used to get a Bremsstrahlung spectrum corrected for self absorption for a particular sample (see chapter 5). This programme works automatically without user's input once the windows of interest are set and name of the experimental spectrum is provided. The experimental and universal background (MBH for formvar corrected for low detector efficiency) spectra are read for the analysis. The universal background spectrum is corrected for different values of absorption path length via subroutine SELF. Each time the corrected spectrum is scaled to the experimental spectrum in the region of interest and the value of reduced chi-square is calculated in the chi-square region. The absorption path length corresponding to best value of reduced chi-square is used to get the fitted background spectrum. This background spectrum is then stored on the disk via subroutine WRSPAN. The programme uses subroutines SETWIND, HEADER, PRESET, and RDSPEC. The subroutine RDSPEC is similar to subroutine RDSPAN, but here some DFLAG values are introduced to enable it to be run on an automatic basis.

A2.4 HALL

This is a short programme, which is based on Hall theory of

quantitation and is used to calculate the mass fractions of the elements present in the a biological sample (see chapter 5). This programme uses two subroutines RQELEMENT and SUMTERM. Initially the programme assumes that in the biological sample under analysis the elements of interest are Na, Mg, Al, P, S, Cl, K, and Ca. The subroutine RQELEMENT asks the user to enter the atomic number of the elements which he/she requires for the analysis. This and some other data e.g peak to white ratio of standard, atomic weight, and g-factors are passed to subroutine SUMTERM through common. Then, the subroutine SUMTERM asks the user to enter the peak to white ratio of each element present in the sample and calculates the sum term of Hall equation (see chapter 5). This value is returned to main programme to calculate the mass fractions of the elements.

A2.5 KVALUE

This is a short programme which is written to calculate the values of K-factors using a theoretical approach (Paterson et al, 1989). It requests the user to provide the data (e.g partition function, fluorescence yield, ionisation energy, etc) for two lines of elements A and B and then using this data calculates the K-factor for these two lines.

A2.6 MABSCO

This programme is used to calculate the mass absorption coefficients, which is based on Heinrich's (1987) model. The original version was provided by Dr. A J Gareett-Reed, M. I. T. Boston USA, and has been modified to run on the Link AN10. The

programme has also been extended to calculate the mass absorption coefficient values for multi-element samples. The mass absorption coefficient values are written in spectrum format upto 2048 channel long.

The subroutine MAC returns the mass absorption coefficient values to the programme. These are then multiplied by a scale factor of 1000. This maintains the precision of the values especially at high photon energies where mass absorption coefficients tend to be small. The subroutine MAC requires the edge energies of the elements used for computation of mass absorption coefficient values. These values are returned to this subroutine via another subroutine EDGE, which reads K, L, M and N1 edge energies of each element from binary data files EEDT1 and EEDT2.

The programme also uses the subroutine HEADER, FORMSPEC, COMPI, COMPO, WRSPAN, and ERRMESS. The subroutine FORMSPEC allows selection and changing of the default spectrum parameters and photon energy range required for the computation. The subroutine COMPI is used to get interactively the number of elements and their proportions in the sample. Then, the subroutine COMPO checks specimen composition from COMPI has been entered correctly. In this subroutine data is passed through common to get round a curious I/O problem in the compiler.

A2.7 MBHBACK

This programme is used to calculate the theoretical background spectrum. It can handle a spectrum upto 2048

channels long and can also be used for multi-element samples. The programme is based on MBH. A subroutine MBHEQ returns the values of the reduced cross-sections for Bremsstrahlung production in units of mb/sr if the electron and photon energies are supplied in keV. This reduced cross-section is converted into an absolute cross-section in the main programme. The other subroutines required for this programme are, HEADER, FORMSPEC, COMPI, COMPO, WRSPAN , and ERRMESS.

A2.8 MINIMISE

This programme is based on the theory of non-linear regression. A detailed review of non-linear regression is given by Bard (1974) and Gill and Murray (1978). The programme MINIMISE was written on an IBM main frame computer type 4361. This has the advantage of having a suitable NAG Fortran Library of subroutines. Two subroutines suitable for non-linear least squares fitting, E04YCF and E04FDF were used from the Library to fit the data as described in chapters 6 and 7. This programme asks the user to enter the number of data points and number of unknown fitting parameters with guess values of the parameters. The input data is read by the programme in the form of a file which is provided by the user at the end of the programme. The subroutine E04FDF generates a sequence of points which is intended to converge to a local minimum of the sum of squares of residuals (FSUMSQ). This subroutine requires another external subroutine which must be named LSFUN1. The subroutine LSFUN1 should state the equation of the theoretical

line to evaluate the residuals. The value of FSUMSQ returned by the subroutine E04FDF is used by the subroutine E04YCF. This second subroutine compares the observed data with the data obtained from the non-linear least-square function. The best values of the fitting parameters are returned corresponding to goodness of the fit.

A2.9 RATIO

This programme is based on Cliff-Lorimer (1975) approach of quantitation and is used to calculate the concentration ratios in the sample $In_{1-x}Ga_xP_{1-y}As_y$ as described in chapter 6. The uncorrected characteristic counts are requested and passed to subroutine CORRECTION via common. The subroutine CORRECTION corrects the In, Ga, P, and As lines for specimen self absorption corresponding to the absorption path length obtained from main method (see chapter 3). The values of the mass path length are entered interactively. This subroutine uses another subroutine FRACTION, which works out the appropriate mass absorption coefficients of four lines. Initially the sample is assumed pure InP (In : P = 0.5 : 0.5), but later on an iterative approach is used to find better values of the mass absorption coefficients of four lines and more accurate concentrations of the four lines in the sample.

A2.10

Main Programme Listings

(The programmes are listed alphabetically.)

```
C FILE-------Analysis
C This programme is for spectrum analyses. Experimental and theoretical
C spectra are read in INSPEC & OUTSPEC arrays.OUTSPEC array is
C corrected for detector efficency and specimen absorption. Windows may
C be selected for scaling the spectra.The final spectrum is written
C on to disk.
C Requires subroutines HEADER, PRESET, RDSPAN, EFFIC, SETWIND, SCALE,
C CHI, WRSPAN, and ERRMESS.
C  Declarations
        INTEGER OPT,WIND,NAME(7),TEXT(10)
        REAL IDE,OUTSPEC ,INSPEC,TEMPSPEC
        COMMON/HEADAN/IHEDAN(0:255)/ARRAY/ISPEC(0:2047)/IARAY/INSPEC(0:2047)/
     1  JARAY/OUTSPEC(0:2047)/KARAY/TEMPSPEC(0:2047)/BLK4/WIND(3,30)
        EQUIVALENCE (IHEDAN(3),MCMIN),(IHEDAN(4),MCMAX),(IHEDAN(7),GF)
        EQUIVALENCE (IHEDAN(9),X0),(IHEDAN(33),SCALNUM)
C  Call header routine
        CALL HEADER  ;Set the header default values.
C  Set Parameters
 20     CALL PRESET (NCHANS,THETA,IDE)
 150    CALL CRLF
        CALL MESS ("SELECT THE OPTION PLEASE. ")
        CALL CRLF
        CALL MESS ("(1) Read an experimental spectrum into INSPEC array.")
        CALL CRLF
        CALL MESS ("(2) Read MBH spectrum(real) into OUTSPEC array.")
        CALL CRLF
        CALL MESS ("(3) Detector efficiency & self absorption correction .")
        CALL CRLF
        CALL MESS ("(4) Set windows.")
        CALL CRLF
        CALL MESS ("(5) Scale OUTSPEC array.")
        CALL CRLF
        CALL MESS ("(6) Chi2 test. ")
        CALL CRLF
        CALL MESS ("(7) File the OUTSPEC to disk.")
        CALL CRLF
        CALL MESS ("(8) Change the presets. ")
        CALL CRLF
        CALL MESS ("(9) End  ")
        CALL CRLF
        CALL IGETNO (OPT,2)
        IF(OPT.LT.1.OR.OPT.GT.9)GO TO 150
C               1   2   3   4   5    6    7   8  9
        GO TO(500,600,700,800,900,1000,1100,110,98),OPT
 500    CALL YESNO (" Read a spectrum in  INSPEC ? ",$150)
        CALL RDSPAN (NAME)
        DO 6 I=0,MCMAX
 6      INSPEC(I)=TEMPSPEC(I)
        CALL CRLF
        CALL MESS ("<15><12> Spectrum in INSPEC named ")
        CALL MESS (NAME)
        GO TO 150
C
 600    CALL YESNO (" Read a spectrum in OUTSPEC ?",$150)
        CALL RDSPAN(NAME)
        DO 7 I=0,MCMAX
 7      OUTSPEC(I)=TEMPSPEC(I)
        CALL CRLF
        CALL MESS ("<15><12> Spectrum in OUTSPEC named ")
        CALL MESS(NAME)
        GO TO 150
C
 700   CALL YESNO ("Efficiency and self absorption correction  ?",$150)
        CALL CRLF
        CALL EFFIC(NCHANS,THETA)
        GO TO 150
C
 800    CALL YESNO ("Set windows   ?",$150)
        CALL SETWIND
        GO TO 150
```

```
C
 900     CALL YESNO ("Scale the spectrum in  OUTSPEC   ? ",$150)
         CALL SCALE(NCHANS,IDE)
         CALL MESS ("<15><12> Spectrum scaled in OUTSPEC.")
         GO TO 150
C
 1000    CALL YESNO (" Reduced chi2 test   ?",$150)
         CALL CHISQUARE(NCHANS,IDE)
         GO TO 150
C
 1100    CALL YESNO ("Write OUTSPEC to disk  ? ",$150)
         CALL WRSPAN(NAME)
         GO TO 150
C
 110     CALL YESNO (" Change the presets   ?",$150)
         GO TO 20
C
 98      CALL YESNO (" Terminate the programme ? ",$150)
         CALL RESET
         STOP
         END


C File-------AUTO
C This programme is for the analysis of biological samples. It models the
C thin (specimen) background with a formvar MBH spectrum corrected for
C detector efficiency.This background spectrum is corrected for specimen
C self absorption by setting path length as a variable parameter.The best
C value of path length is obtained corresponding to the minimum value of
C reduced chi2. It works automatically once the scaling and chi2 windows
C are set and name of the experimental spectrum is provided.
C It can handle upto 2048 channel spectra.
C Requires subroutines HEADER, PRESET, SETWIND, SELF, RDSPEC, WRSPAN, and
C ERRMESS.
C  Declarations
         INTEGER WIND,NAME(7),TEXT(10),DFLAG,EVCH
         REAL IDE,INSPEC,OUTSPEC
         COMMON/HEADAN/IHEDAN(0:255)/ARRAY/ISPEC(0:2047)/IARAY/INSPEC(0:2047)/
     1   JARAY/OUTSPEC(0:2047)/KARAY/TEMPSPEC(0:2047)/BLK4/WIND(3,30)
         COMMON/XARAY/TEMPB (0:2047)/YARAY/TEMPE (0:2047)
         EQUIVALENCE (IHEDAN(3),MCMIN),(IHEDAN(4),MCMAX),(IHEDAN(7),GF)
         EQUIVALENCE (IHEDAN(9),X0),(IHEDAN(33),SCALNUM)
C
         CALL HEADER ; Set up default values for header blocks.
         CALL PRESET (NCHANS,THETA,IDE ); Set necessary parameters.
         CALL SETWIND   ;Set windows for scaling and chi-squared value.
 150     CALL CRLF
         MIN=0
         MAX=2000      ;Maximum range for mass path length (nm).
         INT=100     ;Increase in path length in step of 100 nm.
         IPL=MIN       ;Minimum range for mass path length (nm).
         DFLAG=0       ; To read an experimental spectrum.
C
         CALL RDSPEC (NAME,DFLAG)  ; Read an experimental spectrum.
         CALL CRLF
         CALL MESS ("Please wait I am working out the best value for ")
         CALL MESS ("the path length. ")
         DO 6 I=0,MCMAX
 6       TEMPE(I)=TEMPSPEC(I)
         DFLAG=2          ;To read thin background spectrum.
         CALL RDSPEC (NAME,DFLAG)  ; Read thin background spectrum.
         DO 7 I=0,MCMAX
 7       TEMPB(I)=TEMPSPEC(I)
C
         COMP=0.0   ;Set inital value of comparing parameter to zero.
         DO 999 J=MIN,MAX,INT
         RTX=FLOAT(J)
         DO 8 I=0,MCMAX
         INSPEC(I)=TEMPE(I)
 8       OUTSPEC(I)=TEMPB(I)
         CALL SELF (NCHANS,IDE,RTX) ; Work out specimen self absorption.
```

```
C  Scale to experimental and thin background spectra over a scaling region.
        NWIN=1    ;Number of windows used for scaling.
        A=0.0
        B=0.0
        C=0.0
        DO 100 I=1,NWIN
        NCODE=2  ;Window number used for scaling.
        N1=WIND (2,NCODE) ; Low channel number for scaling window.
        N2=WIND (3,NCODE) ; High channel number for the scaling window.
        DO 100 K=N1,N2
        A=A+INSPEC(K)
        B=B+OUTSPEC(K)
 100    CONTINUE
        SCALF=A/B
        DO 200 I=0,NCHANS
 200    OUTSPEC(I)=OUTSPEC(I)*SCALF
C
C Work out reduced chi-squared value.
        NWIN=1  ; Number of windows used for chi2 test.
        NF=0
        CHI2=0.0
        A=0.0
        DO 300 I=1,NWIN
        NCODE=1  ;Window number used for chi2-test.
        N3=WIND (2,NCODE) ;Low channel number for chi2 window.
        N4=WIND (3,NCODE) ;High channel number for chi2 window.
        NF=NF+N4-N3+1
        DO 300 K=N3,N4
        CHI2=CHI2 + (((ABS(INSPEC(K)-OUTSPEC(K)))**2)/INSPEC(K))
        IF (INSPEC(K).EQ.0.0) GO TO 300
 300    CONTINUE
        NF=NF-1
        REDCHI2=CHI2/NF
C
C  Compare the reduced chi2 value from the previous one.
        IF(COMP.EQ.0.0) GO TO 90
        IF(REDCHI2.GT.COMP) GO TO 99 ;If reduced chi2 value increases
                          ;from the previous(minimum) one, then stop.
 90     COMP=REDCHI2  ;First non-zero value for comparing parameter.
        IPL=IPL+INT   ;Increases path length value by 100 in each step.
 999    CONTINUE
 99     CONTINUE
        CALL ALPH16
        CALL PRTON  ; Set printer on to write best value of path length.
        CALL CRLF
        CALL MESS ("P.LENGTH (in nm )=   ")
        IPL=IPL-INT  ; Find the mass path length corresponding to
                     ; minimum chi2.
        PL=FLOAT(IPL)
        CALL IPUTNO(IPL,6)
        CALL MESS("   REDCHI2=     ")
        CALL PUTNO(COMP,11,6)
        CALL CRLF
        CALL PRTOFF   ;Set printer off.
C
        DO 95 I=0,MCMAX
 95     OUTSPEC(I)=TEMPB(I) ; Take thin background spectrum and correct
        CALL SELF (NCHANS,THETA,PL);it for self absorption effect.
C
        CALL WRSPAN (NAME) ; Write out corrected spectrum on to the disk.
        CALL CRLF
        CALL YESNO (" Teriminate the programme ? ",$150)
        STOP
        END
```

```
C File -------HALL
C This programme is based on Hall theory of quantitation.
C Requires subroutines RQELEMENT and SUMTERM
C ATW is for atomic weight, GF is for G-Factor, R is for the ratio of
C peak to white of specimen to peak to white of standard, PWST and PWSP
C  are for peak to white of standard and specimen respectively, NE is
C number of elements, Z is for atomic number, H is a constant and RQZ is
C for the atomic number of those elements which are required in the analysis.
      COMMON/DT/ATW(8),GF(8),R(8),Z(8),PWST(8),PWSP(8),NE,H,RQZ(8)
      NE=8
      H=3.2Ø
      CALL RQELEMENT  ; Sets up atomic data in arrays.
 22   CONTINUE
      CALL SUMTERM (SUM)
      DO 44 J=1,NE
      IF (Z(J).EQ.Ø.Ø) R(J)=Ø.Ø
      IF (R(J).EQ.Ø.Ø) GO TO 44
      UP=R(J)*ATW(J)*GF(J)*H
      CX=UP/SUM
      CX=CX*1ØØ.Ø
      CALL CRLF
      CALL ALPH16
      CALL PRTON
      CALL CRLF
      CALL MESS (" % Concentration for element Z=   ")
      CALL PUTNO(Z(J),6,1)
      CALL MESS ("   =    ")
      CALL PUTNO (CX,8,4)
      CALL CRLF
      CALL PRTOF
 44   CONTINUE
      CALL CRLF
      CALL YESNO ("ANY MORE ?   ",$99)
      GO TO 22
 99   CONTINUE
      STOP
      END

C File ------KVALUE
C Programme to calculate K-factors theoretically.
       INTEGER NAME1(7),NAME2(7)
       REAL KAB
C SET UP THE VALUES.
 1Ø    CALL CRLF
       CALL MESS ("I WILL CALCULATE K-FACTOR OF TWO ELEMENTS(THEORETICALLY)")
       CALL CRLF
       CALL MESS ("PLEASE ANSWER ME CAREFULLY   ")
       CALL CRLF
       CALL DEFAULT ("Enter name of element A  ",NAME1,"S",1Ø)
       CALL CRLF
       CALL DEFAULT ("Enter name of element B  ",NAME2,"S",1Ø)
       CALL CRLF
       CALL MESS("Enter partitation function of element  A    ")
       CALL GETNO(SA,5,3)
       CALL CRLF
       CALL MESS("Enter partitation function of element  B    ")
       CALL GETNO(SB,5,3)
       CALL CRLF
       CALL MESS("Enter fluorescence yield of element  A    ")
       CALL GETNO(WA,5,3)
       CALL CRLF
       CALL MESS("Enter fluorescence yield of element  B    ")
       CALL GETNO(WB,5,3)
       CALL CRLF
       CALL MESS ("Enter ionisation energy (kev) of element  A    ")
       CALL GETNO(EIA,5,2)
       CALL CRLF
       CALL MESS ("Enter ionisation energy(kev) of element   B     ")
       CALL GETNO(EIB,5,2)
```

```
      CALL CRLF
      CALL MESS ("Enter electron energy(kev)  default=100.0     ")
      NCH=5
      CALL GETNO(T0,NCH,1)
      IF(NCH.EQ.0) T0=100.00
      CALL CRLF
      CALL MESS ("Enter value of constant BK. default= .89 ")
      NCH=6
      CALL GETNO (BK,NCH,3)
      IF (NCH.EQ.0) BK=0.89 ;Beth equation parameter (Paterson, 1989)
      X=(T0/EIA)*BK
      SIGMAA=((SA*WA)/EIA)*ALOG(X)
      Y=(T0/EIB)*BK
      SIGMAB=((SB*WB)/EIB)*ALOG(Y)
      KAB=SIGMAB/SIGMAA
C Ask for detector efficiencies of the two lines.
      CALL CRLF
      CALL MESS ("Enter detector efficiency at K line of element A   ")
      CALL GETNO (EFFA,4,3)
      CALL CRLF
      CALL MESS("Enter detector efficiency at K line of element B   ")
      CALL GETNO(EFFB,4,3)
      KAB=KAB*(EFFB/EFFA)
C Set printer on.
      CALL CRLF
      CALL ALPH16
      CALL PRTON
      CALL CRLF
      CALL MESS("KEY: K-FACTOR  A=     ")
      CALL MESS(NAME1)
      CALL MESS ("   B=   ")
      CALL MESS(NAME2)
      CALL CRLF
      CALL MESS("      KAB=      ")
      CALL PUTNO(KAB,6,3)
      CALL CRLF
      CALL PRTOFF
      CALL YESNO (" Any more  ?      ",$19)
      GO TO 10
 19   CONTINUE
      STOP
      END


C....file MABSCO
C Programme to calculate mass absorption coefficient spectrum upto 2048
C channels long, using Heinrich's Formulation, using subroutine MAC, which
C returns the mass absorption coefficient value. This value is multiplied by
C a scale factor 1000, to mantain the precision of the data at higher
C energy end.
C Program also uses subroutines WRSPAN, ERRMESS, FORMSPEC, COMPO, COMPI,
C HEADER, EDGE and two data files EEDT1 and EEDT2, which contain values
C of edge  energies for elements Z=1 to Z=96 in binary format.
C F.Pt Scale factor saved in header 33 & 34
C Calculates mass absorption coefficients values for multielements.
C
C .....declarations .......
      COMMON /HEADAN/IHEDAN(0:255) /JARAY/OUTSPEC(0:2047)
      COMMON /ATCONS/ATNOS(20),ATWTS(20),ATFRS(20),WTFRS(20)
     1  /BLK3/EEDGE(10,96)/BLK4/FEDGE(5,96)/BLK5/SEDGE(5,96)
      EQUIVALENCE (IHEDAN(1),MHDSIZE),(IHEDAN(3),MCMIN), (IHEDAN(4),MCMAX)
      EQUIVALENCE (IHEDAN(7),GF), (IHEDAN(9),X0), (IHEDAN(33),SCALENUM)
      INTEGER ATNOS,NAME(7),LABEL(16),EVCH,DFLAG,RQMAX,RQMIN
      REAL OUTSPEC,PK,M0C2,NORMFAC,INTENS,MACV
C
 1    CALL HEADER ;set up spectrum header block default values
      CALL FORMSPEC(RQMIN,RQMAX) ;get photon Energy range/ Spectrum Format
      DFLAG=2                  ; for MABSCO don't need atomic fractions etc.
      CALL COMPI(DFLAG,NUMELS)      ;get atomic Nos & mass fractions
C
```

```
C ..............................................................
        CALL EDGE          ; Read up edge energies for element 1 to 96.
C
        DO 1Ø I=MCMIN,MCMAX
1Ø      OUTSPEC(I)=Ø.Ø              ;zero spectrum array for new data
C Create theoretical spectrum of Absolute cross-sections as reals
        CALL CRLF
        CALL MESS ("MABSCO calculation takes  about  3Øs")
        CALL MESS (" per element for 1Ø24 channels ")
        EVCH=IFIX(1ØØØ.Ø/GF)       ;eV per channel
        SCALENUM=1ØØØ.Ø            ;suitable scale factor for mass absorption
                                   ;coefficients
        DO 18 J=1,NUMELS
        NORMFAC=WTFRS(J)*SCALENUM
        DO 19 I=RQMIN,RQMAX
        PK=(FLOAT(I)-XØ)*EVCH                    ;Pk in eV
        CALL MAC (ATNOS(J),PK,ATWTS(J),MACV)
        INTENS = MACV*NORMFAC
        OUTSPEC(I)=OUTSPEC(I) + INTENS
 19     CONTINUE
 18     CONTINUE
        CALL CRLF
C  set up default spectrum file name
        CALL DOCOPY("MABSCOEF",NAME,5)
C  File the Data to disk in spectrum format. F.Pt. data
C  becomes 32 bit integers.
        CALL MESS ("<15><12> Calculation complete.")
        CALL WRSPAN( NAME)
        CONTINUE
C
        CALL CRLF
        CALL YESNO ("Exit programme?",$1) ;or compute another one.
        STOP
        END

C....file MBHBACK
C Programme to calculate backgound spectrum upto 2Ø48 channels long
C using Cross-sections using subroutine MBHEQ, which returns the reduced
C cross-section, s''. The intensity is s''*Z*Z/TØ/Pk Here TØ & Pk have to be
C in units of mØc^2. Z= atomic No., TØ=electron energy, Pk = photon energy
C Program also uses subroutines WRSPAN, ERRMESS, FORMSPEC, COMPO, COMPI and
C HEADER. F.Pt Scale factor saved in header 33 & 34.
C Also calculates  MBH for multielements.
C
C .....declarations .......
        COMMON /HEADAN/IHEDAN(Ø:255) /JARAY/OUTSPEC(Ø:2Ø47)
        COMMON /ATCONS/ATNOS(2Ø),ATWTS(2Ø),ATFRS(2Ø),WTFRS(2Ø)
        EQUIVALENCE (IHEDAN(1),MHDSIZE),(IHEDAN(3),MCMIN), (IHEDAN(4),MCMAX)
        EQUIVALENCE (IHEDAN(7),GF), (IHEDAN(9),XØ), (IHEDAN(33),SCALENUM)
        INTEGER ATNOS,NAME(7),LABEL(16),EVCH,DFLAG,RQMAX,RQMIN
        REAL OUTSPEC,PK,MØC2,NORMFAC,INTENS
C
 1      CALL HEADER      ;set up spectrum header block default values
        CALL FORMSPEC(RQMIN,RQMAX);get photon Energy range/ Spectrum Format
        DFLAG=1                    ; for MBH don't need atomic weights etc.
        CALL COMPI(DFLAG,NUMELS)      ;get atomic Nos & atomic fractions
C
C....... dialog to determine Z,To,theta ................
 9      CALL MESS("<15><12> Enter electron energy (default = 1ØØkeV) ")
        NCH=6
        CALL GETNO(ELEN,NCH)
        IF(NCH .EQ. Ø) ELEN=1ØØ.Ø
        THETA=11Ø.Ø      ;HB5 window less detector
        CALL CRLF
        CALL DEFAULT("Enter detector angle. Default= ",THETA,"F",6,2)
        CALL CRLF
        CALL MESS ("  Electron energy (keV) = ")
        CALL PUTNO (ELEN,5,1)
        CALL MESS (" MBH  Angle = ")
        CALL PUTNO (THETA,6,2)
        CALL YESNO ("  Are these ok?  ", $9)
```

```
C ..........................................................
        DO 10 I=MCMIN,MCMAX
10      OUTSPEC(I)=0.0              ;zero spectrum array for new data
C Create theoretical spectrum of Absolute cross-sections as reals
        CALL CRLF
        CALL MESS ("MBH calculation takes  about  40s")
        CALL MESS (" per element for 1024 channels ")
        PI=3.14159
        THETAR=PI*THETA/180.0       ;radians
        EVCH=IFIX(1000.0/GF)        ;eV per channel
        M0C2=511.0                  ;m0c^2
        SCALENUM=10.0               ;suitable scale factor for spectra
C
        DO 18 J=1,NUMELS
        NORMFAC=ATFRS(J)*FLOAT(ATNOS(J)*ATNOS(J))*M0C2/ELEN
        NORMFAC=NORMFAC*SCALENUM
        DO 19 I=RQMIN,RQMAX
        PK=(FLOAT(I)-X0)*EVCH/1000.0                ;Pk in keV
        CALL MBHEQ(ELEN,PK,ATNOS(J),THETAR,SIGMA) ;sigma = reduced
        INTENS = SIGMA * NORMFAC*M0C2/PK            ; Cross-section
        OUTSPEC(I)=OUTSPEC(I) + INTENS
 19     CONTINUE
 18     CONTINUE
C  set up default spectrum file name
        CALL DOCOPY("MBHSPEC",NAME,5)
C  File the Data to disk in spectrum format. F.Pt. data
C  becomes 32 bit integers
        CALL MESS ("<15><12> Calculation complete.")
        CALL WRSPAN( NAME)
        CONTINUE
C
        CALL CRLF
        CALL YESNO ("Exit programme?",$1) ;or compute another b'ground
        STOP
        END
```

```
C File ------ MINIMISE
C This programme is written on IBM main frame computer to
C cope with the nonlinear least-squares fitting. It uses the two
C  NAG Libraray subroutines.
C Start of the Programme--------
//SS27BE JOB SS27,KHAN,CLASS=M,TIME=(00,59)
// EXEC FVCLG,SYSLIB='SYS1.NAGLIB'
C
C Declarations
    IMPLICIT LOGICAL(A-Z)
    INTEGER I,IFAIL,J,LIW,LW,N,M,NS,NV
C      M is the number of data points used for the fitting and N is
C       number of unknown fitting parameters.
   PARAMETER (M=6, N=2)
   REAL*8  X(M),Y(M),Z(M),T(M)
   REAL*8  FSUMSQ
     PARAMETER (LW=7*N+N*N+2*M*N+3*M+N*(N-1)/2)
   REAL*8  CJ(N),W(LW),A(N)
   INTEGER IW(1)
   COMMON /USER/ Y,X,Z,T
```

```
C Read the data required for the fitting (shown at the end). In Y,
C X and Z arrays the counts of the line of element B, counts of
C the line of element A and the mass absorption coefficient of
C line of element B at each point are read respectively.
      DO 20 I=1,M
       READ (5,*) Y(I),X(I),Z(I)
20    CONTINUE
C Insert guss values of unknown fitting parameters.
      A(1)=4
      A(2)=90.
      LIW=1
      IFAIL=1
C Find minimum of FSUMSQ.
      CALL E04FDF(M,N,A,FSUMSQ,IW,LIW,W,LW,IFAIL)
      WRITE (6,*) 'IFAIL FROM E04FDF EQUALS ',IFAIL
      IF (IFAIL.EQ.1) THEN
      STOP
      END IF
      WRITE (6,*) 'FSUMSQ EQUALS ', FSUMSQ
       WRITE (6,96) (A(J), J=1,N)
        NS=6*N+2*M+M*N+1+MAX0(1,(N*(N-1))/2)
      NV=NS+N
       IFAIL=1
C
      CALL E04YCF(0,M,N,FSUMSQ,W(NS),W(NV),N,CJ,W,IFAIL)
C
      IF (IFAIL.NE.0) THEN
       WRITE(6,93) IFAIL
      STOP
      END IF
       WRITE (6,92) (SQRT(CJ(J)),J=1,N)
       STOP
97    FORMAT (//1X,'ON EXIT,THE SUM OF SQUARES IS', F12.4)
96    FORMAT (1X,'AT THE POINT',/4F12.4)
93    FORMAT (//1X,'ERROR EXIT FROM E04YCF.IFAIL=',I3/1X,'SEE
          ROUTINE')
92    FORMAT (/1X,'AND ESTIMATES OF THE S.D.S OF THE SAMPLE'/
     & ' REGRESSION COEFFICIENTS ARE'/4F12.4)
      END
C
C     Routine to evaluate the residuals
      SUBROUTINE LSFUN1(M,N,AC,FVECC)
       IMPLICIT LOGICAL(A-Z)
```

```
      INTEGER M,N,MM
      PARAMETER (MM=6)
      REAL*8 FVECC(M),AC(N)
      REAL*8 X(MM),Y(MM),Z(MM),T(MM)
      INTEGER I
      COMMON /USER/ Y,X,Z,T
      DO 30 I=1,MM
C Convert counts of element A (X(I)) into cm.
        T(I)=X(I)/10000000.0
C   Now multiply by the value of mass absorption coefficient of
C   element B at each point.
        T(I)=T(I)*Z(I)
C write down theoretical equation for data fitting. AC(1) and
C  AC(2) are two unknown parameters to be returned.
          FVECC(I)=AC(1)*X(I)*(1.0-EXP(-AC(2)*T(I)))/(AC(2)*T(I))
      FVECC(I)=FVECC(I)-Y(I)
        FVECC(I)=FVECC(I)/FLOAT(M)
 30     CONTINUE
      RETURN
      END
C Create a file of known data of each point. This data will be
C read and used by the programme. The data shown in this file is
C  an example data of 6 points.
/ *
//G.FT06F001 DD SYSOUT=T
//G.SYSIN DD *
      3387.          823.          1390.
      4066.          1192.         1391.
      6305.          1846.         1379.5
      6697.          2033.         1378.
      8458.          2609.         1364.5
      9224.          3010.         1369.
```

```
C File....RATIO.....................
C This programme will correct PK, GaK AND AsK lines for absorption effect.
C Then it will work out concentration of P, Ga, As and In in InGaAsP sample.
C Requires subroutines FRACTION and CORRECTION.
C
        COMMON/CDATA/ NC(4),T(4),PT(4),X(4),N(4),COUNT(4)
        COMMON/DT/ IZ(4),WT(4),WF(4),AF(4),MAC(4)
        REAL KGAP,KINGA,KPAS,MAC
        INTEGER DFLAG
C Ask for net uncorrected counts for each line involved.
 111    DO 89 I=1,4
        CALL MESS ("Enter uncorrected net counts of line number  ")
        CALL IPUTNO(I,2)
        CALL CRLF
        CALL IGETNO(NC(I),8)
        CALL CRLF
 89     CONTINUE
        DFLAG =Ø ; Set to start from pure InP.
C Correct the counts of each line for absorption effect.
 5      CALL CORRECTION (DFLAG)
C K-factors, for GaP experimental, for PAs and InGa theoretical.
        KINGA=4.5Ø8
        KGAP=Ø.8869
        KPAS=1.Ø18
C Assign counts to each particular line.
        XIN=X(1)
        XGA=X(2)
        XP= X(3)
        XAS=X(4)
C Work out concentrations.
        XX=KINGA*(XIN/XGA) ; CIn/CGa = KInGa * (NIn/NGa)
        Y=KGAP*(XGA/XP)    ; CGa/CP  = KGaP  * (NGa/NP)
        Z=KPAS*(XP/XAS)    ; CP/CAs  = KPAs  * (NP/NAs)
        Q=1/Y              ; CP  = 1/KGaP  * (NGa/NP)
        R=Q/Z              ; CAs = CP/KPAs * (NP/NAs)
        CGA=1.Ø/(1.Ø+XX+Q+R)      ; Ga concentration in the sample.
        CIN=XX*CGA                ; In concentration in the sample.
        CP=CGA*Q                  ; P  concentration in the sample.
        CAS=CGA*R                 ; As concentration in the sample.
        CALL ALPH16
        CALL PRTON
        CALL CRLF
        CALL MESS ("  KInGa  ")
        CALL MESS ("  KGaP  ")
        CALL MESS ("  KPAs ")
        CALL CRLF
        CALL PUTNO(KINGA,7,3)
        CALL PUTNO(KGAP,7,3)
        CALL PUTNO (KPAS,7,3)
        CALL CRLF
        CALL MESS ("Atomic fractions are as follows=     ")
        CALL CRLF
        CALL MESS("    In         ")
        CALL MESS("    Ga         ")
        CALL MESS("    P         ")
        CALL MESS ("   As       ")
        CALL CRLF
        CALL PUTNO(CIN,7,4)
        CALL PUTNO(CGA,7,4)
        CALL PUTNO(CP,7,4)
        CALL PUTNO(CAS,7,4)
        AF(1)=CIN
        AF(2)=CGA
        AF(3)=CP
        AF(4)=CAS
        CALL CRLF
        CALL PRTOFF
        CALL YESNO ("Repeat the same data   ? ",$1Ø)
        DFLAG =1 ; Set to treat it InGaAsP sample.
        GO TO 5
```

```
10      CALL CRLF
        CALL YESNO ("Continue for other spectrum  ?   ",$99)
        GO TO 111
99      CONTINUE
        STOP
        END
```

A2.11

Subroutine Listings

(All subroutines are listed alphabetically.)

```
C  --File CHI-----
C This subroutine computes a reduced chi-squared value by comparing
C experimental spectrum to its background equivalent over a selected
C range of channels.
C
        SUBROUTINE CHISQUARE(NCHANS,IDE)
        INTEGER OPT,WIND
        REAL IDE,INSPEC,OUTSPEC
        COMMON/IARAY/INSPEC(0:2047)/JARAY/OUTSPEC(0:2047)/BLK4/WIND(3,30)
 30     CALL CRLF
        CALL MESS ("How many regions to be used in chi2 evaluation ?  ")
        CALL IGETNO (NWIN,2)
        NF=0
        CHI2=0.0
        A=0.0
        DO 100 J=1,NWIN
        CALL CRLF
        CALL MESS ("Next window number ?        ")
        CALL IGETNO (NCODE,2)
        N1=WIND(2,NCODE)
        N2=WIND(3,NCODE)
        CALL CRLF
        CALL MESS ("Chi2 comparison from channel    ")
        CALL IPUTNO (N1,4)
        CALL MESS ("  to channel  ")
        CALL IPUTNO (N2,4)
        NF=NF+N2-N1+1
        DO 100 I=N1,N2
        A=(ABS(INSPEC(I)-OUTSPEC(I)))**2
        IF(INSPEC(I).EQ.0.0) GO TO 100
        CHI2=CHI2 + A/INSPEC(I)
100     CONTINUE
        NF=NF-1
        REDCHI2=CHI2/NF
        CALL MESS ("FOR ")
        CALL IPUTNO (NF,4)
        CALL CRLF
        CALL MESS ("Degrees of freedom reduced chi2 value is  ")
        CALL PUTNO (REDCHI2,11,6)
        CALL CRLF
        CALL YESNO (" Another range ?   ",$3)
        GO TO 30
3       RETURN
        END

C ..........file COMPI .......................
C subroutine COMPI is to get interactively the number of elements and
C their proportions in the sample.
C DFLAG=1, only Atomic numbers, and atomic fractions are requested.
C DFLAG=2 atomic number, mass fractions, and atomic weights are requested.
C Calls COMPO to check input data is acceptable.
C
        SUBROUTINE COMPI(DFLAG,NUMELS)
C .....declarations .......
        COMMON /ATCONS/ ATNOS(20),ATWTS(20),ATFRS(20),WTFRS(20)
        INTEGER ATNOS,DFLAG,FLAG
C
C........ dialog to get atomic numbers, fractions & weights ......
        CALL CRLF
 11     CALL MESS ("<15><12> Enter number of elements     ")
        CALL IGETNO (NUMELS,2)
C
        DO 100 I=1,NUMELS
        CALL MESS( "<12><15> For element  ")
        CALL IPUTNO (I,3)
        CALL MESS ("<15><12> Enter Atomic Number ")
        CALL IGETNO (ATNOS(I),2)
        IF (DFLAG.EQ.2) GO TO 19
        CALL MESS ("   Atomic Fraction ")
        CALL GETNO (ATFRS(I),6,4)
        IF (DFLAG .EQ. 1) GO TO 100
```

```
 19      CALL MESS ("   Weight Fraction  ")
         CALL GETNO (WTFRS(I),6,4)
         CALL MESS ("   Atomic Weight ")
         CALL GETNO (ATWTS(I),8,3)
 100     CONTINUE
         CALL COMPO(DFLAG,NUMELS,FLAG)
         IF (FLAG .NE. 1) GO TO 11       ;because data not correct
         RETURN
         END



C file COMPO checks specimen composition from COMPI is ok. Data is
C passed through common to get round Links curious I/O **.** problem.
C
         SUBROUTINE COMPO(DFLAG,NUMELS,FLAG)
C .....declarations .......
         COMMON /ATCONS/ ATNOS(20),ATWTS(20),ATFRS(20),WTFRS(20)
         INTEGER ATNOS,DFLAG,FLAG
C
C check input is correct
         CALL MESS ("<12><15>..... Specimen    Composition .....")
         DO 200 I=1,NUMELS
         CALL MESS ( "<12><15> Element ")
         CALL IPUTNO (I,3)
         CALL MESS ("   Atomic No = ")
         CALL IPUTNO (ATNOS(I),3)
         IF (DFLAG. EQ. 2 ) GO TO 9
         CALL MESS ("  Atomic Fraction =  ")
         CALL PUTNO (ATFRS(I),6,4)
         IF (DFLAG .EQ. 1) GO TO 200
  9      CALL MESS ("  Weight fraction =    ")
         CALL PUTNO (WTFRS(I),6,4)
         CALL MESS ("  Atomic Wt = ")
         CALL PUTNO (ATWTS(I),8,3)
 200     CONTINUE
         CALL CRLF
C .....................
         CALL YESNO(" Are these values O.K.?",$300)
         FLAG=1                    ; data accepatable
         GO TO 310
 300     FLAG=0                    ; data not correct
 310     RETURN
         END


C FILE------CORRECTION-
 C This programme will correct PK, GaK AND AsK lines for absorption effect
 C and returns the corrected values to the main programme for quantitation.
 C       DECLARATIONS.
         SUBROUTINE CORRECTION (DFLAG)
         COMMON/CDATA/NC(4),T(4),FT(4),X(4),N(4),COUNT(4)
         COMMON/DT/IZ(4),WT(4),WF(4),AF(4),MAC(4)
         REAL DE,IDE,KGAP,KINGA,KPAS,MAC
         INTEGER DFLAG
         IF ( DFLAG.EQ.1 ) GO TO 5
 C Set initially pure InP concentration.
         AF(1)=0.5
         AF(2)=0.0
         AF(3)=0.5
         AF(4)=0.0
 5       CONTINUE
         CALL FRACTION
         CALL CRLF
         CALL MESS ("Enter mass path length (nm)       ")
         CALL GETNO (PL,8,1)
         PL=PL/1000000000.0 ; Convert mass path length number to cm.
 C Correct In Line for absorption effect.
  113    DO 97 I=1,4
         T(I)=(1.0-EXP(-MAC(I)*PL))/(MAC(I)*PL)
```

```
          PT(I)=T(I)*100.0
          CALL CRLF
          CALL MESS("% Transmission of signal number = ")
          CALL IPUTNO (I,2)
          CALL CRLF
          CALL PUTNO(PT(I),8,4)
          N(I)=NC(I)      ; Take the uncorrected value of a line (NC)
          COUNT(I)=FLOAT(N(I))/T(I)
          N(I)=IFIX(COUNT(I))
          X(I)=FLOAT(N(I))    ; Corrected counts of a line in real.
          CALL CRLF
          CALL MESS ("Net counts of line number  ")
          CALL IPUTNO (I,2)
          CALL CRLF
          CALL IPUTNO (N(I),8)
   97     CONTINUE
          CALL CRLF
          CALL YESNO ("Is it O.K ? ",$113)
          RETURN
          END


C .... File EDGE.................
C This subroutine reads the edge energy data from two binary file EEDT1
C and EEDT2 and values are returned to subroutine MAC.
C
          SUBROUTINE EDGE
          COMMON/BLK4/FEDGE(5,96)/BLK5/SEDGE(5,96)/BLK3/EEDGE(10,96)
C ASK FOR NUMBER OF CHANNELS.
          CALL CRLF
          NBLOCK=4
          CALL OPEN (3,"EEDT1",1,IER,$30)
          CALL RDBLK (3,0,FEDGE,NBLOCK,IER)
          CALL CRLF
   30     CALL CLOSE (3,IER)
          CALL OPEN (1,"EEDT2",1,IER,$31)
          CALL RDBLK (1,0,SEDGE,NBLOCK,IER)
          CALL CRLF
   31     CALL CLOSE (1,IER)
          DO 111 J=1,96
          DO 222 I=1,5
   222    EEDGE(I,J)=FEDGE(I,J)
   111    CONTINUE
          DO 333 I=1,96
          DO 444 J=1,5
          K=J+5
   444    EEDGE(K,I)=SEDGE(J,I)
   333    CONTINUE
          RETURN
          END

C file----------EFFIC
C KHALID . M .KHAN ----------JULY:88 --------
C This subroutine corrects the theoretical background
C to take into account a detector absorption effect and specimen self
C self absorption effect. The  mass absorption coefficients will have
C created and filed by MABSCO. This subroutine will read them in via
C subroutine RDSPAN.
C
          SUBROUTINE EFFIC(NCHANS,THETA)
C         DECLARATIONS.
          INTEGER ZX,NAME(7)
          REAL OUTSPEC
          COMMON /JARAY/OUTSPEC(0:2047)/KARAY/TEMPSPEC(0:2047)
C         READ IN DATA
   150    CALL CRLF
          CALL MESS ("SELECT THE OPTION PLEASE.")
          CALL CRLF
          CALL MESS (" (1) Specimen self absorption. ")
          CALL CRLF
          CALL MESS (" (2) Detector efficiency for high energy end. ")
```

```
      CALL CRLF
      CALL MESS (" (3) Detector efficiency for low energy end.    ")
      CALL CRLF
      CALL MESS (" (4) Return to main programme.")
      CALL CRLF
      CALL IGETNO (NEXT,1)
      IF(NEXT.LT.1.AND.NEXT.GT.4) GO TO 150
      CALL CRLF
      GO TO (250,350,450,98),NEXT
250   CALL YESNO (" Specimen self absorption ? ",$150)
260   CALL CRLF
      CALL MESS ("Enter absorption path length (nm)  ")
      CALL GETNO(RTX,8,2)
      CALL CRLF
      CALL MESS (" Enter density of specimen (g/cm2). ")
      CALL GETNO (RO,6,3)
      CALL CRLF
      CALL MESS ("  P.Length=  ")
      CALL PUTNO (RTX,8,2)
      CALL MESS ("   Density=  ")
      CALL PUTNO (RO,6,3)
      CALL YESNO ("  Are these o.k ? ",$260)
      TX=RTX*0.1E-06
      CALL CRLF
      PLRO=TX*RO
      GO TO 500
350   CALL YESNO ("Detector efficiency for high energy end ? ",$150)
360   CALL CRLF
      CALL MESS ("Enter effective crystal thickness(mm).")
      CALL GETNO (RTX,6,2)
      CALL CRLF
      CALL MESS (" Enter density (g/cm2) ")
      CALL GETNO (RO,6,3)
      CALL CRLF
      CALL MESS ("  Crystal thickness= ")
      CALL PUTNO (RTX,6,2)
      CALL MESS ("    Density= ")
      CALL PUTNO (RO,6,3)
      CALL YESNO ("  Are these o.k?",$360)
      TX=RTX*0.1
      PLRO=TX*RO
      CALL CRLF
      CALL MESS ("The Mass Abs: Coeff: values direct from tne disk")
      CALL RDSPAN(NAME)
      DO 200 I=0,NCHANS
      X=TEMPSPEC(I)*PLRO
      IF (X.GE.0.0.AND.X.LT.50.0) GO TO 370
      CF=1.0
      GO TO 380
370   CF=1.0-EXP(-X)
380   OUTSPEC(I)=OUTSPEC(I)*CF
200   CONTINUE
      CALL CRLF
      CALL MESS ("CORRECTION FOR HIGH EFFICENCY COMPLETED.")
      GO TO 150
450   CALL YESNO ("Detector efficiency for low energy end ?",$150)
460   CALL CRLF
      CALL MESS ("Enter absorption thickness(nm).")
      CALL GETNO(RTX,8,1)
      CALL CRLF
      CALL MESS ("Enter density (g/cm2).")
      CALL GETNO(RO,6,3)
      CALL CRLF
      CALL MESS(" Thickness=  ")
      CALL PUTNO(RTX,8,1)
      CALL MESS("    Density=  ")
      CALL PUTNO(RO,6,3)
      CALL YESNO ("   Are these o.k  ?",$460)
      TX=RTX*0.1E-06
      THETAR=3.14159*THETA/180.
      PLRO=(TX/COS(THETAR))*RO
```

```
500     CALL CRLF
        CALL MESS("The Mass Abs: Coeff: values direct from the disk.")
        CALL RDSPAN(NAME)
        DO 600 I=0,NCHANS
        X=TEMPSPEC(I)*PLRO
        IF(X.GE.0.0.AND.X.LT.50.0) GO TO 479
        CALL MESS ("<15><12> **  WARNING. 100% ABS ASSUMED .  ")
        CF=0.1001E-09
        GO TO 492
479     IF (X.NE.0.0) GOTO 180
        CF=1.0
        GO TO 492
180     IF(NEXT.EQ.1) GO TO 181
        CF=EXP(-X)
        GO TO 492
181     CF=(1.0-EXP(-X))/X
492     OUTSPEC(I)=OUTSPEC(I)*CF
600     CONTINUE
        CALL MESS ("<15><12> Correction completed.     ")
        GO TO 150
98      RETURN
        END

C  Subroutine ERRMESS outputs to the console error messages
C  corresponding to the error numbers in the LINK  Fortran Manual
C  p 14-12 modified to run on AN10 with DEMON operating system.
C
        SUBROUTINE ERRMESS(TEXT,IER)
        INTEGER TEXT(20)
C
        IF (IER .EQ. 1) GO TO 90
C
        CALL LINK("ANXM.LT","MDR:ANXM.LT",IER)
        CALL PALETTE(16,"ANXM.LT")
        CALL ALPH16
C
        CALL PALETTE(16,"ANXM.LT");palette & alph16 called twice because
        CALL ALPH16               ; of some system bug
C
        CALL MESS("<15><12>  Fortran Runtime Error Messages     ")
        CALL CRLF
        CALL MESS  (".....................................")
        CALL CRLF
        CALL CRLF
        CALL MESS ( TEXT )
        CALL MESS ("        . Error Number= ")
        CALL IPUTNO (IER,5)
        CALL CRLF
        IF(IER .EQ.  4)  CALL MESS ( "Illegal File name")
        IF(IER .EQ.  9)  CALL MESS ( "End of File" )
        IF(IER .EQ.  8)  CALL MESS ( "File Already Exists")
        IF(IER .EQ. 10)  CALL MESS ( "File is Read Protected")
        IF(IER .EQ. 11)  CALL MESS ( "File is Write Protected")
        IF(IER .EQ. 12)  CALL MESS ( "File Already Exists")
        IF(IER .EQ. 13)  CALL MESS ( "File does not Exist")
        IF(IER .EQ. 16)  CALL MESS ( "File is not Open")
        IF(IER .EQ. 20)  CALL MESS ( "Channel in Use")
        IF(IER .EQ. 26)  CALL MESS ( "File Space Exhausted")
        IF(IER .EQ. 27)  CALL MESS ( "File Read Error")
        IF(IER .EQ. 33)  CALL MESS ( "Device not in system")
        IF(IER .EQ. 40)  CALL MESS ( "Device Already in system")
        IF(IER .EQ. 41)  CALL MESS ( "Insufficient Contiguous Blocks")
        IF(IER .EQ. 33)  CALL MESS ( "Directory in use by another Programme")
        IF(IER .EQ. 84)  CALL MESS ( "Disk Format Error")
        CALL CRLF
C
C create a pause to read message. Answer is irrelavant.
        CALL YESNO("  Do you know what went wrong? ",$99)
  90    CONTINUE
  99    RETURN
        END
```

```
C  ............file FORMSPEC.....................................
C  FORMSPEC allows selection  and changing of  the default spectrum parameters
C  and photon energy range required for the computation.
C  NCHANS is the number of channels in the spectrum array
C  MCMAX is the index of the last  non-zero channel. Usually MCMAX=NCHANS-1
C  as LINK arrays are e.g. (0:1023)
C  RQMIN,RQMAX are the maximum and minimum photon energies requested for
C  the calculation
C  EVCH is the eV per channel;
C  X0 is the F.Pt. offset.  GF is the gain factor.
C  Usually GF is equal to 1000.0/EVCH
C
       SUBROUTINE FORMSPEC(RQMIN,RQMAX)
C
C .....declarations .......
       COMMON /HEADAN/IHEDAN(0:255) /JARAY/OUTSPEC(0:2047)
       EQUIVALENCE (IHEDAN(3),MCMIN), (IHEDAN(4),MCMAX)
       EQUIVALENCE (IHEDAN(7),GF), (IHEDAN(9),X0), (IHEDAN(33),SCALENUM)
       REAL OUTSPEC,PMAX,PMIN
       INTEGER EVCH,RQMAX,RQMIN
C
 111   EVCH=IFIX(1000.0/GF)
       CALL DEFAULT("<12><15> eV per channel         = ",EVCH,"I",4)
       GF=1000.0/EVCH
C
       CALL MESS  ("<12><15> Yes for nominal 1K channel spectrum, ")
       CALL YESNO ("<12><15> No  for nominal 2K channel spectrum  ",$10)
       NCHANS=1024
       GOTO 20
 10    NCHANS=2048
 20    MCMAX=NCHANS-1
       IF (NCHANS .EQ. 2048)  X0=20.0     ;(from experimental observ'n)
       CALL CRLF
       CALL DEFAULT("Change offset with CAUTION. Currently = ",X0,"F",6,3)
C
C .. get ReQuested MAX and MIN channel Nos. (photon energies) ...
C  ... maximum ...
       PMAX =(MCMAX-X0)*EVCH  ;maximum possible photon energy in array
       CALL CRLF
       CALL DEFAULT("Maximum photon energy (eV) = ",PMAX,"F",8,1)
       RQMAX = IFIX(PMAX/EVCH+X0  ;highest channel requested
       IF ( RQMAX .GT. MCMAX) THEN
       CALL MESS("<12><15> For this energy, No. of channels = ")
       CALL IPUTNO (RQMAX,7)
       CALL MESS("<12><15> 2K channels selected")
       MCMAX=2047
       X0=20.0
       RQMAX=MCMAX
       PMAX=(MCMAX-X0)*EVCH
       CALL MESS(" Maximum Photon energy (eV) = ")
       CALL PUTNO (PMAX,8,1)
       ENDIF
C .... minimum ...
       PMIN=200.0 ;Theory and data unreliable for less than 200eV
       CALL CRLF
       CALL DEFAULT("Enter minimum photon energy =",PMIN,"F",5,1)
       RQMIN=IFIX(PMIN/EVCH+X0)
C
C ............. check input data is correct ................
C
       CALL CRLF
       CALL MESS("<12><15>       ..... Spectrum  Data ..... ")
       CALL MESS ("<12><15> Gain Factor = ")
       CALL PUTNO(GF,8,4)
       CALL MESS("    eV/Chan = ")
       CALL IPUTNO (EVCH,5)
       CALL MESS ("  Offset X0 =")
       CALL    PUTNO(X0,5,2)
C
       CALL MESS("<12><15>  No. of Spectrum channels = ")
       CALL IPUTNO (MCMAX,7)
C
```

```
        CALL MESS ("<12><15> Maximum requested photon energy eV = ")
        PMAXR = (RQMAX-XØ)*EVCH
        CALL PUTNO(PMAXR,8,1)
        CALL MESS ("<12><15> minimum requested photon energy eV = ")
        PMINR = (RQMIN-XØ)*EVCH
        CALL PUTNO(PMINR,8,1)
        CALL CRLF
C
        CALL YESNO( " Are these O.K? ",$111)
        RETURN
        END

C .....File FRACTION .....
C This subroutine takes the values of the atomic fractions from the main
C programme via common and calculates the corresponding values of mass
C fractions. Using these values of mass fractions, the values of the mass
C absorption coefficients are calculated for four lines and then are
C returned to the subroutine CORRECTION.
        SUBROUTINE FRACTION
        REAL MAC
        COMMON /DT/ IZ(4),WT(4),WF(4),AF(4),MAC(4)
        DATA IZ / 49,31,15,33/
        DATA WT / 114.8,69.72,3Ø.97,74.922 /
111     CONTINUE
        NE=4
        SUMWT=Ø.Ø
C Calculate weight fractions.
        DO 77 I=1,NE
        WF(I)=AF(I)*WT(I)     ; Atomic fraction and atomic weight.
77      SUMWT=SUMWT+WF(I)
        DO 31 I=1,NE
31      WF(I)=WF(I)/SUMWT     ; Output calculated weight fractions.
        CALL CRLF
        DO 78 I=1,NE
        CALL MESS ("Atomic number=    ")
        CALL IPUTNO(IZ(I),2)
        CALL CRLF
        CALL MESS ("Weight fraction=    ")
        CALL PUTNO (WF(I),6,4)
        CALL CRLF
78      CONTINUE
        CALL CRLF
        CALL YESNO ("IS IT O.K   ?   ",$111)
C Calculate mean mass absorption coefficient for each line.
        MAC(1)=12.111*WF(1)+23.63*WF(2)+3.Ø3*WF(3)+27.891*WF(4)
        MAC(3)=1594.Ø*WF(1)+2615.Ø*WF(2)+287.4*WF(3)+3Ø52.Ø*WF(4)
        MAC(2)=166.1*WF(1)+42.8*WF(2)+5Ø.5*WF(3)+51.5*WF(4)
        MAC(4)=116.6*WF(1)+221.4*WF(2)+34.5*WF(3)+35.9*WF(4)
        RETURN
        END

C ........file HEADER ..........................................
C subroutine HEADER is used to set up default values for spectrum
C file header block to allow writing files to disk in LINK AN1Ø
C format that can be read into the Analyser.
C 32 bit double precision integer format is used.
C A F.Pt. scale factor is stored in the header block (words 33 & 34).
C
        SUBROUTINE HEADER
C .....declarations .......
        COMMON /HEADAN/IHEDAN(Ø:255) /JARAY/OUTSPEC(Ø:2Ø47)
        EQUIVALENCE (IHEDAN(3),MCMIN), (IHEDAN(4),MCMAX)
        EQUIVALENCE (IHEDAN(7),GF), (IHEDAN(9),XØ), (IHEDAN(33),SCALENUM)
        REAL OUTSPEC
C
        IHEDAN(Ø)=152501K          ;X-ray flag for AN1Ø analyser
        IHEDAN(1)=255              ;header block size
        IHEDAN(2)=44ØK             ;data type flag (+/-2G = 32 bit)
        MCMIN= Ø                   ;1st non-zero channel
        MCMAX=1Ø23                 ;last   "          "
        CALL DOCOPY ("keV ",IHEDAN(5),2)   ;store energy units in 5,6
```

```
C  7,8 are GF  F.Pt. gain, 9,10 XO the F.Pt. Offset such that
C  the value of the units (e.g. keV) Y is    Y=(I-XO)/GF
C  i.e. XØ is exact channel no. for Øev
        GF=5Ø.Ø     ; GF=(I-XØ)/Y = 5Ø.Ø   for 2Øev/ch & Y in keV
        XØ=1Ø.Ø     ;LINK offset to allow zero strobe to be seen
        DO 5 I=11,255     ;Note XØ=2Ø.Ø for 2Ø47 channel spectra
 5      IHEDAN(I)=Ø
C 11-27=label (Ascii), 28=Ø string terminator, 29,3Ø= Link Scale
C factors(Ints),  33 - 35 not used by Link
        CALL DOCOPY (" Theoretical Spectrum",IHEDAN(11),15)
        SCALENUM=1.Ø              ;default value sometimes overwritten
                                  ;in main programme.
        IHEDAN(36)=Ø              ;live time
        IHEDAN(37)=Ø              ;real time
C If 42=1 strobe is with spectrum;. =16,(32) the strobe is in header at
C  16,(32) bit precision starting at 128 (with XO offset ??)
      IHEDAN(42)=32
C
        RETURN
        END


C........File MAC
C This subroutine calculates mass absorption coefficient values and is
C based on Heinrich (1987) formulation. The values are returned to main
C programme. This requires the data for edge energies of the element.
        SUBROUTINE MAC(IZ,E,WT,MU)
        COMMON/BLK3/EEDGE(1Ø,96)
        REAL MU,N
        Z=FLOAT(IZ)  ; Convert integer value to real
        IF(.NOT.(E.GT.EEDGE(1,IZ))) GO TO 2ØØ
C REGION E>K EDGE
C SUBREGION Z<6
        IF(.NOT.(Z.LT.6.Ø))GO TO 12Ø
        C=-2.87536E-4+1.8Ø8599E-3*Z
        N=3.34745+Ø.Ø2652873*Z-.Ø1273815*Z**2
        BIAS=-1Ø3.+18.2*Z
        A=24.4545+155.6Ø55*Z-14.15422*Z**2
        GO TO 199
C SUBREGION Z>5
  12Ø   C=5.253E-3 +1.33257E-3*Z -7.5937E-5*Z**2
        C=C+1.69357E-6*Z**3 -1.3975E-8*Z**4
        N=3.112 -.Ø121*Z
        BIAS=Ø.Ø
        A=.Ø +47.Ø*Z +6.52*Z**2 -.152624*Z**3
  199   GO TO 2ØØØ
  2ØØ   IF(.NOT.(E.GT.EEDGE(2,IZ))) GO TO 3ØØ
C REGION K>E>L1:
        C=-9.24E-5 +1.41478E-4*Z -5.24999E-6*Z**2
        C=C+9.85296E-8*Z**3 -9.Ø7306E-1Ø*Z**4 +3.19245E-12*Z**5
        N=2.7575 + 1.889E-3*Z - 4.982E-5*Z**2
        BIAS=Ø.Ø
        A=.Ø+17.8Ø96*Z+6.7429E-2*Z**2
        A=A+1.253775E-2*Z**3 - 1.16286E-4*Z**4
        GO TO 2ØØØ
  3ØØ   IF(.NOT.(E.GT.EEDGE(3,IZ))) GO TO 4ØØ
C REGION L1>E>L11:
        C=-9.24E-5+1.41478E-4*Z-5.24999E-6*Z**2
        C=C+9.85296E-8*Z**3-9.Ø7306E-1Ø*Z**4+3.19245E-12*Z**5
        N=2.7575+1.889E-3*Z-4.982E-5*Z**2
        BIAS=.Ø
        A=.Ø+17.8Ø96*Z+6.7429E-2*Z**2
        A=A+1.253775E-2*Z**3-1.16286E-4*Z**4
        C=C*.858
        GO TO 2ØØØ
  4ØØ   IF(.NOT.(E.GT.EEDGE(4,IZ)))GO TO 5ØØ
C REGION L11>E>L111.
        C=-9.24E-5+(1.41478E-4*Z)-(5.24999E-6*Z**2)
        C=C+(9.85296E-8*Z**3)-(9.Ø7306E-1Ø*Z**4)+(3.19245E-12*Z**5)
        N=2.7575+(1.889E-3*Z)-(4.982E-5*Z**2)
        BIAS=.Ø
```

```
          A=.Ø+17.8Ø96*Z+6.7429E-2*Z**2
          A=A+(1.253775E-2*Z**3)-(1.16286E-4*Z**4)
          C=C*(.8933-8.29E-3*Z+6.38E-5*Z**2)
          GO TO 2ØØØ
  5ØØ     IF (.NOT.(E.GT.EEDGE(5,IZ))) GO TO 6ØØ
C REGION L111>E>M1
C SUBREGION Z<3Ø
          IF (.NOT.(Z.LT.3Ø.Ø)) GO TO 52Ø
          C=1.889757E-2 - 1.8517159E-3*Z + 6.96Ø2789E-5*Z**2
          C=C-1.1641145E-6*Z**3 + 7.2773258E-9*Z**4
          N=.5385 + 8.4597E-2*Z - 1.Ø8246E-3*Z**2 + 4.45Ø9E-6*Z**3
          BIAS=.Ø+5.654*Z - .536839169*Z**2
          BIAS=BIAS + 1.8972278E-2*Z**3 - 1.683474E-4*Z**4
          A=.Ø+1Ø.2575657*Z - .822863477*Z**2 + 2.63199611E-2*Z**3
          A=A-1.8641Ø19E-4*Z**4
          GO TO 599
C SUBREGION 29<Z<61
  52Ø     IF (.NOT.(Z.LT.61.Ø))GO TO 53Ø
          C=3.ØØ39E-3 - 1.73663566E-4*Z + 4.Ø424792E-6*Z**2
          C=C - 4.Ø585911E-8*Z**3 + 1.497763E-1Ø*Z**4
          N=.5385 + 8.4597E-2*Z - 1.Ø8246E-3*Z**2 + 4.45Ø9E-6*Z**3
          BIAS=.Ø + 5.654*Z - .536839169*Z**2 + 1.8972278E-2*Z**3
          BIAS=BIAS - 1.683474E-4*Z**4
          A=.Ø + 1Ø.2575657*Z - .822863477*Z**2
          A=A+2.63199611E-2*Z**3 - 1.8641Ø19E-4*Z**4
          GO TO 599
C SUBREGION Z>6Ø
  53Ø     CONTINUE
          C=3.ØØ39E-3 - 1.73663566E-4*Z + 4.Ø424792E-6*Z**2
          C=C-4.Ø585911E-8*Z**3 + 1.497763E-1Ø*Z**4
          N=.5385 + 8.4597E-2*Z - 1.Ø8246E-3*Z**2 + 4.45Ø9E-6*Z**3
          BIAS=.Ø - 1232.4Ø22*Z + 51.114164*Z**2
          BIAS=BIAS-.699473Ø97*Z**3 + 3.1779619E-3*Z**4
          A=.Ø+1Ø.2575657*Z - .822863477*Z**2 + 2.63199611E-2*Z**3
          A=A-1.8641Ø19E-4*Z**4
  599     GO TO 2ØØØ
  6ØØ     IF (.NOT.(E.GT.EEDGE(6,IZ)))GO TO 7ØØ
C REGION M1<E<M11.
          C1=7.7708E-5 - 7.83544E-6*Z + 2.2Ø9365E-7*Z**2 - 1.29Ø86E-9*Z**3
          C2=1.4Ø6 + 1.62E-2*Z - 6.561E-4*Z**2
          C2=C2+4.865E-6*Z**3
          C3=.584+1.955E-2*Z - 1.285E-4*Z**2
          C=C1*C2*C3
          N=3.-4.ØE-3*Z
          A=.Ø+4.62*Z - .Ø4*Z**2
          BIAS=2.51 - 5.2E-2*Z + 3.78E-4*Z**2
          BIAS=BIAS*EEDGE(8,IZ)
          GO TO 2ØØØ
  7ØØ     IF (.NOT.(E.GT.EEDGE(7,IZ)))GO TO 8ØØ
C REGION M11<E<M111.
          C1=7.7708E-5 - 7.83544E-6*Z + 2.2Ø9365E-7*Z**2 - 1.29Ø86E-9*Z**3
          C2=1.4Ø6 + 1.62E-2*Z - 6.561E-4*Z**2 + 4.865E-6*Z**3
          C=(1.Ø82 + 1.366E-3*Z)*C1*C2
          N=3. - 4.ØE-3*Z
          A=.Ø+4.62*Z - .Ø4*Z**2
          BIAS=2.51 - 5.2E-2*Z + 3.78E-4*Z**2
          BIAS=BIAS*EEDGE(8,IZ)
          GO TO 2ØØØ
  8ØØ     IF (.NOT.(E.GT.EEDGE(8,IZ))) GO TO 9ØØ
C REGION M111>E>M1V:
          C1=7.7708E-Ø5 - 7.83544E-Ø6 *Z + 2.2Ø9365E-Ø7*Z**2 - 1.29Ø86E-Ø9*Z**3
          C2=1.4Ø6+1.62E-Ø2*Z - 6.561E-Ø4*Z**2 + 4.865E-Ø6*Z**3
          C=.95*C1*C2
          N=3.Ø - 4.ØE-Ø3 *Z
          A=.Ø+4.62*Z - .Ø4*Z**2
          BIAS=2.51-5.2E-Ø2*Z + 3.78E-Ø4*Z**2
          BIAS=BIAS*EEDGE(8,IZ)
          GO TO 2ØØØ
  9ØØ     IF (.NOT.(E.GT.EEDGE(9,IZ))) GO TO 1ØØØ
C REGION M1V>E>MV:
          C1=7.7708E-5 - 7.83544E-6*Z + 2.2Ø9365E-7*Z**2 - 1.29Ø86E-9*Z**3
```

```
        C2=1.406 + 1.62E-2*Z - 6.561E-4*Z**2 + 4.865E-6*Z**3
        C=(1.6442 - .048*Z + 4.0664E-4*Z**2)*C1*C2
        N=3. - 4.0E-3*Z
        A=.0+4.62*Z - .04*Z**2
        BIAS=2.51 - 5.2E-2*Z + 3.78E-4*Z**2
        BIAS=BIAS*EEDGE(8,IZ)
        GO TO 2000
 1000   IF(.NOT.(E.GT.EEDGE(10,IZ)))GO TO 1100
C REGION MV>E>N1
        C=4.3156E-3 - 1.4653E-4*Z + 1.707073E-6*Z**2 - 6.69827E-9*Z**3
        C=C*1.08
        N=.3736 + 2.401E-2*Z
        BIAS=-113.0 + 4.5*Z
        A=.0+19.64*Z - .61239*Z**2 + 5.39309E-3*Z**3
        GO TO 2000
 1100   CONTINUE
        C=4.3156E-3 - 1.4653E-4*Z + 1.707073E-6*Z**2 - 6.69827E-9*Z**3
        C=C*1.08
        N=.3736+2.401E-2*Z
        BIAS=-113. + 4.5*Z
        A=.0+19.64*Z - .61239*Z**2 + 5.39309E-3*Z**3
        CUTOFF=1042.0 - 31.1812*Z + .252*Z**2
        GO TO 3000
 2000   CONTINUE
C Calculate mass absorption coefficient for region 1-10.
        MU=C*(12397.0/E)**N * Z**4.0 / WT * (1.0-EXP((BIAS-E)/A))
        GO TO 999
 3000   CONTINUE
C Calculate mass ab:co: for region 11
        MU=1.02*C*(12397./E)**N * Z**4.0/WT*(1.-EXP((BIAS-EEDGE(10,IZ))/A))
        MU=MU*(E-CUTOFF)/(EEDGE(10,IZ)-CUTOFF)
 999    RETURN
        END


C File MBHEQ  . .... . ......................
C
C MBHEQ evaluates the doubly differential reduced cross-section for
C Bremsstrahlung Production ( i.e. cross-section *T0*E0/Z/Z)
C       Z=Atomic number, Pk,K= photon energy in keV,m0c^2
C       T0 is the incident electron energy in keV
C       THETAR is the angle between the incident electron vector and the
C       emergent x-ray vector in radians (=THETA in degrees).
C The reduced cross-section is in cb/sr
C
        SUBROUTINE MBHEQ(T0,PK,Z,THETAR,SIGMA)
        REAL KSQ,K,NUM
        INTEGER Z
C  terms not a function of THETAR
        PI=3.1415927
        M0C2=511.0
        E0=T0+M0C2
        E0=E0/M0C2              ;total incident energy=K.E.+ m0c^2
        K=PK/M0C2               ;energy in m0c^2 units
        E=E0-K                  ;emergent electron energy
        P0=SQRT(E0*E0-1)        ;incident momentum of electron
        P=SQRT(E*E-1)           ;emergent     "          "
        BETA0=P0/E0             ;=v0/c
        BETA=P/E                ;=v/c
        ESQ=E*E
        E0SQ=E0*E0
        E0E=E*E0
        P0SQ=P0*P0
        PSQ=P*P
        KSQ=K*K
        ALPHA=108.0/(Z**(1.0/3.0))
        ALPHSQ=ALPHA*ALPHA
        EPS=ALOG((E+P)/(E-P))
C .   .   .   . terms a function of THETAR
        CTHETA=COS(THETAR)
        SINSQ=(SIN(THETAR)**2.0)
        DELTA0=E0-P0*CTHETA
```

```
      DELSQ=DELTAØ*DELTAØ
      DEL4=DELSQ*DELSQ
      PØDEL=PØSQ*DELTAØ
      PDELSQ=PØSQ*DELSQ
      PØDEL4=PØSQ*DEL4
      QSQ=PØSQ+KSQ - 2.Ø*PØ*K*CTHETA
      Q=SQRT(QSQ)
      EPSQ=Ø.5*ALOG(((Q+P)**4.Ø)/(4.Ø*(KSQ*DELSQ+PØSQ/ALPHSQ)))
      REL=ALOG(((EØE-1+(P*PØ))**2.Ø)/(KSQ+PØSQ/(ALPHSQ*DELSQ)))
      A=(8.Ø*SINSQ*(2.Ø*EØSQ+1.Ø))/PØDEL4
      B=2.Ø*(5.Ø*EØSQ + 2.Ø*EØE+3.Ø)/PDELSQ
      C=2*(PØSQ-KSQ)/(QSQ*DELSQ)
      D=4.Ø*E/PØDEL
      E=(4.Ø*EØ*SINSQ*(3.Ø*K-PØSQ*E))/PØDEL4
      F=4.Ø*EØSQ*(EØSQ+ESQ)/PDELSQ
      G=(2.Ø - 2.Ø*(7.Ø*EØSQ - 3.Ø*EØE +ESQ))/PDELSQ
      H=2.Ø*K*(EØSQ+EØE-1)/PØDEL
      RI=4.Ø*EPS/(P*DELTAØ)
      RJ=4.Ø/DELSQ
      RK=6.Ø*K/DELTAØ
      R=2.Ø*K*(PØSQ-KSQ)/(QSQ*DELTAØ)
      XPON1=2.Ø*PI*Z/137.Ø/BETAØ
      IF (XPON1 .GT. 178.Ø) THEN XPON1=178.Ø
      XPON2=2.Ø*PI*Z/137.Ø/BETA
      IF (XPON2 .GT. 178.Ø) THEN XPON2=178.Ø
      NUM=1-EXP(-XPON1)
      DEN=1-EXP(-XPON2)
      S=2.31E-2*(BETAØ/BETA)*NUM/DEN*(P/PØ*TØ/MØC2)
      T=REL/(P*PØ)
      U=EPSQ/(P*Q)
      SIGMA=S*(A-B-C+D + T*(E+F+G+H) -RI + U*(RJ-RK-R))
      RETURN
      END

C  ............file PRESET.....................................
C  PRESET allows selection  and changing of  the default spectrum
C  parameters and take off angle for the detector.
C  NCHANS is the number of channels in the spectrum array
C  MCMAX is the index of the last  non-zero channel. Usually MCMAX=NCHANS-1
C  as LINK arrays are e.g. (Ø:1Ø23)
C  EVCH is the eV per channel;
C  XØ is the F.Pt. offset.  GF is the gain factor.
C  Usually GF is equal to 1ØØØ.Ø/EVCH
C
      SUBROUTINE PRESET (NCHANS,THETA,IDE)
C
C .....declarations .......
      COMMON /HEADAN/IHEDAN(Ø:255) /JARAY/OUTSPEC(Ø:2Ø47)
      EQUIVALENCE (IHEDAN(3),MCMIN), (IHEDAN(4),MCMAX)
      EQUIVALENCE (IHEDAN(7),GF), (IHEDAN(9),XØ), (IHEDAN(33),SCALENUM)
      REAL OUTSPEC,IDE,XØ,GF
      INTEGER EVCH
C
 111  EVCH=IFIX(1ØØØ.Ø/GF)
      CALL DEFAULT("<12><15> eV per channel      = ",EVCH,"I",4)
      GF=1ØØØ.Ø/EVCH
      MCMIN=Ø
C
      CALL MESS  ("<12><15> Yes for nominal 1K channel spectrum, ")
      CALL YESNO ("<12><15> No  for nominal 2K channel spectrum  ",$1Ø)
      NCHANS=1Ø24
      GOTO 2Ø
 1Ø   NCHANS=2Ø48
 2Ø   MCMAX=NCHANS-1
      IF (NCHANS .EQ. 2Ø48)  XØ=2Ø.Ø    ;(from experimental observ'n)
      CALL CRLF
      CALL DEFAULT(" Change offset with CAUTION. Currently = ",XØ,"F",6,3)
C Enter take off angle
      CALL CRLF
      CALL MESS (" Enter MBH angle (Degrees) Default=1ØØ.5  ")
      NCH=5
```

```
        CALL GETNO (TMBH,NCH,2)
        IF (NCH.EQ.0) TMBH=100.5 ; For HB5 angle for MBH is 100.5 degrees.
C
C ..... check input data is correct .....
C
        CALL CRLF
        CALL MESS("<12><15>          ..... Spectrum  Data ..... ")
        CALL MESS ("<12><15> Gain Factor = ")
        CALL PUTNO(GF,8,4)
        CALL MESS("     eV/Chan = ")
        CALL IPUTNO (EVCH,5)
        CALL MESS ("  Offset X0 =")
        CALL    PUTNO(X0,5,2)
C
        CALL MESS("<12><15>  No. of Spectrum channels = ")
        CALL IPUTNO (MCMAX,7)
        CALL MESS ("<12><15> MBH angle (Degrees)=  ")
        CALL PUTNO (TMBH,5,2)
        IDE = FLOAT (EVCH)
        NCHANS = MCMAX
        THETA=TMBH - 90. ;Detector angle.
        CALL YESNO( " Are these O.K? ",$111)
        RETURN
        END


C FILE RDSPAN-------
C Subroutine RDSPAN reads a spectrum from disk.It reads both 16 bit integer
C and 32 bit +/-2G spectrum in array TEMPSPEC.
C uses subroutines ERRMESS,
C
         SUBROUTINE RDSPAN(NAME)
C .....declarations .......
         COMMON /HEADAN/IHEDAN(0:255)
         COMMON/KARAY/ TEMPSPEC(0:2047)
         EQUIVALENCE(IHEDAN(1),MHDSIZE),(IHEDAN(3),MCMIN),(IHEDAN(4),MCMAX),
     &       (IHEDAN(7),GF), (IHEDAN(9),X0),(IHEDAN(33),SCALNUM)
        INTEGER NAME(7),TEXT(20)
C ask for filename
 3      CALL CRLF
        CALL DEFAULT("Enter spectrum filename ",NAME,"S",10)
C add extension to spectra file name (.SP) & copy into label
        CALL AEXTN (NAME, "SP")
C
C Open file for read (1) on channel got by GCHAN
 20     CALL DOCOPY( "Get channel",TEXT,10)
        CALL GCHAN(ICHANO,IER,$999)
        CALL DOCOPY( "Open channel",TEXT,10)
        CALL OPEN(ICHANO,NAME,1,IER,$90)
C   READ  header block data
        CALL DOCOPY( "Read header.",TEXT,10)
        DO 30 I=0,255
 30     CALL RDBIN (ICHANO,1, IHEDAN(I),IER,$90)
C CHECK THE SPECTRUM FORMAT (i.e 32 bit or 16 bit integer)
        MFORMAT=IHEDAN(2)
        ICHECK=MFORMAT/16 -17
        IF(ICHECK.GT.0) GO TO 50
        CALL CRLF
        CALL MESS ("I am reading 16 bit integer spectrum. ")
        DO 51 I=MCMIN,MCMAX
        CALL RDBIN (ICHANO,1,TEMPSPEC(I),IER,$90)
        IF (TEMPSPEC(I).LT.0) TEMPSPEC(I)=0
 51     CONTINUE
        GO TO 90
C Read 32 bit spetrum
 50     CALL CRLF
        CALL MESS ("I am reading 32 bit double precision spectrum.")
        CALL DOCOPY( "Read Spectrum.",TEXT,10)
C Convert 32 bit double precision to floating point.
        DO 40 I= MCMIN,MCMAX
        CALL RDBIN(ICHANO,1,IHIGH,1,ILOW,IER,$900)
        CALL DPFL(IHIGH,ILOW,XTEMP)
        TEMPSPEC(I)=XTEMP
```

```
 4Ø      CONTINUE
 9ØØ     CONTINUE
         CALL CRLF
         IF(SCALNUM.EQ.Ø.Ø) SCALNUM=1.Ø
         CALL MESS ("Array is scaled to get F.Pt number.  ")
         CALL CRLF
         CALL MESS ("The scale factor =.  ")
         CALL PUTNO (SCALNUM,8,2)
         IF (SCALNUM.LE.1Ø.Ø) GO TO 8Ø ;Only mass absorption coefficient
                              ; value is divided, for which SCALNUM > 1Ø.
         DO 335 I=MCMIN,MCMAX
 335     TEMPSPEC(I)=TEMPSPEC(I)/SCALNUM
 8Ø      CONTINUE
         CALL DOCOPY(" Close channel",TEXT,1Ø)
 9Ø      CALL CLOSE (ICHANO,IER)
 999     CALL ERRMESS(TEXT,IER)
         IF (IER.EQ.1) GO TO 99
         CALL YESNO ("<12><15> Read a new file ?  ",$99)
         GO TO 3      ; Read a new file
         IF (SCALNUM.GT.1Ø.Ø) SCALNUM=1Ø.Ø ;Set the value 1Ø for others.
  99      RETURN
          END


C FILE RDSPEC------
C Subroutine RDSPEC reads a spectrum from disk.It reads both 16 bit integer
C and 32 bit +/-2G spectrum in array TEMPSPEC. In order to run the programme
C AUTO on automatic basis, some DFLAGs are introduced.
C With DFLAG = Ø, reads experimental spectrum.
C With DFLAG = 1, reads mass absorption coefficients file of soft tissue.
C With DFLAG = 2, reads thin background spectrum of formvar (Z=6).
C uses subroutine ERRMESS.
C
         SUBROUTINE RDSPEC(NAME,DFLAG)
C .....declarations .......
         COMMON /HEADAN/IHEDAN(Ø:255)
         COMMON/KARAY/ TEMPSPEC(Ø:2047)
         EQUIVALENCE (IHEDAN(1),MHDSIZE), (IHEDAN(3),MCMIN), (IHEDAN(4),MCMAX),
     &       (IHEDAN(7),GF), (IHEDAN(9),XØ),(IHEDAN(33),SCALNUM)
         INTEGER NAME(7),TEXT(1Ø),IHIGH,ILOW,DFLAG
C ask for filename
         IF (DFLAG.EQ.Ø ) GO TO 3
         IF (DFLAG.EQ.1.OR.DFLAG.EQ.2 ) GO TO 2Ø
  3      CALL CRLF
         CALL DEFAULT("Enter spectrum filename ",NAME,"S",1Ø)
C add extension to spectra file name (.SP)
         CALL AEXTN (NAME, "SP")
C
C Open file for read (1) on channel got by GCHAN
 2Ø      CALL DOCOPY( "Get channel",TEXT,1Ø)
         CALL GCHAN(ICHANO,IER,$999)
         CALL DOCOPY( "Open channel",TEXT,1Ø)
         IF (DFLAG.EQ.1) GO TO 39
         IF (DFLAG.EQ.2) GO TO 41
 21      CALL OPEN(ICHANO,NAME,1,IER,$9Ø)
         GO TO 51
C 39      CALL OPEN(ICHANO,"MACZ6.SP",1,IER,$9Ø)
  39     CALL OPEN (ICHANO,"MACSOFT.SP",1,IER,$9Ø)
         GO TO 51
 41      CALL OPEN (ICHANO,"THINBG.SP",1,IER,$9Ø)
C   READ  header block data
 51      CALL DOCOPY( "Read header.",TEXT,1Ø)
         DO 3Ø I=Ø,255
 3Ø      CALL RDBIN (ICHANO,1, IHEDAN(I),IER,$9Ø)
C Check the spectrum format (i.e 32 bit or 16 bit integer).
         MFORMAT=IHEDAN(2)
         ICHECK=MFORMAT/16 -17
         IF(ICHECK.GT.Ø) GO TO 5Ø
         DO 52 I=MCMIN,MCMAX
         CALL RDBIN (ICHANO,1,ITEMP,IER,$9Ø)
         IF (ITEMP.LT.Ø) ITEMP=Ø
 52      TEMPSPEC(I)=FLOAT(ITEMP)
         GO TO 9Ø
```

```
C Read 32 bit spectrum
 50      CONTINUE
         CALL DOCOPY( "Read Spectrum.",TEXT,10)
C Convert 32 bit double precision to floating point.
         DO 40 I= MCMIN,MCMAX
         CALL RDBIN(ICHANO,1,IHIGH,1,ILOW,IER,$900)
         CALL DPFL(IHIGH,ILOW,XTEMP)
 40      TEMPSPEC(I)=XTEMP
 900     CONTINUE
         IF(SCALNUM.EQ.0.0) SCALNUM=1.0
         IF(SCALNUM.LE.10.0) GO TO 981;Only mass absorption coefficient
                                     ; spectrum is divided by SCALNUM, for
                                     ; which SCALNUM is greater than 10.
         DO 335 I=MCMIN,MCMAX
 335     TEMPSPEC(I)=TEMPSPEC(I)/SCALNUM
 981     CONTINUE
         CALL DOCOPY(" Close channel",TEXT,10)
 90      CALL CLOSE (ICHANO,IER)
 999     CALL ERRMESS(TEXT,IER)
         SCALNUM=1.0; Fix SCALNUM to 1 for corrected spectra
         RETURN
         END


C File .......RQELEMENT
C This subroutine stores the known and some required data in a COMMON block.
      SUBROUTINE RQELEMENT
      COMMON/DT/ATW(8),GF(8),R(8),Z(8),PWST(8),PWSP(8),NE,H,RQZ(8)
      DATA PWST/1.0,1.0,0.0,1.0,8.17,1.0,1.0,1.0/
      DATA Z/11.0,12.0,13.0,15.0,16.0,17.0,19.0,20.0/
      DATA ATW/22.99,24.312,26.982,30.974,32.064,35.454,39.102,40.08/
      DATA GF/.000652,0.00223,0.0,.0001692,.00168,.0001532,.000125,0.00/
C             Na      , Mg     , Al , P       , S     , Cl      , K      , Ca
 11   CALL CRLF
      CALL CRLF
      CALL MESS ("Enter values carefully.I expect eight values namely Z=11 TO")
      CALL MESS(" 13, 15 to 17 AND 19 to 20. If you want to exclude any value")
      CALL MESS(" press return, the value will be assumed to zero. ")
      CALL CRLF
      DO 330 J=1,NE
      CALL MESS (" Enter atomic numbers of elements of interest ")
      NCH=6
      CALL GETNO (RQZ(J),NCH,1)
      IF (NCH.EQ.0) RQZ(J)=0.0
      IF (RQZ(J).EQ.0.0) Z(J)=0.0
      IF (Z(J).EQ.0.0) PWST(J)=0.0
      CALL CRLF
 330  CONTINUE
      CALL CRLF
      DO 440 J=1,NE
      IF (Z(J).EQ.0.0) GO TO 44
      CALL MESS (" The requested atomic numbers for this sample are   =")
      CALL PUTNO (Z(J),6,1)
 44   CALL CRLF
 440  CONTINUE
      CALL CRLF
      CALL YESNO (  "Is this choice O.K ?     ",$11)
      RETURN
      END
```

```
C .........File SCALE.....
C This subroutine allows scaling of the background and real experimental
C spectra according to the ratio of counts in a chosen region or
C regions of the spectrum.
C
        SUBROUTINE SCALE(NCHANS,IDE)
C       DECLARATIONS.
        INTEGER WIND
        REAL IDE,INSPEC,OUTSPEC
        COMMON /IARAY/INSPEC(0:2047)/JARAY/ OUTSPEC(0:2047)/BLK4/WIND(3,30)
C       CHOOSE WINDOWS,CALCULATE SCALE FACTOR AND SCALE OUTSPEC TO INSPEC.
 20     CALL CRLF
        CALL MESS ("How many windows do you want to use ? (Less than 31) ")
        CALL IGETNO (NWIN,2)
        IF (NWIN.GT.30) GO TO 20
        A=0.0
        B=0.0
        C=0.0
        DO 100 I=1,NWIN
        CALL CRLF
        CALL MESS ("Next window code is ?     ")
        CALL IGETNO (NCODE,2)
        CALL CRLF
        CALL MESS ("Window number =    ")
        CALL IPUTNO (NCODE,2)
        CALL MESS ("Used for scaling.    ")
        CALL CRLF
        N1=WIND(2,NCODE)
        N2=WIND(3,NCODE)
        DO 100 J=N1,N2    ; Integrate the counts over all windows chosen.
        A=A+INSPEC(J)
        B=B+OUTSPEC(J)
 100    CONTINUE
        CALL CRLF
        CALL MESS (" Total counts in INSPEC =  ")
        CALL RPRINT (A,9)
        CALL CRLF
        CALL MESS (" Total counts in OUTSPEC =  ")
        CALL RPRINT (B,12)
        CALL CRLF
        SCALF=A/B
        CALL MESS ("<15><12> The scale factor is       ")
        CALL PUTNO (SCALF,12,9)
        CALL CRLF
        CALL YESNO (" Is it O.K  ?",$160)
        GO TO 161
 160    CALL CRLF
        CALL MESS (" Enter new scale factor. ")
        CALL GETNO (SCALF,12,9)
 161    CONTINUE
        DO 200 I=0,NCHANS
 200    OUTSPEC(I)=OUTSPEC(I)*SCALF
        RETURN
        END


C file----------SELF
C This subroutine called SELF corrects the thin background spectrum for
C specimen absorption effect.It will read the mass absorption coefficient
C file via subroutine RDSPEC when DFLAG is set to 1.
C
        SUBROUTINE SELF(NCHANS,THETA,RTX)
        INTEGER DFLAG,ZX,NAME(7)
        COMMON /JARAY/OUTSPEC(0:2047)/KARAY/TEMPSPEC(0:2047)
C       READ IN DATA
        TX=RTX*0.1E-06 ; Convert mass path length into cm.
        DFLAG=1
        CALL RDSPEC (NAME,DFLAG)
        DO 600 I=0,NCHANS
        X=TEMPSPEC(I)*PLRO
        IF(X.GE.0.0.AND.X.LT.50.0) GO TO 479
```

```
        CF=0.1001E-09
        GO TO 492
479     IF (X.NE.0.0) GOTO 181
        CF=1.0
        GO TO 492
181     CF=(1.0-EXP(-X))/X
492     OUTSPEC(I)=OUTSPEC(I)*CF
600     CONTINUE
        RETURN
        END


C  FILE Setwind----------
C  This subroutine is used to set regions (windows) as required for
C  analysis. Low and High channel numbers of the windows are asked.
C  Upto 30 windows can be set. The information is stored in common.
C
        SUBROUTINE SETWIND
C       DECLARATIONS
        INTEGER WIND,LCHAN,HCHAN
        COMMON /BLK4/WIND(3,30)/HEADAN/IHEDAN(0:255)
        EQUIVALENCE (IHEDAN(7),GF), (IHEDAN(9),X0)
C       TYPE UP THE WINDOWS PREVIOSLY SET.
 40     CALL CRLF
        CALL MESS ("New window ? Enter code number ")
        CALL CRLF
        CALL MESS ("Enter a code greater than 30 to exit routine. To erase")
        CALL CRLF
        CALL MESS(" a window enter 0 for both high and low energies.")
        CALL IGETNO (NWIN,2)
        IF (NWIN.GT.30) GO TO 200
C       IF BOTH START AND STOP ENERGIES ARE ZERO DELETE THE WINDOW.
 100    WIND(1,NWIN)=1
        CALL CRLF
        CALL MESS (" Enter low channel number. ")
        NCH=4
        CALL IGETNO (LCHAN,NCH)
        WIND(2,NWIN)=LCHAN
        NS=WIND(2,NWIN)
        E1=(FLOAT(NS)-X0)/GF
        CALL CRLF
        CALL MESS (" Enter high channel number. ")
        NCH=4
        CALL IGETNO (HCHAN,NCH)
        WIND(3,NWIN)=HCHAN
        N2=WIND(3,NWIN)
        E2=(FLOAT(N2)-X0)/GF
        CALL CRLF
        CALL MESS("  You are setting window # ")
        CALL IPUTNO(NWIN,2)
        CALL CRLF
        CALL MESS (" Window set from energy (keV) ")
        CALL PUTNO (E1,8,3)
        CALL MESS("  to energy (keV) ")
        CALL PUTNO (E2,8,3)
        IF(WIND(2,NWIN).EQ.0.AND.WIND(3,NWIN).EQ.0) GO TO 170
        CALL CRLF
        CALL YESNO (" Is it O.K   ?",$100)
        GO TO 40
        CALL CRLF
 170    CALL MESS ("Deleting window number .")
        CALL IPUTNO (NWIN,2)
        CALL CRLF
        CALL YESNO ("Is this O.K. ?     ",$40)
        DO 180 I=1,3
 180    WIND(I,NWIN)=0
        GO TO 40
        CALL CRLF
        CALL YESNO (" Is this  O.K   ? ",$40)
 200    RETURN
        END
```

```
C File .........SUMTERM
C This subroutine works out the sum term of main Hall equation.
      SUBROUTINE SUMTERM (SUM)
      COMMON/DT/ATW(8),GF(8),R(8),Z(8),PWST(8),PWSP(8),NE,H,RQZ(8)
      DIMENSION CC(8)
      CALL CRLF
      CALL MESS("Enter white window counts for this spectrum ")
      CALL GETNO(WW,10,1)
      CALL CRLF
      CALL MESS ("Enter characteristic counts for peaks of interest.  ")
      DO 10 J=1,NE
      IF (Z(J).EQ.0.0) GO TO 10
      CALL CRLF
      CALL MESS ("Enter counts for element   ")
      CALL IPUTNO(J,2)
      CALL CRLF
      CALL GETNO (CC(J),10,1)
      PWSP(J) = CC(J)/WW        ; Calculate peak/white ratio (specimen)
 10   CONTINUE
      DO 15 J=1,NE
 15   R(J) = PWSP(J)/PWST(J)
      SUM=0.0
      SUM1=0.0
      SUM2=0.0
      DO 33 J=1,NE
      ZSQ=(Z(J))**2
      D1=R(J)*ZSQ*GF(J)
      D2=R(J)*ATW(J)*GF(J)
      SUM1=SUM1+D1
      SUM2=SUM2+D2
 33   CONTINUE
      SUM=1.0-SUM1+H*SUM2
      CALL CRLF
      CALL MESS ("SUM=     ")
      CALL PUTNO(SUM,8,4)
      RETURN
      END


C Subroutine WRSPAN writes a spectrum to disk.
C AN10000 format selected is 32bit +/-26 to preserve precision
C uses subroutine ERRMESS
C
      SUBROUTINE WRSPAN(NAME)
C .....declarations .......
      COMMON /HEADAN/IHEDAN(0:255) /JARAY/OUTSPEC(0:2047)
      EQUIVALENCE (IHEDAN(1),MHDSIZE),(IHEDAN(3),MCMIN), (IHEDAN(4),MCMAX)
      EQUIVALENCE (IHEDAN(7),GF), (IHEDAN(9),X0), (IHEDAN(33),SCALENUM)
      INTEGER ATNOS,NAME(7),EVCH,DFLAG,RQMAX,RQMIN,TEXT(20)
      REAL OUTSPEC,PK,M0C2
C
C ask for filename
 3    CALL CRLF
      CALL DEFAULT("Enter spectrum filename ",NAME,"S",10)
C add extension to spectra file name (.SP)
      CALL AEXTN (NAME, "SP")
      CALL MESS ("<12><15>Enter 20 char. Label. ")
      CALL DEFAULT(" Default = ",IHEDAN(11),"S",21)
      CALL CRLF
C
C create file
 11   NBLOCK=9        ;No. of blocks for 1024 x 32 bit spectrum
      IF (MCMAX .GE. 2047) THEN
      CALL DOCOPY( "Create random ",TEXT,20)
      CALL CRAND (NAME,IER,$915)
      ELSE
      CALL DOCOPY( "Create contig. ",TEXT,20)
      CALL CCONT (NAME,NBLOCK,IER,$915)
      ENDIF
```

```
C
C Open file for read/write (2) on channel got by GCHAN
 20      CALL DOCOPY( "Get channel",TEXT,20)
         CALL GCHAN(ICHANO,IER,$999)
         CALL DOCOPY( "Open channel",TEXT,20)
         CALL OPEN(ICHANO,NAME,2,IER,$90)
C write header block data
         CALL DOCOPY( "Write header.",TEXT,20)
         DO 30 I=0,MHDSIZE
 30      CALL WRBIN (ICHANO,1, IHEDAN(I),IER,$90)
C convert F.Pt. spectrum data to Double Precision integer
C and write to disk.
         CALL DOCOPY( "Write Spectrum.",TEXT,20)
         DO 40 I= MCMIN,MCMAX
         XTEMP=OUTSPEC(I)
         CALL FLDF(XTEMP,IHIGH,ILOW)
         CALL WRBIN (ICHANO,1, IHIGH,1,ILOW,IER,$90)
 40      CONTINUE
         CALL DOCOPY( "Close channel",TEXT,20)
 90      CALL CLOSE(ICHANO,IER)
         CALL CRLF
         IF (IER .EQ. 1) GO TO 900
C Is error file already exist? Overwrite old file or create new file?
 915     IF (IER .EQ. 8 .OR. IER .EQ. 12) THEN
         CALL YESNO(" <15><12>File already exists. Overwrite ",$3)
         CALL DOCOPY( "Delete old file",TEXT,20)
         CALL DELETE(NAME,IER,$90)
         GO TO 11                    ; and create file with old NAME
         ELSE                ; some other error
         GOTO 999            ; call error message routine
         ENDIF
C
 999     CALL ERRMESS(TEXT,IER)
         IF (IER .NE. 1) GO TO 950
 900     CALL MESS("<12><15> Spectrum ")
         CALL MESS(NAME)
         CALL MESS(" filed.")
 950     CONTINUE
         RETURN
         END
```

APPENDIX 3

Geometry of X-ray Absorption Path Length

A3.1 Introduction

The assumption, implied in chapter 3, that the specimen is a parallel-sided non-tilted thin film (figure 3.1) is rarely the case in practical thin film microanalysis because of the way in which materials specimens are typically produced. Electropolishing and ion-beam thinning both give rise to a wedge-shaped specimens (figure A3.3), which complicates the situation considerably. The effect of the variation of x-ray absorption path length with detector orientation was studied by Glitz et al (1981).

If the specimen is of a simple geometry (constant wedge angle) the correction is relatively simple (Glitz et al, 1981), but this is rarely the case. The situation can be quite complex, particularly in multilayer samples since the layers may be thinned at different rates. In the following sections two geometries used for x-ray microanalysis are discussed.

A3.2 Parallel-Sided Thin Foil Tilted with Respect to the Primary Electron Beam

Zaluzec (1979) and Zaluzec et al (1981) have developed an equation for calculating the actual path length caused by non-normal incidence of the electron beam on parallel sided thin

foils of thickness t. Figure A3.1 shows the geometry. The x-ray path length can be given,

$$L = t \frac{\sin.\beta}{\cos.(\beta - \theta)} \qquad \text{(A3.1)}$$

Hence,

$$G = \frac{\sin.\beta}{\cos.(\beta - \theta)} \qquad \text{(A3.2)}$$

where the angle β specifies the relative tilt of the specimen surface measured with respect to the incident electron beam and θ is the detector elevation angle measured between the specimen surface and the detector axis. τ is the specimen tilt angle. For the special case when the tilt axis of the specimen is oriented perpendicular to the plane of the detector axis, the angle $\beta = 90 - \tau$. θ_0 is the MBH Bremsstrahlung angle which is measured between the emergent electron beam and the axis of the emergent x-ray (detector axis). The detector elevation angle θ can be related with θ_0 through simple relation, $\theta = \theta_0 - 90$.

A3.3 Effective Tilt Angle in Terms of X and Y Stage Tilts

In the more general case where the stage tilts in X and Y, the effective tilt is a function of these stage tilts and the detector azimuthal angle (Fig A3.2). This is shown in figure A3.2 (a). Figures A3.2 (b) and (c) represents in detail the X and Y stage tilts and X-Z and X-Y planes respectively. The Z-axis is taken as beam axis and stage tilts are shown by X and Y. N is normal to the specimen, ϕ is the azimuthal angle measured from

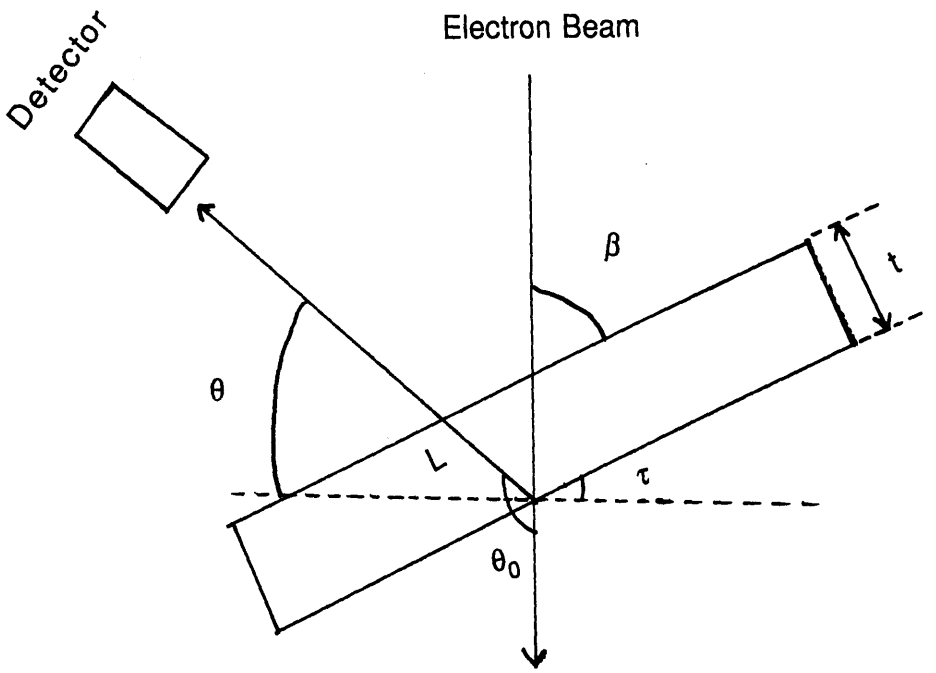

Figure A3.1

Geometry of a parallel sided thin foil tilted with respect to the incident electron beam.

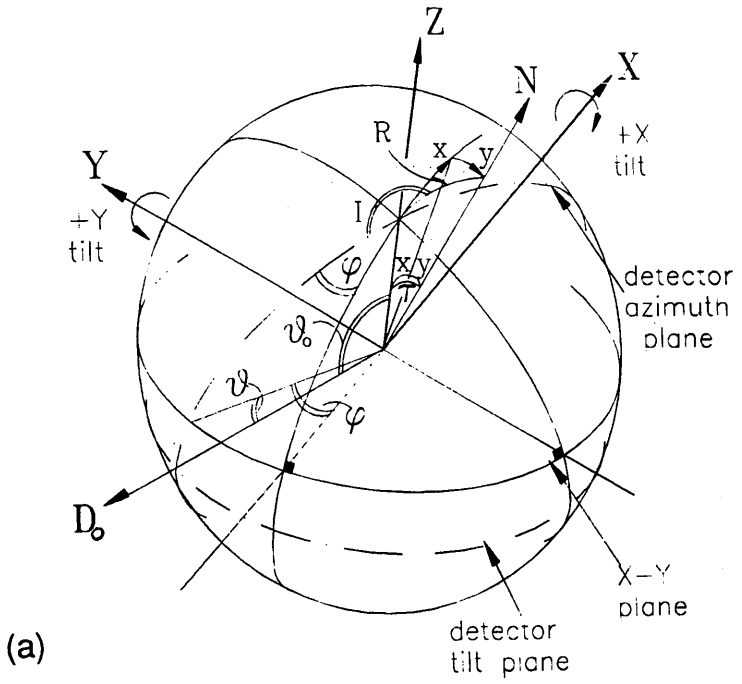

(a)

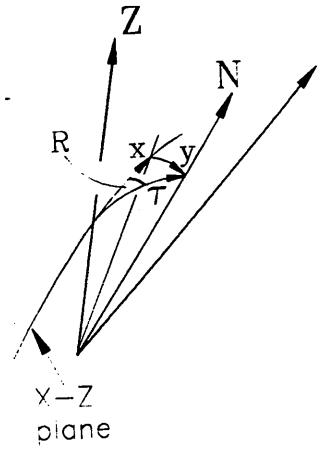

(b)

$I = \pi + R - \varphi$

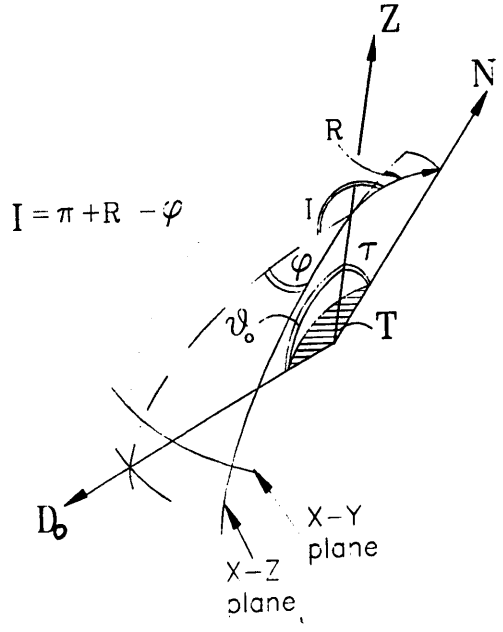

(c)

Figure A3.2

Geometry of specimen tilt in terms of X and Y stage tilts.

the rotation of the detector axis from the X-Z plane, and D_0 is the inclination of detector to X-Y plane.

The general cosine formula for a spherical triangle can be written as,

$$\cos a = \cos b \cos c + \sin b \sin c \cos A$$

Where A is the included angle of spherical triangle and a, b, c are the three side angles. Applying this formula to the N-Z spherical triangle [figure A3.2 (b)], where A is 90°, a is τ, b is X, and c is Y. Therefore,

$$\cos \tau = \cos X \cos Y \qquad \text{(A3.3)}$$

The angle R which is the rotation of normal N, from X-Z plane [figure A3.2 (b)] is given as,

$$\sin R = \frac{\sin X}{\sin \tau} \qquad \text{(A3.4)}$$

The angle I which is the angle between the detector azimuthal plane and the N-Z plane [figure A3.2 (c)] can be given as,

$$I = \pi + R + \phi$$

The angle T, between N and D may be calculated from,

$$\cos T = \cos \theta_0 \cos t + \sin \theta_0 \sin t \cos I$$

In the HB5 electron microscope the Be window x-ray detector is tilted up at 10.5° and is half way between X and Y planes.

Therefore, for the HB5 electron microscope $\theta = 10.5^\circ$; $\theta_0 = 100.5^\circ$ and $\phi = 45^\circ$.

If the specimen is tilted in such a way that N lies in the detector azimuthal plane i.e $R = \phi$ (for our case where $\phi = 45^\circ$; this is closely approximated when the X and Y stage tilts are equal), then $I = \pi$ and therefore equation A3.7 simplifies to,

$$\cos T = \cos (\theta_0 + \tau)$$

Therefore, $T = \theta_0 + \tau = \theta + \pi/2 + \tau$

Hence the specimen take of angle ($A_0 = T - \pi/2$) can be given as,

$$A_0 = \theta + \tau \qquad \text{(A3.5)}$$

For an example, for a typical case when X and Y stage tilts are 5° use of above equations give, $\tau = 7.1^\circ$, $R \approx 45^\circ$, $T = 107.6^\circ$ and $A_0 = 17.6^\circ$.

A3.4 Wedge-Shaped Thin Foil Tilted with Respect to the Primary Electron Beam

Zaluzec (1984b) has calculated the path length and the thickness of a wedge-shaped specimen which is tilted with respect to the incident electron beam. The geometry is shown in figure A3.3. The x-ray absorption path length can be given,

$$L = t \frac{\sin(\beta \pm \alpha/2)}{\cos[(\beta \pm \alpha/2) - \theta]} \qquad \text{(A3.6)}$$

Hence,

$$G = \frac{\sin(\beta \pm \alpha/2)}{\cos[(\beta \pm \alpha/2) - \theta]} \qquad \text{(A3.7)}$$

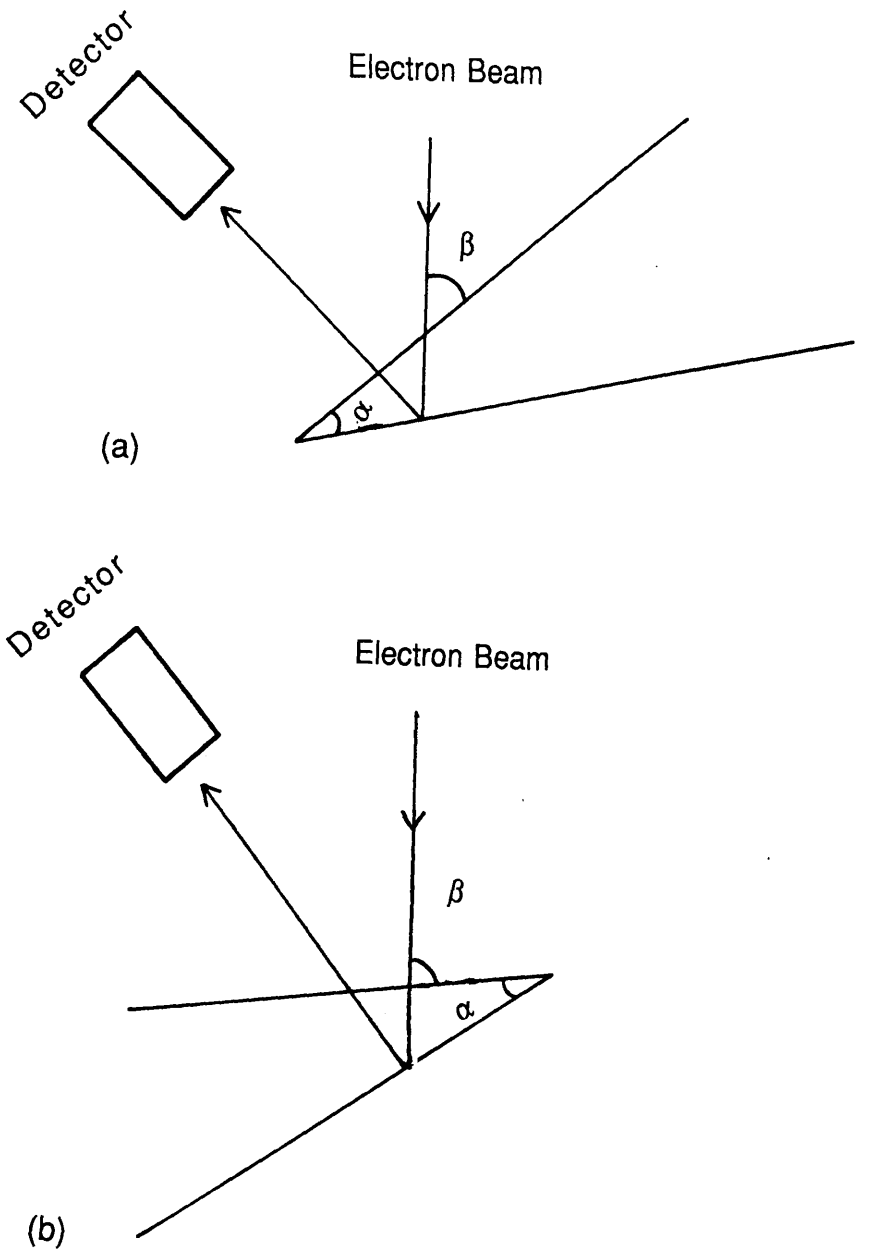

Figure A3.3

(a) Absorption path length decreased relative to a parallel sided sample.

(b) Absorption path length increased relative to a parallel sided sample.

where α is the wedge angle and $+\alpha/2$ applies when the detector is positioned such that the path length is increased relative to a parallel sided sample, while $-\alpha/2$ applies when the detector is positioned such that the path length is decreased relative to a parallel sided sample.

APPENDIX 4

Preparation of Thin Biological Samples

A4-1 Introduction

The biological aspects of the work as described in chapter 5 were carried out in collaboration with Dr H Y Elder and J D Pediani in the Institute of Physiology, University of Glasgow. The preparation of the samples was performed by J D Pediani. In this appendix a description of the preparation of samples, aminoplastic standards and epoxy resin are presented.

A4-2 Preparation of Biological Specimens

Cells of the bovine adrenal zona glomerulosa, known to exhibit an increased potassium efflux in response to angiotensin stimulation (Lobo and Marusic, 1986), were used to produce test data. A batch of cells was divided into two samples A and B. Using a hot water bath samples were incubated at 37 C°. After a five minutes incubation period sample B was stimulated with 10^{-6} M Angiotensin. The treated cells were then smeared onto small pieces of millipore filter (Millipore Ltd, pore size = 0.22 μm) which were then mounted onto a liberal layer of viscous PVP (Polyvinylpyrrolidone, Sigma) covering the end of 4.8 mm

diameter brass stub. The samples were then cryofixed (Elder et al, 1982) by rapidly plunging them into a condensed mixture, of propane with 30 % isopentane, and the temperature of the coolant was 83 K°. Sample A was untreated, cryofixed exactly by the same technique at approximately the same time interval. All the samples were normally quenched 15-20 seconds after mounting onto the stub. The addition of 30-40% isopentane to propane is advantageous since it depresses the melting point of the mixture below that of liquid nitrogen (Jehl et al, 1981) so the liquid cryogen will remain constantly liquid. The coolant vessel was filled to the top to minimize pre-cooling in the vapour phase and the coolant pool was constantly stirred to avoid the production of temperature gradients. The frozen specimens were then stored in a liquid nitrogen fridge until further preparative techniques (Freeze-drying) were undertaken.

A4.3 Protocol for Aminoplastic standards

This protocol is based on the method as described by Roos and Barnard (1984). The standards were prepared by using 70% double distilled glutaraldehyde (Agar Scientific Ltd) and urea (Analar BDH Chemicals Ltd). The salts used were NaCl(molecular weight 58.44), NaH_2PO_4 (molecular weight 119.98), and KCl (molecular weight 74.55).

Two standard solutions A and B were prepared using the same protocol as described by Pease and Peterson(1972). Solution A was prepared by adding 5 ml of 50% glutaraldehyde (takes 10ml of 70% glutaraldehyde and 4ml of distilled water) to 16 grames of urea in a conical flask. This mixture was then

gently heated (37 C°) and constantly stirred using a magnetic stirrer hotplate (Gallenkamp M.S.H. 400) until the urea was completely dissolved and the solution became clear. The flask was then cooled down and 1ml of distilled water was added. The final volume of solution A was approximately 16 ml.

Solution B was 70% glutaraldehyde diluted with salt concentrations of known concentrations to a 50% glutaraldehyde/salt mixture. Equal parts of solutions A and B were then mixed, stirred and polymerized at room temperature. If the blocks display a milky appearance after the overnight polymerization then this indicates water is still present. However, this can be overcome by drying the blocks in an oven at 60 C° for two hours.

A4.4 Preparation of Epoxy Resin

Araldite (Glauert, 1975) was used as the epoxy resin in this work, which was obtained by first mixing thoroughly Araldite CY212 10ml and DDSA 10ml and then adding this mixture to 0.4ml of BDMA accelerator the whole mixture was polymerized for 48 hours at 60 C°.

A choice of resin for embedding the specimen after freeze drying is dependent on a number of factors. The ideal resin should have a low viscosity to allow good infiltration, be hydrophobic to prevent section xehydration, contain no elements which will influence quantitation and lastly have good sectioning properties. Using microanalysis to compare epoxy resins it was found that small quantities of Na and K were detectable in some and a high concentrations of Cl was

measured in Epon Araldite and Emix. In Pallaghy resins (Pallaghy, 1973) the Cl content was approximately half of that measured in Araldite, however this resin does not always polymerize in a homogeneous manner. Araldite was chosen as the best resin because it contained the least contaminants (no Na, almost no K, and a little Cl) and had better sectioning properties.

A4.5 Freeze-Drying and Vacuum Resin Embedding

The frozen biological specimens were freeze-dried in an Edwards vacuum coating unit modified for freeze drying (Elder et al, 1986). The specimen stage was precooled to -195 C° and the specimen chamber was flooded with dry nitrogen gas to prevent frosting. Highly activated molecular sieve was added to the specimen holder to trap any residual water molecules escaping from the specimen during the drying process. The frozen specimens were then rapidly transferred still under liquid nitrogen to the specimen stage. It is important that good thermal contact is made between the specimen holder and cold finger. The chamber was brought under vacuum (less than 10^{-5} Torr) and drying was initially started at -195 C°, then continued at -85 C° for four days, followed by a slow warm up (1 C°/6 minutes) to room temperature (18 C°). On completion of drying, the specimens were vacuum infiltrated with degassed araldite resin (Elder et al, 1986) without breaking the vacuum seal via a copper feed through pipe. The chamber was then restored to atmospheric pressure, the specimens removed, embedded in

araldite resin and polymerized at 60 C° in an oven for 48 hours. The blocks were then stored in a desiccator until sectioning took place.

A4.6 Sectioning

Ultrathin sections (100-150 nm) from the aminoplastic concentration standards and the araldite resin embedded biological specimens (adrenal cortex cells) were cut dry using a Dupont diamond knife on a L.K.B. 4. ultratome. The sections were collected from the knife edge and transferred to the center of a nylon support film covering Titanium single hole mounts (Nichloson, 1974). The sections were then carbon coated (25 nm) in an Emscope T.B. 500 coating unit to provide a thermally and electrically conducting protective cover to the sections. For morphological imaging purposes, ultrathin sections (50 nm) from blocks were sectioned wet and collected using the Arbuthnot technique (Arbuthnot, 1974). The sections were then carbon coated by the same process. The Cl values in table 5.1 were corrected for the Cl content of the resin using the method described in Willson et al (1989).

APPENDIX 5

Derivation of the Hall Equation

As mentioned in chapter 5, the Hall (1971) CN method is frequently used for the quantitation of biological data. Derivation of the Hall equation which is used in CN method is presented here. The formulation follows that of Hall (1971) closely with minor alterations.

According to the theory of Kramers (1923), an electron generates an average number of continuum quanta in certain quantum energy range,B, which can be expressed as,

$$BdEdS = \frac{q}{T_0}\left[(dE / E)\sum_r n_r Z_r^2 \, dS\right] \qquad \text{(A5.1)}$$

where the quantum energy range is between E and (E+dE), q is constant, T_0 is the energy of electron beam, n is the number of atoms (atom/cm^3) with index r which is running over all constituent elements of specimen or standard, Z is atomic number, and dS is the distance through which electron beam travels in the specimen.

Simultaneously the electron beam generates an average number of quanta of the selected spectral lines, P, given by,

$$PdS = \omega_X \sigma_{iX} n_X dS \qquad \text{(A5.2)}$$

where ω_X is for fluorescence yield, σ_{iX} is ionization cross section (cm^2/atom), and X is subscript identifying the assayed element. The peak to background (P/B) intensity ratio (i.e the continuum normalisation) eliminates the need to know dS. It also removes dependence on beam current, counting time and detector solid angle which enter into the equation for detected counts of peak and continuum in the same way. Then comparing the intensities from the specimen (subscript sp) and from a standard of known composition (subscript st) we get,

$$\frac{(P/B)_{sp}}{(P/B)_{st}} = \frac{\left[n_X / \sum_r (n_r Z_r^2)_{sp}\right]}{\left[n_X / \sum_r (n_r Z_r^2)_{st}\right]} \qquad \text{(A5.3)}$$

Let us introduce,

$$n_X / \sum_r (n_r Z_r^2)_{st} = G_X$$

$G_X / (P/B)_{st} = g_X$

and $(P/B)_{sp} = R_X$

then above equation can be re-arranged to give,

$$n_X = R_X g_X \sum_r (n_r Z_r^2) \qquad \text{(A5.4)}$$

From here it should be noted that the index r will run over all constituent elements of specimen only. If W_X is the atomic weight of element X, then equation A5.4 can be related with weight fraction w'_X by using the relation,

$$w'_X = \frac{n_X W_X}{\sum_r (n_r W_r)}$$

$$\text{or} \quad \frac{w'_X}{W_X} = n_X / \sum_r (n_r W_r) \qquad \text{(A5.5)}$$

From equation A5.5 it can be written,

$$\sum_r (n_r W_r) = \frac{(n_r W_r)}{w'_r} \qquad \text{(A5.6)}$$

Thus equation A5.6 reduces to the form,

$$\frac{w'_X}{W_X} = \frac{n_X w'_r}{n_r W_r}$$

Using equation A5.4, it can be further written as,

$$w'_X = R_X g_X W_X \sum_r \left(w'_r Z_r^2 / W_r \right) \qquad \text{(A5.7)}$$

From equation A5.7, it follows that for two elements a and b,

$$\frac{w'_a}{w'_b} = \frac{R_a g_a W_a}{R_b g_b W_b} = \frac{(R g W)_a}{(R g W)_b}$$

So that,

$$\frac{w'_X}{\sum_r w'_r} = \frac{(R g W)_X}{\sum_r (R g W)_r}$$

Since $\sum_r w'_r = 1$

it can be written as,

Dividing through by w'_r and summing over r

$$1 = \sum_r (RgW / w')_r (Z^2 w' / W)_r$$

Separating the summation over m & n,

$$1 = \frac{\sum_m (RgW)_m (Z^2 w' / W)_m}{\sum_m w'} + \frac{\sum_n (RgW)_n (Z^2 w'. W)_n}{\sum_n w'}$$

Cancelling in the second term gives,

$$1 = \frac{\sum_m (RgW)_m}{\sum_m w'} \left[\sum_m (Z^2 w'. W)_m \right] + \sum (RgZ^2)_n$$

$$w'_x = \frac{(R\,g\,W)_x}{\sum_r (R\,g\,W)_r} \qquad \text{(A5.8)}$$

The summation in the denominator of equation A5.8 can be taken in two parts. One summation over matrix elements (m), and the other over other elements including X (n). Therefore, equation A5.8 becomes,

$$w'_x = \frac{(R\,g\,W)_x}{\left[\sum_m (R\,g\,W)_m + \sum_n (R\,g\,W)_n\right]} \qquad \text{(A5.9)}$$

Equation A5.7, can be written as,

$$w'_r \cdot = \cdot (R\,g.W)_r \sum_r \left(Z^2 w' / W\right)_r$$

or summing over r

$$1 = \sum_r (R\,g\,W / w')_r \sum_r \left(Z^2 w' / W\right)_r$$

Separating summation over m and n , it can be written as,

$$1 = \frac{\sum_m (R\,g\,W)_m}{\sum_m w'_m} \left[\sum_m \left(Z^2 w' / W\right)_m\right] + \sum_n \left(R\,g\,Z^2\right)_n$$

Let us define a quantity w_k for a matrix element k as,

$$w_k = \frac{w'_k}{\sum_m w'_m}$$

Where w_K is the relative concentration of the matrix elements in the matrix. Therefore, it can be written as,

$$\sum_m (R\,g\,W)_m = \frac{\left[1 - \sum_n (R\,g\,Z^2)_n\right]}{\sum_m (wZ^2 / A)_m}$$

Let us introduce a constant H,

$$\sum_m (wZ^2 / W)_m = H$$

When matrix is soft tissue H=3.28, when matrix is Araldite H=3.20.

Therefore above equation implies,

$$\sum_m (R\,g.W)_m = \frac{\left[1 - \sum_n (R\,g\,Z^2)_n\right]}{H}$$

Putting this value in equation A5.9, we get

$$w'_x = \frac{(R\,g\,W)_x H}{\left[1 - \sum_n (R\,g\,Z^2)_n + H \sum_n (R\,g\,W)_n\right]} \qquad \text{(A5.10)}$$

This is the general equation which is used in the quantitation of the biological samples. The computer programme, listed in appendix 2, was written to evaluate this equation.

REFERENCES

Adam P F (1986), Ph.D Thesis, Glasgow University.

Alavi K, Petroff P M, Wagner W R and Cho A Y (1983), J. Vac. Sci. Technol. ***B1***, 146.

Allen S M (1981), Phill. Mag., ***A 43***, 325.

Arbuthnot E R (1974), J. Microscopy, ***101 (2)***, 219.

Bambynek W, Crasemann B, Fink R W, Freund H U, Mark H, Swift R E, Price P and Venugopala Rao (1972), Rev. Mod. Phys., ***44***, 716.

Barbi N C (1979), SEM/1979, ***2***, 658.

Bard Y (1974), Nonlinear Parameter Estimation (Academic Press), London.

Barnett S J, Brown G T, Courtney S J, Bass S J and Taylor L L (1988), J. Appl. Phys., ***64***, 1185.

Bass S J, Barnett S J, Brown G T, Chew N G, Cullis A G, Pitt A D and Skolnick M S (1986), J. Cryst. Grow. ***79***, 378.

Bass S J, Barnett S J, Brown G T, Chew N G, Cullis A G, Skolnick M S and Taylor L L (1987), in: Thin Film Growth Techniques for Low Dimensional Structures (Plenum Press), London, 137.

Bean J C, Feldman L C, Fiory A T, Nakahara S and Robinson I K (1984), J. Vac. Sci. Technol., ***A2***, 436.

Bearden J A (1967), Rev. Mod. Phys., ***39***, 78.

Bentley J, Zaluzec N J, Kenik E A, and Carpenter R W (1979), SEM/1979, ***2***, 581.

Berenyi B, Hock G, Ricz S, Schlenk B and Valek A (1978), J. Phys., ***B 11***, 709.

Berenyi B and Hock G (1978), Jap. J. Appl. Phys., ***17 (2)***, 78.

Beth H A (1930), Ann. der. Phys., ***5***, 325.

Bethe H A and Heitler W (1934), Proc. Roy. Soc., London, ***A 146***, 83.

Bethe H A and Salpeter E A (1957), Quantum Mechanics of One and Two Electron Atoms, 323.

Bracewell and Veigele (1970), in: Developments in Appl. Spectros., ed. Perkins A (Plenum Press), New York, **Vol. 9**.

Bullock J F, Humphreys C J, Norman A G and Titchmarsh J M, Microscopy of Semiconducting Materials 1987 (Inst. Phys. Conf. Ser. No. 87, Adam Hilger Ltd), Bristol, 643.

Burhop E H S (1952), in: The Auger Effect and Other Radiationless Transitions (Camberidge University Press).

Champness P E, Cliff G and Lorimer G W (1980), Bull. de. Min., Orleans.

Chapman J N, Gray C C, Robertson B W and Nicholson W A P (1983), X-Ray Spectrom., ***12 (4)***, 153.

Chapman J N, McGibbon A J, Cullis A G, Chew N G, Bass S J and Tayler L L (1987), Microscopy of Semiconducting Materials 1987 (Inst. Phys. Conf. Ser. No. 87, Adam Hilger Ltd), Bristol, 649.

Chew N G, Cullis A G (1987), Ultramicroscopy ***23***, 175.

Chew N G, Cullis A G, Bass S J, Tayler L L, Skolnick M S and Pitt A D (1987), Micros. of Semiconduc. Materials 1987 (Inst. Phys. Conf. Ser. No. 87, Adam Hilger Ltd), Bristol, 231.

Cliff G and Lorimer G W (1975), J. Micros., ***103***, 203.

Cliff G and Lorimer G W (1981), in: Quantitative Microanalysis with High Spatial Reslution, eds. Lorimer G W, Jacobs M H and Doig P (The Metals Soc.), London.

Craven A J and Adam P F (1985), Proc. 8th European Cong. on E.M., Budapest.

Craven A J, Adam P F and Howe R (1985), Proc. of EMAG 85 Conf., New castle.

Crozier P A (1986), Ph.D Thesis, Glasgow University.

Cullis A G, Chew N G, Irvine S J C and Geiss J (1987), Micros. of Semiconducting Materials 1987, (Inst. Phys. Conf. Ser. No. 87, Adam Hilger Ltd), Bristol, 141.

Davies G J and Andrews D A (1985), Br. Telcom. Technol. J., ***3***, 59.

Ekelund S, Thuren A and warlefors T (1979), X-Ray Spectrom., ***8 (1)***, 2.

Elder H Y, Gray C C, Jardine A G, Chapman J N and Biddbcomb W H (1982), J. Microsc., ***126***, 45.

Elder H Y, Biddlecombe W H, Tetley L, Wilson S M, and Jenkinson D.Mc EWan (1986), EMSA Bull, ***16***, 111.

Elwert G (1939), Ann. Phys., ***34***, 178.

Esaki L and Tsu R (1970), IBM J. Res Dev., 14 61.

Fiori C E and Newbury D E (1978), SEM/1978, ***1***, 401.

Fiori C E and Newbury D E (1980), SEM/1980, ***2***, 250.

Freund H U (1975), X-Ray Spectrom., ***4***, 90.

Garrett-Read A J and Furdanowicz W (1987), in: EMAG 87, Proc. of Workshop, 7.

Gill P E and Murray W (1978), Algorithms for the Solution of Nonlinear Least-square Problom., SIAM J. Numer. Anal., ***15***, 977.

Glas F (1986), Ph.D thesis, University de Paris-Sud.

Glitz R W, Notis M R, Williams D B and Goldstein J I (1981), In: Microbeam Analysis-1981, ed. Geiss R H. (San Francisco Press), San Francisco, 309.

Glauert A M (1975), In: Fixation, Dehydration and Embedding of biological specimens, ed. Glauert A M.

Gluckstern R L and Hull M H (1953), J. Phys. Rev., ***90***, 1030.

Goldberg M (1961), J. Phys. Radium, ***22***, 743.

Goldstein J I, Costley J L, Lorimer G W and Reed S J B (1977), SEM/77, ed. O Johari, Chicago, ***1***, 315.

Goldstein J I and Williams D B (1977), SEM/1977, ***1***, 427.

Goodhew P J and Chescoe D (1980), Micron 1980, ***11***, 153.

Goodhew P J and Castle J E (1983), in: Proc. EMAG 1983 (Inst. Phys. Conf. Ser. No. 68), eds. Doig P, 515.

Gray C C (1981), Ph.D Thesis, Glasgow University.

Gray C C, Chapman J N, Nicholson W A P, Robertson B W and Ferrier R P (1983), X-Ray Spectrom., ***12 (4)***, 163.

Gupta B L, Berridge M J, Hall T A, and Moretoy R B (1978), J. Exp. Biol., **72**, 261.

Hall T A (1971), in: Physical Techniques in Biochemical Research, ed. G. Oster, (Academic Press), New York, ***1A***, 157.

Hall T A and Gupta B L (1979), in: Introduction to Analytical Electron Microscopy 1979, eds. Hern J J, Goldstein J I, and Joy D C (Plenum Press), New York, 169.

Heinrich K F J (1966), in: The Electron Microprobe, eds. McKinley T D, Heinrich K F J and Wittery D B (John Wiley), New York, 296.

Heinrich K F J, Fiori C E and Myklebust R L (1979), J. Appl. Phys., ***50***, 5589.

Heinrich K F J (1987), from National Bureau of Standards, Gaitbersdanrg, Md 20899.

Heitler W (1954), in: The Quantum Theory of Radiation (Oxford University Press), London, 242.

Henke B L and Ebisu E S (1974), in: Advances in X-Ray Analysis (Plenum Press), New York, ***17***, 150.

Hirst H and Alexander E (1935), Phil. Mag., ***19***, 918.

Horita Z, Sano T and Nemoto M (1986), J. Micros., ***143 (3)***, 215.

Horita Z, Sano T and Nemoto M (1987), Ultramicroscopy,

21, 271.

Hull R, Carey K W, Fouquet J E, Reid G A, Rosner S J, Bimberg D and Oertcl D (1986), Proc. GaAs and related comp. (Inst. Phys. Conf. Ser. No. 83), Las Vegas, Nevada, 209.

Hutchins R, Loretto M H, Jones I P and Smallman R E (1979), Ultramicroscopy, *3*, 401.

Inokuti M (1971), Rev. Mod. Phys., *43*, 297.

Jehl B, Bauer R Dorge A and Rick R (1981), J. Microscopy, *123 (3)*, 307.

Joyce B A (1985), Rep. Prog. Phys., *48*, 1637.

Joy D C (1979), in: Introduction to Analytical Electron Micros., eds. Hren J J, Goldstein J I and Joy D C (Plenum Press), New York.

Joy D C and Maher D M (1975), Proc. 33rd Annl. EMSA Mtg., ed. Bailey G W (Claitor's Pub. Div.), Baton Rouge, 242.

Keith H D and Loomist T C (1978), X-Ray Spectrom.,*7*, 217.

Kelly P M, Jostsons A, Blake R G and Napier J G (1975), Phys. Stat. Sol., *31*, 771.

Kirkpatrick P and Wiedmann L (1945), Phys. Rev., *67*, 321.

Kissel L, Quarles C A and Pratt R H (1983), At. Data and Nuc. Data Tables, *28*, 381.

Khan Md. R and Karimi M (1980), X-Ray Spectrom., *9*, 32.

Koch H W and Motz J W (1959), Rev. Mod. Phys., *31*, 920.

Kramers A (1923), Phill. Mag., *46*, 836.

Kyser D F and Geiss R H (1977), Proc. 12th Anual. Confs. MAS, 110.

Langenberg A and Van Eck J (1979), J. Phys., *B 12*, 1331.

Link Systems Detector Information Manual, Link Systems, High Wycombe.

Lobo M V and Marusic E T (1986), Am. J. Phyiol., **250 E**, 125.

Lorimer G W, Cliff G and Clark J N (1976), in: Developments in Electron Micros. and Analysis, ed. Venables J A (Acad. Press), London, 153.

Lorimer G W, in: Quantitative Electron Microscopy, eds. Chapman J N and Craven A J, Scottish Universities Summer School in Physics, 305.

Love G, Cox M G C and Scott V D (1977), in: Developments in Electron Micros. and Analysis, ed. Misell D L (Inst. Phys. Conf. Ser. No. 36), Inst. of Phys., Bristol and London, 347.

Mallard R E, Waddington W G and Spurdens P C (1987), Micros. of Semiconducting Materials 1987, (Inst. Phys. Conf. Ser. No. 87, Adam Hilger Ltd), Bristol, 21.

McGibbon A J (1989), Ph.D Thesis, Glasgow University.

McGibbon A J, Chapman J N, Cullis A G, Chew N G, Bass S J and Tayler L L (1989), J. Appl. Phys., ***65 (6)***, 2293.

Nicholson W A P (1974), in: Microprobe Analysis as Applied to Cells and Tissues, eds. Hall T A, Echlin P and Kaufmann R (Academic Press), New York, 239.

Nicholson W A P and Dempster D W (1980), SEM/1980,***2***, 517.

Nicholson W A P, Gray C C, Chapman J N, and Robertson B W (1982), J. Microscopy, ***125***, 25.

Nicholson W A P and Chapman J N (1983), Microbeam Analysis 1983, ed. R.Gooley (San Francisco Press), San Francisco, 215.

Nicholson W A P, Craven A J, Adam P F, and Steele J D (1984), Analytical Electron Microscopy 1984, eds. Willams D B and Joy D C (San Francisco Press), San Francisco, 258.

Osbourne G G (1983), Phys. Rev., ***B27***, 5126.

Pallaghy C K (1973), Australian J. Biol. Sci., ***26***, 1015.

Panessa B J, Warren J B, Hern J J, et-all (1978),

SEM/1978, ***2***, 1055.

Pears K, Private Communications.

Pease D C and Peterson R G (1972), J. Ultrastruct. Res., ***41***, 133.

Peterson J H (1988), Ph.D Thesis, Glasgow University.

Paterson J H, Chapman J N, Nicholson W A P and Titchmarsh J M (1989), J. Microscopy, ***154 (1)***, 1.

Powell C J (1976), Rev. Mod. Phys., ***48***, 33.

Pratt R H, Tseng H K, Lee C M, Kissel L, MacCallum C and Riley M (1977), A. Data Nucl. Data Tables, ***20***, 175.

Rae D A, Scott V D and Love G (1981), in: Quantitative Microanalysis with High Spatial Reslution, eds. Lorimer G W, Jacobs M H and Doig P (The Metals Soc.), London, 57.

Rao-Sahib T S and Wittry D B (1974), J. Appl. Phys., ***45***, 5060.

Rez P (1984), X-Ray Spectrom., ***13 (2)***, 55.

Roomans G M and Kuypers G A J (1980), Ultramicros.***5*** 81.

Roos N and Barnard T (1984), Ultramicroscopy, ***15***, 277.

Rosbeck J P and Herper M E (1987), J. Appl. Phys., ***62***, 1717.

Sauter F (1933), Ann. Phys., ***18***, 486.

Schreiber T P and Wims A M (1981), Ultramicros., ***7***, 323.

Scofield T H (1974), Phys. Rev., ***A 9***, 1041.

Shuman H, Somlyo A V, and Somlyo A P (1976), Ultrmicroscopy, ***1***, 317.

Sommerfeld A (1931), Ann. Phys., ***11***, 257.

Springer G and Nolan (1976), Canad. J. Spectros., ***21***, 134.

Statham P J (1976), X-Ray Spectrom., ***5***, 16.

Statham P J (1981), in: Proc. of a Workshop on Energy Dispersive X-Ray Spectrom., NBS Publ. No. ***604***, 127.

Stenton N, Notis M R, Goldstein J I and Williams D B (1981), in: Quantitative Microanalysis with High Spatial Reslution, eds. Lorimer G W, Jacobs M H and Doig P (The Metals Soc.), London, 35.

Thinh T P and Leroux J (1979), X-Ray Spectrom., ***8***, 85.

Thomas L E (1984), in: Analytical Electron Microscopy 1984, eds. Williams D B and Joy D C (San Francisco Press), San Francisco, 358.

Tixier R and Philibert J (1969), Proc. 5th Intl. Cong. on X-ray Optics and Microanalysis, eds. Mollenstedt G and Gaukler K H (Springer-Verlag), Berlin, 180.

Tseng H K and Pratt R H (1971), Phys. Rev., ***A3***, 100.

Venables J N (1981), in: Quantitative Microanalysis with High Spatial Reslution, eds. Lorimer G W, Jacobs M H and Doig P (The Metals Soc.), London, 205.

Victor C (1961), Ann. Phys., ***6***, 183.

Willson et al (1989), Tissue and Cell, ***20***, 691.

Zaluzec N J (1979), in: Introduction to Analytical Electron Micros., eds. Hren J J, Goldstein J I and Joy D C (Plenum Press), New York, 121.

Zaluzec N J (1981), Microbeam Analysis-1981, ed. Geiss R H (San Francisco Press), San Francisco, 329.

Zaluzec N J, Maher D M and Mochel P E (1981), In: Analytical Electron Microscopy-1981, ed. Geiss R H (San Francisco Press), San Francisco, 25.

Zaluzec N J (1984 a), in: Analytical Electron Microscopy 1984, eds. Williams D B and Joy D C (San Francisco Press), San Francisco, 443.

Zaluzec N J (1984 b), EMSA Bulletin, ***14 (2)***, 61.